Tampere University

HAMED POURKHEIROLLAH

Printed Supercapacitors for Energy Storage and Functional Applications, Modeling, Analysis, and Integration

Tampere University Dissertations 929

Tampere University Dissertations 929

HAMED POURKHEIROLLAH

Printed Supercapacitors for Energy Storage and Functional Applications, Modeling, Analysis, and Integration

ACADEMIC DISSERTATION
To be presented, with the permission of
the Faculty of Information Technology and Communication Sciences
of Tampere University,
for public discussion in the Auditorium TB109
of the Tietotalo building, Korkeakoulunkatu 7, 33720 Tampere,
on 15th December 2023, at 12 o'clock.

ACADEMIC DISSERTATION
Tampere University, Faculty of Information Technology and Communication Sciences
Finland

Responsible supervisor and Custos	Professor Donald Lupo Tampere University Finland	
Supervisors	Professor Donald Lupo Tampere University Finland	Professor Matti Mäntysalo Tampere University Finland
Pre-examiners	Professor Pertti Kauranen LUT University Finland	Assoc. Professor Darren Southee Loughborough University England, United Kingdom
Opponent	Professor Davide Deganello Swansea University Wales, United Kingdom	

The originality of this thesis has been checked using the Turnitin OriginalityCheck service.

Cover design: Roihu Inc.

ISBN 978-952-03-3219-8 (print)
ISBN 978-952-03-3220-4 (pdf)
ISSN 2489-9860 (print)
ISSN 2490-0028 (pdf)
http://urn.fi/URN:ISBN:978-952-03-3220-4

Carbon dioxide emissions from printing Tampere University dissertations have been compensated.

PunaMusta Oy – Yliopistopaino
Joensuu 2023

Acknowledgments

The research work has been conducted at the Laboratory for Future Electronics located in Tampere University, Finland. This project has been financially supported by the European Union's Horizon 2020 research and innovation programme under the Marie Skłodowska-Curie grant agreement No 814299, referred to as CHARISMA. Additionally, certain aspects of the research utilized the Academy of Finland Research Infrastructure "Printed Intelligence Infrastructure" (PII-FIRI, Grant Number 320019).

I extend my heartfelt gratitude to my supervisors, Professor Donald Lupo and Professor Matti Mäntysalo, for their unwavering support and invaluable guidance during the entire duration of my work. Additionally, I would like to express my appreciation to Doctor Jari Keskinen for being an exceptional mentor and providing active support throughout the research process. Their contributions have been instrumental in the success of this endeavor.

Furthermore, I would like to extend my special acknowledgment to the co-authors of the publications and my past and present colleagues at the Laboratory for Future Electronics. I would also like to extend my heartfelt appreciation to my fellow Ph.D. students within the 'CHARISMA' project for their collaborative spirit and invaluable contributions throughout my research journey. Their support has been indispensable, and I am grateful for their contributions, which have enriched this research endeavor.

Last but not least, I want to express my deepest gratitude to my beloved wife "Zahra" for her constant presence and support throughout this journey. Her enduring encouragement has been a source of strength, and without her, this work would not have been possible. I am truly grateful for her love and understanding. I wholeheartedly dedicate this thesis to her, as her unwavering love, encouragement, and steadfast support have been my driving force and constant inspiration throughout this remarkable journey. Her presence in my life has illuminated every step, and it is with profound gratitude that I honor her for the immeasurable role she has played in shaping both my academic achievements and the person I have become.

Abstract

Supercapacitors (SCs), also known as ultracapacitors or electrochemical double-layer capacitors (EDLCs), have emerged as a remarkable class of energy storage devices that bridge the gap between conventional capacitors and batteries. These devices exhibit exceptional power density and long lifecycle, making them well-suited for a wide range of applications, from powering portable electronics to enabling rapid energy storage and release in various industrial systems. Unlike batteries, SCs store energy through the physical separation of charges at the electrode-electrolyte interface, leading to rapid charging and discharging capabilities. However, SCs are not without their challenges, notably leakage current and self-discharge, which can impact their long-term performance and practical utility. As the demand for energy-efficient and responsive power solutions intensifies, a thorough understanding of SCs' behavior, coupled with accurate modeling techniques, becomes imperative. This thesis delves into this intricate realm, offering insights, models, and practical applications that collectively contribute to harnessing the potential of SCs across diverse domains.

In the realm of energy storage and power management, this thesis presents a cohesive exploration of SCs' behavior and its practical implications through a series of five interrelated research papers. Focusing on the context of charging and discharging within series-connected SC modules under varying load conditions, the research advances an innovative exponential model that elegantly captures complex behaviors with less than 4% simulation error over extended time frames (31 days).

The initial study introduces an improved exponential equivalent circuit model (ECM) that elegantly characterizes the charging and discharging dynamics of series-connected SC modules. Leveraging a single-variable leakage resistance (VLR) approach, the model adeptly accounts for diverse self-discharge mechanisms. Unlike existing literature ECMs, this ECM's simplicity and accuracy render it suitable for real-world applications in both short and long terms. The investigation extends to the modeling of multiple SC energy storage modules, providing insights into the behavior of SCs within varying configurations.

Expanding into the domain of Internet of Things (IoT) applications, the research highlights the significance of energy storage devices for wireless sensor nodes. Acknowledging the limitations of traditional batteries, the study advocates for SCs as a viable solution. A refined exponential model is then proposed as a novel approach to predict the discharge behavior of disposable printed flexible SCs, ensuring concordance with experimental findings. This approach involves employing an innovative method to model the non-linearity of self-discharge in printed SCs, effectively capturing this phenomenon. This ECM's adaptability and alignment with measured self-discharge results offer a promising avenue for optimal IoT device performance.

Confronting the challenges of leakage current and self-discharge in SCs, the thesis presents a comprehensive framework. By proposing practical exponential ECMs, the study encapsulates non-linear leakage and self-discharge phenomena. The empirical basis of these ECMs allows accurate prediction of discharge behaviors over extended periods, thereby holding potential for widespread practical application. A linear correlation was identified among the variables governing the exponential function of the equivalent parallel resistance (EPR) within the SC's ECMs and the capacitance. The precision of the proposed ECMs was substantiated over an extended duration of 31 days, employing a diverse array of four distinct methodologies.

The thesis also takes a statistical turn by conducting a meticulous analysis of experimental parameters across printed SCs. Employing established ECMs, the research unveils statistical distributions and correlations, empowering safer operation, and more informed decision-making. Monte Carlo simulation technique unveils the long-term performance of SCs, offering insights into consistency and aiding in risk assessment. The conducted statistical analysis has revealed a normal distribution pattern

for all the parameters characterizing the printed SCs. Additionally, this thesis presents a methodology to ascertain the upper limit of potential standard deviation (std) in capacitance values across SCs within a module, aiming to ensure the seamless operation of the module without encountering malfunctions. Furthermore, an observed linear correlation has been established between the maximum potential std of capacitance values among SCs and the cumulative voltage stored within the module.

Finally, the exploration expands to the activation of irreversible visual indicators (IVIs) through printed SCs, highlighting the potential of diverse monomer systems. The interplay of activation potential, coloration efficiency, and initial voltage underscores the feasibility of fully activating IVIs through series-connected SCs.

In summary, this thesis intricately weaves together five research papers to construct a comprehensive narrative about the behavior, modeling, and application of SCs. From exponential models to statistical analyses and practical implementations, this work contributes to the broader understanding of SC dynamics and their potential within contemporary energy storage systems and IoT applications. The results-driven approach solidifies SCs' impact as a versatile energy storage device, emphasizing real-world performance, and evidence-based decisions.

TABLE OF CONTENTS

List of Figures

List of Tables

Abbreviations and symbols

A	Area
AC	Activated Carbon
Al	Aluminum
BLE	Bluetooth Low Energy
C	Capacitance
CE	Coloration Efficiency
CV	Cyclic Voltammetry
d	distance
E	Energy
Ea	Activation Potential
ECM	Equivalent Circuit Model
EDLC	Electrochemical Double-layer Capacitor
EPR	Equivalent Parallel Resistance
ESR	Equivalent Series Resistance
EV	Electric Vehicle
GCD	Galvanostatic Charge-Discharge
I	Current
IC	Integrated Circuit
IoT	Internet of Things
IVI	Irreversible Visual Indicator
M	Mean value
MC	Monte-Carlo
OPV	Organic Photovoltaic
PE	Printed Electronics
PET	Polyethylene Terephthalate
PI	Polyimide
ppm	Parts Per Million
Q	Charge
R2R	Roll-to-Roll
RF	Radio Frequency
SC	Supercapacitor

SoC	System on a Chip
SP	Screen Printing
SSA	Specific Surface Area
std	Standard Deviation
t	time
V	Voltage
VLR	Variable Leakage Resistance
WSN	Wireless Sensor Network
ε_0	dielectric constant of vacuum
ε_r	dielectric constant of the insulating material

List of Publications

I. **Pourkheirollah, Hamed**, Jari Keskinen, Matti Mäntysalo, and Donald Lupo. "An improved exponential model for charge and discharge behavior of printed supercapacitor modules under varying load conditions." Journal of Power Sources 535 (2022): 231475.

II. **Pourkheirollah, Hamed**, Jari Keskinen, Donald Lupo, and Matti Mäntysalo. "A Modified Exponential Equivalent Parallel Resistance (EPR) Model for Predicting Self-Discharge Behavior of Printed Flexible Supercapacitors." In 2022 IEEE 9th Electronics System-Integration Technology Conference (ESTC), pp. 264-268. IEEE, 2022.

III. **Pourkheirollah, Hamed**, Jari Keskinen, Matti Mäntysalo, and Donald Lupo. "Simplified exponential equivalent circuit models for prediction of printed supercapacitor's discharge behavior-Simulations and experiments." Journal of Power Sources 567 (2023): 232932.

IV. **Pourkheirollah, Hamed**, Jari Keskinen, Matti Mäntysalo, and Donald Lupo. "Statistical analysis and Monte-Carlo simulation of printed supercapacitors for energy storage systems." Journal of Power Sources 585 (2023): 233626.

V. Howard, E. L., **Hamed Pourkheirollah**, Carlos Pinheiro, C. A. T. Laia, A. Jorge Parola, Matti Mäntysalo, and Donald Lupo. "Integration of Supercapacitors to Trigger In-Situ Electropolymerization for Irreversible Visual Indicators." In 2023 IEEE International Conference on Flexible and Printable Sensors and Systems (FLEPS), pp. 1-4. IEEE, 2023.
*First two Authors contributed equally to this work

1- INTRODUCTION

The quest for efficient and reliable energy storage solutions has gained paramount importance in the face of growing global energy demands and the increasing adoption of renewable energy sources. Among various energy storage technologies, supercapacitors (SCs) have emerged as a promising option due to their exceptional power density, rapid charge and discharge capabilities, and extended lifecycle compared to conventional batteries. These attributes make SCs particularly attractive for a wide range of applications, including powering Internet of Things (IoT) devices, wearable electronic devices, and renewable energy systems.

However, despite their numerous advantages, SCs are not without challenges. One of the significant drawbacks is their susceptibility to leakage current and self-discharge, which can lead to performance degradation over time and hinder their long-term reliability. Addressing these issues is of utmost importance for the practical and widespread adoption of SCs in real-world applications.

The current state-of-the-art in SC modeling involves complex equivalent circuit models (ECMs) that attempt to capture the intricate electrochemical processes occurring within these energy storage devices. While these models provide valuable insights, they often suffer from computational complexity, making them impractical for real-time simulations and long-term performance predictions. Thus, there is a growing demand for simplified yet accurate models that can represent the behavior of SCs under varying load conditions and extended periods of operation.

In light of these challenges, this Ph.D. thesis embarks on a journey to develop improved exponential models for characterizing the charging and discharging behavior of series-connected SC modules. These models aim to strike a balance between simplicity and accuracy, allowing for practical implementation and enabling their use in both short-term and long-term applications. The proposed models leverage a single variable leakage resistance (VLR) with an exponential current/voltage profile to effectively model different self-discharge mechanisms of SCs. By incorporating experimental results and electrical parameters of printed SCs, the thesis explores the behavior of different energy modules and compares the performance of the proposed exponential models with existing literature-reported models.

Furthermore, this thesis delves into the challenges faced in IoT applications where SCs are employed as energy storage options for powering autonomous wireless sensor nodes. The uncertainty of dynamic leakage current behavior during repeated charging and discharging in IoT scenarios is thoroughly investigated. An improved simplified exponential model is presented to simulate the non-linear discharge behavior of fabricated printed flexible SCs over an extended period (31 days). The model is well adapted to experimental self-discharge results, offering a more accurate representation of SC behavior in IoT applications.

To complement the modeling efforts, this research explores statistical analysis techniques to assess the performance of printed SCs and predict their behavior over time. The statistical analysis of experimental parameters for multiple SCs using proposed ECMs helps identify key statistical distributions, providing insights into capacitance variations within an energy storage module. This aids in ensuring safe operation and optimal performance. Monte-Carlo simulation technique is employed to predict long-term charge and discharge behavior, offering valuable information for performance evaluation, design validation, and risk assessment.

Additionally, this thesis explores the utilization of printed SCs to activate Irreversible Visual Indicators (IVIs) based on different electrochromic monomers. The key parameters influencing the activation of IVIs and the potential of using series-connected SCs for full activation are thoroughly explored. These findings contribute to the understanding of printed SCs' applicability in visual indicators and other energy-harvesting applications.

1.1- AIMS AND SCOPE OF THE THESIS

The main research questions of this Ph.D. thesis are:

1. How can we develop an accurate exponential model to predict the charging, discharging, leakage current, and self-discharge behavior of series-connected SC modules, considering both short-term and long-term performance in various IoT applications?

2. Can an empirical exponential equivalent circuit model effectively capture the complex interactions between leakage current, self-discharge, and nonlinear behavior in SCs, and how well does it compare with existing models?

3. Through statistical analysis, how can we estimate and predict the dynamic leakage current and self-discharge behavior during repeated charging and discharging for IoT applications, ensuring safe operation and determining energy storage module performance with an acceptable standard deviation range?

4. What is the impact of different monomer systems and key parameters on the activation of Irreversible Visual Indicators (IVIs) based on printed SCs, and can series-connected SCs achieve full activation of IVIs, thereby enabling irreversible visual indicators for various applications?

Below is also a succinct summary outlining the content of each publication:

In **Publication I**, we propose a simple equivalent circuit model for SC energy modules, utilizing experimental parameters of printed SCs. The model incorporates the equivalent series resistance (ESR) and an exponential equation to represent non-linear leakage current and self-discharge. The model successfully predicts the performance of different energy modules, showcasing its potential for real-world applications.

Publication II introduces an improved simplified exponential model to simulate the dynamic self-discharge effects of printed SCs over a month-long period. The proposed model exhibits high accuracy and matches well with experimental results. It addresses the uncertainty of leakage current behavior during repeated charging and discharging in IoT applications, making it valuable for IoT device power management strategies.

In **Publication III**, we propose a simplified equivalent circuit model based on experimentally identified parameters of SCs. The model accurately represents the discharge and self-discharge behavior of electrochemical double-layer capacitors (EDLCs) type SCs over an extended period. The study also presentes three sub-ECMs, offering a straightforward approach for predicting SC behavior with reasonable accuracy.

Publication IV focuses on a comprehensive statistical analysis of experimental parameters for printed SCs, employing previously proposed equivalent circuit models. The statistical distributions and descriptive statistics indicate normal distributions for various SC parameters. Additionally, we

introduce a statistical method to determine the maximum potential standard deviation in capacitance within an energy storage module, ensuring safe operation and predicting energy window ranges.

Publication V explore the activation of Irreversible Visual Indicators (IVIs) based on printed SCs with different monomer systems. The study identifies key parameters influencing IVI activation and their dependence on series-connected SCs. The results highlight promising monomer systems for IVI activation and potential applications in the smart label market.

In conclusion, this Ph.D. thesis presents a comprehensive study that addresses critical challenges in SC modeling, IoT applications, statistical analysis, and activation of IVIs. The proposed exponential models, combined with statistical techniques, offer valuable insights into the behavior and performance of SCs, empowering researchers and engineers to make informed decisions and unlock the full potential of these energy storage devices in practical applications. The knowledge gained from this research contributes to advancing the field of energy storage and opens up new avenues for efficient and sustainable energy solutions.

1.2- STRUCTURE OF THE THESIS

This thesis comprises seven chapters and is augmented by five peer-reviewed publications. Chapter 1 delineates the thesis' objectives, its structure, and offers an overarching introduction to the subject. Chapter 2 elucidates the fundamental operational principles of supercapacitors, contrasting them with alternative energy storage methods, and surveys various supercapacitor types. This chapter also covers the materials employed in supercapacitors and the printing techniques utilized for producing printed supercapacitors. Moving to Chapter 3, a brief description of the device fabrication and characterization methods utilized in this research is provided.

Chapter 4 encompasses the modeling of supercapacitors, covering both the equivalent circuit models (ECMs) documented in existing literature and those proposed within this thesis. The principal results and discoveries are discussed in Chapter 5. Chapter 6 presents a summary and conclusion of the thesis, coupled with a discussion on potential avenues for future research. Chapter 7 includes all the references cited within the thesis. The publications are appended at the end of the thesis.

1.3- AUTHORS' CONTRIBUTION

Through collaborative efforts with fellow researchers, the articles referenced in this thesis have been published, outlining the author's specific contributions as outlined below:

Publication I, II, III and IV: **Hamed Pourkheirollah**: Conceptualization, Methodology, Software, Validation, Formal analysis, Investigation, Data curation, Writing original draft, Visualization. **Doctor Jari Keskinen**: Conceptualization, Methodology, Resources, Writing – review & editing. **Professor Matti Mäntysalo:** Conceptualization, Methodology, Resources, Writing – review & editing, Supervision. **Professor Donald Lupo**: Resources, Writing – review & editing, Supervision, Project administration, Funding acquisition.

Publication V: This work has two main authors as Elin Howard and Hamed Pourkheirollah collaborated equally on all parts of this work. The author contributed to planning the experiments,

fabricating the samples, and conducting the measurements. The author also shared an equal role on performing the characterization, analyzing the data and writing the first version of the manuscript.

2- BACKGROUND

This chapter commences with an exploration of the indispensability of energy storage systems. We embark on a thorough review of the merits and demerits inherent in both SCs and batteries. Subsequent to this analysis, we elucidate the fundamental principles underpinning the operation of SCs, providing a foundational understanding of their operational mechanism.

Our inquiry then extends to the different applications that harness the potential of SCs, accompanied by a categorization of their diverse types. Furthermore, we delve into a meticulous examination of the materials integral to SC composition, underscoring their pivotal role in optimizing overall device efficiency and performance.

As we conclude this chapter, our focus turns towards the convergence of printing technologies and the realm of manufacturing printed SCs. This review opens the gateway to further exploration in subsequent chapters, laying a robust groundwork for deeper comprehension.

2.1 ENERGY STORAGE SYSTEMS

The depletion of fossil fuels, combined with the detrimental impact of their CO2 emissions, climate change, and global warming, has driven extensive research into renewable energy sources such as solar, radio frequency, bio-energy, mechanical vibration, and wind [1]. However, due to the intermittent nature of these resources, energy storage systems are of paramount importance in the efficient utilization of harvested energy from renewable sources [2]. In addition to the advent of renewable energy generation technologies, the rising demand for portable power has also underscored the significance of efficient electrical energy storage [3].

Besides, from an environmental perspective, the imperative to reduce energy consumption is evident. Nevertheless, it is noteworthy that effective energy management practices can significantly mitigate associated drawbacks [4]. Energy management entails the decoupling of energy utilization from its immediate production, instead enabling its storage for subsequent utilization [5,6].

Energy storage systems act as energy buffers and serve the critical function of optimally storing the clean energy generated and supplying it to the system when there is a high demand for power or when the primary energy source is unavailable [7]. A notable example lies within the realm of the energy autonomous Internet of Things (IoTs), where seamless interconnectivity among a multitude of objects is achieved through ubiquitous, inexpensive, thin, and flexible wireless sensor networks (WSNs) [8]. WSNs are networks consisting of spatially distributed autonomous sensors to monitor physical or environmental conditions, such as temperature, sound, pressure, etc., and to cooperatively pass their data through the network to a main location. The reliable operation and functionality of these interconnected systems rely heavily on effective energy storage capabilities [9].

Furthermore, with the increasing adoption of integrating energy harvesting and storage devices to achieve self-powered flexible, stretchable, and wearable electronic devices and power systems [10-13], and the proliferation of interconnected self-charging smart devices for various applications like healthcare, security, and smart home automation systems, the research interest in energy storage

systems continues to grow [14-16]. This has led to a rising need for cost-effective and environmentally friendly energy storage solutions. The primary objective of these systems is to store energy obtained from diverse sources and provide instantaneous electrical power as per the system's requirements. Key criteria for designing energy storage systems include high specific power and energy density, fast charging capabilities, reliability, low power dissipation, safety, and long lifespan [17,18].

Supercapacitors (SCs), also known as electric double-layer capacitors (EDLCs), have received significant research attention as potential forms of environmentally friendly energy storage technologies [19,20]. Despite having larger capacity than regular capacitors, SCs have been analyzed and modeled in a similar manner. They have emerged as a key component in energy storage systems, and extensive studies have been conducted over the past decade to understand and optimize their performance [21]. Specifically, in recent years, there has been a focused effort to develop and explore the potential of the SCs in energy storage systems [22].

SCs offer several unique promising characteristics that make them suitable for energy harvesting and storage applications. They exhibit large specific power density, high efficiency, fast charge and discharge times, minimal heating losses due to the small equivalent series resistance (ESR), and long lifespan in terms of charge/discharge cycles and overall duration [23-25]. ESR represents the internal resistance of the SC. This includes the resistance of the electrolyte, electrodes, and any other internal components that contribute to the overall resistance. These attributes make them highly desirable for integration into energy storage systems and hybrid energy systems alongside batteries [12].

2.2 SUPERCAPACITOR VS. BATTERY

Batteries and SCs both serve as electrical energy storage systems. The key distinction lies in the methods they employ to store energy. SCs store energy in the form of an electric field [26]. They consist of two electrodes separated by an electrolyte. Applying a voltage across the electrodes results in the accumulation of positive and negative charges on the surfaces of the electric double layers, leading to the formation of electric fields that span between the electrodes. This electric field stores the energy, and it can be quickly discharged when needed [26]. To explain further, in SCs, ions are only required to diffuse solely through the electrolyte towards the electrode surface, without the need to penetrate the electrode itself. For this reason, SCs have the ability to charge and discharge at a faster rate, making them capable of serving as high-peak power energy storage devices. Moreover, owing to the absence of electrochemical reactions, SCs often exhibit significantly longer cycle lives compared to batteries.

On the other hand, batteries store energy in a chemical form. They typically contain one or more electrochemical cells, which consist of two electrodes (an anode and a cathode) separated by an electrolyte [27]. During charging, a chemical reaction takes place, converting the electrical energy into chemical potential energy. When the battery is discharged, the chemical reactions reverse, converting the stored chemical energy back into electrical energy [28].

It is also worth mentioning that SCs of EDLC type are energy storage devices that utilize the electric double-layer formed at the electrode-electrolyte interface for energy storage through electrostatic charge accumulation. On the other hand, pseudocapacitors, another type of SCs, involve redox Faradaic reactions at the electrode-electrolyte interface, in addition to the double-layer capacitance, to store energy. This unique characteristic gives pseudocapacitors higher energy densities and better performance, making them an attractive choice for various energy storage applications. In other words, while both EDLCs and pseudocapacitors are types of SCs, their energy storage mechanisms differ, with pseudocapacitors employing redox reactions in addition to the double-layer capacitance.

Hence, in summary, SCs of the EDLC type, store energy by creating an electric field, while batteries store energy through chemical reactions. In other words, in ideal circumstances, SCs of the EDLC type rely solely on electrostatic processes for charging and discharging, without involving reduction-oxidation (redox) Faradaic reactions between the electrodes and electrolyte [29]. Accordingly, these kind of SCs exhibit capacitive behavior at the interfaces between the electrodes and electrolytes, resulting in the absence of direct current conduction between the two components. The absence of Faradaic reactions occurring at the electrode-electrolyte interface leads to a reduction in the maximum energy density of these type of SCs [30]. As a consequence, SCs have a lower energy storage capacity per unit weight compared to batteries [31]. Conversely, the surface storage mechanism observed in SCs enables rapid charging and discharging processes, thereby enhancing their power performance capabilities. In contrast, the operation principle of batteries is founded on chemical reduction and oxidation processes between the ions and the bulk electrode materials [32]. Consequently, in batteries, both the charging and discharging rate can be constrained by the diffusion of charges within the electrodes and the occurrence of redox reactions. Likewise, within batteries, the occurrence of Faradaic reactions during charge and discharge processes induces swelling in the active materials [33]. This swelling phenomenon imposes limitations on the cycle life of batteries, typically restricting it to a few thousand cycles at most [34].

SCs offer a compelling alternative to batteries in various applications, thanks to their disposability, safety, and long lifespan. Compared to conventional capacitors, SCs possess larger capacitance values and higher energy density. Nevertheless, batteries still possess significantly higher energy density in comparison to SCs. SCs also exhibit other superior characteristics such as higher power density, lower internal resistance, increased charge/discharge efficiency allowing frequent charging and discharging at high current densities, shorter charging time, recyclability, operating effectively within a wide temperature range, and longer cycle life when compared to batteries [30,35]. These attributes make them highly suitable for a wide range of applications.

Rechargeable battery approaches like NiMH and Li-ion have been widely used as primary energy storage devices due to their high energy density and low self-discharge [36]. However, the aging process during charge-discharge cycles leads to an increase in internal resistance and a decrease in capacity over time, limiting the lifetime of many applications [37]. They are also limited by low charge/discharge rates, and safety concerns associated with the use of toxic or problematic materials, as well as relatively high cost of flexible Li-ion batteries [38]. Additionally, batteries may experience disruptions in their power delivery capabilities under high current loads due to their low power density. High current rates and transient load conditions also negatively impact the cycle life of rechargeable batteries, often necessitating their replacement after 1-2 years. These limitations can restrict the practical applications of rechargeable batteries [39]. In contrast, SCs can be used in high current rate and transient load conditions which offer significantly higher energy density than conventional capacitors and provide a promising alternative for energy storage systems technology, despite having relatively lower energy density compared to batteries. On the other hand, SCs also provide a promising alternative by allowing the harvesting of energy from ambient sources like wind, light, or temperature gradients.

Moreover, SCs can be manufactured using non-toxic materials, ensuring safety and stability while minimizing environmental impact [40]. Their flexibility, especially when fabricated through printing techniques, enables their integration into energy-autonomous flexible and wearable electronic systems, such as electronic skin [41,42]. As a result, SCs hold great promise as next-generation energy storage devices for future electronic systems.

As an illustration, energy storage devices are primarily characterized by their energy and power capabilities for a load, typically depicted through Ragone plot [43]. The Ragone plot serves as a tool for comparing the performance of various energy storage systems. In a Ragone plot (Fig. 1), the y-axis

represents specific energy (Wh/kg), while the x-axis represents specific power (W/kg). The diagonal lines in the graph represent time constants derived from the ratio of energy density to power density. This plot allows for the visualization and comparison of energy storage systems based on these two parameters.

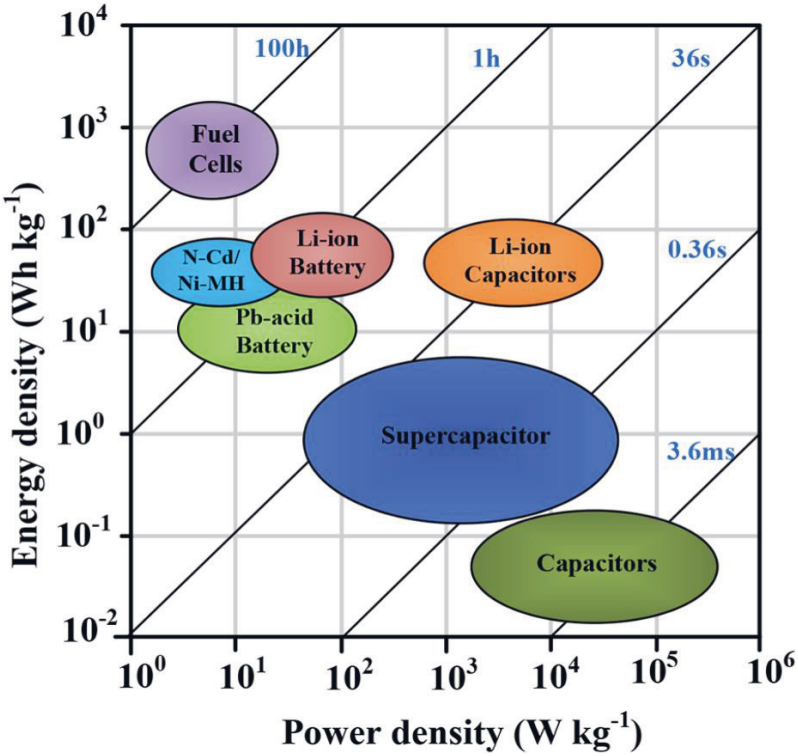

Fig. 1. Ragone plot for different energy storage systems. Reprinted from [22] with permission.

Table 1 presents a comprehensive comparison of the primary distinctions between SCs and batteries, while Table 2 provides a comparative analysis of the characteristic features exhibited by SCs, batteries, and capacitors.

Table 1. Comparison between batteries and supercapacitors [44].

Parameter	Battery	Supercapacitor
Storage mechanism	Chemical	Physical or surface redox reactions
Power limitation	Reaction kinetics, mass transport	Electrolyte conductivity
Energy storage	High (bulk)	Limited (surface area)
Charge rate	Kinetically limited	High, same as discharge
Cycle life limitations	Mechanical stability, chemical reversibility	Side reactions

Table 2. Comparison among selected electrochemical energy storage technologies [44].

Characteristics	Capacitor	Supercapacitor	Battery
Specific energy (W h kg-1)	< 0.1	1-10	10-100
Specific power (W kg-1)	⩾10,000	500- 10,000	< 1000
Charge time	10-6 to 10 -3	s to min	1-5 h
Discharge time	10-6 to 10 -3	s to min	0.3- 3h
Coulombic efficiency (%)	about 100	85-98	70-85
Cycle-life	almost infinite	> 500,000	about 1000

Fig. 2 illustrates the schematic representation highlighting the distinctions in energy and power density, as well as charge and discharge rates between batteries and SCs. In the canvas of energy storage, SCs resemble a small jug with a wide spout, symbolizing high power density - quickly delivering energy when needed (Fig. 2a). In contrast, batteries are akin to a large gallon with a narrow spout, representing high energy density - storing more energy for extended use, but a lower power density. On the other hand, the disparity between SCs and batteries is evident in their charge and discharge characteristics as shown in Fig. 2b. SCs showcase rapid energy transfer due to their inherent design, making them suitable for applications requiring quick bursts of power. While batteries demand more time for their chemical processes during charge and discharge cycles, and they provide a relatively constant voltage output throughout these phases. These visuals encapsulate the trade-off between SCs' swift energy exchange and batteries' steadier, longer-lasting energy delivery.

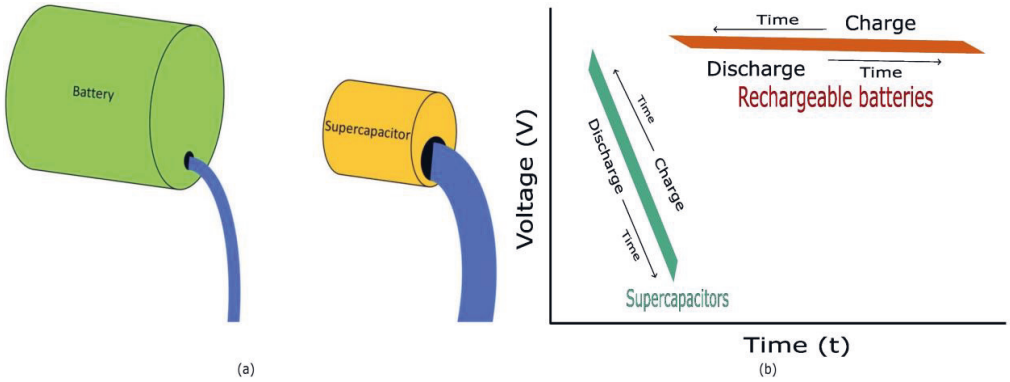

Fig. 2. Schematic representation of the distinctions in (a) energy and power density (reprinted from [45] with permission), and (b) charge and discharge rates between batteries and supercapacitors.

2.3 BASIC PRINCIPLES OF SUPERCAPACITORS

This section delves into the fundamental principles of EDLC SCs, as these specific SC types were manufactured, characterized, modelled, subjected to statistical analysis, and utilized in an application within this thesis. Section 2.5 will cover the explanation of the other SC types, Pseudocapacitors and hybrid capacitors. An EDLC type SC, comprises two electrodes featuring porous microstructures, that possess a significant surface area. These electrodes are separated by a liquid electrolyte and separator layer. Fig. 3 and 4 illustrate the fundamental operational mechanism of a SC. The energy storage mechanism of SCs primarily relies on the electrostatic separation of charge from the electrolytic ion sorption occurring on the electrode surface [46]. In fact, the accumulation of negative and positive ions at the interfaces, induced by Coulombic forces, is a result of the electronic charges present on the electrode surfaces. This process operates through a highly reversible mechanism. In other words, as shown in Fig. 4, upon application of an external voltage, the device undergoes a process in which an electric double layer is established and the storage of charges in SCs occurs within double layers at the interface between the active electrode and the electrolyte [47]. The double layer formed on each electrode essentially functions as a plate capacitor, wherein the distance between the charged layers is on the order of molecular dimensions [48]. As a result, SCs are capable of storing a significantly higher amount of energy compared to conventional capacitors.

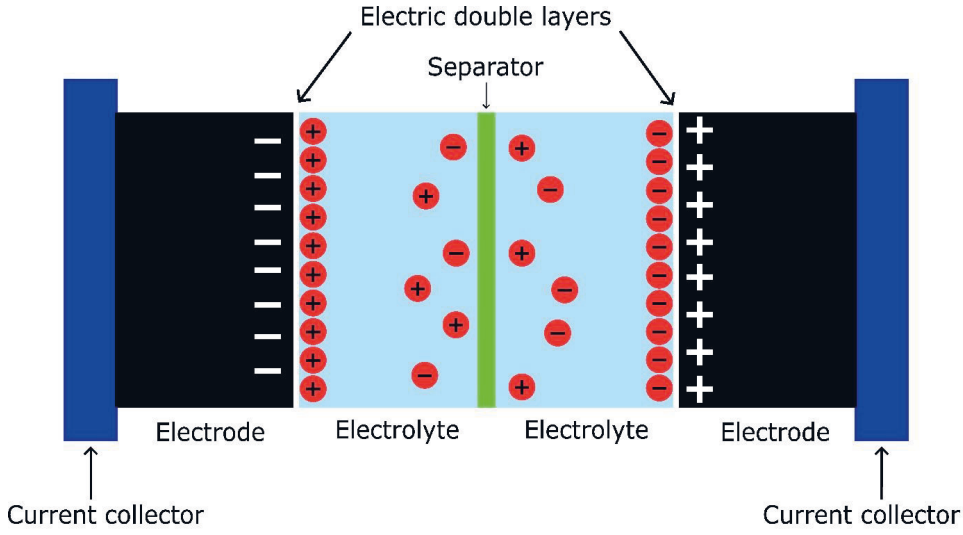

Fig. 3. Operational principle of a supercapacitor.

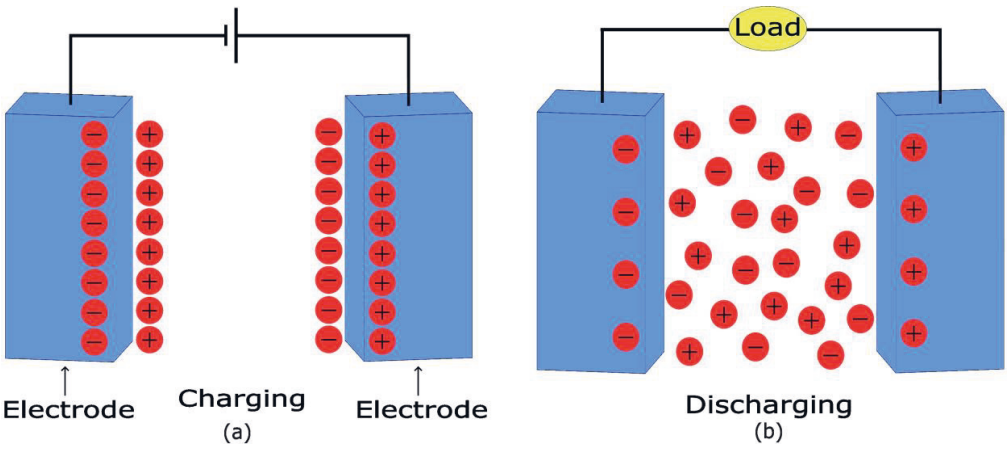

Fig. 4. Charge and discharge mechanism in a supercapacitor. a) charging, and b) discharging.

Fig. 3 and 4 clearly demonstrate the formation of two capacitors, each positioned between the electrolyte and the corresponding electrode. The capacitance of each capacitor can be computed using the following formula:

$$C = \varepsilon_0 \varepsilon_r A/d \quad (1)$$

In the provided equation, the relative dielectric constant (ε_r) represents the relative dielectric constant of the insulating material, while ε_0 denotes the dielectric constant of vacuum. The area (A) corresponds to the surface area of the conducting surfaces, including the rough electrode and the adjacent ionic layer, which can be conceptually regarded as two plates of a capacitor. The capacitance is enhanced by this substantial surface area provided by the porous electrode material. Lastly, the parameter d signifies the distance between the charge layers. In this particular scenario, the value of d represents the distance between charges in electrodes and electrolyte, which is significantly small, in the order of a few ångströms (0.3–0.8 nm) [49]. Accordingly, the capacitors exhibit a high capacitance, approximately in the range of 10-20 $\mu F/cm^2$ [50].

As already mentioned, within each SC, there exist two capacitors located at the surfaces of the electrodes. The two capacitors in a SC are connected in series, and the total capacitance (C) of the SC can be calculated by utilizing the capacitances of the individual capacitors, C_1 and C_2, through the following equation:

$$1/C=1/C_1+1/C_2 \rightarrow C= (C_1 \times C_2)/(C_1+C_2) \quad (2)$$

C_1 and C_2 represent the capacitance values of the double layer at each respective electrode. In theory, the values of C_1 and C_2 can be determined through calculations based on electric double-layer models. Due to the variation in double layer ions between the positive and negative electrodes, the double layers and consequently the capacitances of the electrodes are not identical, even in cases where the electrode structure is symmetric [51]. In other words, this disparity arises due to the ability of smaller ions to occupy positions in closer proximity to the electrode surface. Therefore, the capacitance values of C_1 and C_2 often differ, even in cases where the electrodes are identical and symmetric. This discrepancy in capacitance can reach up to a twofold difference.

Numerous theories have been proposed to serve as the foundation for the microscopic structure modeling of an electric double layer. Helmholtz's discovery in 1853 led to the proposal of the double-layer model in 1874, which describes capacitive characteristics at the interface between a solid conductor and a liquid ionic conductor. The model assumes uniform charge distribution at the

electrode-electrolyte interface, resembling a conventional capacitor [52,53]. However, the poor conductivity of the electrolyte prevents even charge distribution, resulting in an overestimated capacitance value. Nonetheless, the model effectively illustrates the energy storage principle of SCs in a simple and intuitive manner, making it a classic representation in the field.

Gouy proposed the model of side charge dispersion distribution in solution in 1910, and Chapman conducted a detailed mathematical analysis of this model in 1913. The model considers the spatial distribution of charge in the electrolyte, known as the diffusion layer [51-53]. However, the model overestimates the capacitance value because it assumes that ions are point charges and can approach the electrode-electrolyte interface infinitely close.

Stern presented an enhanced model building upon the Gouy and Chapman double-layer model that includes a compact layer and a diffusion layer in the double electric layer at the electrode-solution interface [51-53]. The model suggests that the electric double layer capacitance can be understood as a series combination of the capacitance of the compact layer and the capacitance of the diffusion layer.

Subsequently, Graham developed the metal-solution interface model, wherein he divided the compact layer into two distinct layers: the inner Helmholtz layer and the outer Helmholtz layer [51-53]. This can be attributed to the fact that the most prevalent cations are typically smaller in size compared to commonly encountered anions, thereby allowing them to retain their solvation shells. The three basic electrochemical models of a SC are shown in Fig. 5 schematically.

In spite of all that, it is worth noting that electrochemical models, while offering high accuracy, tend to exhibit low computational efficiency.

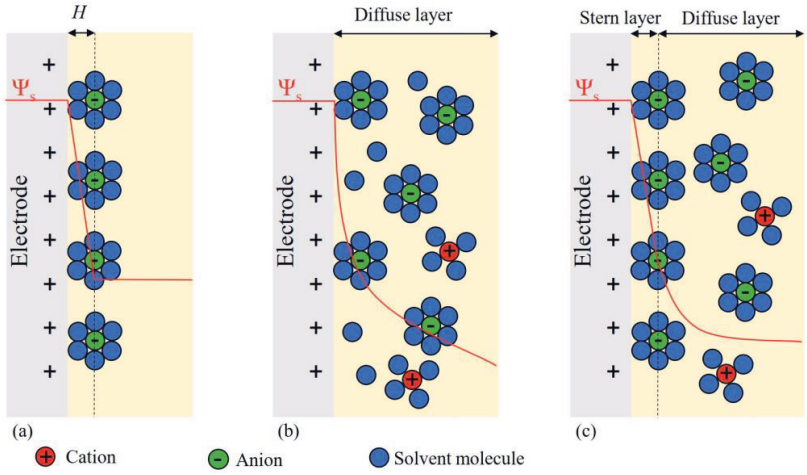

Fig. 5. Schematic of three basic electrochemical models of the supercapacitor: (a) Helmholtz model, (b) Gouy-Chapman model, (c) Stern model (combined model). Adapted from [53].

2.4 APPLICATIONS OF SUPERCAPACITORS

SCs exhibit significant benefits including a high magnitude of power density, an extensive operational temperature range, and a prolonged lifespan characterized by millions of cycles as opposed to thousands observed in batteries. Moreover, SCs are capable of handling rapid fluctuations in energy levels, rendering them highly suitable as auxiliary or primary energy storage devices for a wide range of

applications including uninterrupted power supplies, quick start mechanisms, peak pulse power systems, fast charging, and memory backup applications [54-57]. SCs can also enhance the quality of electric power by mitigating voltage fluctuations, thereby safeguarding electronic devices against potential damage [58]. Given that voltage disturbances typically have a relatively short duration, the limited energy capacity of a SC is not a significant concern.

Besides, in order to achieve a sustained operational lifetime in industrial applications like self-powered energy harvesting wireless sensor networks (WSNs), energy autonomous Internet of Things (IoT) devices, as well as flexible and wearable electronics, SCs have been proposed as the primary energy storage system [59-62]. A potential approach to enhance the eco-friendliness of powering connected objects in IoT systems is the replacement of primary and secondary batteries with energy harvesting techniques, such as utilizing light, electromagnetic radio frequency (RF), or kinetic energy and subsequently storing the harvested energy in thin, flexible, and non-toxic SCs [63,64]. SCs are also utilized as the primary energy storage devices in several other applications, such as switched-mode power supplies, system on a chip (SoC) design, and Bluetooth Low Energy (BLE) technology [65-67]. A SoC refers to an integrated circuit (IC) that incorporates most or all the components of a complete computer system or other electronic system onto a single chip. BLE, is a wireless communication technology designed for short-range communication between devices. It is a power-efficient version of the classic Bluetooth technology, optimized for applications where low power consumption and intermittent communication are crucial. The approach of powering these systems using SCs is motivated by the limitations of conventional power methods, which often involve challenges such as wiring to power outlets or the reliance on batteries that necessitate frequent recharging or replacement. Furthermore, typically microcontrollers utilized in embedded systems are engineered to minimize energy consumption, making SCs a promising choice as an energy storage solution for such applications [68].

Other research works have also explored the combination of SCs with rechargeable batteries to optimize energy storage capabilities. For instance, recently, there have been reports on the emerging trend of combining lithium-ion batteries with SCs in a hybrid configuration, serving as an advanced energy storage system [69,70]. This hybrid system demonstrates suitability for various applications, including toys, drones, and low-cost microelectronics devices [71]. It offers notable advantages such as higher power density, fast charging, and extended lifespan. However, it is important to note that this configuration also presents certain disadvantages, including power discontinuity and the need for power matching, as well as the challenges associated with synchronizing it with a feedback system [71].

The anticipated expansion of the worldwide SC market in the forthcoming years can be attributed to the increasing need for SCs across diverse applications [72]. Modern society is characterized by the widespread prevalence of portable and flexible electronics, including smartwatches, cameras, phones, and various other smart devices. SCs hold great potential as the main energy storage system to effectively power these smart devices, thereby playing a crucial role in their operation. There have also been reports of integrating flexible SCs with wearable textiles and sensors, enabling the power supply for electronic devices in the context of wearable technology [61,73,74]. Furthermore, the integration of SCs with energy harvesters, such as organic photovoltaic (OPV) modules or piezoelectric transducers, offers the capability to store harvested energy efficiently [75-78].

In addition, incorporating SCs in electric vehicles (EVs) to capture and store kinetic energy generated through regenerative braking could contribute to enhanced vehicle fuel efficiency [69,70,79]. In order to improve efficiency in EVs, the power level may become too high to directly charge batteries; hence, having the advantage of the combination of batteries and SCs could be a practical solution to address this issue [79]. Besides, in order to compensate for the fluctuations inherent in renewable energy sources like wind or solar power, an intermittent energy storage system is necessary to equalize the

energy levels and maintain a consistent power supply. Currently, approximately 20 to 30% of wind turbines are outfitted with a SC-based pitch control system [80].

Overall, SCs can be regarded as the optimal solution when there is a requirement for short-duration operation, outstanding cycle lifetime, reliable performance, and a wide temperature range.

Fig. 6 illustrates a schematic representation of the diverse applications of SCs across various fields.

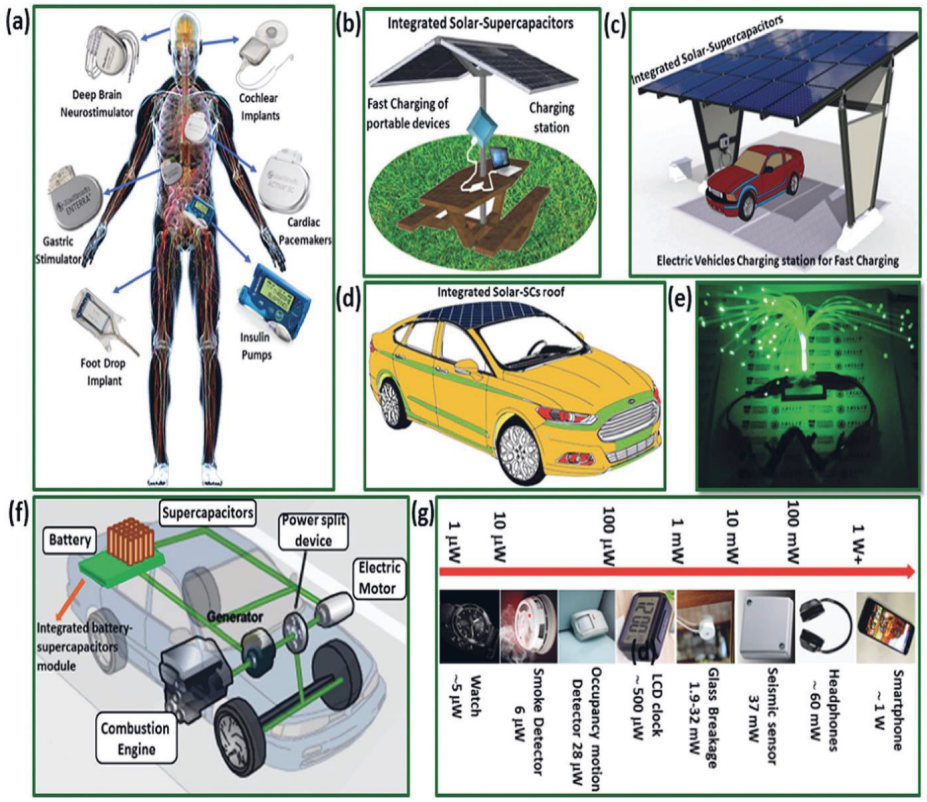

Fig. 6. An overview of several applications of supercapacitors across diverse domains. Reprinted from [81] with permission.

The broad range of available capacitance values for commercially accessible SCs, as some of them demonstrated in Table 3, reflects the necessity to cater to the diverse energy capacity demands in different applications.

Table 3. Commercial supercapacitors and their manufacturer-specified feature values [22].

Manufacturer	Voltage (V)	Capacitance (F)	ESR (mΩ)	Energy Density (W h kg-1)	Power Density (Kw kg-1)
Cellergy	2.7-5.5	0.5-470	-	-	-
Ioxus	2.3-128	100-5000	0.22-16.8	3.7-6.4	6.3-34
Maxwell Technologies	2.2, 2.7	10-3000	0.24-700	0.91-9.1	1.4-2.4
Murata Manufacturing	4.2-5.5	0.035-1	40-300	-	-
Nanoramic Laboratories	2.5	-	110-160	-	-
Nec Tokin	2.7, 3.8	350-2300	0.01-0.3	4.2	3.5-6.1
Nippon Chemi-Con	2.5-7.5	1-3000	0.4-13.2	4	4.9-6.5
Panasonic	2.3-2.7	2.5-100	0.01-0.3	5	0.0035-0.29
Paper Battery Company	2.7-16	0.1-5000	-	-	-
Skeleton Technologies	2.85, 3	300-3400	0.14-1.7	5.4-8.4	17.1-45
Yunasko	2.7	400-3000	0.08-0.25	4.2-6.2	7.1-41
ZapGo	2.7-3	-	-	5-10	-
LS Mtron	2.7-3	100-3000	0.23-9	5.9	0.9-2.4

2.5 TYPES OF SUPERCAPACITORS

In the early stages of SC technology development, there was some lack of clarity in terminology, and the distinctions between ultracapacitors, SCs, hybrid capacitors, and pseudocapacitors were not well-established. However, over time, as research and development in the field progressed, a more clear and consistent nomenclature emerged. Today, the distinctions between these energy storage devices are better defined:

- Ultracapacitors and SCs are often used interchangeably to describe high-capacitance, low-energy-density devices that store energy electrostatically, typically using double-layer capacitance (EDLC).

- Pseudocapacitors are a distinct type of SC that store energy through fast and reversible faradaic redox reactions at the electrode-electrolyte interface.

- Hybrid capacitors combine aspects of both SCs and batteries, offering a balance between energy density and power density, typically by combining EDLC and pseudocapacitive behavior.

This clarity in nomenclature is crucial for the understanding and development of energy storage technologies, and it reflects the progress made in the field to distinguish and define these devices more precisely. Fig. 7 depicts the graphical representation of diverse categorizations of SCs. The classification scheme is predicated on the utilization of distinct material compositions in the fabrication of SC

devices including activated carbon, graphene, or conducting polymers as positive and negative electrodes of an electrochemical cell. Additionally, the classification accounts for the structural configuration, which can either be symmetric or asymmetric. The term "symmetric" is used to describe a structural configuration wherein the positive and negative electrodes of a device exhibit similar characteristics and compositions.

2.5.1 ELECTRIC DOUBLE-LAYER CAPACITORS

EDLCs exhibit a symmetrical configuration and are commonly constructed using two carbon electrodes that are identical in nature. Activated carbon (AC) is the most commonly employed electrode material in EDLCs [82]. However, alternative materials such as carbon nanotubes and graphene have also been utilized in some instances [83,84]. These materials possess favorable characteristics such as ready availability, cost-effectiveness, a significant surface area, and a porous structure, enabling them to achieve a higher specific capacitance when compared to electrostatic capacitors [85]. Table 4 presents a comparative analysis of the energy density and power density of the EDLC SCs utilizing various carbon-based electrode materials.

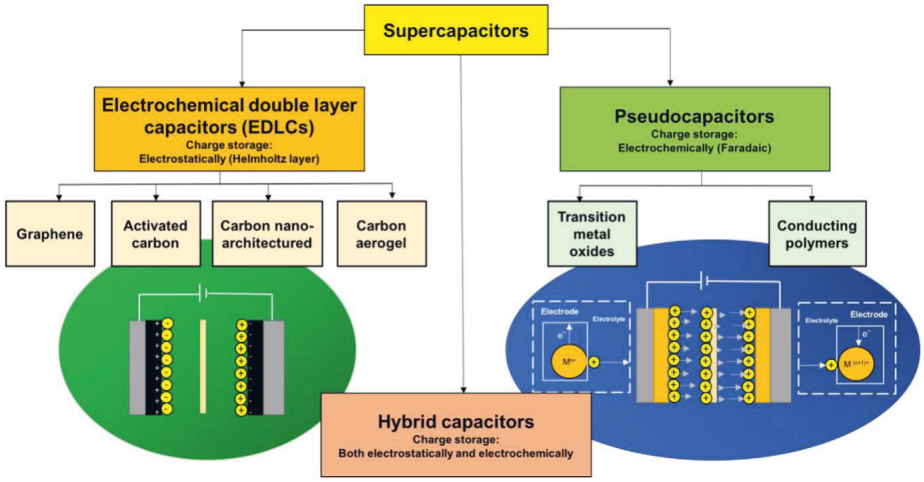

Fig. 7. Classification of supercapacitors. Adapted from [53].

Table 4. Characteristics of specific energy and power densities achieved utilizing diverse electrode materials [47].

Carbon material	Energy density (Wh.kg–1)	Power Density (kW.kg–1)	Electrode Capacitance (F.g–1)
Carbon fiber cloth	2–36	5 to 11	3.5 to 60
Activated carbon	5 to 25	10 to 40	50 to 125
Carbon nanofiber	10 to 20	5 to 20	50 to 100
Templated carbon	5 to 60	5 to 40	30 to 150
Carbon nanotube	0.5 to 40	30 to 1000	12 to 120
Graphene	20 to 70	40 to 250	100 to 200

2.5.2 PSEUDOCAPACITORS

Pseudocapacitors are comprised of an electrode constructed from conducting polymers like polyaniline or polypyrrole, or metal oxides such as lithium cobalt oxide (LiCoO2), ruthenium oxide (RuO2), nickel oxide (NiO), or manganese dioxide (MnO2) [86]. Pseudocapacitance arises from reversible fast reduction-oxidation (redox) reactions occurring in proximity to, or directly at the surface interface between a material and the electrolyte, enabling efficient charge storage [29]. Pseudocapacitors exhibit a greater energy density in comparison to EDLCs [87]. Conductive polymers, such as polyaniline or polypyrrole, can be utilized either on both electrodes or on a single electrode in conjunction with another electrode comprised of activated carbon [88]. Polyaniline demonstrates a charge density of approximately 140 mAhg-1, slightly lower than that achieved by metal oxides like LiCoO2 but significantly higher than carbon-based devices that typically offer around 15 mAhg-1 [89].

2.5.3 HYBRID CAPACITORS

Hybrid capacitors are commonly referred to as asymmetric SCs due to their distinctive characteristics. These SCs employ active electrode materials that combine the mechanisms of electric double-layer capacitance and pseudo capacitance, thereby integrating the benefits of both processes [90,91]. Hybrid capacitors exhibit a combination of non-Faradaic (electric double-layer) and Faradaic (battery-type) behavior [91]. A notable illustration is the lithium-ion capacitor, which incorporates a positive electrode composed of high surface area activated carbon and a negative electrode containing a lithium ion-containing material [92]. These capacitors possess the capability to store energy that is approximately 5-10 times higher than that of conventional EDLCs [93]. Additionally, they demonstrate a prolonged cycle life, indicating their ability to endure repeated charge and discharge cycles without significant performance degradation [94].

2.6 MATERIALS USED IN SUPERCAPACITORS

The utilization of materials in the fabrication of SCs is determined by the specific requirements and intended purposes of the device. The fundamental constituents of SCs encompass various components, including electrodes, electrolytes, separators, current collectors, and the substrate(s) onto which these materials are deposited (see Fig. 3). The preference lies in employing recyclable, non-toxic, abundant, and low-cost materials in the fabrication of SCs.

2.6.1 ELECTRODES

Electrodes are fabricated using materials that exhibit high conductivity. In the context of SCs, it is advantageous to utilize materials possessing a high surface area as electrodes. This is due to the fact that capacitance is directly proportional to the surface area, making materials with larger surface areas more conducive to achieving higher capacitance values [95]. Carbon electrodes such as carbon nanotube, carbon fiber, carbon aerogel, graphene and AC exhibit notable characteristics, including high porosity, surface areas reaching up to 3000 m^2g^{-1}, and capacitance values of around 588 Fg^{-1} [96]. Additionally, other materials such as carbon black, conducting polymers, and transition metals have also found application in this domain [88,97,98]. AC is a widely employed electrode material in SCs as it is an economically viable option that can be fabricated using relatively cost-effective raw materials, resulting in low manufacturing expenses [99]. Moreover, AC possesses the fundamental prerequisites as an electrode material, characterized by a notable specific surface area (SSA) ranging from 1000 to 2500 m2/g [100]. SSA refers to the surface area per unit mass of a material and represents the amount of material available for interactions with other substances, and it plays a significant role in processes such as adsorption, chemical reactions, and the electrical properties of materials. Besides, AC exhibits exceptional chemical and thermal compatibility and stability with the electrolyte utilized within the system, along with commendable electrical conductivity [99].

From a microstructural perspective, AC materials can be regarded as assemblies comprised of graphene layers exhibiting structural defects [101]. The raw materials employed for AC production can include various sources such as wood, coal, coconut shells, oil, or polymers [102]. The predominant choice of raw material for manufacturing AC grades intended for SC applications is primarily focused on coconut shells [103]. The synthesis AC involves a sequential process wherein the raw materials undergo carbonization, which entails heat treatment under an inert atmosphere [104]. Subsequently, the carbonized materials are activated through methods such as steam or carbon dioxide treatment at elevated temperatures, leading to the development of a porous structure [103,104]. In order to ensure desirable electrical properties and prolonged lifespan in SCs, it is imperative for the AC to exhibit a high degree of purity [105]. This entails maintaining an ash content below 1% and limiting the concentration of halogens and iron to below 100 parts per million (ppm) [106,107]. The activation process enhances the SSA and pore volume of the AC, leading to the formation of micropores (with diameters less than 2 nm), mesopores (with diameters ranging from 2 to 50 nm), and macropores (with diameters exceeding 50 nm) [108].

In addition to possessing a high surface area, the pore diameter of electrodes plays a crucial role in attaining high capacitance levels in SCs [109]. Although the behavior of ions in micropores is not fully comprehended, it is generally observed that if the pores are too small, ions cannot penetrate them [110]. Consequently, the surface area inside the micropores may not contribute to an increase in capacitance. Previous studies have indicated that in order to effectively utilize all available pores, the pore size in electrodes should be approximately twice the size of the ions involved [26]. As a result, the ions are able to move unhindered into and out of the pores, facilitating efficient charge storage and leading to high-capacity retention. For this reason, the size and distribution of pores in electrodes play a crucial role in enabling high capacitance values to be achieved in SCs. Pyun et al. conducted a study where they reported that the performance of EDLCs is influenced by the distribution of pore sizes [111]. They found that electrodes with smaller pore sizes exhibit a higher time constant due to slower ion penetration into the pores, in contrast to electrodes with larger pore sizes.

In general, a larger pore size promotes enhanced ion flow between the electrode and electrolyte. Conversely, a smaller pore size increases the SSA. Ideally, the pore size should be sufficiently large to facilitate effective ion diffusion while also providing a substantial surface area.

2.6.2 ELECTROLYTE

The energy storage capacity in SCs is governed by two primary factors: the electrochemical window of the electrolyte, dictating the uppermost voltage limit, and the capacitance, predominantly reliant on the electrode properties. The energy storage capacity demonstrates a direct proportionality to the square of the applied voltage [112]. Consequently, the choice of electrolyte significantly influences the energy density of SCs. In a word, the selection of electrolyte plays a significant role in determining the properties of SCs, including capacitance, temperature range, and voltage range [113].

The electrolyte is composed of solvents and ions, with aqueous and organic electrolytes being the most prevalent types. In general, the selection of an electrolyte type relies on the intended application. Aqueous electrolytes are cost-effective and simpler to fabricate compared to organic electrolytes, which necessitate an inert atmosphere during the fabrication process. Aqueous electrolyte solutions encompass potent acidic and basic substances, including sulfuric acid (H2SO4), potassium hydroxide (KOH), as well as neutral salts such as sodium chloride (NaCl) and potassium chloride (KCl) [114-118]. On the other hand, propylene carbonate and acetonitrile are frequently employed as predominant organic electrolyte solvents [119,120], whereas tetraethylammonium tetrafluoroborate is the prevailing salt compound commonly utilized [121].

The conductivity of the electrolyte has a direct impact on the ESR of the SC [122]. A rise in ionic conductivity leads to a reduction in the ESR of the device. Aqueous electrolytes in SCs often exhibit relatively high conductivity [123], which enhances the current output capability of the device. The ionic conductivity of aqueous electrolytes can vary depending on their concentration. For instance, electrolytes such as H2SO4 (sulfuric acid) and KOH (potassium hydroxide) can achieve ionic conductivities exceeding 500 mS cm-1 [124]. In the case of NaCl (sodium chloride)-based solutions, the ionic conductivity typically falls around 100 mS cm-1 [117]. These high conductivities enable efficient ion mobility within the electrolyte, facilitating enhanced performance in SCs. On the other hand, organic electrolytes typically exhibit ionic conductivity ranging from 10 to 60 mS cm-1 [125].

Furthermore, the voltage window of the SC, which constrains the cell voltage and the energy storage capacity of the device, is determined by the properties of the electrolyte [126]. Aqueous electrolytes exhibit a working voltage window ranging up to around 2 V [127], while organic electrolytes offer a broader range, typically spanning from 2.5 V to 4 V [128]. Due to their higher maximum voltage

capability, organic electrolyte SCs are often favored by manufacturers. Despite organic electrolytes being predominantly used by commercial SC manufacturers, there is a higher prevalence of publications in research and development focusing on aqueous electrolytes. The prevalence of aqueous electrolytes in SC research and development can be attributed to several reasons. Firstly, aqueous electrolytes are advantageous due to their low cost, non-toxicity, and non-flammability compared to organic solvents. Secondly, the use of organic solvents and ionic liquids requires special handling conditions to prevent moisture-induced performance degradation and increased self-discharge. Hence, the utilization of water-based electrolytes in SCs leads to lower manufacturing costs [129].

The accessibility of electrolyte ions to electrode pores is enhanced by reducing the ion size, which is evident. However, the larger organic ions are unable to penetrate small pores as effectively as ions present in aqueous electrolytes, leading to a decrease in specific capacitance when organic electrolytes are utilized [130]. Regarding the advantages of organic electrolytes, in addition to their higher voltage compared to aqueous electrolytes, they enable the use of metallic materials like aluminum for current collectors and encapsulation in SCs [44]. Additionally, PC electrolyte exhibits some other advantageous attributes including convenient availability, thermal stability, safety, and cost-effectiveness [131]. PC is known to possess a reported melting point of -48 °C [132]. However, the preparation of organic electrolyte necessitates a controlled environment within an inert atmosphere, such as a glove box, to ensure the removal of moisture [75]. The presence of moisture can result in undesirable side reactions when the electrochemical window of water is surpassed. On the contrary, aqueous electrolyte offers several advantages such as enhanced ionic conductivity, environmental friendliness, non-flammability, and affordability. However, its utilization is constrained to a voltage range below 2 V.

Furthermore, there are advantages to transforming the electrolyte into a gel form. The solid-like structure of gel electrolytes reduces the risk of electrolyte leakage [133], while the presence of a liquid phase within the solid scaffold allows for reasonably high ionic conductivity to be maintained. When a gel electrolyte is utilized, the need for a separate separator in a SC is eliminated since the gel electrolyte serves the dual function of both an electrolyte and a separator. Examples of commonly used gel electrolytes include mixtures of polyvinyl alcohol with potassium hydroxide or sulfuric acid, as well as gelatin-based hydrogels [134-136].

2.6.3 SEPARATOR

In order to safeguard against short circuits, a separator is introduced between the two electrodes in the device. Its purpose is to provide a physical barrier and prevent direct contact between the electrodes [137]. The separator used in the device should possess a porous structure that enables the passage of ions [138]. This characteristic is essential to facilitate ion transport while maintaining the required physical separation between the electrodes. The ideal separator for the device should exhibit several key characteristics. Firstly, it should possess flexibility and lightness, allowing for easy handling and integration within the system. In addition, when impregnated with the electrolyte, the separator should be wettable and display high ionic conductivity, facilitating efficient ion transport between the electrodes. Furthermore, chemical, electrochemical, thermal, and mechanical stability is crucial to ensure the separator's integrity and performance under various operating conditions. Several types of separators are available for use in SCs. The commonly reported separators utilized in various applications include paper separators composed of cellulose fibers with a thickness of 15-50 μm, as well as polymer separators such as polypropylene (PP), polyethylene (PE), polyethylene terephthalate (PET), polytetrafluoroethylene (PTFE), and polyimide (PI) [139]. These separators offer a range of properties and characteristics that make them suitable for different SC applications.

2.6.4 CURRENT COLLECTOR

The primary role of the current collector is to gather electrons from the electrode material and facilitate their transfer to the external circuit. In other words, current collector serves as the electrical connection between the electrode and the external junction of the SC [140]. In order to maximize the utilization of the high power provided by a SC cell, it is crucial to optimize all the components that contribute to the ESR. This includes minimizing the resistance of current collectors and the contact resistance between the electrodes and current collectors. Keeping these resistances as low as possible is essential for efficient power delivery and enables a higher energy density and a faster charge-discharge time constant. Additionally, it should be acknowledged that the energy density of SCs may not be significantly affected by the ESR when a low current is flowing.

Typically, current collectors in SCs are composed of metals, including aluminum, nickel, copper, and stainless steel [141]. In SCs, two current collectors are employed, with one positioned at the anode terminal and the other at the cathode terminal. The stability and conductivity of a SC are influenced by the characteristics of the current collector [140].

In addition to possessing satisfactory electrical conductivity, critical properties of current collectors include their electrochemical and chemical stability in relation to the electrolyte, cost factors such as purity and availability, density, and processability [142]. Consideration of the electrolyte is essential as the requirements for current collectors differ between aqueous and organic electrolytes, primarily due to electrochemical stability challenges specific to each electrolyte type.

2.7 PRINTED SUPERCAPACITORS

The field of printed electronics (PE) is recognized as an emerging domain that has been garnering increasing research interest. In contrast to traditional electronics, PE technology exhibits exceptional efficacy in the fabrication of stacks comprising microscale and nanoscale devices [143]. In addition to its simplicity, time and material efficiency, cost-effectiveness, versatility, eco-friendliness, and scalability for high-volume production, PE encompasses a diverse array of manufacturing technologies suited for various SC architectures, such as micro, asymmetric, and flexible designs [63]. This is achieved through the utilization of a broad selection of flexible substrates, enabling the realization of the full potential of SCs.

Solution-based processes, including different coating and printing methods, can be readily scaled up to facilitate the production of a significant quantity of devices or the coating of large-area substrates [144]. This capability enables cost-effective manufacturing of electronic components and devices. Printing methods distinguish themselves from coating techniques by their capacity to generate irregularly shaped images in two dimensions [143].

There are two types of PE technologies, contact and non-contact, as shown in Fig. 8.

- In contact printing, the printing plate comes into direct contact with the substrate (screen printing, gravure, pad, flexographic printing, offset lithography, and soft lithography).
- In non-contact techniques, the deposition material is only in contact with the substrate (inkjet printing, aerosol-jet, organic vapor-jet printing, and laser direct writing).

Each of these methods possesses distinct properties, such as line width, line thickness, and speed, which contribute to their unique characteristics. The selection of a suitable printing method for SCs primarily hinges upon the desired thickness of the film. Unlike many other printed electronic devices, SCs typically necessitate relatively thick films of the active material, typically ranging in the order of tens of micrometers. This unique requirement should be considered when determining the appropriate printing technique for fabricating SC devices. In commercial SCs, the typical thickness of the activated carbon electrodes is on the order of 100 μm [145]. Among the printing methods mentioned above, screen printing is a viable technique for creating layers with thicknesses ranging from 10 to 100 μm [146]. Conversely, the other methods are commonly employed for producing thinner layers. Screen printing is a highly suitable method for the fabrication of thick, patterned SC electrodes [147]. It has garnered significant attention and utilization in numerous research studies owing to its effectiveness in achieving the desired thickness and patterning requirements essential for optimal supercapacitor performance [148-150].

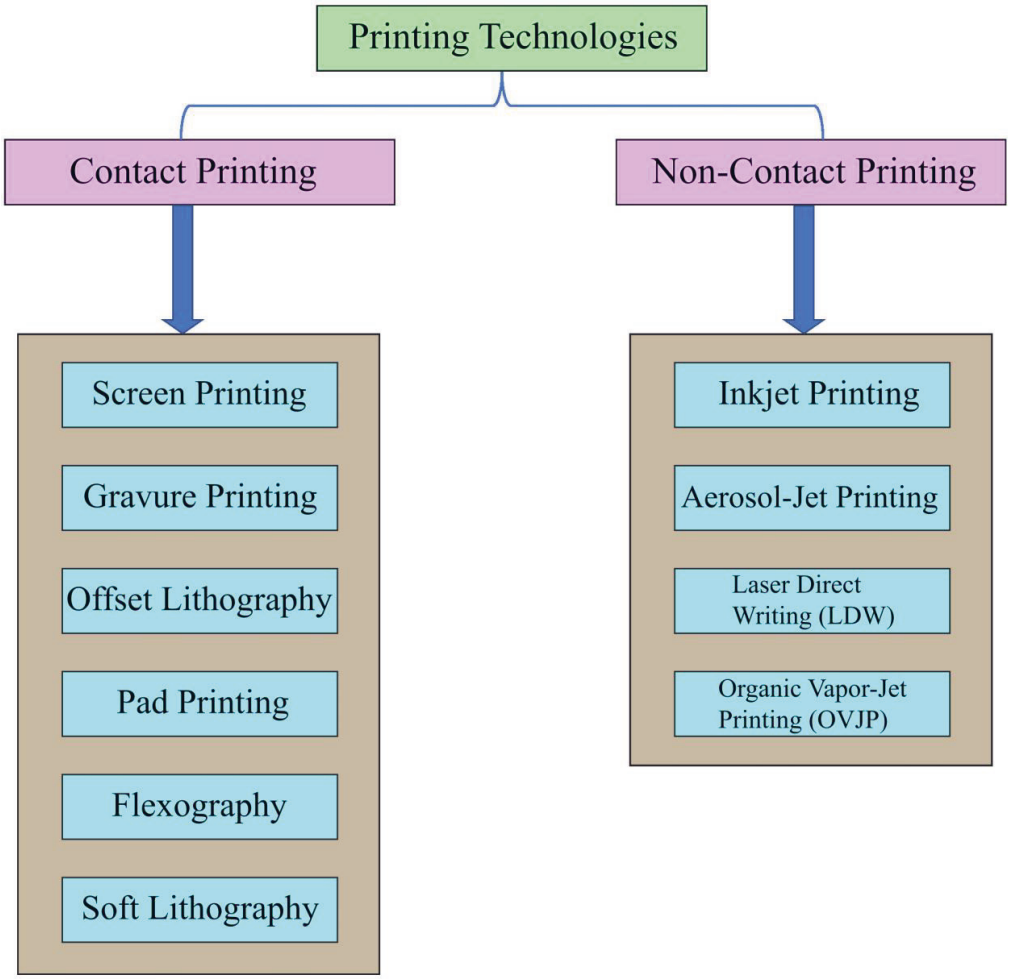

Fig. 8. Classification of printing technologies.

In contrast, the resolution of the print image is not considered a critical factor in SC fabrication. Unlike applications where high image resolution is essential, such as in display technologies, the print image

resolution is of lesser significance in the context SCs. The focus primarily lies on achieving the desired film thickness and ensuring proper electrode and electrolyte integration, rather than attaining fine detail in the printed image.

The majority of studies focusing on printed SCs typically depict devices where the electrodes are printed onto distinct substrates and subsequently assembled by sandwiching them together with a separator paper, resulting in the formation of the complete device. Additionally, there have been notable demonstrations of utilizing gel electrolytes in printed SCs, eliminating the need for a separate separator layer [151]. This advancement enables a more simplified design and assembly process for such devices. Moreover, there have been reported instances of successfully printing all the layers of a SC on a single substrate, known as monolithic printing [152,153]. However, there are a few significant challenges in monolithic printing such as high ESR and leakage current as well as challenges with the design of the separator layer [154]. The separator must exhibit impermeability to the ink used for printing the top electrode, while simultaneously enabling efficient movement of the electrolyte through it. Achieving this delicate balance is crucial for ensuring optimal performance of the printed SC.

The devices described in this thesis were fabricated using the doctor blade method. A concise introduction to screen printing is also included here to highlight its significance in the context of scale-up processes.

2.7.1 DOCTOR BLADING

The blade coating method, also referred to as doctor blade or knife coating, is a technique employed for the application of solution layers with a thickness on the order of 100 μm [155]. Doctor blade coating is a precise technique employed to create relatively uniform films with precisely controlled thicknesses on flexible or rigid substrate [156]. The technique operates by positioning a sharp blade at a predetermined distance from the surface to be coated. Subsequently, the coating solution is positioned in front of the blade, and the blade is moved along the surface in line with it, resulting in the formation of a wet film as shown in Fig. 9. The resulting thickness of the film is dictated by the spacing between the blade and substrate, the velocity at which the coating is applied, and the viscoelastic characteristics of the solution [157]. Patterning can be achieved by utilizing stencils as a means to apply ink or paste onto the desired surface [158]. Ideally, the technique should exhibit solution losses of approximately 5% [156]. However, in practice, it often requires a certain amount of time to establish optimal conditions for achieving this ideal level of solution loss. The inks or pastes utilized in these processes typically demand significant quantities of binders and thickeners to attain the high viscosities (1000–10,000 mPa s) necessary for consistent and dependable production of films [156]. Viscosities can be augmented by incorporating polymeric additives such as glycerol, ethylene glycol, or ethyl cellulose into the system [159].

The use of a hot plate during the doctor blade coating technique is common, and it serves a specific purpose. The hot plate is employed to control the drying and curing process of the coated film [160]. The application of heat facilitates solvent evaporation, accelerates film formation, and enhances the bonding and adhesion properties of the deposited material. Additionally, the hot plate helps in achieving uniformity and consistency in the coated film by controlling the drying rate and minimizing defects.

Blade coaters are characterized by their affordability and user-friendly operation. Furthermore, there are laboratory-scale single sheet coaters accessible for experimental purposes. Hence, the primary advantage of doctor blade coating resides in its inherent simplicity, as it allows for the manual

preparation of electrodes, enabling expedited testing procedures. Nevertheless, since the coaters operate in an open system configuration, solvents are prone to evaporate readily, potentially leading to alterations in the rheological properties of the ink. The fluid dynamics occurring in the vicinity of the blade near the substrate during the blade coating process exhibit a highly intricate nature. Attaining a uniform film can be challenging due to the propensity for uneven substrate thickness, which can lead to the formation of an uneven film.

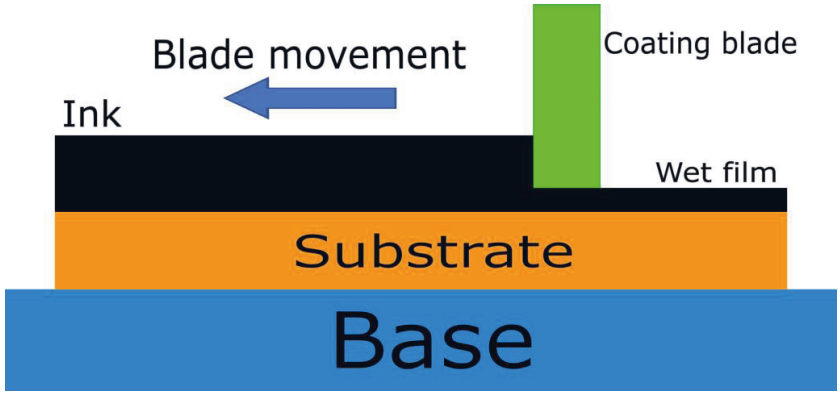

Fig. 9. Illustration depicting the doctor blade coating process in a schematic manner.

2.7.2 SCREEN PRINTING

The screen-printing (SP) technique has a rich history dating back approximately 2000 years, with its utilization spanning across Asia, Europe, and Africa [146]. Its primary purpose has been to generate consistent patterns, symbols, and labels on various textile materials. SP has emerged as a favorable option for the production of thick, patterned electrodes and has been widely employed in numerous research investigations [161]. SP is a well-established printing technique that can be carried out in either a planar or roll-to-roll (R2R) format [162]. A SP mesh possessing a designated configuration is used for the planar system, which is directly in contact with the substrate; Initially, the ink is administered onto the screen, which is positioned at a minor elevation above the substrate, as shown schematically in Fig. 10. A rubber squeegee is employed to exert pressure and facilitate the passage of ink through the mesh onto the substrate. Through the standard pattern in the mesh, the ink passes down onto the substrate and defines the final image. In other words, the screen used in SP is subjected to a patterning process where certain meshes are blocked. When the mesh is flexed, the ink adheres to the substrate and is subsequently transferred onto it. A variety of substrates can be used, including epidermis, paper, glass, metal, ceramic, wood, textiles, and polymers [164-168].

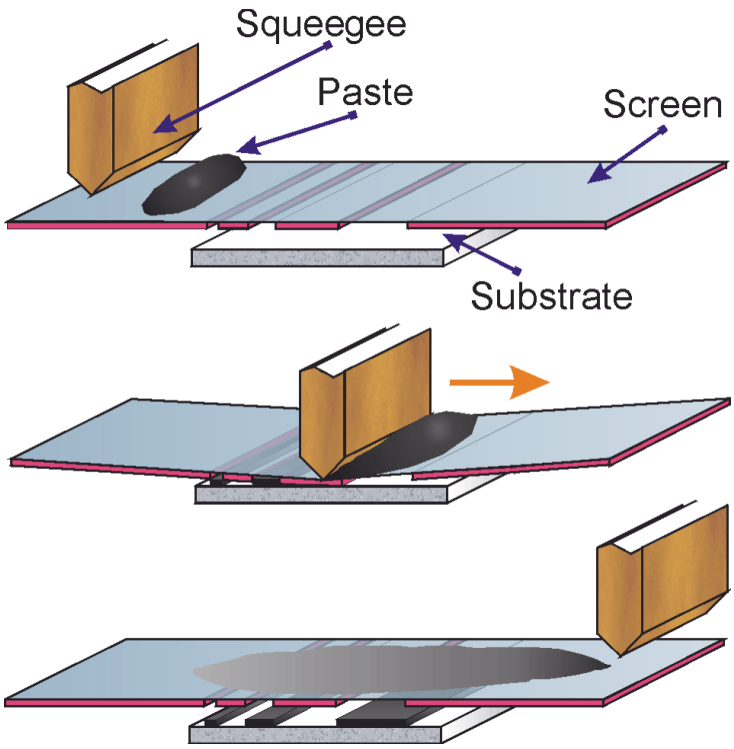

Fig. 10. The fundamental methodology of the screen-printing technique. Adapted from [163].

Subsequently, the next stage involves the removal of the mesh, a process referred to as relaxation. Following the printing process, the desired pattern becomes visible. Subsequently, in preparation for the subsequent manufacturing step, the fluid inks undergo a transition from the liquid to the solid state through a drying process, which involves the removal of solvents. The drying phase can be accomplished through various methods depending on the nature of the ink and the intended film application. Options include ambient air drying at room temperature, thermal drying utilizing equipment such as ovens, hotplates, infrared devices, or hot air blowers, or employing UV radiation as a drying mechanism. It is important to acknowledge that the drying process represents the final stage in blade coating as well. In many cases, it is also necessary to remove surface-bound stabilizing agents from the particles' surfaces. During the drying process, structural transformations of the ink can occur, such as polymerization and crosslinking. This alteration highlights the potential need for supplementary treatments to enhance particle bonding and optimize the performance of the printed film [169], particularly in the context of SCs. Enhanced particle-to-particle contact can be achieved by subjecting them to high-temperature sintering, facilitating diffusion within the particles and promoting the formation of interconnecting necks between them [170].

In the R2R process, the static flat screen is substituted with a rotating screen. In other words,, the R2R process replaces the squeegee with a roller and places the blade and ink within the roller and the ink is forced through the mesh by the blade [171]. Unlike the planar system, the R2R processing is continuous, allowing fast production, although rotary setups are expensive and difficult to maintain.

In PE, SP is a widely used technology. However, a large amount of production material (including the ink) is wasted as a result of carrying this technique out. Besides, the level of resolution is the most significant limitation. Furthermore, the planar printing process is slower than other conventional printing methods.

3- EXPERIMENTS AND METHODS

This chapter provides a concise overview of the materials employed in the fabrication of SCs, the manufacturing techniques utilized, and the characterization methods employed for assessing their performance. The selection of materials for SCs was primarily driven by the specific requirements established for the devices. Emphasis was placed on utilizing materials that possess non-toxic properties, are recyclable, and can be effectively incinerated. Furthermore, to enable widespread application and affordability, inexpensive materials were favored for incorporation in the SC design.

3.1 DEVICE FABRICATION

The manufacturing procedure for this particular class of printed aqueous SCs has been documented in prior publications by the research group [172-178] and is also outlined concisely herein. The schematic representation in Fig. 11 illustrates the fabrication process for the SCs used within this thesis. The initial substrate used was a double-sided Al/PET flexible substrate (Pyroll) with an aluminum (Al) thickness of 9 μm and a PET thickness of 50 μm (Figure 11a). Prior to fabrication, the Al/PET substrate underwent pre-heating at 95°C for 15 minutes (Figure 11b). The PET side of the substrate was coated with a graphite ink (Acheson Electrodag PF-407C) to create a current collector layer, while the Al layer acted as a barrier (Figure 11c). The graphite ink was dried in an oven at 95°C for 1 hour, resulting in a graphite thickness of 40-50 μm (Figure 11d). Subsequently, an electrode layer composed of activated carbon with chitosan as a binder was applied onto the current collector layer (Figure 11e). The activated carbon ink was dried at room temperature overnight, forming a film with a thickness of 50-70 μm (Figure 11f). These layers were deposited using a laboratory scale doctor blade coater. Next, a heat-sealing dispersion adhesive material (Paramelt Aquaseal X2277 polyolefin) was applied to the PET and a portion of the current collector layer (Figure 11g). The samples were placed in an oven at 80°C for 15 minutes (Figure 11h). An aqueous electrolyte with a 1:5 mass ratio of NaCl to H2O was then added onto the electrode layer (Figure 11i). A paper separator impregnated with the aqueous electrolyte was placed onto the electrode layer (Figure 11j). The second half of the SC, shown in Figure 11k, had the same electrode pattern as Figure 11j but without the paper separator, with the electrode facing downwards. In the final step, the two electrodes were packed and heat-sealed face to face using annealed Aquaseal, as depicted in Fig. 11l (upside down). The resulting SC, including the packaging, has dimensions of 50 mm in length, 50 mm in width, and a thickness ranging from 0.4 to 0.5 mm.

In a comprehensive assessment, the primary technical prerequisites for current collectors entail possessing low electrical resistance and exhibiting resistance to electrolytic corrosion [140]. In conjunction with current collectors, substrates collectively constitute the packaging of the component. Moreover, the packaging should effectively inhibit the evaporation of the electrolyte solution while providing the necessary mechanical robustness or strength. Furthermore, enhanced encapsulation and robust sealing of a device have the potential to mitigate or minimize the leakage current. By implementing improved encapsulation techniques and ensuring a secure and reliable sealing mechanism, the ingress of external factors, such as moisture or contaminants, can be restricted [178,179]. This, in turn, reduces the likelihood of undesired current paths and leakage within the device.

In brief, effective encapsulation and sealing practices contribute to the overall stability and longevity of the device by safeguarding against external influences and optimizing its electrical performance.

In **Publication I**, we have provided a comprehensive overview of the fabrication steps and characterization techniques employed for the development of our disposable and flexible printed SCs. Our focus was on utilizing low-cost and non-toxic processes and materials.

3.2 DEVICE CHARACTERIZATION

Cyclic voltammetry (CV) and galvanostatic charge-discharge (GCD) measurement are widely employed methods for the characterization of the SCs [180]. These techniques provide valuable information about the electrochemical performance and behavior of the device under different operating conditions. During CV, the electrode potential is systematically varied in a linear manner with respect to time, starting from the initial value and reaching a maximum potential. Subsequently, the potential is swept back in the opposite direction to the original value, forming a cyclic pattern. The resulting current is measured at each point during the potential sweep, providing valuable information about the electrochemical processes occurring at the electrode-electrolyte interface. In fact, the value of the current is extracted from the discharge curve, which represents the current profile during the discharge process of the SC. By analyzing the shape and magnitude of the current over time, valuable insights can be gained about the performance and behavior of the SC, including its discharge rate, energy storage capacity, and efficiency.

The area enclosed by CV curve is utilized to determine the capacitance of the SC. On the other hand, In the CV experiment, the total charge transferred during the cyclic sweep can be obtained by integrating the current with respect to time (duration of the experiment). Moreover, dividing the current by the scan rate allows for the calculation of the capacitance value. In ideal SCs, CV curve exhibits a rectangular shape, indicating fast and reversible charge storage. However, in practical devices, the CV curve deviates from the ideal rectangular shape due to the presence of ESR and leakage current, leads to inflections or deviations in the CV curve. These inflections can affect the performance and efficiency of the SC by introducing additional losses and limiting the maximum achievable capacitance.

Furthermore, in addition to the previously mentioned approach, an alternative method for determining the capacitance value involves dividing the total charge of the device by the applied voltage. The total charge of the device can be measured by integrating the current with respect to time, providing a comprehensive assessment of the charge accumulation over the entire duration of the measurement.

On the other hand, GCD is a well-established method utilized for the determination of both capacitance and ESR of the SCs. This technique involves applying a constant current during the charging and discharging processes of the SC and monitoring the resulting voltage profile. By analyzing the charge-discharge characteristics and the voltage drop, valuable information regarding the capacitance and ESR of the SC can be obtained. GCD is widely employed due to its effectiveness in quantifying the energy storage capacity and internal resistance of SC devices.

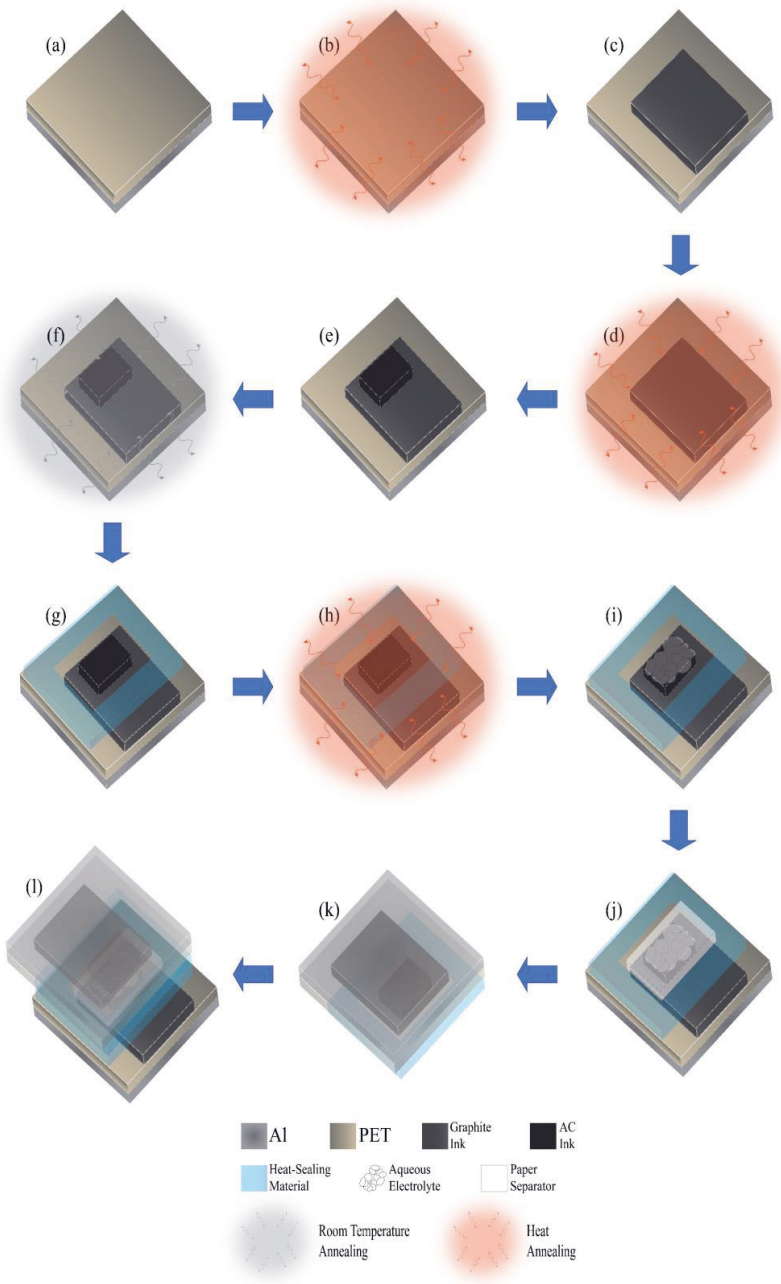

Fig. 11. Overview of the fabrication process. The process includes: a) Starting with a double-sided Al/PET substrate (9 µm Al, 50 µm PET). b) Pre-heating the substrate at 95°C for 15 minutes. c) Applying graphite ink to form the current collector layer. d) Drying the graphite ink in an oven at 95°C for 1 hour. e) Developing the electrode layer using activated carbon ink with chitosan binder. f) Allowing the activated carbon ink to dry overnight at room temperature. g) Applying a heat-sealing adhesive layer to the PET and part of the current collector layer. h) Annealing the heat-sealing layer in an oven at 80°C for 15 minutes. i) Introducing the NaCl: H2O aqueous electrolyte with a mass ratio of 1:5. j) Adding a paper separator. k) Placing a second cell upside-down without the separator. l) Heat-sealing and packaging the two cells together face to face upside-down using the annealed heat-sealing adhesive layer." Adapted from **publication I**.

The fundamental electrical characteristics of printed SCs used in this thesis, including capacitance, ESR, and leakage current, were evaluated according to the guidelines outlined in the international industrial standard IEC 62391-1 [181]. In order to perform electrical characterization of the SCs, a Maccor 4300 workstation (Maccor Inc., USA) was employed. The Maccor 4300 workstation is a specialized instrument designed for such characterization purposes. The SCs underwent a charging and discharging cycle, repeated three times, within the voltage range of 0 to 1.2 V. The charging and discharging processes were conducted using a constant current of 1 mA, 3 mA, and 10 mA. Subsequently, the SCs were maintained at a constant voltage of 1.2 V for a duration of 30 minutes. The capacitance of the SCs was determined by measuring the discharge current while maintaining a constant current discharge process between the voltage limits of 0.96 V and 0.48 V.

Following that, the SCs were subjected to a constant voltage of 1.2 V for a duration of 1 hour, during which the leakage current was measured and recorded. Subsequently, the current required to maintain the voltage level during the float state is recorded as the leakage current. This procedure was repeated for each of the three specified currents of 1 mA, 3 mA, and 10 mA. This leakage current represents the small amount of current that flows through the SC when it is not actively being charged or discharged, indicating the inherent electrical losses in the device. By measuring and monitoring the leakage current, valuable insights into the self-discharge behavior and overall electrical performance of the SC can be gained. The presence of impurities may result in small residual leakage currents attributed to Faradaic charge-transfer reactions occurring at the electrodes [182]. Transition metal ions are commonly encountered impurities in carbon materials. Finally, the ESR was determined by calculating the voltage drop (IR drop) across the SC and dividing it by the current applied during the measurement, specifically using a discharge current of 10 mA.

Fig. 12 presents the characterization results of a printed SC obtained using the Maccor system. This figure encompasses both CV curves and GCD results.

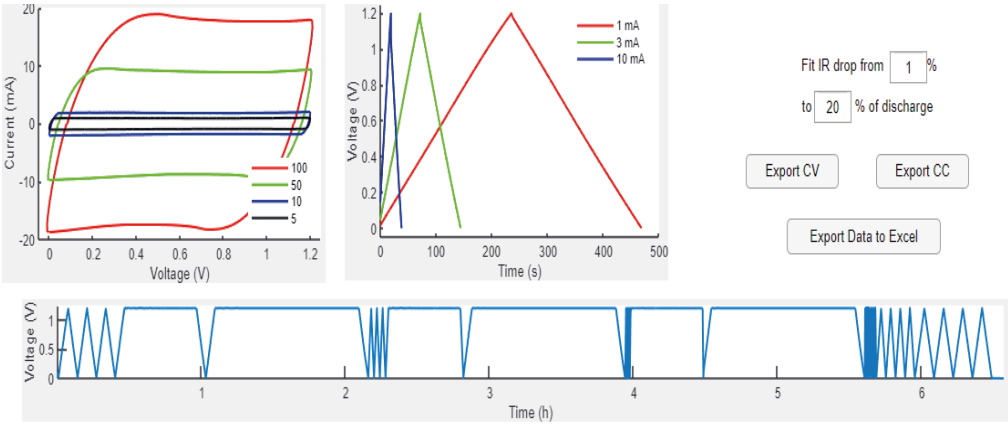

Fig. 12. Characterization results of a printed SC obtained using the Maccor system, showcasing both cyclic voltammetry (CV) curves and galvanostatic charge-discharge (GCD) results.

4- MODELING OF SUPERCAPACITORS

SCs have traditionally been approached in modeling and analysis similarly to standard capacitors, despite their higher capacity. The modeling of SC energy modules holds a pivotal role in anticipating design outcomes and enabling condition monitoring. The characterization of diverse electrical attributes of SCs and the anticipation of how these attributes influence the charging and discharging dynamics of energy modules, both in loaded and unloaded scenarios, represent crucial pre-deployment steps in harnessing SCs for energy applications. Notably, considering the potential divergence in electrical parameters among devices, notably evident in printed SCs, it is of utmost significance to conceptualize and gauge the impact of these variations on the performance of series-connected modules. Literature encompasses a multitude of models designed to accurately depict the electrical behavior, thermal characteristics, self-discharge tendencies, and aging phenomena of SCs across varying operational conditions [208-210].

The paramount approach for emulating the electrical behavior of SCs is the employment of an equivalent circuit model (ECM), rooted in parametric RC (resistor-capacitor) networks. Despite not explicitly revealing the intrinsic physical parameters and internal intricacies of SCs, this model is derived from empirical observations and experimental data. Furthermore, its straightforward composition and impressive precision render it suitable for real-time energy management endeavors. The precision of the ECM within the parametric RC networks paradigm varies contingent upon the electrical circuit's configuration and the number of components employed.

Considering the primary focal point of this thesis, which centers on the modeling and simulation of self-discharge and leakage current phenomena intrinsic to printed SCs, an optimal strategy involves initiating this chapter by providing contextual information concerning self-discharge and leakage current.

4.1 SELF-DISCHARGE AND LEAKAGE CURRENT

SCs hold immense potential for practical applications; however, their widespread use is limited by the presence of self-discharge and leakage current. Self-discharge in a SC is observed when the external resistance becomes effectively infinite, leading to a spontaneous decrease in voltage. This occurs when the SC is left in an open circuit, but it is also important to note that self-discharge is not solely a result of an infinite external resistance. This phenomenon significantly impacts the SC's dynamic behavior during rest periods, potentially disrupting its function and leading to the unintended dissipation of stored energy. Self-discharge in SCs primarily arises from three mechanisms: Ohmic leakage, charge redistribution, and Faradaic reactions [183,184]. Among these, Faradaic reactions are considered the dominant cause.

Leakage current, on the other hand, refers to the small current that flows through a SC while the rated voltage is continuously applied [185]. Over time, the leakage current stabilizes and diminishes [186]. Considering the detrimental effects of self-discharge and leakage current, it is crucial to account for these characteristics when designing electronic circuits involving SCs. However, it is noteworthy that self-discharge and leakage current have received relatively little attention in the literature.

The study of self-discharge in SCs is complex, due to the involvement of ions and the diverse range of electrode structures. Unlike conventional capacitors, self-discharge in SCs cannot be solely explained by leakage resistance. Several material properties, such as electrode structure, porosity, impurities, ionic size of the electrolyte, and accessible surface area, also influence the self-discharge process [187]. Charge redistribution occurs due to differences in the accessibility of electrolyte ions to the electrode surfaces, primarily if the cells are overcharged [188]. During the initial hours of open-circuit period, Faradaic redox reactions dominate the self-discharge, while internal ohmic leakage typically dominates thereafter [189]. Additionally, leakage current in SCs primarily results from Faradaic redox reactions at the electrode-electrolyte interface [190].

Despite the significance of self-discharge and leakage current in SCs, these characteristics have remained largely unexplored in the literature. Understanding and addressing these phenomena are essential for optimizing the long-term performance of SCs and accurately estimating available energy, particularly in applications such as power supply for WSNs, IoT, and wearable electronic devices.

To summarize, several factors contribute to self-discharge in SCs, including impurities in the electrolyte solution triggering electrochemical reactions, ohmic leakage resulting from resistive losses, redox reactions occurring within the electrodes or at interfaces, and excessive voltage during overcharging events [191]. These various causes gradually dissipate stored energy in the SC, leading to self-discharge. Moreover, the rate of self-discharge is influenced by the charging duration, with longer charging times promoting more uniform charging of the electrode surface, improved ion penetration into electrode pores, balanced charge distribution, and efficient ion transport. This enhanced charging process reduces self-discharge and improves voltage retention characteristics in SCs.

In order to quantify self-discharge in electrochemical SCs, a defined procedure is employed. The SC device undergoes full charging for a predetermined duration, typically ranging from 24 to 72 hours, to ensure reliable data. Following complete charging, the device is disconnected, and the open-circuit voltage output is measured at various time intervals to document the decay in voltage over time.

4.2 EQUIVALENT CIRCUIT MODELS REPORTED IN THE LITERATURE

SCs are increasingly used in energy storage systems, making it essential to accurately model their electrical behavior for effective design prediction and condition monitoring. Various equivalent circuit models (ECMs) have been proposed to describe the electrical characteristics of SCs, including the classical ECM, two-branch models with equivalent parallel resistance (EPR), three-branch models, and models based on variable leakage resistance (VLR) [53], [192-206], [207-213]. EPR is a parameter used to represent the internal losses and leakage current within the SC. However, these existing ECMs have limitations when it comes to predicting the nonlinear self-discharge effect of SCs in the long term and are not suitable for practical applications.

The classical ECM, commonly used to represent SCs, consists of a capacitor and an ESR to account for internal losses [197]. While this ECM is simple and accurate for short-term charge/discharge times, it fails to capture the effects of self-discharge and leakage current over extended periods. The addition of a constant parallel resistance in the classical model attempts to address these effects [198], but it still falls short in accurately modeling the nonlinear behavior of self-discharge.

More complex ECMs, such as the two-branch model with EPR and the three-branch model, offer additional elements to represent the redistribution of charges and diffusion-controlled Faradaic redox

reactions [199-202]. However, despite their increased complexity, these ECMs are also inadequate for estimating the nonlinear self-discharge effect of SCs over the long term.

In order to address these limitations, some ECMs incorporate VLR to describe the self-discharge behavior of SCs [195]. These ECMs utilize multiple distinct exponential functions with different time constants to represent the varying leakage resistances. However, the determination of a large number of distinct exponential functions for different periods complicates the parameters identification and hinders long-term simulations in SC energy modules.

The ECMs for a SC reported in the literature are illustrated in Fig. 13.

In summary, the existing ECMs reported in the literature have multiple branches and numerous RC network elements, which make them impractical for implementation in energy storage modules that require simplified models. Moreover, these ECMs fail to accurately capture the nonlinearity of self-discharge in SCs over extended time periods. Therefore, there is a need for a simpler and more effective ECM that can accurately predict the behavior of SC energy storage systems in practical applications, especially in long-term scenarios involving series-connected SC energy storage modules.

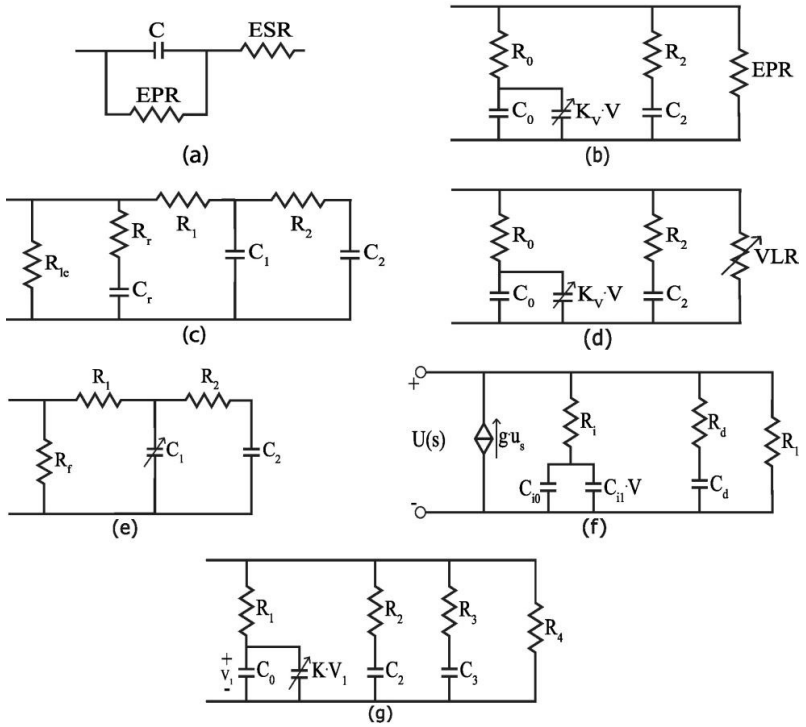

Fig. 13. Various ECMs for a Single SC as documented in the literature; a) Spyker et al. Model [198], b) Two-Branch Model with EPR [201], c) Three-Branch Model [202], and d) Two-branch ECM with VLR [195,205]. e) Two-branch ECM [203,204]. f) Two-branch ECM with a controlled current source [194]. g) Three-branch ECM with EPR [189,206]. Adapted from **publication I** and **publication III**.

4.3 PROPOSED EQUIVALENT CIRCUIT MODELS

In **publication I**, we focused on addressing the limitations of existing ECMs for SCs in the long-term applications, particularly the insufficient treatment of leakage and self-discharge effects. In order to overcome these limitations, we developed an ECM that incorporates the nonlinearity of leakage and self-discharge. Our approach involved charging each fabricated SCs to approximately 1 V and recording the voltage during a 31-day self-discharge period. Then we calculated current at each data point based on the capacitance of each SC and from the experimental data, we fitted the current-voltage exponential equation, as demonstrated in Fig. 14b, with a good level of approximation. This process was repeated for all 12 printed SCs utilized in this study, resulting in a unique exponential and nonlinear equation for the leakage of each SC.

In order to model the internal parameters of an SC (Fig. 14a), we employed a capacitor, an ESR, and a variable exponential element connected in parallel to the SC. This parallel component accounted for the nonlinearity of SC self-discharge and leakage current. The ECM incorporated capacitance and ESR values obtained through characterization of the printed SCs using the Maccor system, as well as 'a' and 'b' values derived from the experimental self-discharge data. It is worth noting that each of the 12 fabricated SCs had its own unique capacitance, ESR, 'a,' and 'b' values.

In **publication II**, a new ECM is proposed, which incorporates the nonlinearity of leakage and self-discharge over time. Although, the ECM presented in **publication II** utilizes identical elements to the model described in **publication I**, the exponential equation used for EPR and the method of obtaining EPR parameters differ in this study. The equation $I=V\times e^{-(a+ b\times V)}$ is employed as the exponential equation for EPR, which demonstrates a better fit with experimental self-discharge data. Moreover, this exponential equation is better suited for Monte-Carlo simulations, which would be the focus of the next research topic by the authors.

In order to determine the EPR equation, the discharge potential difference formula of the capacitor is utilized. By characterizing the printed SCs using the Maccor system, the capacitance value 'C' is already determined. Additionally, based on experimental self-discharge data, the initial potential difference 'V0', time 't', and potential difference 'V' for each SC at a specific time are determined. Subsequently, the dynamic resistance can be calculated for each data point, and the resistance curve (R(V)) can be plotted as a function of potential difference. The exponential equation $e^{(a+ b\times V)}$ is then fitted to the R(V) data points to obtain 'a' and 'b' parameters for each individual SC. A visual representation of this fitting process is illustrated in Fig. 15, showing the good fit between the exponential fitting curve and the experimental data points.

To incorporate the self-discharge and leakage of SCs into the ECM, the leakage current is defined as a function of the potential difference. As $R=V/I = e^{(a+ b\times V)}$, this relationship leads to $I=V\times e^{-(a+ b\times V)}$, which represents the SC's EPR in the proposed ECM. The ECM of an SC, as presented in **publication II**, is depicted in Fig. 16.

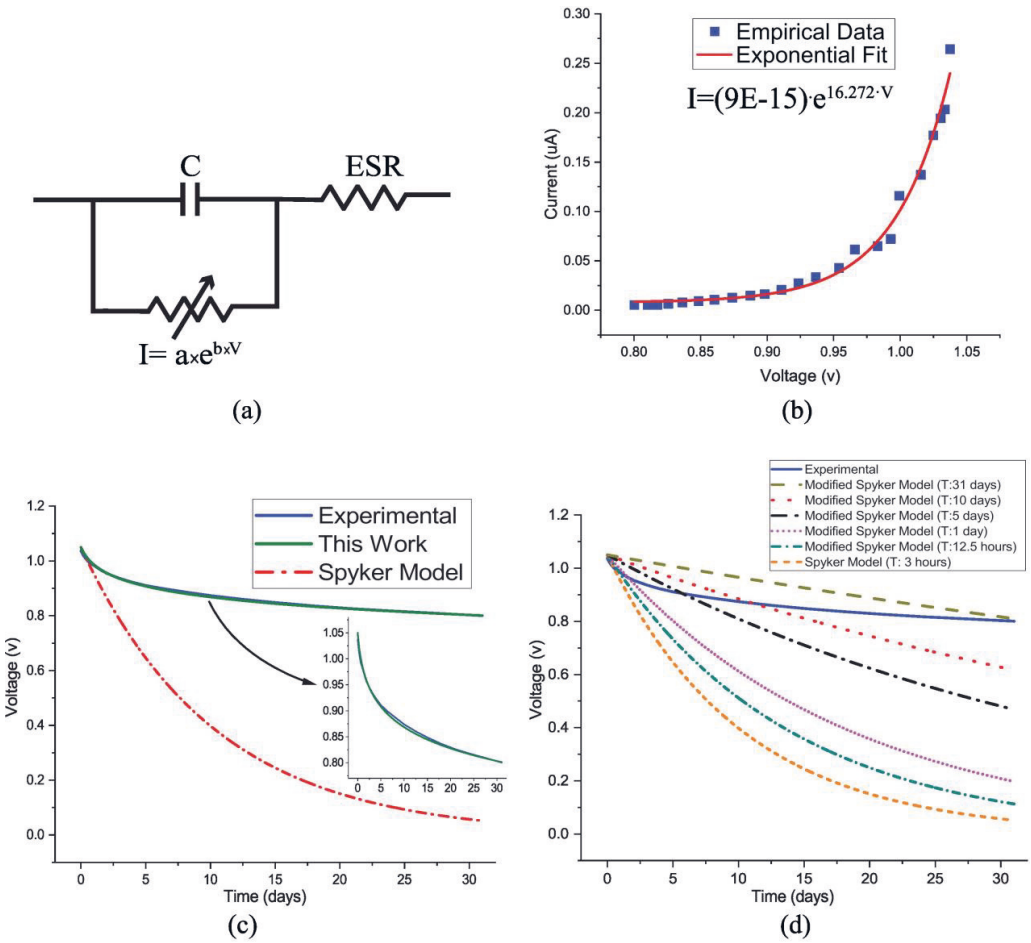

Fig. 14. a) Suggested ECM for a SC in **publication I**.b) Derivation of the I-V exponential equation for modeling leakage current and self-discharge characteristics. c) Comparison of self-discharge behavior between the SC ECMs: Spyker linear model and the exponential model proposed in this study, along with experimental results. d) Enhancing the Spyker model by incorporating a longer self-discharge time constant (T) in the proposed equation, resulting in closer agreement with experimental data but not achieving complete conformity. Adapted from **publication I**.

In **publication III**, in order to model the internal parameters of a single SC, the same ECM comprising conventional capacitor (C), an ESR, and a parallel variable EPR are utilized. Although this model shares similarities with **publication I** and **II**, the exponential EPR function used in this study and the method for obtaining this element differ. The proposed exponential equation in **publication III**, $I = e^{(a+ b\times V)}$, accurately describes the self-discharge and leakage current effects, exhibiting a better fit with empirical self-discharge data. Moreover, this exponential equation is well-suited for Monte-Carlo simulations due to the normal distribution of parameters involved in the equation.

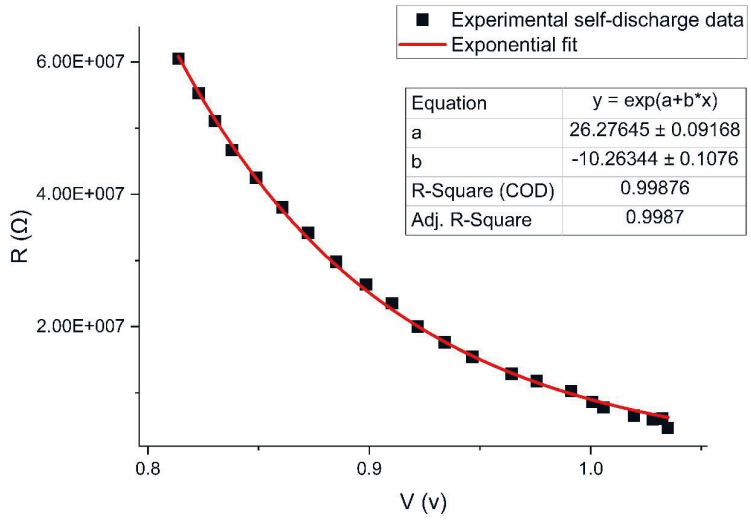

Fig. 15 . Exponential curve fitting of R(V) for a SC. Reprinted from **publication II** with permission.

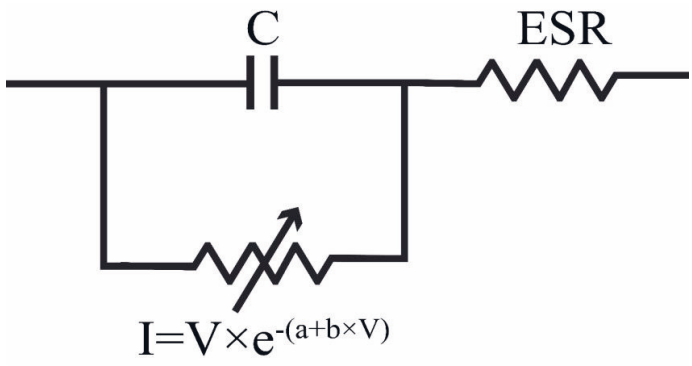

Fig. 16. Proposed ECM for a SC in **publication II**. Reprinted from **publication II** with permission.

The experimental self-discharge potential difference data for each SC over time is used to determine the exponential function of the EPR in the proposed ECM (Fig. 17 b). By employing basic capacitance and current formulas (3), the numerical values of the current (4) at any given voltage for each SC can now be calculated using the capacitance (C) and self-discharge data.

$$Q = C \times V,\ I = dQ/dt \tag{3}$$

$$I_m = C \times dV_m/dt_m = C \times (V_{m-1}-V_m)\ /(t_m-t_{m-1}) \tag{4}$$

Using the calculated current data points, the I (V) diagram for each SC is plotted (Fig. 17c and d). Subsequently, the exponential equation $e^{(a+b\times V)}$ is fitted to the I (V) data points of each SC. This fitting process uniquely determines the parameters 'a' and 'b' for each SC, as depicted in Fig. 17c and d. The fitting results demonstrate excellent statistical parameters, including high R-square and Adj. R-square values, indicating a strong fit between the exponential function and the I (V) data points. Notably, all

12 SCs in the study exhibit R-square values exceeding 0.99, highlighting the excellent fit of the exponential function for all SCs.

Based on the successful fitting of the exponential function, the numerical values of 'a' and 'b' parameters, along with the characterization parameters 'C' and 'ESR', are determined, revealing all four parameters of the proposed ECM (Fig. 17a). This model, referred to as ECM 1 in this study, provides a comprehensive representation of the SC behavior.

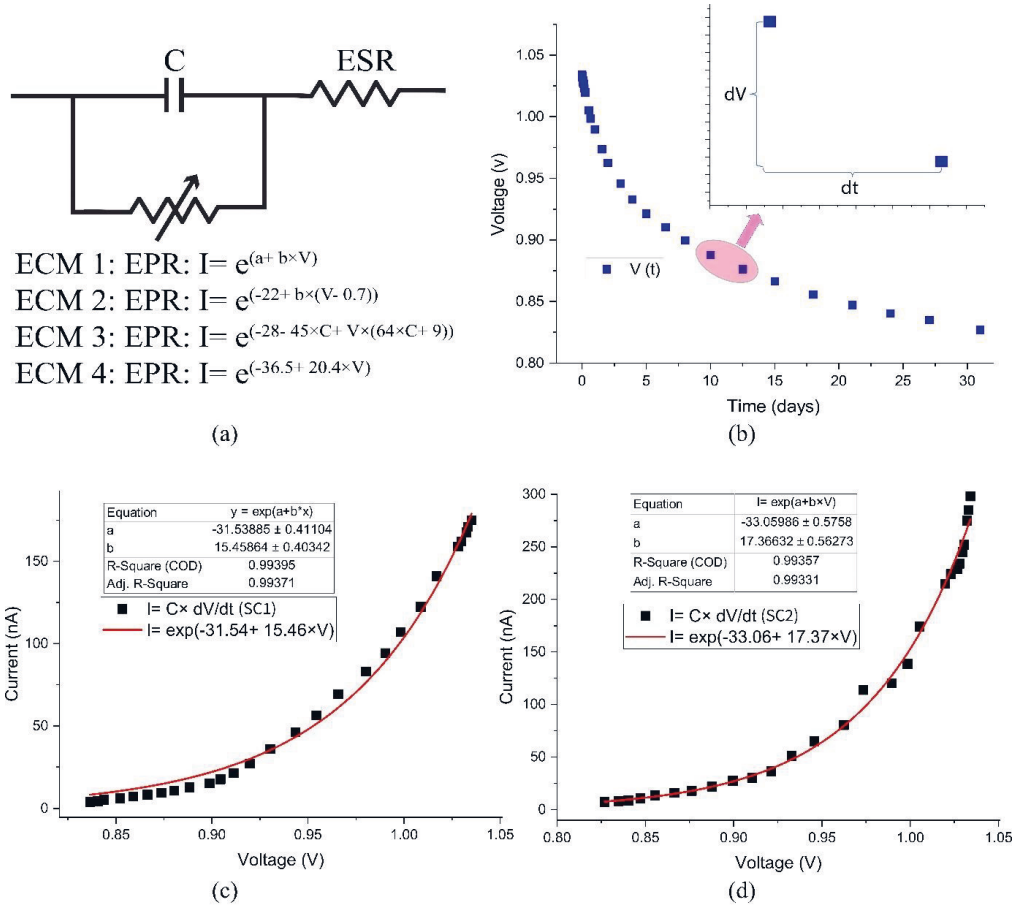

Fig. 17. a) Proposed ECMs for a single SC. b) experimental self-discharge data of a SC. c) fitting the exponential function to the I(V) datapoints of SC1. d) fitting the exponential function to the I(V) datapoints of SC2. Adapted from **publication III.**

In **publication III**, ECM 1 is introduced as a simple model with four parameters. However, the aim is to further simplify the model by reducing the number of parameters and formulating an EPR exponential I(V) function based on a single parameter. The parameters 'C', 'a', and 'b' in ECM 1 demonstrate a relatively good linear relationship, as depicted in Fig. 18a and 18b. Linear fits are used to approximate this linear relationship, yielding two linear equations with high R-square and Adj. R-square values.

With the linear relationship among the parameters established, two simplified models are formulated. ECM 2 utilizes only parameter 'b' in the exponential equation, while ECM 3 incorporates only parameter 'C'. The EPR exponential I(V) functions for ECM 2 and ECM 3 are derived accordingly. The simplified ECM 2 has three and ECM 3 has two parameters instead of four, making them even more practical.

$$\text{EPR: } I = e^{(a + b\times V)},\ a = -0.7\times b - 22 \rightarrow I = e^{(-22 + b\times(V - 0.7))} \text{ :ECM 2} \quad (5)$$

$$b = 64\times C + 9 \rightarrow I = e^{(-28 - 45\times C + V\times(64\times C + 9))} \text{ :ECM 3} \quad (6)$$

Another approach to simplifying ECM 1 is to replace the 12 SCs' mean values of parameters 'a' and 'b' in the EPR exponential function. This alternative model, referred to as ECM 4 ($I = e^{(-36.5 + 20.4\times V)}$), utilizes only two parameters ('C' and 'ESR') and eliminates the need for parameters in the exponential EPR function.

Overall, ECM 2, ECM 3, and ECM 4 offer increasingly simplified representations compared to the previous models in this work, with ECM 4 being the simplest and most straightforward, providing practical advantages for various applications.

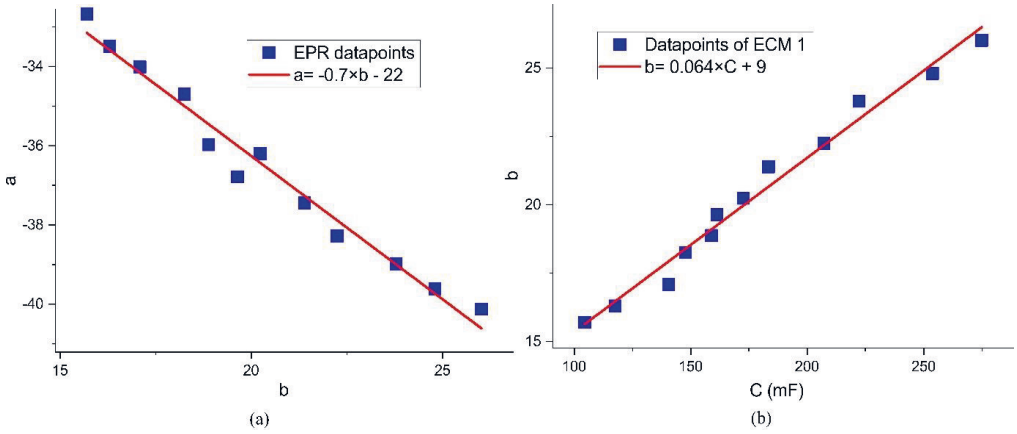

Fig. 18. Linear relationships in ECM 1 parameters a) A linear relationship with a good approximation between parameters 'a' and 'b'. b) Another linear relationship with a good approximation between parameters 'b' and 'C'. Adapted from **publication III**.

Overall, compared to linear ECMs reported in the literature [195-199], [201-203], [208-214], our exponential ECMs for SC self-discharge and leakage offers enhanced accuracy while maintaining a simplified circuit structure.

5- RESULTS AND DISCUSSION

In this pivotal section, we unravel the culmination of our investigative efforts, illuminating the intricacies of SC behavior within the context of diverse scenarios. Through rigorous analysis and simulation, we discerned the accuracy of our proposed ECMS, enabling a nuanced understanding of its performance characteristics. The interplay between leakage current and charging dynamics is expounded upon, unravelling its effects on energy management. Moreover, we delve into the influence of resistive loading on the intricate landscape of leakage current in SCs, unearthing insights into their performance under varying load conditions.

A statistical prism is cast over printed SCs, unveiling patterns and trends that drive their electrical response. This analysis is further enriched by our pioneering endeavour to integrate SCs, leveraging their potential as an energy storage device for in-situ electropolymerization, thereby catalyzing the creation of irreversible visual indicators.

As we navigate through these results, we concurrently engage in a comprehensive discussion that contextualizes our findings within the broader scientific landscape. By embracing both quantitative evidence and qualitative reasoning, we chart a course towards a more profound comprehension of SC behavior, paving the way for their optimized integration and application.

5.1 ACCURACY OF THE PROPOSED ECMS

In **publications I**, **II**, and **III**, the accuracy of the proposed ECMs is assessed through five different approaches. By employing these five approaches, all the proposed ECMs are rigorously evaluated, ensuring their reliability and effectiveness in modeling the behavior of SCs.

5.1.1 COMPARING THE ACCURACY OF THE PROPOSED ECMS WITH LITERATURE

In **publication I**, in order to demonstrate the accuracy of the proposed ECM, we simulated the self-discharge behavior of an SC using both the linear model proposed by Spyker et al. [198] and our exponential ECM. The results were then compared with experimental data. The Spyker linear model, as depicted in Fig. 13a, proved unsuitable for simulating the long-term discharge behavior of an SC. In contrast, our ECM exhibited remarkable accuracy, with simulation results closely aligning with the experimental findings. Notably, we modified the Spyker method to calculate the EPR by considering self-discharge values over longer time constants, as shown in Table 5. Although this modification improved the agreement between the self-discharge behavior and experimental results, some discrepancies still remained.

Table 5. Calculated EPR values with extended time constants using the Spyker method [198] from previous studies. Reported in **publication I**.

Time Constant	EPR (M Ω)
3 hours	4.9
12.5 hours	6.6
1 day	8.8
5 days	18.1
10 days	27.5
31 days	56.4

In **publication III**, the verification process involves comparing the self-discharge experimental results of two commercially available EDLCs with the simulation results based on ECM 4, the most simplified ECM in **publication III**. ECM 4 requires only the knowledge of capacitance and ESR values to simulate the charge and discharge behavior of SCs.

The experimental self-discharge results for the two commercial SCs, referred to as SC1 and SC2, were obtained from literature sources [202,215]. SC1 is a carbon-based SC with an acetonitrile electrolyte and a capacitance of 600 F [215]. SC2 is also a carbon-based SC with an organic electrolyte and a capacitance of 2600 F [202]. SC1 was charged to 1.3 V and kept at that voltage for 24 hours, while SC2 was charged to 1.5 V with a charging time of one hour. Subsequently, the open circuit potential difference, which represents the self-discharge behavior, was monitored, and recorded for 15 days for SC1 and 7 days for SC2.

Fig. 21a demonstrates the close agreement between the simulation results and experimental results over time for both SC1 and SC2. The residual voltage (subtracting the simulation from the experiment) over time is also presented in Fig. 21b. The maximum simulation error for SC1 is approximately 34 mV, corresponding to approximately 2.6% of the initial voltage, over the 15-day period. For SC2, the maximum simulation error is approximately 17 mV, which is approximately 1.1% of the initial voltage, over the 7-day period. These findings indicate the high accuracy of the proposed ECM for these two commercial EDLC SCs.

However, it remains uncertain whether our proposed ECMs can accurately replicate the self-discharge patterns of organic SCs within the higher charging voltage ranges (2.5-3 V). It is possible that our proposed ECMs may not achieve accurate simulation, as the higher initial voltage of these organic SCs exceeds the voltage range upon which our ECMs are developed. Further experiments and simulations are essential to assess the precision of the proposed ECMs on commercial SCs with varied electrolyte types and within different voltage ranges.

5.1.2 SCS USED TO DEVELOP THE ECMS: SIMULATION RESULTS VS. EXPERIMENTS

Publications I, **II**, and **III** involve comparing the self-discharge simulation results with the experimental data obtained from the SCs used in developing the ECMs. This allows for a direct evaluation of how well the ECMs capture the behavior of the SCs.

For example, in **publication II**, in order to assess the accuracy of the proposed ECM, the potential difference of four SCs in self-discharge mode was simulated and compared with experimental data collected over a 31-day period. The comparison, as shown in Fig. 19, reveals a close correspondence between the simulation results and the experimental data, indicating a reasonable agreement. Even after 31 days, the disparity between the measured experimental data and the simulation results is negligible, with an estimation error of less than two percent when employing the ECM presented in **publication II**.

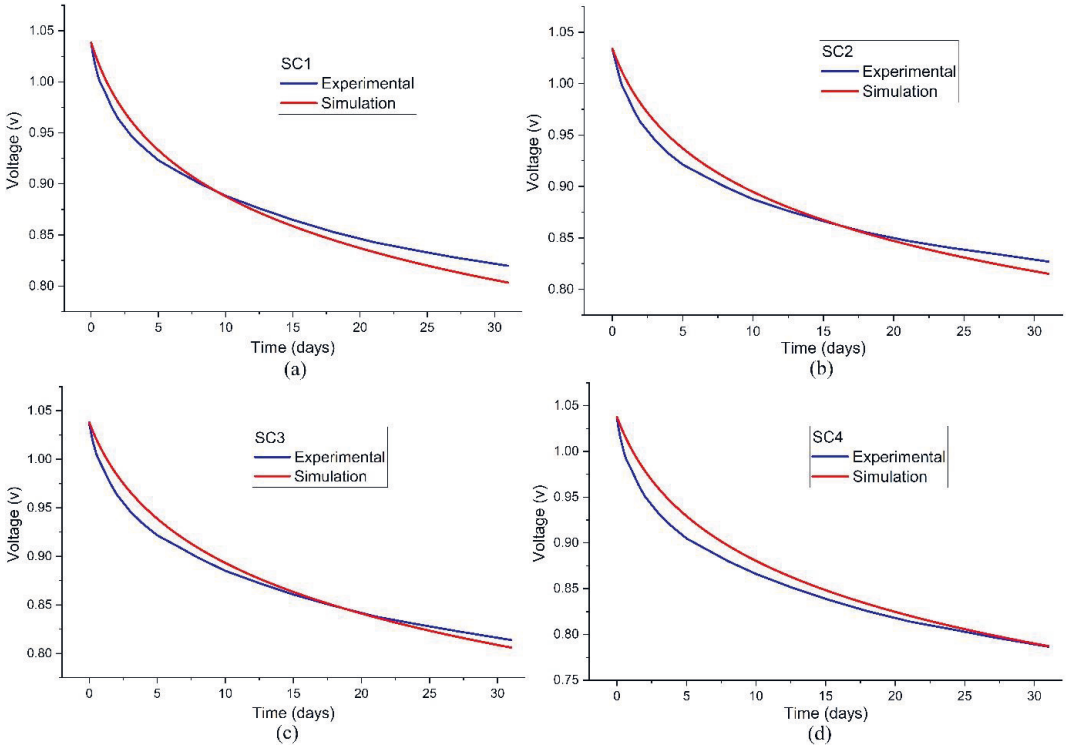

Fig. 19. Experimental data and simulation results depicting the potential difference during self-discharge mode for four SCs over 31 days. Reprinted from **publication II** with permission.

In all three publications, the accuracy of the proposed ECMs is quantitatively evaluated through this approach, demonstrating their reliability in capturing the self-discharge behavior of SCs.

5.1.3 SCS NOT USED TO DEVELOP THE ECMS: SIMULATION RESULTS VS. EXPERIMENTS

As a third method of evaluating the accuracy of the proposed ECMs, in **publication III**, the proposed ECMs are applied to new printed SCs that were not used in their development. The self-discharge behavior of four randomly selected SCs is experimentally measured and compared with the simulation results obtained using the ECMs. The selected SCs include both those similar to the ones used in ECM development and those with different substrates, allowing for a comprehensive assessment of the ECMs.

Fig. 20 demonstrates the effectiveness of all proposed ECMs in **publication III**, in predicting the self-discharge behavior of the new SCs over a 31-day period. The simulation results align well with the experimental data. ECM 1 exhibits a maximum error of 17.64 mV (2.21% of the SC's final voltage), while ECM 2, ECM 3, and ECM 4 have maximum errors of 26.49 mV (3.29%), 12.48 mV (1.56%), and 13.87 mV (1.74%), respectively.

It is interesting to note that ECMs 3 and 4, the simplest ECMs with only two parameters ('C' and 'ESR') for each SC, demonstrate slightly higher accuracy than ECMs 1 and 2, with maximum errors of less than 2%. However, the difference falls within the experimental uncertainty. These findings imply that by knowing the capacitance and ESR values, the self-discharge behavior of an SC over a 31-day period can be predicted with an error of less than 2% using ECMs 3 and 4. Considering their simplicity, it can be concluded that all proposed ECMs in **publication III** exhibit negligible maximum simulation errors for the new SCs over the long term and demonstrate excellent accuracy.

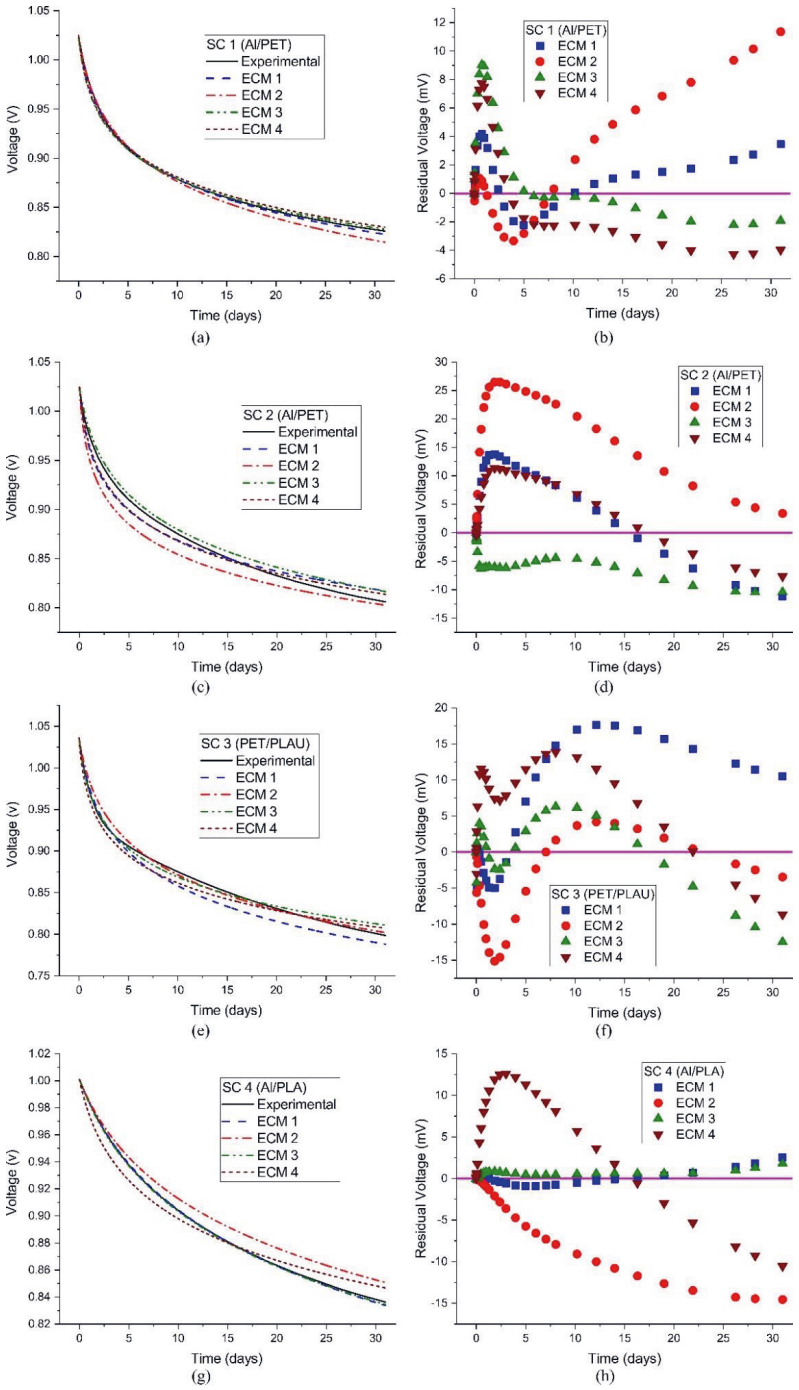

Fig. 20. a, c, e, g) Experimental and simulation results of self-discharge over 31 days using newly proposed ECMs, applied to four randomly selected SCs not utilized during ECM development. b, d, f, h) Residual voltage (the variance between experimental and simulation data). Adapted from **publication III**.

5.1.4 VERIFICATION USING DISCRETE LOAD RESISTORS: SIMULATION RESULTS VS. EXPERIMENTS

In **publication I, II**, and **III**, two separate SC energy modules, each consisting of three SCs connected in series, are formed (see Fig. 21c). These modules are then connected to discrete resistors with different resistance values. The voltage delivered to the discrete resistor during the discharge of the SC module is measured and compared with the simulation results based on the EPR function model proposed in each publication. This test verifies the accuracy of the ECMs in predicting the behavior of SCs in practical applications.

For example, in **publication III**, two SC modules are fully charged to 3 V each, after which the main power source is disconnected, and a resistive load is connected to the SC modules. The voltage across the resistive load during the discharge of the SC modules is measured using a digital multimeter.

Fig. 21d, e, f, and g present the discharge behavior of the SC energy modules while 1 kΩ and 4.7 kΩ discrete resistors are connected. As can be seen, the simulation results closely align with the experimental results, exhibiting a small difference. This difference is almost negligible for the resistive load of 4.7 kΩ. Fig 22e and g illustrate the residual voltage for SC modules 1 and 2, respectively, which can be utilized to determine the simulation error for each module by calculating the absolute value of the residual voltage over time.

For the resistive load of 1.0 kΩ, the maximum simulation error is 47 mV for module 1 and 243 mV for module 2, equivalent to approximately 1.57% and 8.1% of the module's initial voltage, respectively. An interesting finding from these short-term simulations is the full agreement among the simulation results based on ECMs 1 to 4 in **publication III**, indicating that leakage and self-discharge have minimal influence in the initial minutes of SC discharge. Instead, the capacitance values of the SCs play a more significant role in the short-term discharge behavior. Thus, the higher simulation error observed in module 2 compared to module 1 may be attributed to the larger difference in capacitance values among its SCs.

Overall, considering the results obtained from all verification tests using discrete load resistors in **publication I, II**, and **III**, all the proposed ECMs can be deemed acceptable in terms of estimation accuracy, given their simplicity.

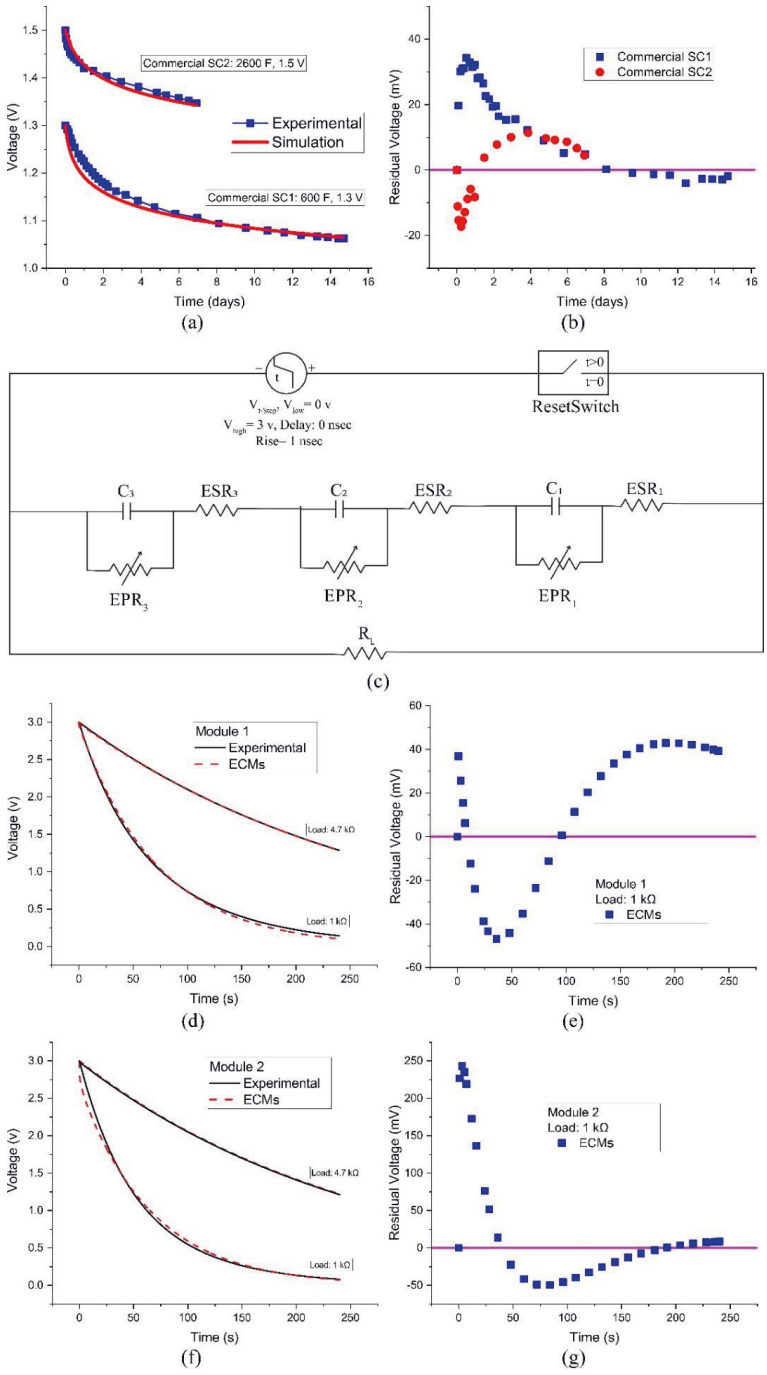

Fig. 21. a) Experimental and simulation results using ECM 4 for self-discharge in two commercially available SCs. b) Comparison of residual voltage (experiment vs. simulation) for the self-discharge of the mentioned SCs. c) Charge and discharge ECM of an SC energy module consisting of three series-connected SCs with a resistive load. d, f) Experimental and simulation results for the resistive load voltage during discharge, utilizing the proposed ECMs. e, g) Residual voltage analysis of the resistive load during the discharge of the SC energy module. Adapted from **publication III**.

5.1.5 SELF-DISCHARGE BEHAVIOR OF SC MODULES: SIMULATION RESULTS VS. EXPERIMENTS

To overcome the limited power storage capacity of individual SCs, multiple SCs can be connected in series to form an SC energy module. However, the stored potential difference in an SC decrease over time due to self-discharge, making it important to estimate the available power stored in the energy module in the long term. The proposed ECMs enable the prediction of the voltage across each SC energy module at any given time.

As an illustration, in **publication III**, four SC energy modules, each comprising three SCs connected in series using the 12 SCs used in developing the ECMs, are formed. Table 6 provides the parameters of the three SCs in each module. The capacitance difference among the SCs within each module increases from module 1 to module 4, with module 4 exhibiting the largest difference. However, the total capacitance value of the modules does not vary significantly. Fig. 22 and table 7 present the experimental and estimated voltage remaining in each of the four modules over a period of 31 days based on the proposed ECMs in **publication III**.

The results indicate that module 4 has a lower voltage remaining on day 31 compared to the other modules, suggesting that a larger capacitance difference among the SCs in a module leads to a lower final voltage value in the long term, influenced by self-discharge and leakage. Specifically, module 1, with a smaller capacitance difference, has a higher experimental and estimated final voltage compared to module 4. Therefore, selecting SCs with similar capacitance values or minimal differences maximizes power storage in an energy module, allowing for more power to be retained in the long term. Moreover, as illustrated in Fig. 22c and d, SC modules 3 and 4, characterized by larger capacitance variations among their three series-connected SCs, exhibit reduced precision in forecasting experimental self-discharge outcomes over the 0 to 20-day period when contrasted with modules 1 and 2, where the capacitance differences among their SCs are smaller. Hence, a substantial divergence in SC capacitance within a module result in diminished simulation accuracy, particularly in the short-term. One important motivation behind this modeling work is to understand how device-to-device variation in printed SCs affects the performance of an energy module comprising multiple SCs connected in series.

Additionally, the simulation results of the four ECMs can be utilized to predict the minimum and maximum voltage remaining in the energy module at any given time. Table 7 presents the estimated final voltage value for each module (at the end of day 31) based on different ECMs. This information enables the determination of the predicted minimum and maximum final voltage values for each module, providing an approximation of the possible voltage range window at the end of the 31st day. Notably, the experimental voltage results for each module at the end of day 31 fall within the predicted final voltage range window, supporting the validity of these predictions.

Table 6. Characteristics of four series-connected SC energy modules, each comprising three SCs. Reported in **publication III**.

Module 1	SC1	SC2	SC3	**Module 2**	SC1	SC2	SC3
C (mF)	147.7	158.8	161.3	**C (mF)**	140.5	183.4	222.2
ESR (Ω)	7.3	8	8	**ESR (Ω)**	7.2	7.8	8.8
a (EPR)	-34.7	-36.0	-36.8	**a (EPR)**	-34.0	-37.4	-39.0
b (EPR)	18.3	18.9	19.6	**b (EPR)**	17.1	21.4	23.8
C-total (mF)	51.9			**C-total (mF)**	58.6		
Module 3	SC1	SC2	SC3	**Module 4**	SC1	SC2	SC3
C (mF)	117.4	176.5	253.7	**C (mF)**	104.4	207.2	274.9
ESR (Ω)	7.5	7.4	8.4	**ESR (Ω)**	6.8	7	8.5
a (EPR)	-33.5	-36.2	-39.6	**a (EPR)**	-32.7	-38.3	-40.1
b (EPR)	16.3	20.2	24.8	**b (EPR)**	15.7	22.2	26.0
C-total (mF)	54.8			**C-total (mF)**	55.4		

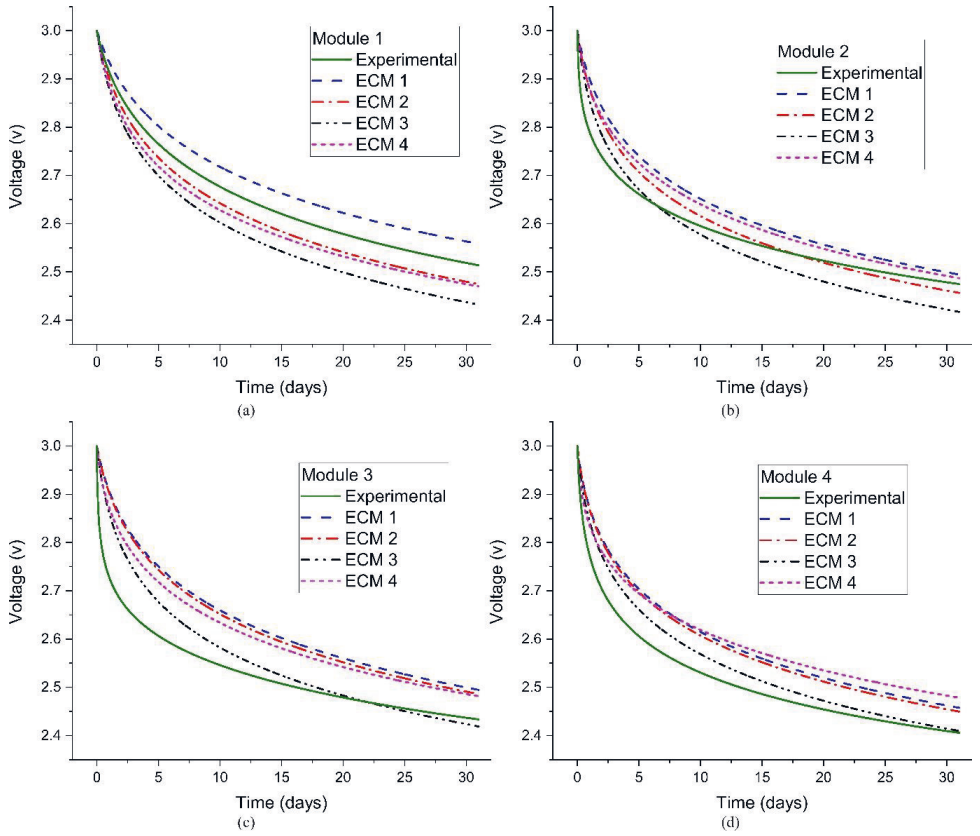

Fig. 22. Comparison of self-discharge behavior: experimental and simulation results based on proposed ECMs for four SC energy modules over time. Adapted from **publication III**.

Table 7. Experimental data and predicted value of the final voltage still stored in each module at the end of day 31 based on the proposed ECMs. Reported in **publication III**.

	Module 1	**Module 2**	**Module 3**	**Module 4**
ECM 1	2.56 V	2.49 V	2.49 V	2.46 V
ECM 2	2.47 V	2.46 V	2.49 V	2.45 V
ECM 3	2.43 V	2.42 V	2.42 V	2.41 V
ECM 4	2.47 V	2.49 V	2.48 V	2.48 V
Min.	2.43 V	2.42 V	2.42 V	2.41 V
Max.	2.56 V	2.49 V	2.49 V	2.48 V
Experiment	2.51 V	2.47 V	2.43 V	2.41 V

5.2 EFFECT OF LEAKAGE CURRENT DURING CHARGING

In order to assess the impact of leakage current on the potential difference stored at the ends of the SCs, simulations were conducted with and without considering the leakage in **publication I**. Fig 24a and 24b depict the voltage stored in an SC in a module over time during the charging process. It is evident that the leakage current has a minimal effect on the stored voltage. This simulation was repeated for all SCs in four energy modules, and consistent results were observed across all cases, demonstrating a negligible difference between the two sets of diagrams. As a result, it can be concluded that the leakage current has an insignificant influence on the charging behavior of SCs in the energy modules. Thus, during the charging phase, it is acceptable to disregard the leakage current, given that it remains considerably smaller than the charging current.

Furthermore, as illustrated in Fig 24c and 24d, the final amount of leakage current is approximately 106 times smaller than the initial amount of displacement current. This simulation was also performed for the remaining three energy modules, yielding similar outcomes for all the modules. These results provide further confirmation that the leakage current has minimal impact on the charging behavior of SCs within the energy modules and can be safely ignored.

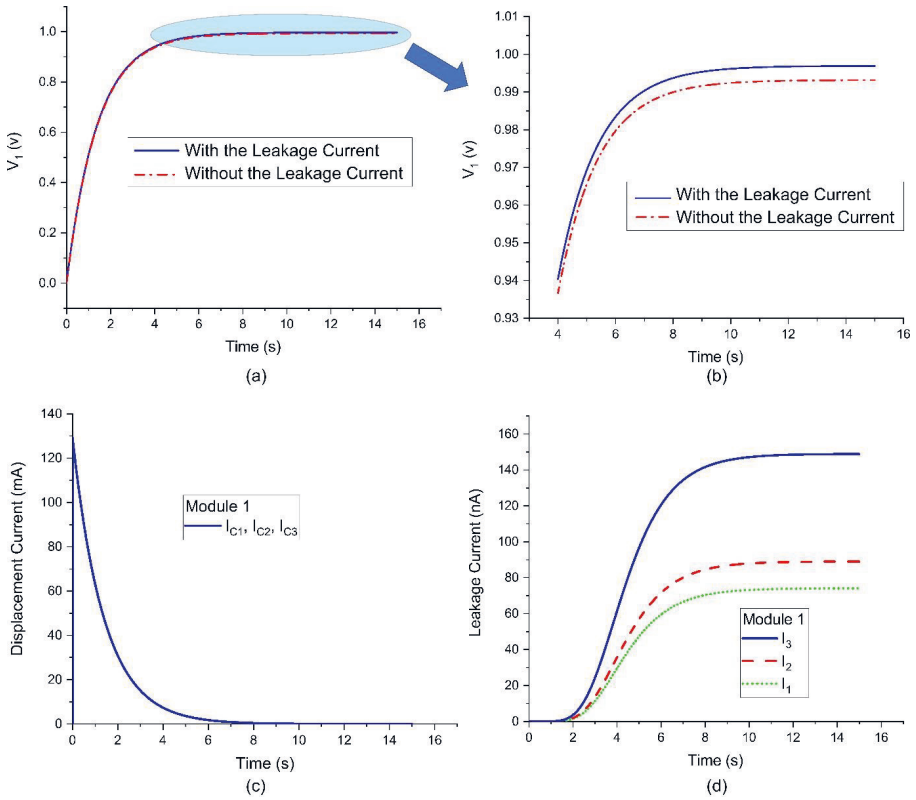

Fig 23. a), b) exploring the impact of leakage current on SCs charge in energy module 1. c), d) contrasting SCs displacement and leakage current during charging in energy module 1. Adapted from **publication I**.

5.3 EFFECT OF RESISTIVE LOAD ON THE LEAKAGE CURRENT OF SCS

In the discharge model of the SC modules (Fig. 15b), the leakage current of the SCs in the energy modules becomes more significant as the resistance load increases. This relationship is evident in Fig. 19e and f, which illustrate the leakage current of SC1 in energy module 1 for different small and large resistive loads. The figure shows that the leakage current is highest during self-discharge and lowest when a 1 kΩ resistive load is connected to the energy module. This behavior can be explained by considering that as the resistive load increases, the SCs deliver less voltage to the load. Consequently, a larger potential difference remains across the SCs. Since the leakage current exhibits an exponential relationship with the potential difference across the SC, the leakage current remains higher due to the larger potential difference between the two ends of the SC.

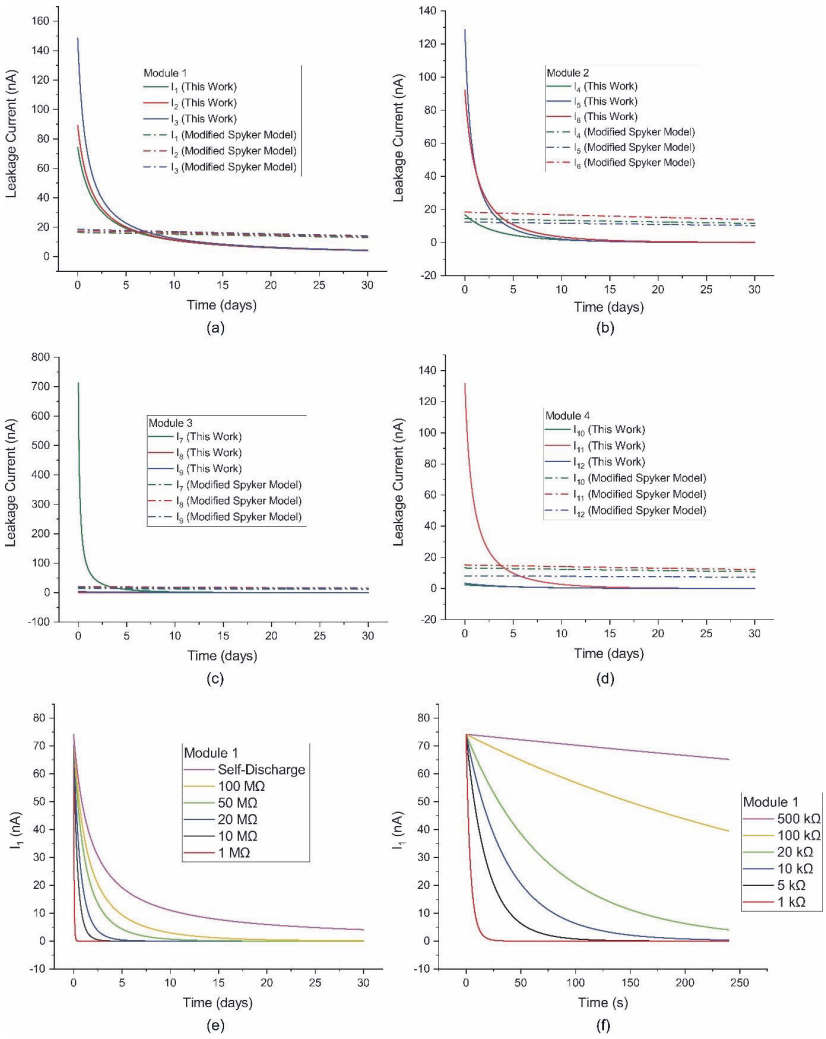

Fig. 24. a, b, c, d) SCs leakage behavior in four energy modules with proposed ECM and modified Spyker model. e, f) Impact of resistance load variation on SCs leakage current. Adapted from **publication I**.

5.4 STATISTICAL ANALYSIS OF PRINTED SCS

In **publication IV**, we investigate the charge and discharge characteristics of printed SCs utilizing statistical methodologies. The findings of this statistical analysis offer the potential to forecast the behavior of series-connected SC energy modules, considering the variations in electrical properties observed among individual devices. This aspect is of significant importance when dealing with PE devices.

Furthermore, the statistical study's applicability extends beyond predicting critical aspects of PE. It can also be utilized to assess the impact of diverse electrical variables, which may differ from one device to another, on the behavior of an energy module comprising several SCs connected either in series or in parallel. In essence, our work enables the analysis of how variations in electrical parameters, such as

self-discharge and leakage current in SCs, influence the performance of series-connected SCs within an energy module.

In **publication IV**, a set of 12 printed SCs is employed to conduct a comprehensive statistical analysis. In this study, we used the same previously proposed ECMs as in **publications I**, **II**, and **III** (Fig. 17a) to model the printed SCs. To apply the MC method, it was essential to define the probability distribution for each of the four parameters that inherently carry uncertainty. These parameters were associated with the 12 printed SCs used in the investigation.

In order to determine the appropriate probability distribution for each parameter, a normality test was conducted. The normality test assesses whether the data can be adequately described by a normal distribution, also known as a Gaussian distribution. A normal distribution is symmetric around the mean, indicating that data close to the mean are more likely to occur than data further away from the mean [218].

The histogram charts (Fig. 25) depict the distribution of each parameter along with their respective bell curves. As clearly shown in the histogram charts, all four parameters conform to a normal distribution, indicating that they can be appropriately represented using this probability distribution.

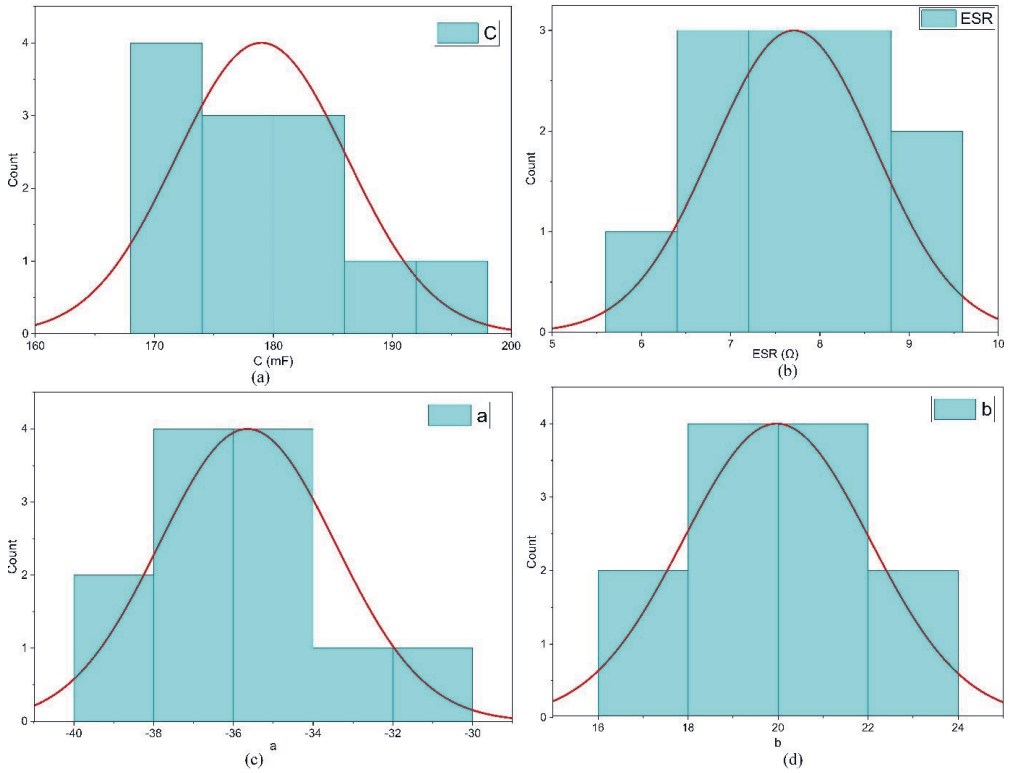

Fig. 25. Histogram chart of the ECM parameters. Adapted from **publication IV**.

In Table 8, a comprehensive summary of the descriptive statistics and normality test results for each parameter can be found. The descriptive statistics include the mean value, standard deviation (Std), P-value, and skewness for each parameter. Std is a measure of the amount of variation or dispersion in a set of values. It provides a way to quantify the degree of spread or scatter in a dataset. P-value is a measure that helps assess the evidence against a null hypothesis. The null hypothesis represents a default assumption that there is no effect, no difference, or no association in the population under

study. The p-value is used in hypothesis testing to determine the strength of the evidence against the null hypothesis. Skewness describes the asymmetry of the probability distribution of a real-valued random variable. In simpler terms, it indicates the degree and direction of skew (departure from horizontal symmetry) in a dataset.

Upon analyzing the numerical results of the descriptive statistics, it becomes evident that all four parameters exhibit a normal distribution. This conclusion is further supported by the P-values obtained for each parameter, which range from 0.74 to 0.98. A P-value greater than 0.05 generally indicates a strong indication of normal distribution.

Moreover, the close similarity between the mean and median values for each of the four parameters serves as additional evidence of their adherence to the normal distribution. The mean and median values being almost identical implies a symmetrical distribution for these variables.

Additionally, the skewness values, which serve as indicators of distribution asymmetry, range between 0.30 and 0.52 for the four parameters. These values suggest that the probability distributions of all variables are approximately symmetrical, further supporting their normality.

Table 8. ECM parameters' descriptive statistics and normality test results. Reported in **publication IV**.

Parameters	C (mF)	ESR (Ω)	a	b
N total	12	12	12	12
Mean	179.0	7.7	-35.6	20.0
Minimum	169.1	6.3	-38.6	16.9
Median	178.2	7.6	-35.8	20.0
Maximum	192.0	9.3	-31.3	23.8
Std	7.18	0.92	2.21	2.07
P-Value	0.83	0.82	0.74	0.98
Skewness	0.35	0.41	0.52	0.30

5.4.1 QUANTIFYING CAPACITANCE VARIATION IN SERIES-CONNECTED SC ENERGY MODULES

The voltage stored in a single SC is limited by the electrochemical potential window of the electrolyte and cannot exceed a certain amount, with a maximum potential value of 1.2 V for the printed SCs in this thesis. However, if this voltage is insufficient for a specific application, the solution is to connect multiple SCs in series to form an SC energy module. When connecting SCs in series, it is crucial to consider the std among their capacitance values. The larger the difference in capacitance among the SCs in a module, the greater the variation in voltage stored across each SC after the charging phase (with more voltage over the SC with the lowest capacitance). Equation 7 can be used to calculate the potential difference across each SC based on the capacitive division of the total charging voltage.

Consequently, if the std of capacitance among SCs within a module exceeds a certain threshold, some SCs may experience voltage levels that surpass the electrochemical potential window of the electrolyte, leading to malfunctioning of the entire module. Therefore, conducting statistical analysis is essential for determining the maximum allowable capacitance std of series-connected SCs within a module.

$$VSC_i = V_0 / (C_i \times (1/C_1 + 1/C_2 + 1/C_3 + \ldots + 1/C_N)) \quad (7)$$

Here, VSC_i represents the voltage stored across SC_i, V_0 represents the charging voltage, C represents the capacitance, and N represents the number of SCs connected in series.

In the preceding section, the normality test and descriptive statistics demonstrated that the capacitance of the printed SCs follows a normal distribution. In **publication IV**, utilizing statistical analysis tools, our objective is to determine the number of SC energy modules (each with three SCs connected in series) out of 100, that will contain at least one SC with a stored voltage higher than 1.2 V when charging each module up to 3 V. We fabricated 300 printed SCs with different std on their capacitance (10%, 15%, and 20%) for this investigation. The results of this statistical study are presented in Table 9.

Based on the results, when the capacitance value of the 300 printed SCs has a std of 10%, there will be only one module with at least one SC having a voltage higher than 1.2 V. With a std of 15% and 20% on the capacitance of the 300 SCs, there will be 12 and 31 modules, respectively, with at least one SC having a voltage of more than 1.2 V. Therefore, the maximum allowable std on the capacitance of three series-connected printed SCs is less than 10%, to prevent the module from malfunctioning when charged up to 3 V.

Table 9. The count of SC energy modules containing at least one SC with a stored voltage exceeding 1.2 V, considering various capacitance standard deviations (10%, 15%, and 20%). Reported in **publication IV**.

	Std (10%)	**Std (15%)**	**Std (20%)**
Number of modules	1	12	31

For this statistical study, we present the distribution plots of the stored voltage across the SCs within an energy module, as depicted in Fig. 26. The distribution plots clearly illustrate a notable trend: the proportion of SCs with a voltage exceeding 1.2 V exhibits an upward trend with increasing capacitance std. In fact, in the case of a 20% std, the voltage of certain SCs may reach approximately 1.6 V.

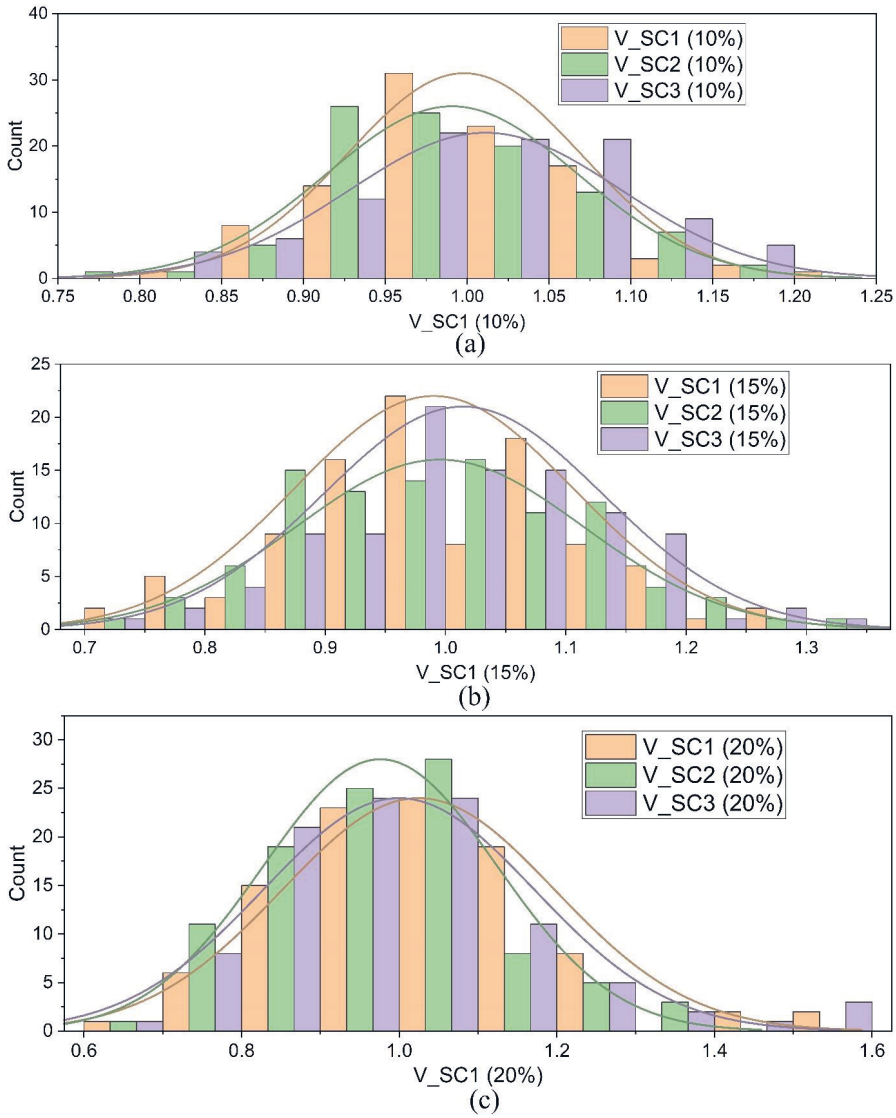

Fig. 26. Distribution plots of the stored voltage within a module SCs, with subplots (a, b, and c) representing different capacitance std of 10%, 15%, and 20% on the SCs' capacitance values, respectively. Adapted from **publication IV**.

5.4.2 STATISTICAL ANALYSIS OF CAPACITANCE STD IN SERIES-CONNECTED PRINTED SCS FOR CHARGING VOLTAGE OPTIMIZATION

Prior to applying a specific voltage to the energy storage module, it is prudent to employ statistical analysis to determine the maximum acceptable std of capacitance for the printed SCs connected in

series within the module. This determination ensures the protection of the energy storage systems from malfunctioning.

Our objective in **publication IV** is to establish the maximum allowable capacitance std for 300 printed SCs when configuring a three series-connected SC module, while applying a specific voltage ranging from 2.5 V to 3.5 V. The maximum allowed capacitance std is inversely related to the applied voltage. For instance, to safely store 3.5 V in the energy storage module, the maximum allowable capacitance std for the printed SCs should be 1.4%. However, when using 2.5 V, this can be increased up to 16.1%.

Furthermore, as depicted in Fig. 27, there exists a linear relationship with high accuracy (indicated by R-square values of the linear fit) between the maximum capacitance std and the total voltage stored in the module. As a result of this linear correlation, the following equation can be deduced:

$$C\text{-}Std_{max} = 54.61 - (15.2 \times V_T) \quad (8)$$

Where $C\text{-}Std_{max}$ represents the maximum allowable std for the capacitance of 300 printed SCs, and V_T represents the maximum voltage that can be safely stored across a three series-connected SC energy module.

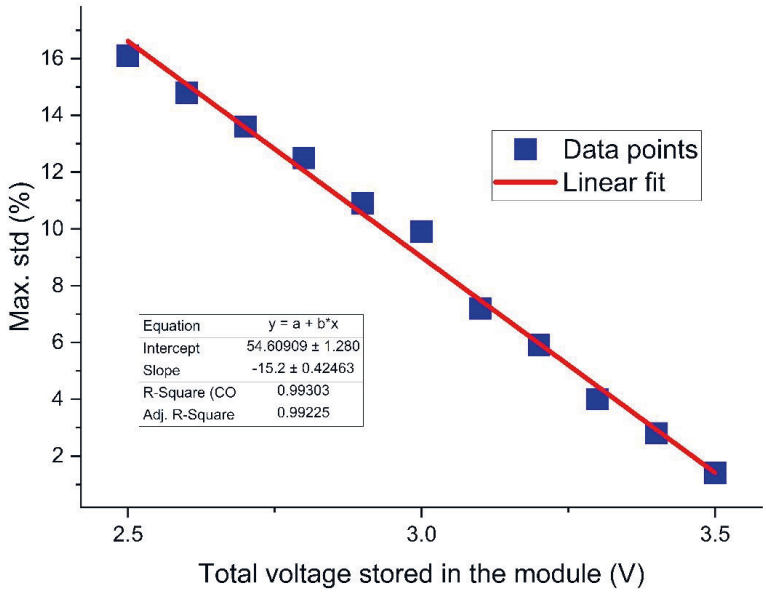

Fig. 27. The linear correlation between capacitance std and the total stored voltage in a series-connected SC module. Adapted from **publication IV**.

5.4.3 ENERGY WINDOW RANGE OF THE PRINTED SC MODULES

To ensure reliable operation during power outages or interruptions, accurately determining the energy output capacity of an energy storage module in various applications is essential. By considering the std

in the capacitance of printed SCs during mass production, statistical analysis can provide valuable insights into the energy window range of SC modules well before their deployment in applications. This knowledge of the energy range that a printed SC module can supply to a specific application facilitates energy management optimization, enhances system performance, extends the module's lifespan, reduces environmental impact, and ensures safe operation [219,220].

Equation (8) allows for the calculation of the maximum potential std of the capacitance of printed SCs within a module to ensure safe storage of a particular potential difference. In **publication IV**, our objective is to determine the energy window range for each module when forming 100 SC modules using 300 printed SCs and storing a specific voltage (ranging from 2.5 V to 3.5 V) within each module.

As shown in Fig. 28a, the energy window range of the three series-connected SC modules is observed when a potential difference of 2.5 V to 3.5 V is stored across the module. For instance, with a safe storage capacity of 3.5 V, the SC module can supply energy within the range of 358 to 370 mJ. However, if the safe storage capacity is reduced to 2.5 V, the SC module is expected to provide an energy output in the range of 125 to 225 mJ. This highlights that reducing the stored voltage in the module leads to an increased allowed std in the capacitance of the SCs, thereby widening the energy window of the module. Specifically, as shown in Fig. 28a, the energy window becomes wider from right to left as the voltage decreases. Nevertheless, it is important to acknowledge that higher voltage across the SC module results in a greater energy span within the module. However, in cases where SC modules hold lower stored voltage, a higher permissible std in capacitance values can lead to a broader energy span, rather than an increase in magnitude.

The integration of printed SC modules with integrated circuit (IC) chips represents a significant and promising advancement, enabling more compact and energy-efficient IC chip systems [221]. However, this integration comes with technical challenges that need to be addressed. One key challenge involves matching the voltage of the SC module with the operating voltage of the IC chip. Another challenge is to ensure that sufficient energy is supplied to meet the IC chip's operational requirements, while avoiding damage to the chip due to excessive voltage. The statistical analysis conducted in **publication IV** has provided some insights into addressing these concerns.

Additionally, considering the remaining energy window of a printed SC module after operating an IC chip is crucial. Computation of the remaining energy within the SC module can be done using Equation (9):

$$E = ½ \times C_{tot} \times (V^2_{module} - V^2_{app}) \quad (9)$$

where E is the remaining energy, C_{tot} is the total capacitance of the SC module, V_{module} is the stored voltage in the SC module, and V_{app} is the minimum operational voltage of the IC chip.

Modern IC chips generally operate at low voltages, typically around 2 V [222]. In this study, printed SC modules were assumed to power IC chips with three different operational voltages (1.8 V, 2 V, and 2.2 V). Fig. 28b, c, and d illustrate the remaining energy window range of three series-connected printed SC modules after operating IC chips at voltages of 1.8 V, 2 V, and 2.2 V, respectively, without recharging. Based on the analysis shown in Fig. 28b, c, and d, it can be concluded that when a printed SC module is charged up to 3.5 V and used to power IC chips with voltages of 1.8 V, 2 V, and 2.2 V, a remaining energy range of 263-273 mJ, 241-250 mJ, and 217-224 mJ, respectively, may still be available within the module. However, in the case of storing 2.5 V across the SC module, the remaining energy range after operating IC chips with voltages of 1.8 V, 2 V, and 2.2 V would be 75-109 mJ, 56-107 mJ, and 19-62 mJ, respectively. These energy window range values, obtained through statistical analysis, offer valuable information to system designers for selecting suitable energy modules and setting realistic expectations for the backup power supply duration.

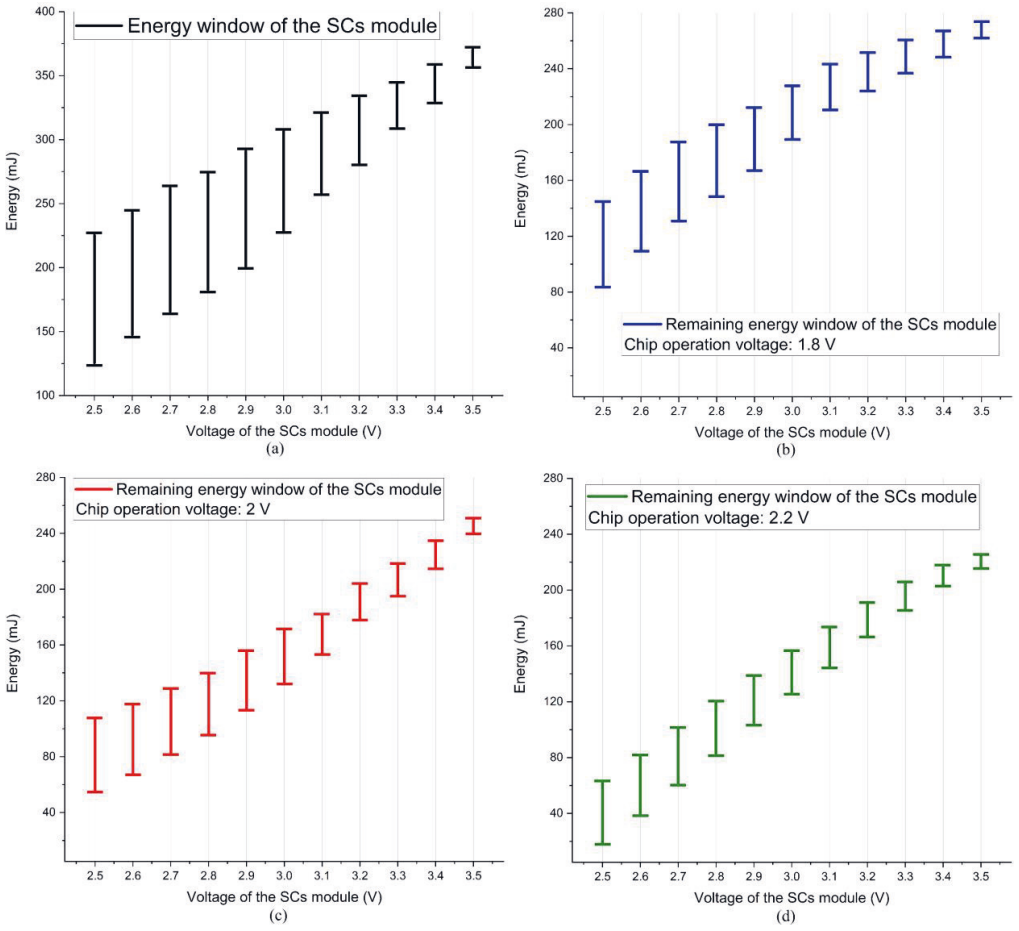

Fig. 28. a) Energy window range of a series-connected SC module with a potential difference of 2.5-3.5 V. b, c, d) Remaining energy window range of series-connected printed SC modules after operating IC chips at a voltage of b)1.8 V; c) 2 V; d) 2.2 V without recharge. Adapted from **publication IV**.

5.4.4 UTILIZING MC TO ANALYZE CHARGING AND DISCHARGING BEHAVIOR OF SC MODULE

To conduct the statistical analysis of the charge and self-discharge behavior of the printed SCs, Monte-Carlo (MC) simulation technique has been employed in **publication IV**. MC simulation method is a powerful technique capable of running a large number of simulations to produce an approximate range or distribution of potential outcomes [216].

The MC simulation method is based on constructing models that anticipate various results by substituting a range of values from a probability distribution for uncertain factors [217]. Probability distributions are employed to represent the potential values of uncertain inputs and their associated probabilities. Consequently, the system repeatedly calculates potential outcomes using diverse sets of randomly generated values from the probability functions. Beyond estimating the probabilities of

different outcomes, researchers can perform a wide array of additional analyses based on this data of potential results.

Compared to traditional "best/worst/most likely" guess analyses, MC simulation offers superior realism in representing uncertainty in variables through probability distributions. This characteristic makes it a highly valuable tool in the field of PE, significantly expediting the research process and leading to substantial savings in time, energy, and expensive materials. By obviating the need to fabricate large quantities of devices, the MC method proves to be an advantageous approach in the context of PE investigations.

Fig. 29a depicts the charging ECM of a SC module comprising three printed SCs connected in series and charging up to 3 V. Fig. 29b illustrates the discharge ECM of the SC module. To model the initial potential difference of the SCs during discharging, a switch and a DC voltage source are employed for each SC. The value of the DC voltage source is determined using capacitive voltage division of the three SCs.

In order to utilize MC simulation, defining various variables in an ECM is required, along with their distribution, mean value, and std. The four ECMs proposed in **publication III** have different numbers of variables for each single SC (see Fig. 17a). ECM1 has four variables (C, ESR, a, and b), ECM2 has three variables (C, ESR, and b), and ECMs 3 and 4 have two variables each (only C and ESR). Furthermore, **publication IV** employs 12 printed SC parameters for conducting MC simulations, with all four parameters of the SCs following a normal distribution. Table 10 provides a summary of the EPR function for each ECM, along with the variables included in each ECM and their respective mean value (M) and std (the abbreviation 'N/A' indicates that the specific variable is not applicable to the corresponding ECM). In **publication IV**, the charging and discharging behavior of the printed SC module is analyzed through 100 trials conducted using the MC simulation tool.

Table 10. Overview of variables of ECMs, elements of EPR functions, mean value (M), and std. Reported in **publication IV**.

Variables / **ECMs**	**C (mF)**	**ESR (Ω)**	**a**	**b**
ECM 1 EPR: $I = e^{(a + b \times V)}$	M: 179.0 Std: 7.18	M: 7.7 Std: 0.92	M: -35.6 Std: 2.21	M: 20.0 Std: 2.07
ECM 2 EPR: $I = e^{(-22 + b \times (V - 0.7))}$			N/A	
ECM 3 EPR: $I = e^{(-28 - 45 \times C + V \times (64 \times C + 9))}$				N/A
ECM 4 EPR: $I = e^{(-36.5 + 20.4 \times V)}$				

Fig. 29c and 29d illustrate the charging behavior of an individual SC (SC 1) and the entire module. The charging profiles of the three printed SCs show a remarkable similarity. However, none of the SCs reaches a charging voltage of 1.2 V. The observed similarity in charging behavior and the consistent maintenance of charging voltage below 1.2 V for each individual SC can be attributed to two factors. Firstly, the printed SCs have low std in capacitance and ESR values, which are 7.18% and 0.92%,

respectively. As previously discussed in this article, this ensures the safe storage of each individual printed SC within the three series-connected SC module when connected to a 3 V power source, as long as the capacitance standard deviation remains below 9.9%. Secondly, as demonstrated in **publication I**, the charging behavior of SCs is minimally affected by the EPR when the charging current is excessively high.

Furthermore, Fig. 29d illustrates the charging behavior of the entire module, which stores 3 V in approximately 10 seconds.

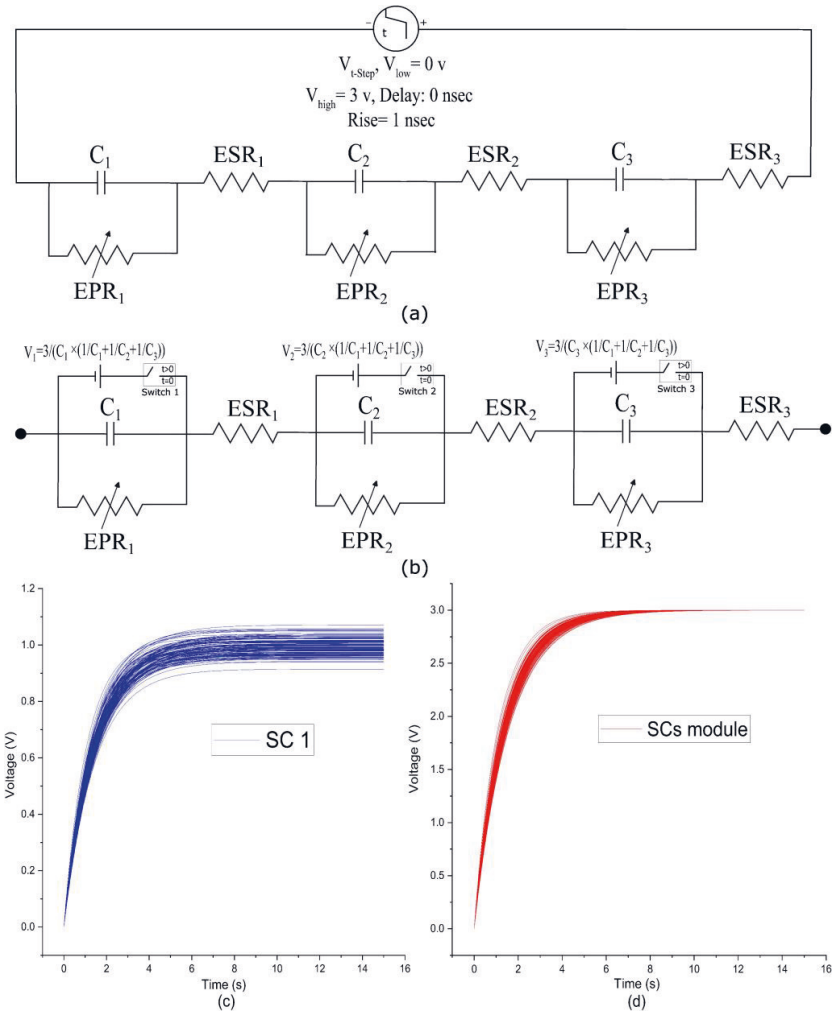

Fig. 29. a) ECM depicting the charging of a three series-connected SC module. b) ECM illustrating the discharging of a three series-connected SC module. c) Charging characteristics of individual SCs within an SC module. d) Charging behavior of the entire SC module. Adapted from **publication IV**.

Fig. 30 and 31 depict the 31-day simulated self-discharge characteristics of an individual SC within the module (SC 1) and the entire three series-connected SC energy module, respectively, using four ECMs through the MC simulation. The figures clearly show that ECM 1 predicts the broadest range of results on day 31, while ECM 3 and 4 predict the narrowest range. This difference is due to the application of the MC tool on four variables in ECM 1 and only two variables in ECM 3 and 4. Nevertheless, ECM

3 and ECM 4 are likely to produce the most probable final outcomes, as their ranges fall within the highest data concentration observed for ECM 1. Employing ECM 1, the SC energy storage module is projected to retain a minimum of 1.87 V power after 31 days of self-discharge in the worst-case scenario, while the best-case scenario anticipates a maximum of 2.89 V power on the 31st day. ECM 2 predicts a module energy range between 2.41 and 2.56 V, whereas ECM 3 and 4 provide a narrower range, approximately 2.40 to 2.43 V. These numerical values suggest that the final results from ECM 3 and ECM 4 are roughly equivalent to the average value of the final results generated by ECM 1.

The same pattern in results is evident when examining the simulation outcomes for a single SC over a 31-day period. MC simulation results using ECM1 yield a broader voltage range at the conclusion of day 31 (0.44 V - 1.03 V), as can be seen in Fig. 30a. In contrast, the result ranges for ECM 2, 3, and 4 are 0.78-0.90, 0.80-0.81, and 0.82-0.83, respectively (Fig. 30 c, 31a, and 31c). It is once again noteworthy that the reduction in the window range from ECM 1 to ECM 4 is attributed to the smaller number of parameters in ECM 3 and 4 (2 parameters) utilized by the MC simulation tool, compared to ECM 1, which employs four parameters. Nevertheless, ECM 3 and ECM 4 are likely to generate the most probable final outcomes for a single SC, as their ranges align within the highest concentration of observed data for ECM 1.

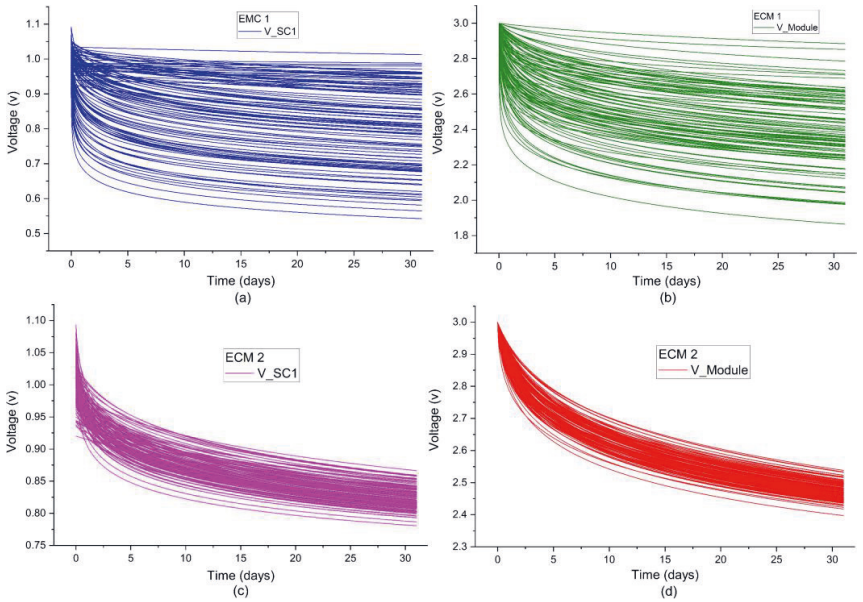

Fig. 30. MC simulated long-term (31 days) self-discharge behavior of individual SCs and the entire series-connected SC energy module using ECM 1 (a, b) and ECM 2 (c, d). Adapted from **publication IV**.

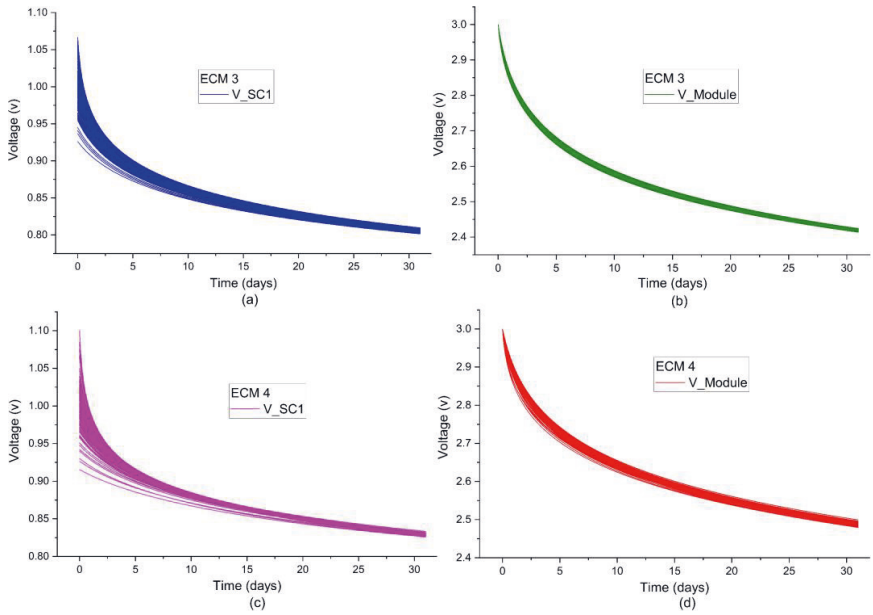

Fig. 31. MC simulated long-term (31 days) self-discharge behavior of individual SCs and entire series-connected SC energy module using ECM 3 (a,b) and ECM 4 (c,d). Adapted from **publication IV**.

5.5 INTEGRATION OF SUPERCAPACITORS TO TRIGGER IN-SITU ELECTROPOLYMERIZATION FOR IRREVERSIBLE VISUAL INDICATORS

Electrochromic indicators and displays have gained commercial interest in various sectors, including logistics, retail, and healthcare, as they provide a dynamic means of conveying information [223]. Traditional methods for producing electrochromic displays involve depositing or coating the chromogenic material during the manufacturing process. However, researchers have proposed the concept of 'in-situ' electropolymerization as a simpler approach for fabricating electrochromic displays [224-227]. With this technique, an electrochromic polymer is formed inside the display electrochemically after the device has been fully manufactured.

While in-situ electropolymerization has been successfully demonstrated for generating electrochromic displays with conventional reversible cycling [228], it can also be utilized to create Irreversible Electrochromic visual Indicators (IVIs). These indicators find applications in scenarios like spoilage labels or tamper labels, where a prominent color change is required that cannot be reversed, as shown in Fig. 32. For commercial application of IVIs, integration with a switching circuit and a power source is necessary to trigger the electropolymerization reaction during use.

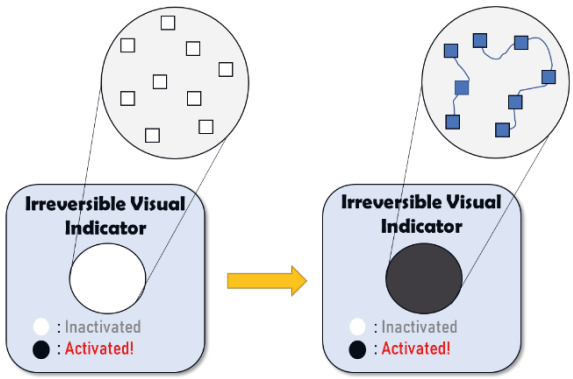

Fig. 32. Schematic representation of an irreversible visual indicator achieved through electropolymerization. Reprinted from **publication V** with permission.

Previous studies [229] have shown reversible switching of electrochromic displays using SC. However, electropolymerization demands a significantly higher voltage and charge compared to reversible redox switching of the corresponding homopolymer.

In **publication V**, printed SCs are employed to trigger in-situ electropolymerization of devices utilizing four different monomer systems: 3,4-Ethylenedioxythiophene (EDOT), bis-3,4-Ethylenedioxythiophene (BiEDOT), 2,2'-Bithiophene (bithiophene), and 2,2':5',2"-Terthiophene (terthiophene). These monomer systems are selected because they offer a wide range of activation potentials (Ea) and coloration efficiencies (CEs). Ea refers to the voltage or potential difference that needs to be applied to an electrochromic material or device to initiate a change in its optical properties. Ea is influenced by the electrochemical properties of the materials used in the electrochromic system, as well as the design and configuration of the device. CE in electrochromics refers to the effectiveness of a material or device in changing its color in response to an applied voltage or electrical stimulus. CE is typically measured in terms of the change in optical density or absorbance per unit change in voltage or current. The results of activation using the printed SCs are evaluated and compared to a 3 V coin-cell battery. Overall, the study finds that for monomer systems with high CE, SCs can provide sufficient voltage and charge to fully activate 1 x 1 cm2 indicators, making them a promising candidate for activating in-situ electropolymerization indicators.

5.5.1 MEASUREMENTS

Optical spectroscopy was conducted using an Agilent Cary 300 UV-Vis Spectrophotometer to assess the activation of the indicators. The activation process was monitored by measuring the transmittance at 555 nm, which corresponds to the peak of human photopic vision. Potentiostatic and cyclic voltammetric measurements were carried out using an AUTOLAB PGSTAT100N potentiostat. The voltage of the SCs was measured using a FLUKE® 115 handheld multimeter digital CAT III 600 V display, which provides a resolution of 6000 counts. Fig. 33 shows the measurement set-up schematically.

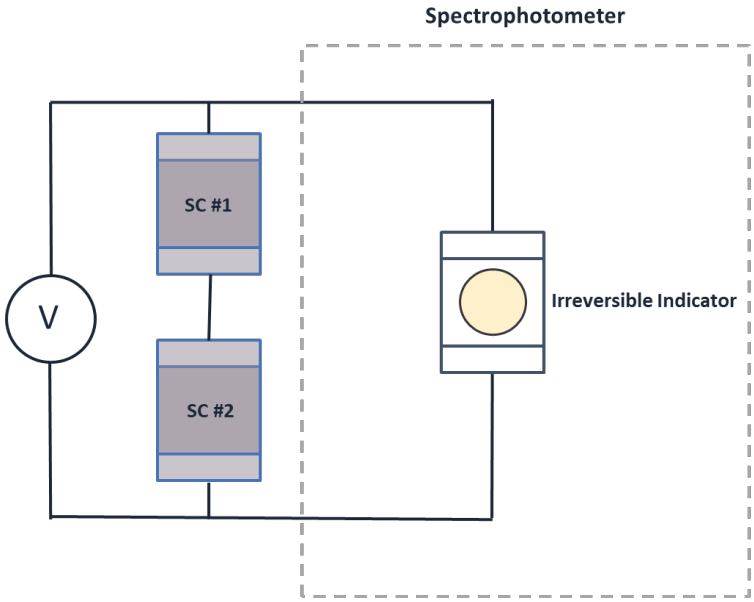

Fig. 33. Schematic of experimental set-up for activation of IVIs using series-connected SCs. Reprinted from **publication V** with permission.

5.5.2 ELECTRICAL AND OPTICAL CHARACTERIZATION OF IVI SYSTEMS

Two crucial electrical properties essential for IVIs are Ea and CE. The Ea of an IVI primarily depends on the oxidation potential of the monomer system, while the CE is mainly influenced by the number of electrons transferred in each cross-linking step [230], along with the length and absorptivity of the resulting polymer. However, additional parameters such as the solvent, salt, monomer concentration, and electrical activation protocol can also impact these values. A summary of the Ea and CE for all four monomers is presented in Table 11. Increasing the conjugation length of a monomer species results in a decrease in the oxidation potential, thereby reducing the number of cross-linking steps required to form the same polymer length. Consequently, the CE of BiEDOT compared to EDOT and TerThiophene compared to BiThiophene is more than double, while the Ea shows a decrease of 0.5 and 0.3 V, respectively.

Table 11. Electrical characteristics of irreversible indicators using various monomer systems. Reported in **publication V**.

Monomer System	Activation Potential (V)	Coloration Efficiency (Cm2/C)
EDOT	2.5	9
BiEDOT	2.0	24
BiThiophene	2.6	21
TerThiophene	2.3	49

5.5.3 ACTIVATION OF IVIS WITH SCS AND COIN-CELL BATTERY

All four IVI systems underwent activation using two and three SCs connected in series. Simultaneous recording of transmittance across the IVIs and voltage across the SCs was performed, and the results are depicted in Fig. 34. In the series connection with IVIs, if the potential of the SCs (E_0) exceeds the activation potential (Ea) of the IVI, in-situ polymerization is initiated. The film-forming process proceeds as the SC module discharges until the module's voltage drops below the Ea of the IVI. At this point, the potential is insufficient to further oxidize monomers within the IVI and sustain the electropolymerization reaction.

While both two and three SCs in series possess a sufficiently high E_0 to initiate activation with EDOT, the low CE of EDOT (9 cm^2/C) requires the use of three SCs in series to achieve full IVI activation with $\Delta T > 80\%$. With only two SCs, a ΔT of only 55% is achieved. Similarly, BiThiophene requires three SCs for full activation, resulting in a ΔT of 33% with only two SCs. Both BiEDOT and TerThiophene can be fully activated with either two or three SCs in series.

For all tested monomer systems, activation using three SCs demonstrates faster kinetics compared to two SCs, as the speed is dependent on the voltage. Additionally, Fig. 34 includes transmittance data for activation using a 3 V coin-cell battery, illustrating that SCs could serve as an alternative to coin-cell batteries in light-harvesting modules for labeling purposes. Nonetheless, although this thesis lacks a cost analysis for this category of printed SCs, it is essential to recognize that the manufacturing cost for such printed SCs in a laboratory environment would likely exceed that of commercial coin cell batteries. Nevertheless, it is worth noting that by transitioning the fabrication process of these printed SCs to extensive roll-to-roll and sheet-to-sheet manufacturing lines, the overall manufacturing cost for these printed SCs could potentially be comparable to or lower than that of commercial coin cell batteries.

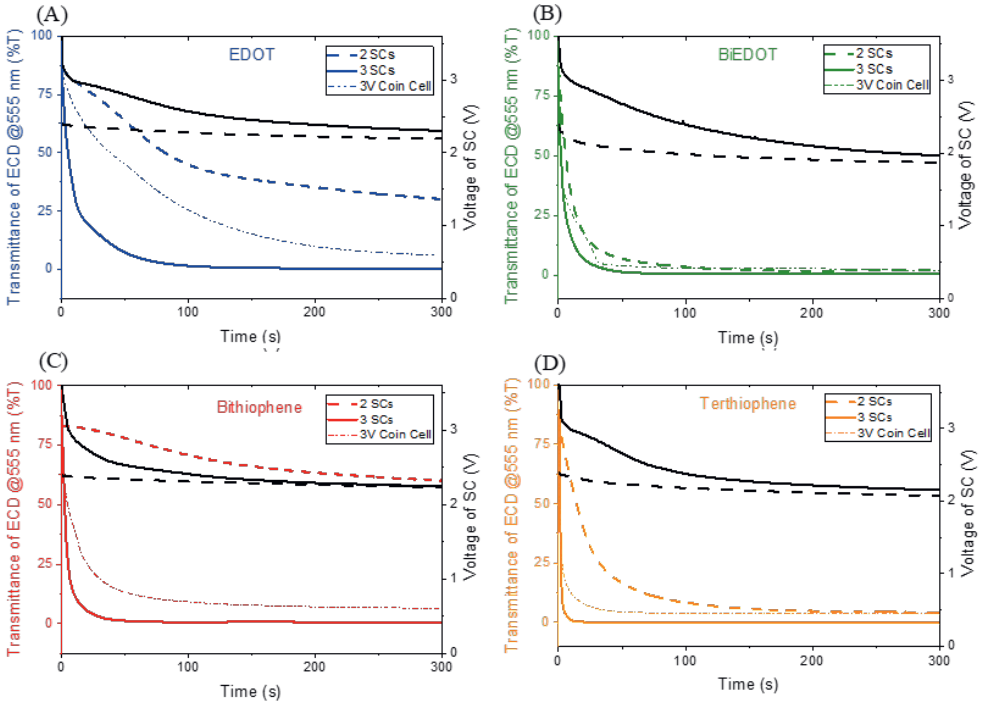

Fig. 34. Transmittance of IVIs during activation using two SCs, three SCs, and a 3 V coin-cell battery for (A) EDOT, (B) BiEDOT, (C) BiThiophene, and (D) TerThiophene. The right y-axis displays the voltage of the SCs during activation. The black solid lines and the black dashed lines represent the voltage of three and two series-connected SCs during activation, respectively. Reprinted from **publication V** with permission.

6- SUMMARY AND CONCLUSION

In summary, this thesis introduces numerical exponential methods to characterize the nonlinear phenomena of self-discharge and leakage current in printed SCs by utilizing experimental electrical parameters. Improved ECMs are presented, derived from experimentally determined quantities of individual devices. Notably, existing ECMs in the literature, such as the two-branch model with EPR, three-branch model, and VLR models, feature multiple branches and numerous RC network elements. However, practical applications demand simplified versions for efficient model implementation. Specifically, the exponential EPRs employing VLR published in the literature use several distinct exponential functions to capture the short-term (several hours) self-discharge behavior of a single SC. Consequently, to simulate the long-term (31 days) self-discharge behavior of energy modules comprising multiple SCs connected in series, an extensive number of exponential functions and parameter definitions are necessary when employing literature-reported exponential models. Despite their complexity, these ECMs are unsuitable for long-term SC module simulations due to the need for simplicity in practical applications.

In contrast, the proposed ECMs consist of only one branch and a few RC elements (only 3), making them more straightforward for use in energy storage modules with multiple SCs in series. Additionally, unlike the literature ECMs using a VLR with an exponential voltage/time profile, the ECMs in this thesis utilize a VLR with an exponential current/voltage profile. The method for obtaining these profiles differs, relying on experimental data of SCs' self-discharge over an extended period (31 days). Furthermore, the proposed ECMs in this thesis do not differentiate between various self-discharge mechanisms. Instead, single VLRs with exponential current/voltage profiles are introduced to account for the effects of different self-discharge mechanisms under normal operating conditions.

Furthermore, unlike literature ECMs, which lack accuracy in simulating the nonlinear self-discharge effect of SCs over the long term, the super-simple ECMs proposed in this thesis demonstrate high accuracy in predicting the discharge behavior of printed SCs in both self-discharge and load-connected modes over an extended period (31 days). Various approaches, including the use of a single SC or three series-connected SC energy modules, were employed to verify the accuracy of the proposed ECMs, and excellent agreements were found.

Additionally, the proposed ECMs predict how the operation of series-connected modules depends on variations in electrical properties from device to device, a crucial consideration in printed devices. In essence, beyond modeling the full charging and discharging behavior of SCs, the ECMs can be employed to investigate the impact of device-to-device variations in electrical parameters, particularly the nonlinear nature of leakage current and self-discharge, on the behavior of series-connected SCs in energy modules.

Moreover, in this thesis, a thorough statistical analysis of printed SCs using proposed ECMs revealed a normal distribution for key parameters. A novel method was introduced to determine the maximum potential std in capacitance, preventing SCs from exceeding the electrolyte's electrochemical potential window and ensuring safe operation. A strong linear relationship was found between applied voltage and capacitance std in series-connected SC energy storage modules. Additionally, a statistical method predicted the energy window post-IC chip operation, aiding in performance optimization and system reliability. Monte-Carlo simulations confirmed consistent charging behavior as long as std remains below a threshold, offering insights into real-world power variations over 31 days.

As a practical application for printed SCs, this thesis demonstrated the effective activation of in-situ polymerization-based intelligent irreversible visual indicators (IVIs) by printed SCs, suggesting their potential in the smart label market. BiEDOT and TerThiophene IVI systems showed promise, but long-term stability requires further investigation. Optimization possibilities include adjusting working area size and monomer concentration. Future work aims to integrate these elements into a flexible substrate prototype for the cold-chain market.

In brief, the present Ph.D. thesis embarked on a comprehensive investigation of SCs' discharging behavior, addressing challenges related to leakage current and self-discharge in various applications. The primary focus was to develop improved exponential models and statistical analysis techniques to enhance the accuracy and practicality of simulating SC performance over extended time periods.

Once more, we revisit the research questions and provide responses to them:

1. How can we develop an accurate exponential model to predict the charging, discharging, leakage current, and self-discharge behavior of series-connected SC modules, considering both short-term and long-term performance in various IoT applications?

Publication I, II, and **III** answered this question. Developing an accurate exponential model to predict the behavior of series-connected SC modules requires a comprehensive approach that considers both short-term and long-term performance in diverse IoT applications. By integrating experimental data from printed SCs, this research seeks to refine the exponential model to accurately depict charging, discharging, leakage current, and self-discharge behaviors. The model's effectiveness was evaluated across different operational conditions in long-term to ensure its applicability in real-world scenarios. Ultimately, this endeavour aims to enhance the predictability and optimization of SC performance in the dynamic context of IoT devices.

2. Can an empirical exponential equivalent circuit model effectively capture the complex interactions between leakage current, self-discharge, and nonlinear behavior in SCs, and how well does it compare with existing models?

Publication I, II, and **III** answered this question. The investigation into the empirical exponential ECM's efficacy in capturing the intricate interactions between leakage current, self-discharge, and nonlinear behavior within SCs is a critical pursuit. By leveraging experimental results and comparing the proposed ECMs with existing alternatives, this research aims to determine the model's accuracy and comprehensiveness. Understanding the strengths and limitations of this model in representing the complex interplay of factors will shed light on its potential for advancing our understanding of SC behavior and optimizing their performance across various applications.

3. Through statistical analysis, how can we estimate and predict the dynamic leakage current and self-discharge behavior during repeated charging and discharging for IoT applications, ensuring safe operation and determining energy storage module performance with an acceptable standard deviation range?

Publication IV answered this question. Estimating and predicting dynamic leakage current and self-discharge behavior during repeated charging and discharging cycles for IoT applications is a multifaceted challenge. Employing advanced statistical analysis techniques, this study seeks to develop a robust methodology to assess the uncertainty associated with these behaviors. By establishing acceptable standard deviation ranges and integrating them into energy storage module performance evaluation, researchers aim to ensure safe and reliable operation while accommodating the inherent variability of SCs. This endeavor contributes to the development of dependable energy management strategies in IoT environments.

4. What is the impact of different monomer systems and key parameters on the activation of Irreversible Visual Indicators (IVIs) based on printed SCs, and can series-connected SCs achieve full activation of IVIs, thereby enabling irreversible visual indicators for various applications?

Publication V answered this question. Examining how various monomer systems and critical factors influence the activation of Irreversible Visual Indicator (IVI) by printed SCs unveils opportunities for pioneering applications. By systematically investigating the activation potential, coloration efficiency (CE), and other influencing factors, researchers aim to elucidate the underlying mechanisms. Additionally, assessing whether series-connected SCs can achieve full IVI activation across various monomer systems enhances our understanding of this technology's versatility. Ultimately, this research paves the way for deploying IVIs in diverse scenarios, leveraging the potential of printed SCs for unique and practical applications.

In conclusion, this Ph.D. thesis has made significant contributions to the understanding and practical implementation of SCs in a low-power application. The developed exponential models and statistical analysis techniques provide accurate predictions for SC behavior, aiding in system design, performance optimization, and risk assessment. The findings hold potential for energy autonomous IoT devices, energy-harvesting wireless sensor nodes, wearable self-charging power systems, and smart label applications. The simplicity and accuracy of the proposed models enable their use in practical scenarios, paving the way for more efficient and sustainable energy solutions. By answering the research questions outlined in the introduction, this thesis has contributed valuable insights to the field of SCs research and opened new avenues for future exploration.

However, this study suggests several potential avenues for future research and development:

Focusing on the practical implementation of findings from this work in large-scale manufacturing. Particularly, in the context of cost-effective production methods such as roll-to-roll and sheet-to-sheet techniques, leveraging the insights from this model could significantly optimize the manufacturing and testing processes. Exploring how printing technologies can be employed for the efficient fabrication of interconnected series SCs at scale holds great potential for advancing the field and facilitating the widespread adoption of printed energy storage devices.

Model Refinement: The proposed exponential models for SCs' charging and discharging behavior can be further refined and validated with experimental data from different types of SCs and energy modules. More sophisticated mathematical and statistical techniques can be explored to improve the accuracy of the models.

Advancing SC modelling: Evaluating the precision of the proposed ECMs in testing them with larger SCs modules and expanding the analysis to encompass modules with tens of printed SCs connected in series. This provides a more complex and realistic scenario, enabling exploration of scalability, performance limits, and optimization challenges.

Monte Carlo Simulation: The use of Monte Carlo simulations can be expanded to explore the robustness and reliability of printed SC energy storage systems under various operating conditions and uncertainties. This will provide a deeper understanding of the system's performance and potential risks.

Verification of the Monte Carlo Results: Experimental validation of the Monte-Carlo results for a limited number of SCs (20) can provide valuable insights into the accuracy of the simulations. By focusing on a representative subset, the experimental efforts are more manageable while still offering meaningful validation of the Monte Carlo outcomes. This approach allows for a more practical and resource-efficient assessment of the simulation results.

Exploring the stability of series-connected heterogeneous printed SCs during cyclic operation. Investigating the system's behavior under repeated charge and discharge cycles is crucial for understanding potential voltage differences between individual series-connected printed SCs over numerous cycles, thereby enhancing practical implementation.

New Material Characterization: Investigate new materials and fabrication techniques for SCs to enhance their performance, reduce self-discharge rates, and improve energy storage capacity. Characterizing the electrochemical properties of these new materials will be crucial for modeling and practical applications.

Integration with IoT Devices: Further research can be done on integrating SCs into IoT devices, such as wireless sensors and wearables. Optimization of power management strategies, considering the variability in leakage current and self-discharge, will enhance the efficiency and longevity of these IoT devices.

Application-Specific Studies: Conduct application-specific studies to evaluate the suitability of SCs in various fields, such as smart labels, cold-chain monitoring, and energy-harvesting systems. Assess the practical challenges and potential benefits for each application.Printed Electronics Optimization: Explore the optimization of printed electronics manufacturing processes to achieve better uniformity and reproducibility of SCs. This will reduce device-to-device variations and enhance the overall performance of energy modules.

New Energy Storage Concepts: Investigate hybrid energy storage systems that combine SCs with other energy storage technologies, such as batteries or fuel cells. Such systems can offer improved energy density and extended lifespan.

Real-World Performance Testing: Conduct extensive real-world testing of SC energy storage systems in different environments and operating conditions to validate their performance and reliability. Long-term field tests will provide valuable insights into practical applications.

Environmental Impact Assessment: Evaluate the environmental impact of printed SCs and their manufacturing processes. Identify potential improvements in materials and production techniques to enhance sustainability.

Cost-Effectiveness Analysis: Perform a cost-effectiveness analysis to determine the economic feasibility of integrating printed SCs in various energy storage systems. This will help identify potential markets and commercialization opportunities.

To conclude, continuing this research will not only advance the understanding of SC behavior but also contribute to the development of efficient and sustainable energy storage solutions for a wide range of applications. The proposed ECMs and statistical analysis techniques open up new possibilities for practical implementation and optimization of SC-based energy storage systems.

7- REFERENCES

[1] Kalyani, Vijay Laxmi, Manisha Kumari Dudy, and Shikha Pareek. "Green energy: The need of the world." Journal of Management Engineering and Information Technology 2, no. 5 (2015): 18-26.

[2] Kalair, Anam, Naeem Abas, Muhammad Shoaib Saleem, Ali Raza Kalair, and Nasrullah Khan. "Role of energy storage systems in energy transition from fossil fuels to renewables." Energy Storage 3, no. 1 (2021): e135.

[3] Tan, Darren HS, Panpan Xu, and Zheng Chen. "Enabling sustainable critical materials for battery storage through efficient recycling and improved design: A perspective." MRS Energy & Sustainability 7 (2020): E27.

[4] Shakib, Mohammed, Hou Yumei, Abdul Rauf, Mahmudul Alam, Muntasir Murshed, and Haider Mahmood. "Revisiting the energy-economy-environment relationships for attaining environmental sustainability: evidence from Belt and Road Initiative countries." Environmental Science and Pollution Research 29, no. 3 (2022): 3808-3825.

[5] do Nascimento, Álvaro Della Justina, and Ricardo Rüther. "Evaluating distributed photovoltaic (PV) generation to foster the adoption of energy storage systems (ESS) in time-of-use frameworks." Solar Energy 208 (2020): 917-929.

[6] Sánchez-Díez, Eduardo, Edgar Ventosa, Massimo Guarnieri, Andrea Trovò, Cristina Flox, Rebeca Marcilla, Francesca Soavi, Petr Mazur, Estibaliz Aranzabe, and Raquel Ferret. "Redox flow batteries: Status and perspective towards sustainable stationary energy storage." Journal of Power Sources 481 (2021): 228804.

[7] Zhang, Ziyu, Tao Ding, Quan Zhou, Yuge Sun, Ming Qu, Ziyu Zeng, Yuntao Ju, Li Li, Kang Wang, and Fangde Chi. "A review of technologies and applications on versatile energy storage systems." Renewable and Sustainable Energy Reviews 148 (2021): 111263.

[8] Khanna, Abhishek, and Sanmeet Kaur. "Internet of things (IoT), applications and challenges: a comprehensive review." Wireless Personal Communications 114 (2020): 1687-1762.

[9] Ahmed, Abdelsalam, Islam Hassan, Maher F. El-Kady, Ali Radhi, Chang Kyu Jeong, Ponnambalam Ravi Selvaganapathy, Jean Zu, Shenqiang Ren, Qing Wang, and Richard B. Kaner. "Integrated triboelectric nanogenerators in the era of the internet of things." Advanced Science 6, no. 24 (2019): 1802230.

[10] Pu, Xiong, Weiguo Hu, and Zhong Lin Wang. "Toward wearable self-charging power systems: the integration of energy-harvesting and storage devices." Small 14, no. 1 (2018): 1702817.

[11] Wang, Zhuo, Shuncheng Yao, Shaobo Wang, Zhirong Liu, Xingyi Wan, Quanhong Hu, Yunchao Zhao, Cheng Xiong, and Linlin Li. "Self-powered energy harvesting and implantable storage system based on hydrogel-enabled all-solid-state supercapacitor and triboelectric nanogenerator." Chemical Engineering Journal 463 (2023): 142427.

[12] Dong, Kai, and Zhong Lin Wang. "Self-charging power textiles integrating energy harvesting triboelectric nanogenerators with energy storage batteries/supercapacitors." Journal of Semiconductors 42, no. 10 (2021): 101601.

[13] Sheng, Feifan, Bo Zhang, Renwei Cheng, Chuanhui Wei, Shen Shen, Chuan Ning, Jun Yang, Yunbing Wang, Zhonglin Wang, and Kai Dong. "Wearable energy harvesting-storage hybrid textiles as on-body self-charging power systems." Nano Research Energy (2023).

[14] Sahoo, Surjit, Satyajit Ratha, Chandra Sekhar Rout, and Saroj Kumar Nayak. "Self-charging supercapacitors for smart electronic devices: A concise review on the recent trends and future sustainability." Journal of Materials Science 57, no. 7 (2022): 4399-4440.

[15] Kwon, O. Hyeon, Jun Ryu, Ji Hye Lee, Hee Woong Kim, Jung Sang Cho, Sang Mun Jeong, Dong-Won Kang, and Jae-Kwang Kim. "Stretchable self-charging energy integrated device of high storage efficiency." Journal of Power Sources 525 (2022): 231079.

[16] Tang, Qian, Hengyu Guo, Peng Yan, and Chenguo Hu. "Recent progresses on paper-based triboelectric nanogenerator for portable self-powered sensing systems." EcoMat 2, no. 4 (2020): e12060.

[17] Acar, Canan. "A comprehensive evaluation of energy storage options for better sustainability." International Journal of Energy Research 42, no. 12 (2018): 3732-3746.

[18] Ibrahim, Hussein, Adrian Ilinca, and Jean Perron. "Energy storage systems—Characteristics and comparisons." Renewable and sustainable energy reviews 12, no. 5 (2008): 1221-1250.

[19] Jinitha, C. G., S. Virgin Jeba, S. Sonia, and Rajendran Ramachandran. "Fundamentals of supercapacitors." In Smart Supercapacitors, pp. 83-100. Elsevier, 2023.

[20] Kumar, Niraj, Su-Bin Kim, Seul-Yi Lee, and Soo-Jin Park. "Recent advanced supercapacitor: a review of storage mechanisms, electrode materials, modification, and perspectives." Nanomaterials 12, no. 20 (2022): 3708.

[21] Patra, Abhinandan, K. Namsheer, Jeena Rose Jose, Surjit Sahoo, Brahmananda Chakraborty, and Chandra Sekhar Rout. "Understanding the charge storage mechanism of supercapacitors: in situ/operando spectroscopic approaches and theoretical investigations." Journal of Materials Chemistry A 9, no. 46 (2021): 25852-25891.

[22] Yadlapalli, Ravindranath Tagore, RamaKoteswara Rao Alla, Rajani Kandipati, and Anuradha Kotapati. "Super capacitors for energy storage: Progress, applications and challenges." Journal of Energy Storage 49 (2022): 104194.

[23] Raghavendra, Kummara Venkata Guru, Rajangam Vinoth, Kamran Zeb, Chandu VV Muralee Gopi, Sangaraju Sambasivam, Madhusudana Rao Kummara, Ihab M. Obaidat, and Hee Je Kim. "An intuitive review of supercapacitors with recent progress and novel device applications." Journal of energy storage 31 (2020): 101652.

[24] Kularatna, Nihal, and Dilini Jayananda. "Supercapacitor-based long time-constant circuits: A unique design opportunity for new power electronic circuit topologies." IEEE Industrial Electronics Magazine 14, no. 2 (2020): 40-56.

[25] Pershaanaa, M., Shahid Bashir, S. Ramesh, and K. Ramesh. "Every bite of Supercap: A brief review on construction and enhancement of supercapacitor." Journal of Energy Storage 50 (2022): 104599.

[26] Sharma, Priyanka, and Vinod Kumar. "Current technology of supercapacitors: A review." Journal of Electronic Materials 49, no. 6 (2020): 3520-3532.

[27] Goodenough, John B., and Kyu-Sung Park. "The Li-ion rechargeable battery: a perspective." Journal of the American Chemical Society 135, no. 4 (2013): 1167-1176.

[28] Revankar, Shripad T. "Chemical energy storage." In Storage and Hybridization of Nuclear Energy, pp. 177-227. Academic Press, 2019.

[29] Minakshi, Manickam, and Kethaki Wickramaarachchi. "Electrochemical aspects of supercapacitors in perspective: From electrochemical configurations to electrode materials processing." Progress in Solid State Chemistry (2023): 100390.

[30] Kim, Brian Kihun, Serubbable Sy, Aiping Yu, and Jinjun Zhang. "Electrochemical supercapacitors for energy storage and conversion." Handbook of clean energy systems (2015): 1-25.

[31] Libich, Jiří, Josef Máca, Jiří Vondrák, Ondřej Čech, and Marie Sedlaříková. "Supercapacitors: Properties and applications." Journal of energy storage 17 (2018): 224-227.

[32] Sun, Tao, Jian Xie, Wei Guo, Dong-Sheng Li, and Qichun Zhang. "Covalent–organic frameworks: advanced organic electrode materials for rechargeable batteries." Advanced Energy Materials 10, no. 19 (2020): 1904199.

[33] Sauerteig, Daniel, Nina Hanselmann, Arno Arzberger, Holger Reinshagen, Svetlozar Ivanov, and Andreas Bund. "Electrochemical-mechanical coupled modeling and parameterization of swelling and ionic transport in lithium-ion batteries." Journal of Power Sources 378 (2018): 235-247.

[34] Popp, Hartmut, Markus Koller, Marcus Jahn, and Alexander Bergmann. "Mechanical methods for state determination of Lithium-Ion secondary batteries: A review." Journal of Energy Storage 32 (2020): 101859.

[35] Molahalli, Vandana, K. Chaithrashree, Muskan Kumari Singh, Manica Agrawal, Syam G. Krishnan, and Gurumurthy Hegde. "Past decade of supercapacitor research–Lessons learned for future innovations." Journal of Energy Storage 70 (2023): 108062.

[36] Olabi, Abdul Ghani, Qaisar Abbas, Pragati A. Shinde, and Mohammad Ali Abdelkareem. "Rechargeable batteries: Technological advancement, challenges, current and emerging applications." Energy (2022): 126408.

[37] Barcellona, Simone, Silvia Colnago, Giovanni Dotelli, Saverio Latorrata, and Luigi Piegari. "Aging effect on the variation of Li-ion battery resistance as function of temperature and state of charge." Journal of Energy Storage 50 (2022): 104658.

[38] Bin, Duan, Fei Wang, Andebet Gedamu Tamirat, Liumin Suo, Yonggang Wang, Chunsheng Wang, and Yongyao Xia. "Progress in aqueous rechargeable sodium-ion batteries." Advanced Energy Materials 8, no. 17 (2018): 1703008.

[39] Nadeem, Furquan, SM Suhail Hussain, Prashant Kumar Tiwari, Arup Kumar Goswami, and Taha Selim Ustun. "Comparative review of energy storage systems, their roles, and impacts on future power systems." IEEE access 7 (2018): 4555-4585.

[40] Akter, Runa, Jaber Bin Abdul Bari, Saidur R. Chowdhury, Muhammad Muhitur Rahman, and Syed Masiur Rahman. "Environmental Aspects of Biomass Utilization in Supercapacitors." Biomass-Based Supercapacitors: Design, Fabrication and Sustainability (2023): 23-39.

[41] Gao, Fengxian, Jingyao Song, He Teng, Xiliang Luo, and Mingming Ma. "All-polymer ultrathin flexible supercapacitors for electronic skin." Chemical Engineering Journal 405 (2021): 126915.

[42] Liang, Jie, Hongwei Sheng, Hongyun Ma, Pengxiang Wang, Qi Wang, Jiao Yuan, Xuetao Zhang et al. "Transparent electronic skin from the integration of strain sensors and supercapacitors." Advanced Materials Technologies 8, no. 4 (2023): 2201234.

[43] https://gnanomat.com/2019/05/16/innovative-energy-storage-systems/ Access Day 11.08.2023.

[44] González, Ander, Eider Goikolea, Jon Andoni Barrena, and Roman Mysyk. "Review on supercapacitors: Technologies and materials." Renewable and sustainable energy reviews 58 (2016): 1189-1206.

[45] https://www.wevolver.com/article/battery-supercapacitor-hybrid-energy-storage-systems Access Day 11.08.2023.

[46] Sinha, Prerna, and Kamal K. Kar. "Introduction to supercapacitors." In Handbook of nanocomposite supercapacitor materials II: Performance, pp. 1-28. Cham: Springer International Publishing, 2020.

[47] Yu, Aiping, Victor Chabot, and Jiujun Zhang. Electrochemical supercapacitors for energy storage and delivery: fundamentals and applications. Taylor & Francis, 2013.

[48] Winter, Martin, and Ralph J. Brodd. "What are batteries, fuel cells, and supercapacitors?." Chemical reviews 104, no. 10 (2004): 4245-4270.

[49] Kötz, Rüdiger, and M. J. E. A. Carlen. "Principles and applications of electrochemical capacitors." Electrochimica acta 45, no. 15-16 (2000): 2483-2498.

[50] Drummond, R., C. Huang, P. S. Grant, and S. R. Duncan. "Overcoming diffusion limitations in supercapacitors using layered electrodes." Journal of Power Sources 433 (2019): 126579.

[51] Zhao, Jingyuan, and Andrew F. Burke. "Review on supercapacitors: Technologies and performance evaluation." Journal of Energy Chemistry 59 (2021): 276-291.

[52] Berrueta, Alberto, Alfredo Ursúa, Idoia San Martin, Ali Eftekhari, and Pablo Sanchis. "Supercapacitors: electrical characteristics, modeling, applications, and future trends." Ieee Access 7 (2019): 50869-50896.

[53] Ma, Ning, Dongfang Yang, Saleem Riaz, Licheng Wang, and Kai Wang. "Aging mechanism and models of supercapacitors: A review." Technologies 11, no. 2 (2023): 38.

[54] Banerjee, Soma, Bibekananda De, Prerna Sinha, Jayesh Cherusseri, and Kamal K. Kar. "Applications of supercapacitors." Handbook of Nanocomposite Supercapacitor Materials I: Characteristics (2020): 341-350.

[55] Mofokeng, Thapelo P., Zikhona N. Tetana, and Kenneth I. Ozoemena. "Defective 3D nitrogen-doped carbon nanotube-carbon fibre networks for high-performance supercapacitor: Transformative role of nitrogen-doping from surface-confined to diffusive kinetics." Carbon 169 (2020): 312-326.

[56] Lei, Chunhong, Richard Fields, Peter Wilson, Constantina Lekakou, Negar Amini, Stephen Tennison, John Perry, Michele Gosso, and Brunetto Martorana. "Development and evaluation of a composite supercapacitor-based 12 V transient start–stop power system for vehicles: Modelling, design and fabrication scaling up." Proceedings of the Institution of Mechanical Engineers, Part A: Journal of Power and Energy 235, no. 4 (2021): 914-927.

[57] Akin, Mert, and Xiangyang Zhou. "Recent advances in solid-state supercapacitors: From emerging materials to advanced applications." International journal of energy research 46, no. 8 (2022): 10389-10452.

[58] Saripalli, Bhanu Prakash, Gagan Singh, and Sonika Singh. "Supercapacitors based energy storage system for mitigating solar photovoltaic output power fluctuations." World Journal of Engineering (2022).

[59] Yue, Xicai, Janice Kiely, Des Gibson, and Emmanuel M. Drakakis. "Charge-based supercapacitor storage estimation for indoor sub-mW photovoltaic energy harvesting powered wireless sensor nodes." IEEE Transactions on Industrial Electronics 67, no. 3 (2019): 2411-2421.

[60] Lethien, Christophe, Jean Le Bideau, and Thierry Brousse. "Challenges and prospects of 3D micro-supercapacitors for powering the internet of things." Energy & Environmental Science 12, no. 1 (2019): 96-115.

[61] Sundriyal, Poonam, and Shantanu Bhattacharya. "Textile-based supercapacitors for flexible and wearable electronic applications." Scientific reports 10, no. 1 (2020): 13259.

[62] Keum, Kayeon, Jung Wook Kim, Soo Yeong Hong, Jeong Gon Son, Sang-Soo Lee, and Jeong Sook Ha. "Flexible/stretchable supercapacitors with novel functionality for wearable electronics." Advanced Materials 32, no. 51 (2020): 2002180.

[63] Zhang, Yi-Zhou, Yang Wang, Tao Cheng, Lan-Qian Yao, Xiangchun Li, Wen-Yong Lai, and Wei Huang. "Printed supercapacitors: materials, printing and applications." Chemical Society Reviews 48, no. 12 (2019): 3229-3264.

[64] Thakur, Anupma, and Pooja Devi. "based flexible devices for energy harvesting, conversion and storage applications: A review." Nano Energy 94 (2022): 106927.

[65] Ariyarathna, Thilanga, Nihal Kularatna, and D. Alistair Steyn-Rosse. "Supercapacitor Assisted Hybrid DC-DC Converter for Applications Powered by Renewable Energy Sources." In 2020 2nd IEEE International Conference on Industrial Electronics for Sustainable Energy Systems (IESES), vol. 1, pp. 194-199. IEEE, 2020.

[66] Zhang, Panpan, Sheng Yang, Honggui Xie, Yang Li, Faxing Wang, Mingming Gao, Kun Guo, Renheng Wang, and Xing Lu. "Advanced three-dimensional microelectrode architecture design for high-performance on-chip micro-supercapacitors." ACS nano 16, no. 11 (2022): 17593-17612.

[67] Elizalde, Jorge, Cristina Cruces, Michael Stiven Sandoval, Xabier Eguiluz, and Iñaki Val. "Self-powered photovoltaic bluetooth® low energy temperature sensor node." IEEE Access 9 (2021): 111305-111314.

[68] Habibzadeh, Mohamadhadi, Moeen Hassanalieragh, Tolga Soyata, and Gaurav Sharma. "Solar/wind hybrid energy harvesting for supercapacitor-based embedded systems." In 2017 IEEE 60th International Midwest Symposium on Circuits and Systems (MWSCAS), pp. 329-332. IEEE, 2017.

[69] Xu, Hui, and Minghai Shen. "The control of lithium-ion batteries and supercapacitors in hybrid energy storage systems for electric vehicles: a review." International Journal of Energy Research 45, no. 15 (2021): 20524-20544.

[70] Ahsan, Muhammad Bin Fayyaz, Saad Mekhilef, Tey Kok Soon, Marizan Binti Mubin, Prashant Shrivastava, and Mehdi Seyedmahmoudian. "Lithium-ion battery and supercapacitor-based hybrid energy storage system for electric vehicle applications: A review." International Journal of Energy Research 46, no. 14 (2022): 19826-19854.

[71] Riaz, Amna, Mahidur R. Sarker, Mohamad Hanif Md Saad, and Ramizi Mohamed. "Review on comparison of different energy storage technologies used in micro-energy harvesting, WSNs, low-cost microelectronic devices: challenges and recommendations." Sensors 21, no. 15 (2021): 5041.

[72] Lasrado, Dylan, Sandeep Ahankari, and Kamal K. Kar. "Global trends in supercapacitors." Handbook of Nanocomposite Supercapacitor Materials III: Selection (2021): 329-365.

[73] Jung, Gyusung, Hanchan Lee, Hyojin Park, Jiyoon Kim, Jung Wook Kim, Dong Sik Kim, Kayeon Keum, Yong Hui Lee, and Jeong Sook Ha. "Temperature-tolerant flexible supercapacitor integrated with a strain sensor using an organohydrogel for wearable electronics." Chemical Engineering Journal 450 (2022): 138379.

[74] Wang, Weiwen, Liqiang Xu, Lun Zhang, Aimin Zhang, and Jihai Zhang. "Self-Powered Integrated Sensing System with In-Plane Micro-Supercapacitors for Wearable Electronics." Small (2023): 2207723.

[75] Rokaya, Chakra, Jari Keskinen, and Donald Lupo. "Integration of fully printed and flexible organic electrolyte-based dual cell supercapacitor with energy supply platform for low power electronics." Journal of Energy Storage 50 (2022): 104221.

[76] Selleri, Giacomo, Federico Poli, Riccardo Neri, Leonardo Gasperini, Chiara Gualandi, Francesca Soavi, and Davide Fabiani. "Energy harvesting and storage with ceramic piezoelectric transducers coupled with an ionic liquid-based supercapacitor." Journal of Energy Storage 60 (2023): 106660.

[77] Kulkarni, Abhishek A., Neha K. Gaikwad, Ankita P. Salunkhe, Rushikesh M. Dahotre, Tejasvinee S. Bhat, and Pramod S. Patil. "An ensemble of progress and future status of piezo-supercapacitors." Journal of Energy Storage 65 (2023): 107362.

[78] Chodankar, Nilesh, Chinmayee Padwal, Hong Duc Pham, Kostya Ken Ostrikov, Sagar Jadhav, Kiran Mahale, Prasad KDV Yarlagadda, Yun Suk Huh, Young-Kyu Han, and Deepak Dubal. "Piezo-supercapacitors: A new paradigm of self-powered wellbeing and biomedical devices." Nano Energy 90 (2021): 106607.

[79] Rajagopal, Sivakumar, Rameez Pulapparambil Vallikkattil, M. Mohamed Ibrahim, and Dimiter Georgiev Velev. "Electrode materials for supercapacitors in hybrid electric vehicles: Challenges and current progress." Condensed Matter 7, no. 1 (2022): 6.

[80] Ghosh, Sourav, Sarita Yadav, Ambika Devi, and Tiju Thomas. "Techno-economic understanding of Indian energy-storage market: A perspective on green materials-based supercapacitor technologies." Renewable and Sustainable Energy Reviews 161 (2022): 112412.

[81] Dubal, Deepak P., Nilesh R. Chodankar, Do-Heyoung Kim, and Pedro Gomez-Romero. "Towards flexible solid-state supercapacitors for smart and wearable electronics." Chemical Society Reviews 47, no. 6 (2018): 2065-2129.

[82] Kim, Ju-Hwan, Sang-Chul Jung, Hye-Min Lee, and Byung-Joo Kim. "Comparison of pore structures of cellulose-based activated carbon fibers and their applications for electrode materials." International Journal of Molecular Sciences 23, no. 7 (2022): 3680.

[83] De, Bibekananda, Soma Banerjee, Kapil Dev Verma, Tanvi Pal, P. K. Manna, and Kamal K. Kar. "Carbon nanotube as electrode materials for supercapacitors." Handbook of Nanocomposite Supercapacitor Materials II: Performance (2020): 229-243.

[84] Niu, Ziyu, Yong Zhang, Yan Zhang, Xiuzhen Lu, and Johan Liu. "Enhanced electrochemical performance of three-dimensional graphene/carbon nanotube composite for supercapacitor application." Journal of Alloys and Compounds 820 (2020): 153114.

[85] Verma, Kapil Dev, Prerna Sinha, Soma Banerjee, and Kamal K. Kar. "Characteristics of electrode materials for supercapacitors." In Handbook of Nanocomposite Supercapacitor Materials I: Characteristics, pp. 269-285. Cham: Springer International Publishing, 2020.

[86] Akhtar, Mainul, and S. B. Majumder. "Hybrid Supercapacitor-Battery Energy Storage." Handbook of Advanced Ceramics and Composites: Defense, Security, Aerospace and Energy Applications (2020): 1259-1296.

[87] Waqas Hakim, M., Sabeen Fatima, Syed Rizwan, and Asif Mahmood. "Pseudo-capacitors: Introduction, Controlling Factors and Future." In Nanostructured Materials for Supercapacitors, pp. 53-70. Cham: Springer International Publishing, 2022.

[88] Sardana, Silki, Anjli Gupta, Kuldeep Singh, A. S. Maan, and Anil Ohlan. "Conducting polymer hydrogel based electrode materials for supercapacitor applications." Journal of Energy Storage 45 (2022): 103510.

[89] Snook, Graeme A., Pon Kao, and Adam S. Best. "Conducting-polymer-based supercapacitor devices and electrodes." Journal of power sources 196, no. 1 (2011): 1-12.

[90] Shao, Yanyan, Fei Shen, and Yuanlong Shao. "Recent advances in aqueous zinc-ion hybrid capacitors: a minireview." ChemElectroChem 8, no. 3 (2021): 484-491.

[91] Chatterjee, Dhruba P., and Arun K. Nandi. "A review on the recent advances in hybrid supercapacitors." Journal of Materials Chemistry A 9, no. 29 (2021): 15880-15918.

[92] Soltani, Mahdi, and S. Hamidreza Beheshti. "A comprehensive review of lithium ion capacitor: development, modelling, thermal management and applications." Journal of Energy Storage 34 (2021): 102019.

[93] Sivakkumar, Seepalakottai R., and A. G. Pandolfo. "Evaluation of lithium-ion capacitors assembled with pre-lithiated graphite anode and activated carbon cathode." Electrochimica Acta 65 (2012): 280-287.

[94] Liang, Jiaxing, and Da-Wei Wang. "Design rationale and device configuration of lithium-ion capacitors." Advanced Energy Materials 12, no. 25 (2022): 2200920.

[95] Ponce, M. Federico, Arminda Mamani, Florencia Jerez, Josué Castilla, Pamela B. Ramos, Gerardo G. Acosta, M. Fabiana Sardella, and Marcela A. Bavio. "Activated carbon from olive tree pruning residue for symmetric solid-state supercapacitor." Energy 260 (2022): 125092.

[96] Selvaraj, Aravindha Raja, Anand Muthusamy, Hee-Je Kim, Karuppanan Senthil, and Kandasamy Prabakar. "Ultrahigh surface area biomass derived 3D hierarchical porous carbon nanosheet electrodes for high energy density supercapacitors." Carbon 174 (2021): 463-474.

[97] Ma, Chang, Liqiang Wu, Mahmut Dirican, Hui Cheng, Junjing Li, Yan Song, Jingli Shi, and Xiangwu Zhang. "Carbon black-based porous sub-micron carbon fibers for flexible supercapacitors." Applied Surface Science 537 (2021): 147914.

[98] Liang, Ruibin, Yongquan Du, Peng Xiao, Junyang Cheng, Shengjin Yuan, Yonglong Chen, Jian Yuan, and Jianwen Chen. "Transition metal oxide electrode materials for supercapacitors: a review of recent developments." Nanomaterials 11, no. 5 (2021): 1248.

[99] Manasa, Pantrangi, Sangaraju Sambasivam, and Fen Ran. "Recent progress on biomass waste derived activated carbon electrode materials for supercapacitors applications—A review." Journal of Energy Storage 54 (2022): 105290.

[100] Chen, Jie, Qiongfen Yu, Ming Li, Shengnan Sun, Danya Zhan, Yunfeng Wang, Zhenhua Gu, and Ying Zhang. "Preparation of high specific surface area activated carbon fiber by high-temperature vacuum activation and its superior water vapor adsorption for air humidity control." Journal of Materials Science 58, no. 6 (2023): 2469-2493.

[101] Marsh, Harry, and Francisco Rodríguez Reinoso. Activated carbon. Elsevier, 2006.

[102] Yusufu, M. I., C. C. Ariahu, and B. D. Igbabul. "Production and characterization of activated carbon from selected local raw materials." African journal of pure and applied chemistry 6, no. 9 (2012): 123-131.

[103] Sujiono, Eko Hadi, D. Zabrian, V. Zharvan, and N. A. Humairah. "Fabrication and characterization of coconut shell activated carbon using variation chemical activation for wastewater treatment application." Results in Chemistry 4 (2022): 100291.

[104] Lai, Jia Yen, Lock Hei Ngu, Siti Salwa Hashim, Jiuan Jing Chew, and Jaka Sunarso. "Review of oil palm-derived activated carbon for CO2 capture." Carbon Letters 31, no. 2 (2021): 201-252.

[105] Sesuk, T., P. Tammawat, P. Jivaganont, K. Somton, P. Limthongkul, and W. Kobsiriphat. "Activated carbon derived from coconut coir pith as high performance supercapacitor electrode material." Journal of Energy Storage 25 (2019): 100910.

[106] Khuong, Duy Anh, Hong Nam Nguyen, and Toshiki Tsubota. "Activated carbon produced from bamboo and solid residue by CO2 activation utilized as CO2 adsorbents." Biomass and Bioenergy 148 (2021): 106039.

[107] Muttil, Nitin, Saranya Jagadeesan, Arnab Chanda, Mikel Duke, and Swadesh Kumar Singh. "Production, types, and applications of activated carbon derived from waste tyres: An overview." Applied Sciences 13, no. 1 (2022): 257.

[108] Khuong, Duy Anh, Kieu Trang Trinh, Yu Nakaoka, Toshiki Tsubota, Daisuke Tashima, Hong Nam Nguyen, and Daisaku Tanaka. "The investigation of activated carbon by K2CO3 activation: Micropores-and macropores-dominated structure." Chemosphere 299 (2022): 134365.

[109] Bhat, Vinay S., Arafat Toghan, Gurumurthy Hegde, and Rajender S. Varma. "Capacitive dominated charge storage in supermicropores of self-activated carbon electrodes for symmetric supercapacitors." Journal of Energy Storage 52 (2022): 104776.

[110] Decaux, C., C. Matei Ghimbeu, M. Dahbi, M. Anouti, D. Lemordant, F. Béguin, C. Vix-Guterl, and E. Raymundo-Pinero. "Influence of electrolyte ion–solvent interactions on the performances of supercapacitors porous carbon electrodes." Journal of Power sources 263 (2014): 130-140.

[111] Pyun, S. Il, C. H. Kim, S. W. Kim, and J. H. Kim. "Effect of pore size distribution of activated carbon electrodes on electric double-layer capacitor performance." Journal of New Materials for Electrochemical Systems 5, no. 4 (2002): 289-296.

[112] Saikia, Binoy K., Santhi Maria Benoy, Mousumi Bora, Joyshil Tamuly, Mayank Pandey, and Dhurbajyoti Bhattacharya. "A brief review on supercapacitor energy storage devices and utilization of natural carbon resources as their electrode materials." Fuel 282 (2020): 118796.

[113] Dhanda, Monika, Rajat Arora, Simran Ahlawat, S. P. Nehra, and Suman Lata. "Electrolyte as a panacea to contemporary scientific world of super-capacitive energy: a condense report." Journal of Energy Storage 52 (2022): 104740.

[114] Taer, E., A. Putri, R. Farma, R. Taslim, and D. A. Yusra. "The effect of potassium iodide (KI) addition to aqueous-based electrolyte (sulfuric acid/H2SO4) for increase the performance of supercapacitor cells." Materials Today: Proceedings 44 (2021): 3241-3244.

[115] Niknam, Ehsan, Homam Naffakh-Moosavy, and Majid Ghahraman Afshar. "Electrochemical performance of Nickel foam electrode in Potassium Hydroxide and Sodium Sulfate electrolytes for supercapacitor applications." Journal of Composites and Compounds 4, no. 12 (2022): 149-152.

[116] Verma, Kapil Dev, Soma Banerjee, and Kamal K. Kar. "Characteristics of electrolytes." Handbook of Nanocomposite Supercapacitor Materials I: Characteristics (2020): 287-314.

[117] Wei, Wutao, Jiaqiang Xu, Weihua Chen, Liwei Mi, and Jiujun Zhang. "A review of sodium chloride-based electrolytes and materials for electrochemical energy technology." Journal of Materials Chemistry A 10, no. 6 (2022): 2637-2671.

[118] Lee, Hee Y., and John B. Goodenough. "Supercapacitor behavior with KCl electrolyte." Journal of Solid State Chemistry 144, no. 1 (1999): 220-223.

[119] Bo, Zheng, Jing Kong, Huachao Yang, Zhouwei Zheng, Pengpeng Chen, Jianhua Yan, and Kefa Cen. "Ultra-Low-Temperature Supercapacitor Based on Holey Graphene and Mixed-Solvent Organic Electrolyte." Acta Phys. Chim. Sin 38 (2022).

[120] Shim, Hwirim, Í. Budak, Veronika Haug, Mathias Widmaier, and Volker Presser. "Comparison of organic electrolytes at various temperatures for 2.8 áV–Li-ion hybrid supercapacitors." Electrochimica Acta 337 (2020): 135760.

[121] Li, Shaohui, Qingyong Tian, Jingwei Chen, Yining Chen, Pengzhi Guo, Cong Wei, Peng Cui, Jingyun Jiang, Xiaomeng Li, and Qun Xu. "An intrinsically non-flammable organic electrolyte for wide temperature range supercapacitors." Chemical Engineering Journal 457 (2023): 141265.

[122] Verma, Sonali, Bhavya Padha, Prerna Mahajan, and Sandeep Arya. "Effect of Electrolyte on the Performance of Supercapacitors." ECS Transactions 107, no. 1 (2022): 10821.

[123] Shao, Yuanlong, Maher F. El-Kady, Jingyu Sun, Yaogang Li, Qinghong Zhang, Meifang Zhu, Hongzhi Wang, Bruce Dunn, and Richard B. Kaner. "Design and mechanisms of asymmetric supercapacitors." Chemical reviews 118, no. 18 (2018): 9233-9280.

[124] Banuprabha, T. R., A. Karthikeyani, and P. Kalyani. "Evaluation and application of phytomass derived activated carbons as electrodes for coin cell supercapacitors." International Journal of Electrochemical Science 16, no. 12 (2021): 211251.

[125] Bhat, T. S., P. S. Patil, and R. B. Rakhi. "Recent trends in electrolytes for supercapacitors." Journal of Energy Storage 50 (2022): 104222.

[126] Guo, Junhong, Yalan Ma, Kun Zhao, Yue Wang, Baoping Yang, Jinfeng Cui, and Xingbin Yan. "High-Performance and Ultra-Stable Aqueous Supercapacitors Based on a Green and Low-Cost Water-In-Salt Electrolyte." ChemElectroChem 6, no. 21 (2019): 5433-5438.

[127] Zang, Xining, Caiwei Shen, Mohan Sanghadasa, and Liwei Lin. "High-voltage supercapacitors based on aqueous electrolytes." ChemElectroChem 6, no. 4 (2019): 976-988.

[128] Yu, Minghao, Yongzhuang Lu, Haibing Zheng, and Xihong Lu. "New insights into the operating voltage of aqueous supercapacitors." Chemistry–A European Journal 24, no. 15 (2018): 3639-3649.

[129] Deng, Yongqi, Hongfei Wang, Kefu Zhang, Jun Qiu, and Lifeng Yan. "Flexible quasi-solid-state high-performance aqueous zinc ion hybrid supercapacitor with water-in-salt hydrogel electrolyte and N/P-dual doped graphene hydrogel electrodes." Advanced Sustainable Systems 6, no. 1 (2022): 2100191.

[130] Wang, Xuehang, Yahao Li, Fengliu Lou, Marthe Emelie Melandsø Buan, Edel Sheridan, and De Chen. "Enhancing capacitance of supercapacitor with both organic electrolyte and ionic liquid electrolyte on a biomass-derived carbon." RSC advances 7, no. 38 (2017): 23859-23865.

[131] Fan, Haiman, Xingwei Liu, Laibing Luo, Faping Zhong, and Yuliang Cao. "All-climate high-voltage commercial lithium-ion batteries based on propylene carbonate electrolytes." ACS Applied Materials & Interfaces 14, no. 1 (2021): 574-580.

[132] Chen, Lihang, Jie Shu, Yunbo Huang, Zhepu Shi, Hao Luo, Zhaoping Liu, and Cai Shen. "Engineering solid electrolyte interphase for the application of propylene carbonate solvent for graphite anode in low temperate battery." Applied Surface Science 598 (2022): 153740.

[133] Yang, Yang. "A mini-review: emerging all-solid-state energy storage electrode materials for flexible devices." Nanoscale 12, no. 6 (2020): 3560-3573.

[134] Almafie, M. R., Z. Nawawi, J. Jauhari, and I. Sriyanti. "Electrospun of Poly (vinyl alcohol)/Potassium hydroxide (PVA/KOH) nanofiber composites using the electrospinning method." In IOP Conference Series: Materials Science and Engineering, vol. 850, no. 1, p. 012051. IOP Publishing, 2020.

[135] Hasan, Khadija, Shahid Bashir, Ramesh Subramaniam, Ramesh Kasi, Kashif Kamran, Javed Iqbal, Hamed Algarni et al. "Poly (Vinyl Alcohol)/Agar Hydrogel Electrolytes Based Flexible All-in-One Supercapacitors with Conducting Polyaniline/Polypyrrole Electrodes." Polymers 14, no. 21 (2022): 4784.

[136] Xu, Ting, Kun Liu, Nan Sheng, Minghao Zhang, Wei Liu, Huayu Liu, Lin Dai et al. "Biopolymer-based hydrogel electrolytes for advanced energy storage/conversion devices: Properties, applications, and perspectives." Energy Storage Materials 48 (2022): 244-262.

[137] Nayem, SM Abu, Santa Islam, Syed Shaheen Shah, Abdul Awal, Nasrin Sultana, AJ Saleh Ahammad, and Abdul Aziz. "Biomass-based Separators for Supercapacitor Applications." Biomass-Based Supercapacitors: Design, Fabrication and Sustainability (2023): 403-415.

[138] Verma, Kapil Dev, Prerna Sinha, Soma Banerjee, Kamal K. Kar, and Manas K. Ghorai. "Characteristics of separator materials for supercapacitors." Handbook of Nanocomposite Supercapacitor Materials I: Characteristics (2020): 315-326.

[139] Ahankari, Sandeep, Dylan Lasrado, and Ramesh Subramaniam. "Advances in materials and fabrication of separators in supercapacitors." Materials Advances 3, no. 3 (2022): 1472-1496.

[140] Abdisattar, Alisher, Mukhtar Yeleuov, Chingis Daulbayev, Kydyr Askaruly, Aidos Tolynbekov, Azamat Taurbekov, and Nikolay Prikhodko. "Recent advances and challenges of current collectors for supercapacitors." Electrochemistry Communications (2022): 107373.

[141] Trivedi, Harish, Kapil Dev Verma, Prerna Sinha, and Kamal K. Kar. "Current collector material selection for supercapacitors." Handbook of Nanocomposite Supercapacitor Materials III: Selection (2021): 271-311.

[142] Verma, Kapil Dev, Prerna Sinha, Soma Banerjee, and Kamal K. Kar. "Characteristics of current collector materials for supercapacitors." In Handbook of Nanocomposite Supercapacitor Materials I: Characteristics, pp. 327-340. Cham: Springer International Publishing, 2020.

[143] Khan, Yasser, Arno Thielens, Sifat Muin, Jonathan Ting, Carol Baumbauer, and Ana C. Arias. "A new frontier of printed electronics: flexible hybrid electronics." Advanced Materials 32, no. 15 (2020): 1905279.

[144] Chaudhary, Kashif Tufail. "Thin film deposition: Solution based approach." In Thin Films. IntechOpen, 2021.

[145] Bo, Zheng, Xiangnan Cheng, Huachao Yang, Xinzheng Guo, Jianhua Yan, Kefa Cen, Zhaojun Han, and Liming Dai. "Ultrathick MoS2 films with exceptionally high volumetric capacitance." Advanced Energy Materials 12, no. 11 (2022): 2103394.

[146] Bommineedi, Lakshmana Kumar, Nakul Upadhyay, and Rafael Minnes. "Screen Printing: An Ease Thin Film Technique." In Simple Chemical Methods for Thin Film Deposition: Synthesis and Applications, pp. 449-507. Singapore: Springer Nature Singapore, 2023.

[147] Liang, Jing, Bin Tian, Shuaiqi Li, Changzhong Jiang, and Wei Wu. "All-printed MnHCF-MnOx-based high-performance flexible supercapacitors." Advanced Energy Materials 10, no. 12 (2020): 2000022.

[148] Li, Hongpeng, Shuiren Liu, Xiran Li, Zhong-Shuai Wu, and Jiajie Liang. "Screen-printing fabrication of high volumetric energy density micro-supercapacitors based on high-resolution thixotropic-ternary hybrid interdigital micro-electrodes." Materials Chemistry Frontiers 3, no. 4 (2019): 626-635.

[149] Xiong, Chuanyin, Mengrui Li, Qing Han, Wei Zhao, Lei Dai, and Yonghao Ni. "Screen printing fabricating patterned and customized full paper-based energy storage devices with excellent photothermal, self-healing, high energy density and good electromagnetic shielding performances." Journal of Materials Science & Technology 97 (2022): 190-200.

[150] Tu, Qian, Xianran Li, Zeyu Xiong, Hongxia Wang, Jun Fu, and Liangzhe Chen. "Screen-printed advanced all-solid-state symmetric supercapacitor using activated carbon on flexible nickel foam." Journal of Energy Storage 53 (2022): 105211.

[151] Say, Mehmet Girayhan, Robert Brooke, Jesper Edberg, Andrea Grimoldi, Dagmawi Belaineh, Isak Engquist, and Magnus Berggren. "Spray-coated paper supercapacitors." npj Flexible Electronics 4, no. 1 (2020): 14.

[152] Arvani, Maedeh, Jari Keskinen, Anna Railanmaa, Sanna Siljander, Tomas Björkqvist, Sampo Tuukkanen, and Donald Lupo. "Additive manufacturing of monolithic supercapacitors with biopolymer separator." Journal of Applied Electrochemistry 50 (2020): 689-697.

[153] Wang, Sen, Linmei Li, Shuanghao Zheng, Pratteek Das, Xiaoyu Shi, Jiaxin Ma, Yu Liu et al. "Monolithic integrated micro-supercapacitors with ultra-high systemic volumetric performance and areal output voltage." National Science Review 10, no. 3 (2023): nwac271.

[154] Li, Jingxue, Hui Jia, Shuaishuai Ma, Lijing Xie, Xian-Xian Wei, Liqin Dai, Hongliang Wang, Fangyuan Su, and Cheng-Meng Chen. "Separator design for high-performance supercapacitors: requirements, challenges, strategies, and prospects." ACS Energy Letters 8, no. 1 (2022): 56-78.

[155] Liu, Gaoyang, Shanlong Peng, Faguo Hou, Xindong Wang, and Baizeng Fang. "Preparation and Performance Study of the Anodic Catalyst Layer via Doctor Blade Coating for PEM Water Electrolysis." Membranes 13, no. 1 (2022): 24.

[156] Patil, Ganesh C. "Doctor Blade: A Promising Technique for Thin Film Coating." In Simple Chemical Methods for Thin Film Deposition: Synthesis and Applications, pp. 509-530. Singapore: Springer Nature Singapore, 2023.

[157] He, Zhengran, Ziyang Zhang, and Sheng Bi. "Tailoring the molecular weight of polymer additives for organic semiconductors." Materials Advances 3, no. 4 (2022): 1953-1973.

[158] Xi, Yue, Tao Wang, Qi Mu, Congcong Huang, Shuming Duan, Xiaochen Ren, and Wenping Hu. "Stencil mask defined doctor blade printing of organic single crystal arrays for high-performance organic field-effect transistors." Materials Chemistry Frontiers 5, no. 7 (2021): 3236-3245.

[159] Kang, Yao-Ting, Kwong-Yang Lee, and Ta-Jo Liu. "The effect of polymer additives on the performance of a two-roll coater." Journal of applied polymer science 43, no. 6 (1991): 1187-1195.

[160] Hsu, Hung-Chieh, Shih-Hsiung Wu, Yung-Liang Tung, and Chuan-Feng Shih. "Long-term stable perovskite solar cells prepared by doctor blade coating technology using bilayer structure and non-toxic solvent." Organic Electronics 101 (2022): 106400.

[161] Zhang, Ying, Yuanyuan Zhu, Shuanghao Zheng, Liangzhu Zhang, Xiaoyu Shi, Jian He, Xiujian Chou, and Zhong-Shuai Wu. "Ink formulation, scalable applications and challenging perspectives of screen printing for emerging printed microelectronics." Journal of Energy Chemistry 63 (2021): 498-513.

[162] Mensing, Johannes P., Tanom Lomas, and Adisorn Tuantranont. "2D and 3D printing for graphene based supercapacitors and batteries: A review." Sustainable materials and technologies 25 (2020): e00190.

[163] Tomchenko, Alexey A. "Printed Chemical Sensors: From Screen-Printing to Microprinting∗." Encycl. Sens 10 (2006): 279-290.

[164] Yáñez-Sedeño, Paloma, Susana Campuzano, and José Manuel Pingarrón. "Screen-printed electrodes: Promising paper and wearable transducers for (bio) sensing." Biosensors 10, no. 7 (2020): 76.

[165] Suresh, Raghavv Raghavender, Muthaiyan Lakshmanakumar, J. B. B. Arockia Jayalatha, K. S. Rajan, Swaminathan Sethuraman, Uma Maheswari Krishnan, and John Bosco Balaguru Rayappan. "Fabrication of screen-printed electrodes: opportunities and challenges." Journal of Materials Science 56 (2021): 8951-9006.

[166] Gao, Jiaqi, Zhongqiu Hua, Shu Xu, Hao Wan, Zinan Zhi, Xinyi Chen, and Shurui Fan. "Amperometric gas sensors based on screen printed electrodes with porous ceramic substrates." Sensors and Actuators B: Chemical 342 (2021): 130045.

[167] Ferri, Josue, Clara Perez Fuster, Raúl Llinares Llopis, Jorge Moreno, and Eduardo Garcia-Breijo. "Integration of a 2D touch sensor with an electroluminescent display by using a screen-printing technology on textile substrate." Sensors 18, no. 10 (2018): 3313.

[168] Cahn, Gabe, Alejandro Barrios, Samuel Graham, Jeff Meth, Antonia Antoniou, and Olivier Pierron. "The role of strain localization on the electrical behavior of flexible and stretchable screen printed silver inks on polymer substrates." Materialia 10 (2020): 100642.

[169] Dubourg, Georges, and Marko Radovic. "Multifunctional screen-printed TiO2 nanoparticles tuned by laser irradiation for a flexible and scalable UV detector and room-temperature ethanol sensor." ACS applied materials & interfaces 11, no. 6 (2019): 6257-6266.

[170] Sharma, N., S. N. Alam, and B. C. Ray. "Fundamentals of spark plasma sintering (SPS): an ideal processing technique for fabrication of metal matrix nanocomposites." Spark plasma sintering of materials: advances in processing and applications (2019): 21-59.

[171] Huttunen, Olli-Heikki, Tuomas Happonen, Johanna Hiitola-Keinänen, Pentti Korhonen, Jyrki Ollila, and Jussi Hiltunen. "Roll-to-roll screen-printed silver conductors on a polydimethyl siloxane substrate for stretchable electronics." Industrial & Engineering Chemistry Research 58, no. 43 (2019): 19909-19916.

[172] Arvani, Maedeh, Jari Keskinen, Donald Lupo, and Mari Honkanen. "Current collectors for low resistance aqueous flexible printed supercapacitors." Journal of Energy Storage 29 (2020): 101384.

[173] Keskinen, Jari, Suvi Lehtimäki, Arman Dastpak, Sampo Tuukkanen, Timo Flyktman, Thomas Kraft, Anna Railanmaa, and Donald Lupo. "Architectural modifications for flexible supercapacitor performance optimization." Electronic Materials Letters 12 (2016): 795-803.

[174] Keskinen, Jari, Saara Tuurala, Martin Sjödin, Kaisa Kiri, Leif Nyholm, Timo Flyktman, Maria Strømme, and Maria Smolander. "Asymmetric and symmetric supercapacitors based on polypyrrole and activated carbon electrodes." Synthetic Metals 203 (2015): 192-199.

[175] Keskinen, Jari. "Supercapacitors on flexible substrates for energy autonomous electronics", Doctoral thesis, Tampere University of Technology, Publ. 1562, (2018). ISBN: 978-952-15-4197-1.

[176] Railanmaa, Anna, Suvi Lehtimäki, Jari Keskinen, and Donald Lupo. "Non-toxic printed supercapacitors operating in sub-zero conditions." Scientific Reports 9, no. 1 (2019): 14059.

[177] Railanmaa, Anna, Ayat Soltani, Suvi Lehtimäki, Nazanin Pournoori, Jari Keskinen, Mikko Hokka, and Donald Lupo. "Skin-conformable printed supercapacitors and their performance in wear." Scientific reports 10, no. 1 (2020): 15194.

[178] Li, Hongpeng, and Jiajie Liang. "Recent development of printed micro-supercapacitors: printable materials, printing technologies, and perspectives." Advanced Materials 32, no. 3 (2020): 1805864.

[179] Wen, Jianfeng, Bingang Xu, Jinyun Zhou, Jiangtao Xu, and Yuejiao Chen. "3D patternable supercapacitors from hierarchically architected porous fiber composites for wearable and waterproof energy storage." Small 15, no. 25 (2019): 1901313.

[180] Sinha, Prerna, and Kamal K. Kar. "Characteristics of supercapacitors." Handbook of Nanocomposite Supercapacitor Materials II: Performance (2020): 71-87.

[181] International Electrotechnical Commission. "International Standard: Fixed Electric Double Layer Capacitors for Use in Electronic Equipment." First. IEC (2006): 62391-1.

[182] Kumar, Arun, Honey Mittal, and Manika Khanuja. "Facile synthesis of 2D acid-etched g-C3N4 nanosheets with 1D ZnO nanorods as a promising electrode material for supercapacitor." Journal of Energy Storage 67 (2023): 107496.

[183] Liu, Kunlun, Chang Yu, Wei Guo, Lin Ni, Jinhe Yu, Yuanyang Xie, Zhao Wang, Yongwen Ren, and Jieshan Qiu. "Recent research advances of self-discharge in supercapacitors: Mechanisms and suppressing strategies." Journal of Energy Chemistry 58 (2021): 94-109.

[184] Shi, Mingwei, Zailei Zhang, Man Zhao, Xianmao Lu, and Zhong Lin Wang. "Reducing the self-discharge rate of supercapacitors by suppressing electron transfer in the electric double layer." Journal of The Electrochemical Society 168, no. 12 (2021): 120548.

[185] Ali, Ziad M., Martin Calasan, Shady HE Abdel Aleem, and Hany M. Hasanien. "On the Exact Analytical Formulas of Leakage Current-Based Supercapacitor Model Operating in Industrial Applications." Energies 16, no. 4 (2023): 1903.

[186] Li, Wei, Xiaomin Yang, Zhimin Chen, Ting Lv, Xiaofeng Wang, and Jieshan Qiu. "Synthesis and structure regulation of armor-wearing biomass-based porous carbon: Suppression the leakage current and self-discharge of supercapacitors." Carbon 196 (2022): 136-145.

[187] Yuan, Renlu, Yue Dong, Ruoyang Hou, Su Zhang, and Huaihe Song. "Influencing Factors and Suppressing Strategies of the Self-Discharge for Carbon Electrode Materials in Supercapacitors." Journal of The Electrochemical Society 169, no. 3 (2022): 030504.

[188] Haque, Mazharul, Qi Li, Anderson D. Smith, Volodymyr Kuzmenko, Per Rudquist, Per Lundgren, and Peter Enoksson. "Self-discharge and leakage current mitigation of neutral aqueous-based supercapacitor by means of liquid crystal additive." Journal of Power Sources 453 (2020): 227897.

[189] Shen, Ji-Fu, Yi-Jun He, and Zi-Feng Ma. "A systematical evaluation of polynomial based equivalent circuit model for charge redistribution dominated self-discharge process in supercapacitors." Journal of Power Sources 303 (2016): 294-304.

[190] Ike, Innocent S., Iakovos Sigalas, and Sunny Iyuke. "Understanding performance limitation and suppression of leakage current or self-discharge in electrochemical capacitors: a review." Physical Chemistry Chemical Physics 18, no. 2 (2016): 661-680.

[191] Shang, Wenxu, Wentao Yu, Xu Xiao, Yanyi Ma, Yi He, Zhongxi Zhao, and Peng Tan. "Insight into the self-discharge suppression on electrochemical capacitors: Progress and challenges." Advanced Powder Materials (2022): 100075.

[192] Hidalgo-Reyes, J. I., José Francisco Gómez-Aguilar, Ricardo Fabricio Escobar-Jiménez, Victor Manuel Alvarado-Martínez, and M. G. López-López. "Classical and fractional-order modeling of equivalent electrical circuits for supercapacitors and batteries, energy management strategies for hybrid systems and methods for the state of charge estimation: A state of the art review." Microelectronics Journal 85 (2019): 109-128.

[193] Zhao, Yanming, Wenchao Xie, Ziwei Fang, and Shuli Liu. "A parameters identification method of the equivalent circuit model of the supercapacitor cell module based on segmentation optimization." IEEE Access 8 (2020): 92895-92906.

[194] Xu, Dan, Le Zhang, Bin Wang, and Guangliang Ma. "Modeling of supercapacitor behavior with an improved two-branch equivalent circuit." IEEE Access 7 (2019): 26379-26390.

[195] Ghanbari, Teymoor, Ehsan Moshksar, Sara Hamedi, Fatemeh Rezaei, and Zahra Hosseini. "Self-discharge modeling of supercapacitors using an optimal time-domain based approach." Journal of Power Sources 495 (2021): 229787.

[196] Reema, N., G. Jagadanand, Nikhil Sasidharan, and M. P. Shreelakshmi. "Parameter Estimation of Variable Leakage Resistance Model of Supercapacitor." In 2022 IEEE International Conference on Power Electronics, Smart Grid, and Renewable Energy (PESGRE), pp. 1-5. IEEE, 2022.

[197] Shi, Lisheng, and M. L. Crow. "Comparison of ultracapacitor electric circuit models." In 2008 IEEE Power and Energy Society General Meeting-Conversion and Delivery of Electrical Energy in the 21st Century, pp. 1-6. IEEE, 2008.

[198] Spyker, Russell L., and R. Mark Nelms. "Classical equivalent circuit parameters for a double-layer capacitor." IEEE transactions on aerospace and electronic systems 36, no. 3 (2000): 829-836.

[199] Zhang, Ying, and Hengzhao Yang. "Modeling and characterization of supercapacitors for wireless sensor network applications." Journal of Power Sources 196, no. 8 (2011): 4128-4135.

[200] Laadjal, Khaled, and Antonio J. Marques Cardoso. "A review of supercapacitors modeling, SoH, and SoE estimation methods: Issues and challenges." International Journal of Energy Research 45, no. 13 (2021): 18424-18440.

[201] Faranda, Roberto. "A new parameters identification procedure for simplified double layer capacitor two-branch model." Electric Power Systems Research 80, no. 4 (2010): 363-371.

[202] Diab, Yasser, Pascal Venet, Hamid Gualous, and Gérard Rojat. "Self-discharge characterization and modeling of electrochemical capacitor used for power electronics applications." IEEE Transactions on power electronics 24, no. 2 (2008): 510-517.

[203] ŞahİN, Mustafa Ergin, Frede Blaabjerg, and Ariya SangwongwanİCh. "Modelling of supercapacitors based on simplified equivalent circuit." CPSS Transactions on Power Electronics and Applications 6, no. 1 (2021): 31-39.

[204] Alsabari, Ali Mohsen, M. K. Hassan, C. S. Azura, and Ribhan Zafira. "Experimental design for an enhanced parametric modeling of supercapacitor equivalent circuit model." Indonesian Journal of Electrical Engineering and Computer Science 23, no. 1 (2021): 63-74.

[205] Yang, Hengzhao, and Ying Zhang. "A study of supercapacitor charge redistribution for applications in environmentally powered wireless sensor nodes." Journal of Power Sources 273 (2015): 223-236.

[206] Naseri, F., S. Karimi, E. Farjah, and E. Schaltz. "Supercapacitor management system: A comprehensive review of modeling, estimation, balancing, and protection techniques." Renewable and Sustainable Energy Reviews 155 (2022): 111913.

[207] Saha, Pankaj, Satadru Dey, and Munmun Khanra. "Modeling and state-of-charge estimation of supercapacitor considering leakage effect." IEEE Transactions on Industrial Electronics 67, no. 1 (2019): 350-357.

[208] Zhang, Lei, Xiaosong Hu, Zhenpo Wang, Fengchun Sun, and David G. Dorrell. "A review of supercapacitor modeling, estimation, and applications: A control/management perspective." Renewable and Sustainable Energy Reviews 81 (2018): 1868-1878.

[209] Lee, Jeongbin, Jaeshin Yi, Daeyong Kim, Chee Burm Shin, Kyung-Seok Min, Jongrak Choi, and Ha-Young Lee. "Modeling of the Electrical and Thermal Behaviors of an Ultracapacitor." Energies 7, no. 12 (2014): 8264-8278.

[210] Berrueta, Alberto, Idoia San Martín, Andoni Hernández, Alfredo Ursúa, and Pablo Sanchis. "Electro-thermal modelling of a supercapacitor and experimental validation." Journal of Power Sources 259 (2014): 154-165.

[211] Kaus, Maximilian, Julia Kowal, and Dirk Uwe Sauer. "Modelling the effects of charge redistribution during self-discharge of supercapacitors." Electrochimica Acta 55, no. 25 (2010): 7516-7523.

[212] Kovaltchouk, Thibaut, Bernard Multon, Hamid Ben Ahmed, Judicael Aubry, and Pascal Venet. "Enhanced aging model for supercapacitors taking into account power cycling: Application to the sizing of an energy storage system in a direct wave energy converter." IEEE Transactions on Industry Applications 51, no. 3 (2014): 2405-2414.

[213] Yang, Hengzhao, and Ying Zhang. "Self-discharge analysis and characterization of supercapacitors for environmentally powered wireless sensor network applications." Journal of Power Sources 196, no. 20 (2011): 8866-8873.

[214] Fletcher, Stephen, Victoria Jane Black, and Iain Kirkpatrick. "A universal equivalent circuit for carbon-based supercapacitors." Journal of Solid State Electrochemistry 18 (2014): 1377-1387.

[215] Kowal, Julia, Esin Avaroglu, Fahmi Chamekh, Armands Šenfelds, Tjark Thien, Dhanny Wijaya, and Dirk Uwe Sauer. "Detailed analysis of the self-discharge of supercapacitors." Journal of Power Sources 196, no. 1 (2011): 573-579.

[216] Rausch, Christopher, Mohammad Nahangi, Carl Haas, and Wanhua Liang. "Monte Carlo simulation for tolerance analysis in prefabrication and offsite construction." Automation in Construction 103 (2019): 300-314.

[217] https://www.palisade.com/monte-carlo-simulation/ Access Day 11.08.2023.

[218] https://statisticsbyjim.com/basics/normal-distribution/ Access Day 11.08.2023.

[219] Bocklisch, Thilo. "Hybrid energy storage approach for renewable energy applications." Journal of Energy Storage 8 (2016): 311-319.

[220] Satpathy, Sambit, Sanchali Das, and Bidyut Kumar Bhattacharyya. "How and where to use super-capacitors effectively, an integration of review of past and new characterization works on super-capacitors." Journal of Energy Storage 27 (2020): 101044.

[221] Zhou, Yang, Hualei Qi, Jinyuan Yang, Zheng Bo, Feng Huang, Mohammad Saiful Islam, Xunyu Lu et al. "Two-birds-one-stone: multifunctional supercapacitors beyond traditional energy storage." Energy & Environmental Science 14, no. 4 (2021): 1854-1896.

[222] Ahmed, Farid Uddin, Zarin Tasnim Sandhie, Liaquat Ali, and Masud H. Chowdhury. "A brief overview of on-chip voltage regulation in high-performance and high-density integrated circuits." IEEE Access 9 (2020): 813-826.

[223] Fan, Hongwei, Wei Wei, Chengyi Hou, Qinghong Zhang, Yaogang Li, Kerui Li, and Hongzhi Wang. "Wearable electrochromic materials and devices: from visible to infrared modulation." Journal of Materials Chemistry C (2023).

[224] Ding, Yujie, Michael A. Invernale, Donna MD Mamangun, Amrita Kumar, and Gregory A. Sotzing. "A simple, low waste and versatile procedure to make polymer electrochromic devices." Journal of Materials Chemistry 21, no. 32 (2011): 11873-11878.

[225] Kumar, Amrita, Michael T. Otley, Fahad Alhasmi Alamar, Yumin Zhu, Blaise G. Arden, and Gregory A. Sotzing. "Solid-state electrochromic devices: relationship of contrast as a function of device preparation parameters." Journal of Materials Chemistry C 2, no. 14 (2014): 2510-2516.

[226] Tao, Yijie, Kai Zhang, Chaoyang Zhang, Haifeng Cheng, Chunlin Jiao, and Yulei Zhao. "Electrochemical synthesis of copolymers based on 2-(anthracen-9-yl) thiophene: A facile and efficient route to a series of multicolor electrochromic polymers." Materials Science in Semiconductor Processing 56 (2016): 66-75.

[227] Yijie, Tao, Cheng Haifeng, Zhang Zhaoyang, Xu Xiaoqian, and Zhou Yongjiang. "Multielectrochromic copolymers of 3, 4-ethylenedioxythiophene and naphthalene prepared via electropolymerization in boron trifluoride diethyl etherate." Journal of Electroanalytical Chemistry 689 (2013): 142-148.

[228] Österholm, Anna M., D. Eric Shen, Aubrey L. Dyer, and John R. Reynolds. "Optimization of PEDOT films in ionic liquid supercapacitors: demonstration as a power source for polymer electrochromic devices." ACS applied materials & interfaces 5, no. 24 (2013): 13432-13440.

[229] Tuukkanen, Sampo, Marja Välimäki, Suvi Lehtimäki, Tiina Vuorinen, and Donald Lupo. "Behaviour of one-step spray-coated carbon nanotube supercapacitor in ambient light harvester circuit with printed organic solar cell and electrochromic display." Scientific reports 6, no. 1 (2016): 22967.

[230] Heinze, Jurgen, Bernardo A. Frontana-Uribe, and Sabine Ludwigs. "Electrochemistry of Conducting Polymers • Persistent Models and New Concepts." Chemical reviews 110, no. 8 (2010): 4724-4771.

PUBLICATION I

An improved exponential model for charge and discharge behavior of printed supercapacitor modules under varying load conditions

Hamed Pourkheirollah, Jari Keskinen, Matti Mäntysalo, Donald Lupo

Journal of Power Sources

https://doi.org/10.1016/j.jpowsour.2022.231475

Journal of Power Sources 535 (2022) 231475

Contents lists available at ScienceDirect

Journal of Power Sources

journal homepage: www.elsevier.com/locate/jpowsour

An improved exponential model for charge and discharge behavior of printed supercapacitor modules under varying load conditions

Hamed Pourkheirollah *, Jari Keskinen, Matti Mäntysalo, Donald Lupo

Faculty of Information Technology and Communication Sciences, Tampere University, Tampere, Finland

HIGHLIGHTS

- Modelling charging and discharging of supercapacitors using an exponential method.
- The key parameters of supercapacitors are modeled based on experimental results.
- Proposed method models the nonlinear behavior of self-discharge and leakage current.
- Modelling supercapacitor modules over a wide range of load conditions in long-term.
- Fabrication steps of flexible printed supercapacitors are schematically summarized.

ARTICLE INFO

Keywords:
Printed supercapacitors
Energy storage systems
Supercapacitor modelling and simulation
Charge and discharge
Energy module
Series connected supercapacitors

ABSTRACT

We report an improved and simple exponential model for the charging and discharging behavior of series-connected modules of supercapacitors under varying load conditions and over extended periods of time. In this work, only a single variable leakage resistance (VLR) with exponential current/voltage profile is used to model the effects of different self-discharge mechanisms of a supercapacitor. Due to the simplicity and accuracy of the simulations, the proposed model can be implemented in practical applications, both short-term and long-term, unlike the two-, three-branch, and exponential models with voltage/time profile reported in the literature. We have modeled four different energy modules using the electrical parameters of 12 printed supercapacitors in order to study and compare the series connected supercapacitors' behavior in each energy module. The key parameters such as capacitance and equivalent series resistance (ESR) of supercapacitors were based on experimental results. The numerical exponential method reported here enables modelling of the nonlinear behavior of self-discharge and leakage current over a wide range of load conditions and time periods. Furthermore, we have modified the linear model reported in the literature for leakage and self-discharge and compared the results with our nonlinear model.

1. Introduction

Energy storage systems [1] play a key role in storing the harvested energy generated from renewable readily available sources like wind [2], light [3], bio-energy [4], and RF radiation [5], as well as delivering the needed energy to the system when high power is required or when the primary energy source is not available [6–8]. Energy-Harvesting Wireless Sensor Nodes [9–12], energy autonomous Internet of Things (IoT) [13–16] and trillions of sensor networks in the near future will connect smart devices for different applications such as healthcare [17], security [18], smart home automation systems [19] and wearable electronics [20]. Hence, energy storage systems are a subject of continually growing research interest, as these systems will play a key role in a variety of future applications. Furthermore, with the increasing attention to directly integrate energy harvesting and storage devices to achieve flexible, stretchable, and wearable self-charging sensors and power systems [21–28], the importance of inexpensive and environmentally friendly energy storage systems is increasing day by day [29,30]. The task of these systems is to store the energy supplied by other sources and to provide the instantaneous electrical power required by the system [31]. The main criteria for an energy storage system include high specific power and energy density, fast charging time, reliability,

* Corresponding author.
E-mail address: hamed.pourkheirollah@tuni.fi (H. Pourkheirollah).

https://doi.org/10.1016/j.jpowsour.2022.231475
Received 27 October 2021; Received in revised form 2 March 2022; Accepted 13 April 2022
Available online 20 April 2022

low power dissipation and longevity [32].

Supercapacitors (SCs) [33,34], sometimes referred to as electric double layer capacitors (EDLCs), have been modeled and analyzed like regular capacitors, despite being larger in capacity. Over the past decade, extensive studies and research have been conducted on SCs as a key element in energy storage systems [23–28,35,36]. SCs are promising elements for use in energy harvesting and storage systems, due to their large specific power density, high efficiency, fast charge and discharge time, low heating losses because of small equivalent series resistance (ESR), and long lifespan (in both charge/discharge cycles and time) and are widely used in energy storage systems and hybrid energy systems with batteries [37–40]. In addition, SCs are, in many cases, a good alternative to batteries due to disposability, safety, and long lifetime [41,42]. The voltage range for a single SC is low, as it is limited to the electrochemical window of the electrolyte. For applications that require high voltage, multiple SCs can be connected in series to form a SC energy module that can be integrated directly to the energy storage systems.

Modelling SC energy modules is essential from the viewpoint of design prediction and condition monitoring [43]. Modelling the various electrical properties of SCs and predicting the effect of these properties on charging and discharging behavior of an energy module, both in the presence or absence of a load, are important steps before utilizing SCs in energy modules. In particular, due to the potential device-to-device variation in electrical properties, especially in printed SCs, it is important to model and understand the effect of these variations on the performance of series-connected modules.

There are numerous models reported in the literature for SCs with the aim of accurately describing their electrical behavior [43–45], thermal behavior [43–45], self-discharge [43–46], and aging [45] under different operating conditions. In order to model the electrical behavior of SCs, one of the most common modelling methods is the equivalent circuit model, which uses parametric RC (resistor-capacitor) networks. Although the equivalent circuit model does not explicitly state the physical parameters and internal information of SCs, this model is derived from experimental data and empirical experience. Furthermore, the simple structure and high accuracy of this model make it suitable for real-time energy management applications [48]. In the parametric RC networks model, depending on the configuration of the electrical circuit and the number of elements, the accuracy of the circuit model varies. The basic equivalent circuit model, known in the literature as the classical equivalent circuit, is a subset of parametric RC networks; it includes a capacitor C and an equivalent series resistance (ESR) to model the internal losses of the SC [49]. The advantage of this classic RC model is its inherent simplicity. On the other hand, in this model, the effects of self-discharge and leakage of SCs in the system cannot be observed and analyzed. Spyker et al. [50] added another constant resistance parallel to the capacitor in the classical model, with the aim of considering the phenomenon of self-discharge and leakage current (Fig. 1a). However, self-discharge and leakage current of SCs is a nonlinear phenomenon and cannot be modeled with a constant parallel resistance. On the other hand, the effects of self-discharge and leakage of SCs during long-term charge/discharge time are significant, and therefore the classical RC model and Spyker model can only be useful in very short-term (several seconds) charge/discharge time; this significantly limits the range of realistic applications of these models.

Moreover, there are somewhat more complicated equivalent circuit models with more RC network elements for SCs reported in the literature, such as a two-branch model with equivalent parallel resistance (EPR) [51] and a three-branch model [52]. In the two-branch model with EPR (Fig. 1b), the first branch is the main branch, where R_0 and the voltage dependent capacitance (C_0 and $Kv \cdot V$) are connected in series. This branch represents the charge and discharge behavior of the SC in the short-term. The second branch, which has R_2 and C_2 in series, determines the redistribution of the SC charge in the mid-term and long-term, and the constant equivalent parallel resistance (EPR) models the self-discharge effect. Since this model uses a constant parallel resistance, it considers only the internal ohmic leakage of the SC and is not a suitable model for estimating the SC non-linear self-discharge effect in the long-term. In the three-branch model (Fig. 1c), another branch, with R_r and C_r in series, is added to define the self-discharge caused by diffusion-controlled Faradaic redox reactions, which is proportional to the concentration gradient of the diffusible redox species. The concentration gradient, at a certain distance from the electrode, is inversely proportional to the square-root of time and, consequently, leads to a decrease in the rate of self-discharge over time. Nevertheless, despite the complexity of the model and a greater number of RC network elements, this model is also not able to well estimate the nonlinear effect of self-discharge in SCs in the mid-term to long-term.

In other work, a variable leakage resistance (VLR) is used to model the self-discharge time dependency in a SC [53,54]. In this model (Fig. 1d), several distinct exponential functions are used to model the self-discharge characteristic, each of which has different time constants at different time and voltage periods of self-discharge, leading to varying leakage resistances. Zhang et al. [53,54] reported to have found by trial and error that modelling the self-discharge effect of a SC for 8 h required five distinct exponential functions for five periods. In another VLR model published by Ghanbari et al. [55], multiple distinct exponential functions with voltage/time profiles have been used to model the effect

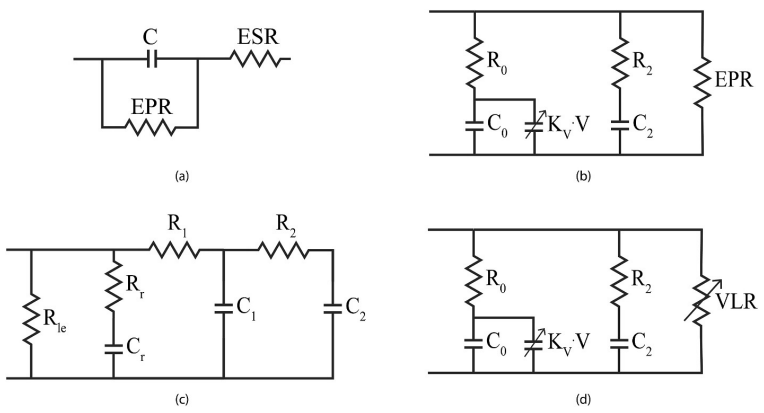

Fig. 1. Equivalent circuit models reported in the literature for a single SC; a) Spyker et al. model [50]. b) two branch model with EPR [51]. c) three-branch model [52] and d) VLR model [53–55].

of supercapacitor self-discharge in the short term (6 h). It is clear that, in order to analyze and study the behavior of series connected SC modules self-discharge using these VLR models [53–55] in the long term (one month for example), a very large number of distinct exponential function characteristics are required for different periods, which requires many parameters determination steps. For this reason, using these VLR proposed models [53–55] would increase the difficulty of parameter identification in SC energy modules, thus practically the reported VLR models are not suitable for long-term simulations.

In this work, we have in brief illustrated the fabrication steps and characterization of our disposable and flexible printed SCs using low-cost and non-toxic processes and materials. In the following, we have presented a numerical exponential method to model the nonlinear behavior of self-discharge and leakage current of SCs using experimental electrical parameters of SCs. We report an improved model based on experimentally determined quantities of individual devices. The model also predicts the dependence of the operation of series-connected modules on variation of electrical properties from device to device, an important issue in printed devices. In other words, in addition to its ability to model the full charging and discharging behavior of the supercapacitors, the model can also be used to study the effect of device-to-device variations in electrical parameters, especially the nonlinear nature of leakage current and self-discharge, on the behavior of series connected supercapacitors in the energy modules. In contrast to the models [53–55] using a variable leakage resistance with exponential voltage/time profile, the model proposed in this work uses variable leakage resistance with exponential current/voltage profile. In addition, the method of obtaining the exponential profiles is different; in our model, it is based on experimental data of SCs self-discharge for a long time (31 days). Furthermore, in the model presented in this paper, no distinction is made between different self-discharge mechanisms. Rather, a single VLR with exponential current/voltage profile has been introduced to consider the effects of various self-discharge mechanisms under the normal operation conditions.

Briefly, the two-branch model with EPR, three-branch model and VLR models reported in the literature, have multiple branches and more RC network elements, while in practical applications, simplified versions are required to enable model implementation. In contrast, the proposed model has only one branch and a few RC elements (only 3), and accordingly is simpler for use in energy storage modules which include several SCs in series.

Furthermore, as an illustration, we have also modeled four different energy modules using the parameters of 12 printed SCs in order to simulate the SCs' behavior in energy modules. We have simulated the charging and self-discharging behavior of the modules to estimate their behavior in the absence of load and the amount of power delivered to different small and large loads in short-term and long-term. We have also modified the Spyker model reported in the literature [50] and compared the simulation results of the model proposed in this work with the modified Spyker model.

2. Experimental and methods

2.1. Fabrication of supercapacitors

The fabrication process for this type of printed supercapacitors (SCs) has been reported in the previous works published by the group [39,40, 56–61] but will be summarized here. The fabrication steps are shown schematically in Fig. 2. A double-sided Al/PET flexible substrate (Pyroll) was used as the starting substrate with an aluminum (Al) thickness of 9 μm and a polyethylene terephthalate (PET) thickness of 50 μm (Fig. 2a). Before fabrication, the Al/PET substrate was pre-heated inside the oven at 95° for 15 min (Fig. 2b).

First, a current collector layer consisting of a graphite ink (Acheson Electrodag PF-407C) was applied onto the PET side of the substrate, while the Al layer acts only as a barrier layer (Fig. 2c). The graphite ink was then dried in the oven for 1 h at 95° (Fig. 2d) and a graphite thickness of 40–50 μm was obtained. Subsequently, activated carbon was applied using an in-house formulation with chitosan as binder to form an electrode layer onto the current collector layer (Fig. 2e). The activated carbon ink was then dried at room temperature overnight (Fig. 2f) and the resulting film was 50–70 μm thick. A laboratory scale doctor blade coater was used to deposit these layers. Then, heat-sealing dispersion adhesive material (Paramelt Aquaseal X2277 polyolefin) was applied onto the PET and part of the current collector layer (Fig. 2g). The samples were then placed in the oven at 80 °C for 15 min (Fig. 2h). NaCl: H_2O aqueous electrolyte with a mass ratio of 1: 5 was then added onto the electrode layer (Fig. 2i). The next step was to add a paper separator onto the electrode, in which the electrode and the paper separator were impregnated with aqueous electrolyte (Fig. 2j). Fig. 2k shows the other half of the SC, which is shown upside down in the figure. The electrode in Fig. 2k was exactly the same pattern as the electrode in Fig. 2j, but facing downwards, and without the paper separator. In the final step, the two electrodes were packed and heat-sealed face to face with the help of annealed Aquaseal, as shown in Fig. 2l, upside down. The final length, width, and thickness of the fabricated SC with the package were 50, 50 and 0.4–0.5 mm, respectively.

2.2. Characterization of supercapacitors

The key electrical parameters of SCs, such as capacitance, equivalent series resistance (ESR) and leakage current were obtained using an international industrial standard, IEC 62391-1 [62]. A Maccor 4300 workstation (Maccor Inc., USA) was used to electrically characterize the SCs. The SCs were charged and discharged three times between 0 and 1.2 v with a constant current of 1, 3 and 10 mA. The SCs were then held at the constant voltage of 1.2 V for 30 min. The capacitance was measured through a constant current discharge step between 0.96 V and 0.48 V. The SCs were then kept at the constant voltage of 1.2 V for 1 h and the leakage current was obtained. This was repeated for all three currents of 1, 3 and 10 mA. Eventually, the ESR was calculated from the IR drop in the measurement with discharge current of 10 mA.

2.3. Improved equivalent circuit model

As mentioned in the introduction, equivalent circuit models reported in the literature are inefficient for long-term applications due to the lack of thorough treatment of leakage and self-discharge effects [43–55]. In order to overcome this limitation, the nonlinearity of leakage and self-discharge is modeled in this work. To do this, each of the fabricated supercapacitors (SCs) was first charged to about 1 V, and then during self-discharge, their voltage and current were recorded for 31 days, and their current-voltage exponential equation was extracted from the experimental data. As shown in Fig. 3b, the exponential equation for the current-voltage curve of one of the SCs is extracted with a good approximation. This was repeated for all 12 printed SCs used in this work, and a unique exponential and nonlinear equation for the leakage of each SCs was obtained.

In order to model the internal parameters of a SC (Fig. 3a), each device is modeled with a capacitor, a series resistor called ESR, as well as a variable exponential element connected in parallel with the SC to model the nonlinearity of SC self-discharge and leakage current. The values of capacitance and ESR from the characterization of the printed SCs using the Maccor system and the values of 'a' and 'b' from the experimental data of SCs during self-discharge are given in the model. 12 SCs were fabricated and characterized, each of which had its own unique capacitance, ESR, 'a' and 'b' values.

This exponential model for SC self-discharge and leakage, while maintaining the simplicity of the circuit structure, also increases the accuracy of the simulation and is suitable for long-term simulations, compared to the linear models reported in the literature [43–55]. To show this, the self-discharge behavior of a SC is simulated using the

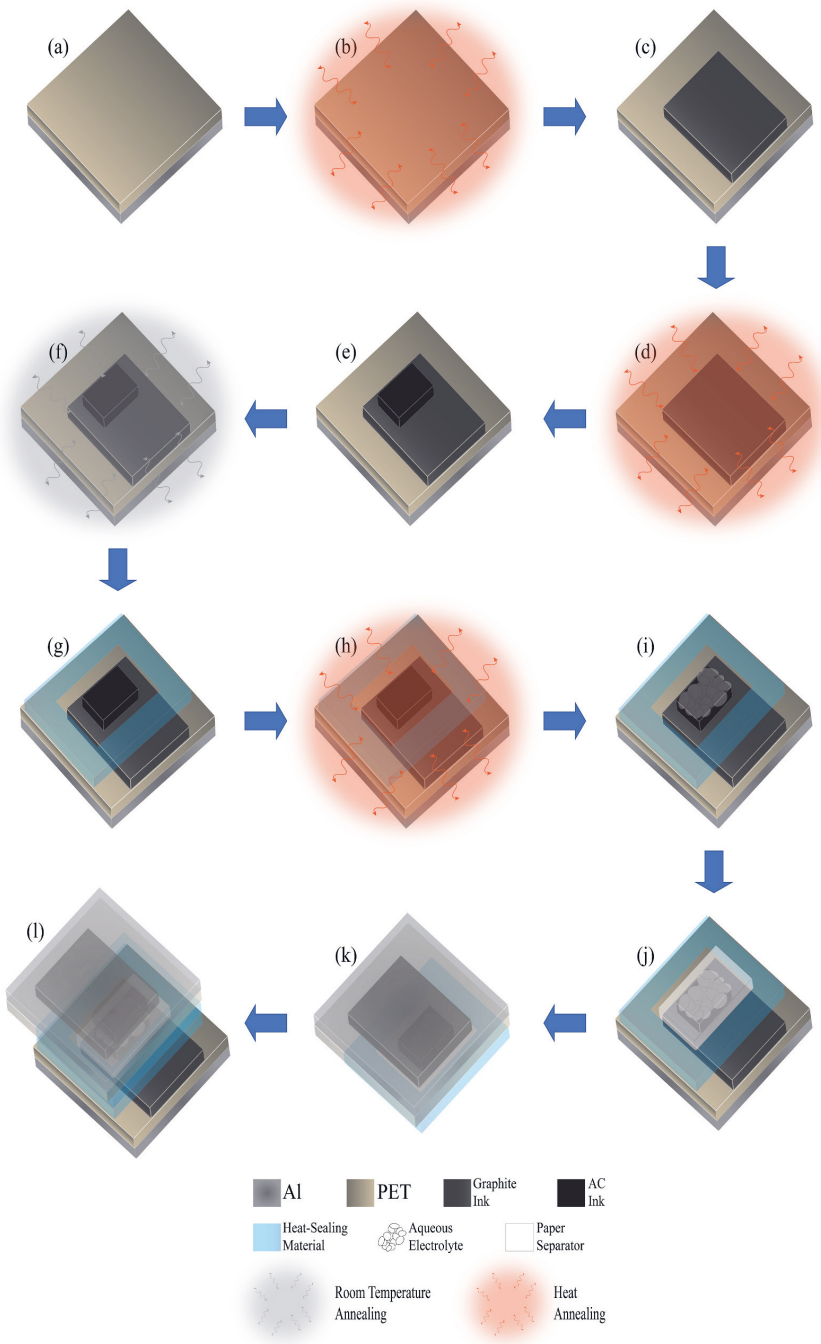

Fig. 2. Complete fabrication steps. a) The starting substrate; A double-sided Al/PET flexible substrate, 9 μm Al, 50 μm PET. b) Pre-heating the substrate in the oven at 95° for 15 min. c) Developing the current collector layer using graphite ink. d) Drying graphite ink in the oven for 1 h at 95°. e) Developing the electrode layer using activated carbon ink with chitosan binder. f) Drying activated carbon ink at room temperature overnight. g) Applying heat-sealing adhesive layer onto the PET and part of the current collector layer. h) Annealing the heat-sealing layer in the oven at 80 °C for 15 min. i) Adding NaCl: H2O aqueous electrolyte with a mass ratio of 1: 5 respectively. j) Adding the paper separator. k) Second cell upside-down without the separator. l) Heat-sealing and packing two cells together face to face upside-down using annealed heat-sealing adhesive layer.

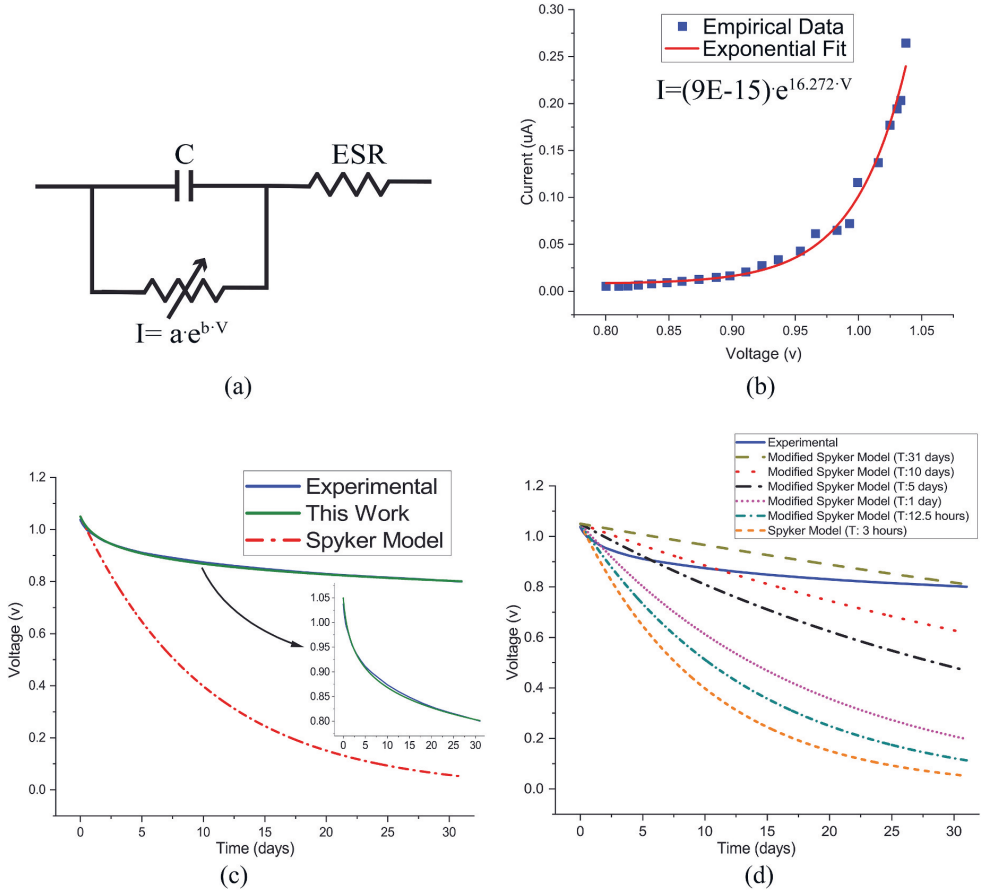

Fig. 3. a) Proposed equivalent circuit model of a SC. b) Extraction of I–V exponential equation for leakage current and self-discharge modelling. c) Self-discharge behavior of a SC modeled by Spyker linear model and the exponential model proposed in this work and comparing the results with the experimental results. d) The modified Spyker model; albeit closer to the experimental results by applying longer self-discharge time constant (T) to the proposed equation, but still does not fully comply with the experimental results.

linear model reported by Spyker et al. [50] and the exponential model presented in this work, and the results are compared with the experimental data. Using the method provided by Spyker et al. [50], the constant equivalent parallel resistance (EPR) for modelling the self-discharge and leakage was calculated and included in the equivalent circuit model in parallel with the capacitor (Fig. 1a) and the SC self-discharge was simulated. As can be seen in Fig. 3c, it is clear that the Spyker linear model is not suitable for simulating the discharge behavior of a SC in long-term applications, and in contrast, the model presented in this work is very accurate and the results obtained from the simulation are in good agreement with the experimental results. However, the equation in the Spyker method for calculating the EPR considers the values of self-discharge voltage only for a period of 3 h. We modified this method and calculated the EPR values by applying the self-discharge values for longer time constants, as can be seen in Table 1. Fig. 3d shows that by applying the self-discharge values to the Spyker equation over longer time constants, the SC self-discharge behavior approaches the experimental results, but is still far from fully consistent with it.

In this work, we have modeled 4 different SC energy modules using 12 SCs, each of modules consists of 3 series connected SCs. To model the SCs, the exponential model described earlier in Fig. 3 was used. Using

Table 1
The calculated EPR values for longer time constants using Spyker method reported in literature [50].

Time Constant	EPR (M Ω)
3 h	4.9
12.5 h	6.6
1 day	8.8
5 days	18.1
10 days	27.5
31 days	56.4

this model, the charging and discharging behavior of SCs in the form of energy modules, the total amount of power delivered to different loads by 4 modeled energy modules, and the self-discharging behavior of the modules are discussed and analyzed. Fig. 4a shows the equivalent circuit model of an energy module while charging. This equivalent circuit, in addition to three SCs in series, has a step-source battery to charge the SCs and a resistor parallel to the whole circuit to model the load connected to the energy module. Fig. 4b shows the equivalent circuit of an energy module during discharge. A DC voltage source is modeled in parallel with each SC, and the voltage value of this source is the final

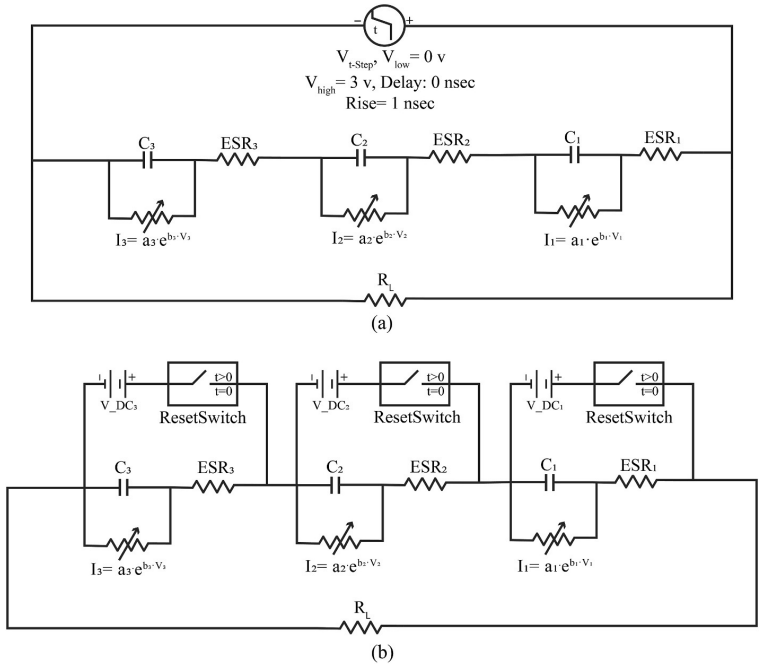

Fig. 4. a) Charging circuit model of a SC energy module. b) Discharging circuit model of a SC energy module.

value of the potential difference stored in the SCs at the end of the charging phase. In order to show that this potential difference is stored at the two ends of the SCs at zero seconds, a reset switch is modeled in series with each source. In this work, we have modeled 4 different scenarios using 12 different SCs. The capacitance, ESR, and exponential equation parameters related to self-discharge of each SCs which used in 4 different energy modules are shown in Table 2. The capacitance of these SCs is between 146 and 222 mF, the equivalent capacitance of each module is about 60 mF and the ESR value of the SCs is between 6.3 and 9.9 Ω.

3. Results and discussion

3.1. Accuracy of the proposed model

In order to verify the performance of the model presented in this work, the test of connecting discrete resistors to SC modules was performed. In this experiment, SC modules 1 and 3 were randomly selected and three different discrete resistors were used as the resistive load. The voltage value of the two ends of the resistor during discharge of the SC modules was measured using a digital multimeter. The resistance values of the resistors used were 1.0, 4.7 and 8.2 kΩ and the measured experimental results were compared with the simulation results. As can be seen in Fig. 5, the difference between the simulation and experimental results is negligible. Therefore, it can be concluded that the proposed model is well verified against experiments.

3.2. Effect of leakage current during charging

In order to understand the leakage current effect of the supercapacitors (SCs) on the potential difference stored at their ends, simulations were performed with and without consideration of the leakage. In Fig. 6a and Fig. 6b, the voltage stored in the SC_1 over time in module 1 during charging is shown. As can be seen, the leakage current has very little effect on the stored voltage. This simulation was repeated for all SCs in all four energy modules, and all the results showed that there was truly a slight difference between the two diagrams. Therefore, it can be said that leakage current has negligible effect on the charging behavior of SCs in the energy modules, and leakage current can be ignored during charging as long as the leakage current is considerably smaller than the charging current.

Furthermore, as can be seen in Fig. 6c and d, the final amount of the

Table 2
Parameters of SCs used in four energy modules; each energy module contains three series connected SCs.

Module 1	SC_1	SC_2	SC_3	Module 2	SC_4	SC_5	SC_6
Capacitance (mF)	181.7	183	176.8	Capacitance (mF)	188.3	158.4	172.6
ESR (Ω)	8.4	7.8	7	ESR (Ω)	7.2	9	7.4
EPR Factors	$a_1 = 7E\text{-}15$	$a_2 = 9E\text{-}15$	$a_3 = 3E\text{-}14$	EPR Factors	$a_4 = 1E\text{-}14$	$a_5 = 1E\text{-}15$	$a_6 = 5E\text{-}14$
	$b_1 = 16.225$	$b_2 = 16.272$	$b_3 = 15.217$		$b_4 = 15.638$	$b_5 = 16.991$	$b_6 = 14.675$
Module 3	SC_7	SC_8	SC_9	**Module 4**	SC_{10}	SC_{11}	SC_{12}
Capacitance (mF)	147.8	178.8	209.3	Capacitance (mF)	145.9	184.8	222.2
ESR (Ω)	9	8.1	7.1	ESR (Ω)	7.3	6.3	9.9
EPR Factors	$a_7 = 7E\text{-}15$	$a_8 = 1E\text{-}15$	$a_9 = 6E\text{-}14$	EPR Factors	$a_{10} = 9E\text{-}14$	$a_{11} = 4E\text{-}15$	$a_{12} = 3E\text{-}15$
	$b_7 = 15.508$	$b_8 = 10.903$	$b_9 = 13.444$		$b_{10} = 8.4903$	$b_{11} = 17.591$	$b_{12} = 17.054$

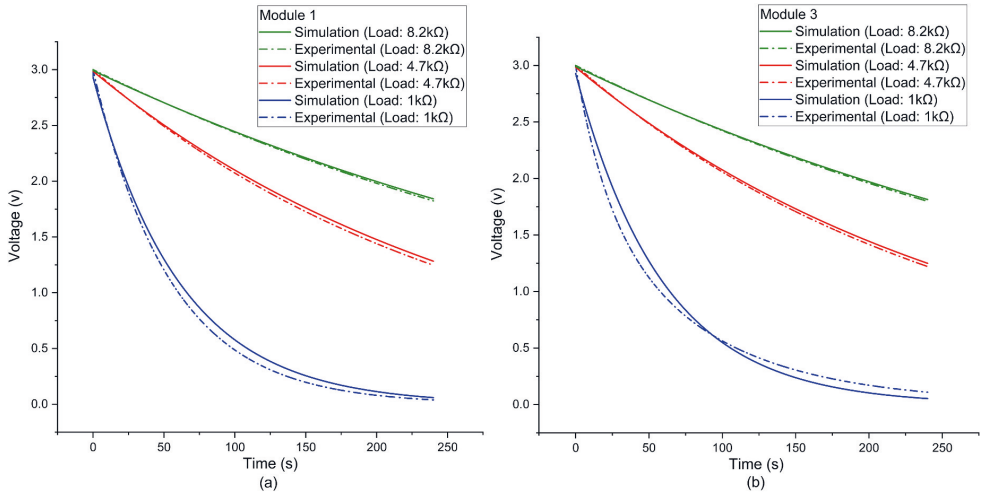

Fig. 5. Verification of the proposed model accuracy against experiments using carbon resistors as resistive loads. Experimental and simulation behavior of a) SCs module 1, b) SCs module 3.

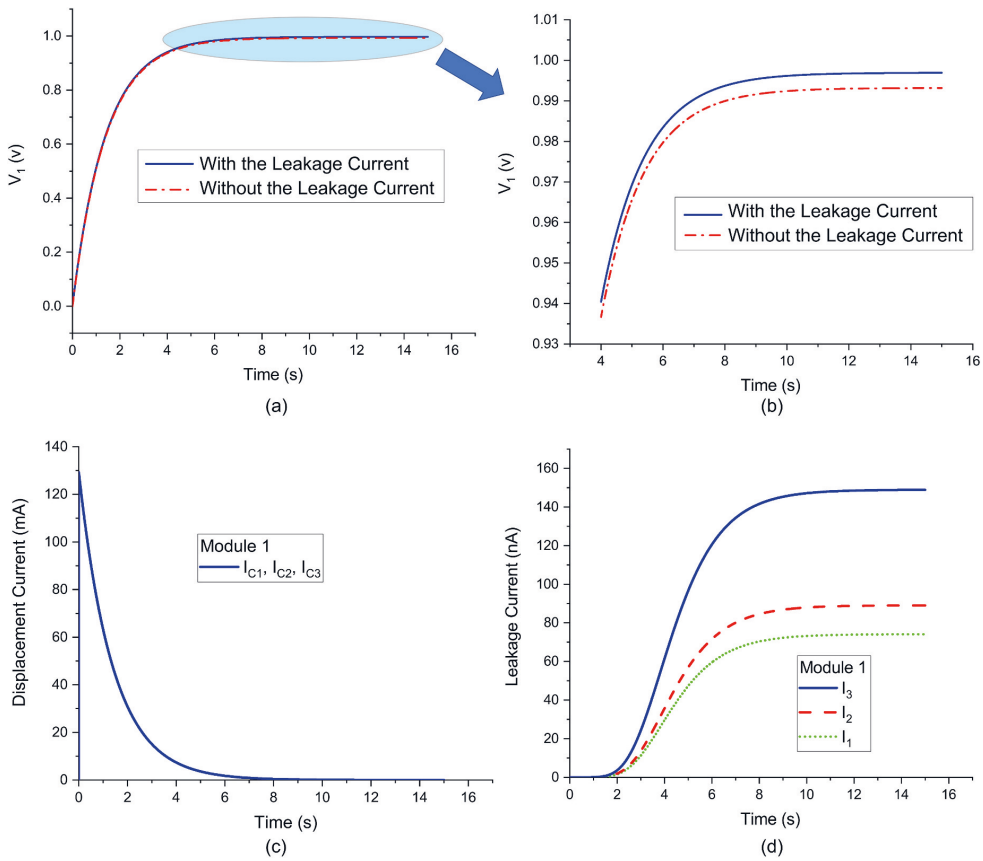

Fig. 6. a), b) Investigation of the leakage current effect on the charge of SCs in energy module 1. c), d) Comparison of the displacement and leakage current of the SCs during charging in energy module 1.

leakage currents is around 10^6 times smaller than the initial amount of the displacement currents. This simulation was also performed for the other three energy modules and similar results were observed for all modules. These results confirm that leakage current has little effect on the charging behavior of the SCs in energy modules and can be ignored.

3.3. Discharging behavior

In order to simulate the discharge behavior of SCs in energy modules, a resistor parallel to the system was used to model the load connected to the energy modules (Fig. 4b). Since these printed SCs can be used in a variety of applications such as Internet of Things (IoT), flexible and wearable electronics, energy harvesting wireless sensor networks, etc., and in both short-term and long-term applications, both large loads in the MΩ range and small loads in the kΩ range were simulated. The self-discharge, as well as the voltage delivered by module 3 to the different large load resistance values using the modified Spyker model (time constant: 31 days) and the model presented in this work, can be seen in Fig. 7a. The results for the simulation using the Spyker model are shown with a dash-dotted line and the results for the simulation using the model presented in this work are shown with a straight line. As can be seen in Fig. 7. a, upon increasing the resistive load in the long-term, especially during self-discharge, the Spyker model does not provide an accurate estimate of the behavior of the energy module. In addition, the modified Spyker model is no longer able to accurately estimate the final amount of the voltage stored in the SC energy module. On the other hand, as the accuracy of the model presented in this work with the empirical results was confirmed earlier in this article, it can be said that, for example, when self-discharging, there is still more than 2.5 V potential differences stored in this module after 30 days. While the 100 MΩ load is connected, the module, after 20 days of delivering power, is still able to deliver more than 2 V to the load. For other modules, similar results were obtained. In Fig. 7b, the amount of voltage delivered to the relatively small loads (range in kΩ) by module 3 using the model proposed in this work is shown over time. For example, when a 5 kΩ resistance load is connected to the module 3, after 2 min, there is still about 2 V stored in the energy module containing three series connected SCs.

We now compare the performance of the different modules when connected to the same resistive load during discharge as well as the self-discharge using the modified Spyker model, and the model proposed in this work. Fig. 7c shows the voltage delivered from the four modules to the same resistive load (100 MΩ) over time. As can be seen, module 4 shows better performance than the other modules. Module 3 delivers less voltage initially than modules 1 and 2, but performs better later on, and delivers higher voltage after the 6th day. The simulations were repeated for additional resistive loads in the range of MΩ, and in all simulations, module 4 had better performance in delivering more power to the loads over time. Fig. 7d shows the self-discharge of the four energy modules over time using the modified Spyker model and the proposed model; Straight lines show the results of the simulation using the proposed model and dash-dot lines also show the results of the modified Spyker model. Module 4 has again a relatively better performance than the other three modules using both models. However, the simulation using the modified Spyker model cannot even accurately estimate the final values of the potential difference stored in the modules while self-discharge and differs significantly from the simulation results using the proposed model.

The same comparison for delivering voltage from the energy modules was carried out for smaller resistance loads (in the range of kΩ) over shorter time (120 s). In Fig. 7e and f, the voltage delivered by different modules to a 5 kΩ resistive load using the model proposed in this work and the Spyker model can be seen, respectively. For this load, all four modules have almost the same performance using both models. The same simulations were performed for several other resistive loads in the kΩ range, from 1 to 500 kΩ; similar results were obtained for both models and there was no significant difference between the modules' performance. This is due to the fact that the simulations for small resistive loads were performed for a short time (120 s), and as already mentioned in the Introduction, leakage current has little effect on the discharge behavior of SCs in the short-term. Therefore, all four energy modules show almost identical self-discharge and leakage behavior. As a result, the modules have the same performance in delivering power to the small resistive loads.

The reason for the better performance of Module 4 in delivering more power to the loads in long-term is related to the leakage behavior of the SCs in this module. By comparing the leakage currents of the 12 SCs in the four energy modules, it can be seen that the three SCs in module 4 have smaller leakage current than the SCs in the other modules. Fig. 8a, 8b, 8c, 8d shows the leakage current of the SCs in each of the four energy modules and it is clear that the three SCs that form module 4 have a lower total leakage current than the other SCs, and therefore module 4 has a better performance in delivery of more power to the different loads in the long-term. Therefore, based on the simulation results of the proposed model, it can be said that device-to-device variations in electrical properties, especially leakage current in printed SCs, which are typically encountered in printed devices can affect the performance of series-connected SC modules, but not to the extent that their usability or stability is significantly reduced. In addition, the leakage behavior of the SCs that form each module using the modified Spyker model can be seen in Fig. 8a, 8b, 8c, 8d. As can be seen in this figure, using the modified Spyker model, linear curves are obtained for the leakage currents, which does not correspond to the nonlinear leakage behavior of SCs in reality.

3.4. Effect of resistive load on the leakage current of supercapacitors

According to the discharge model of the SC modules (Fig. 4b), as the resistance load increases, the significance of the leakage current of the SCs in the energy modules increases. For example, Fig. 8e and 8f shows the leakage current of the SC1 in the energy module 1 for the different small and large resistive loads. As can be seen in this figure, the highest leakage current is for the self-discharge and the lowest is when a 1 kΩ resistive load is connected to the energy module. This happens because as the resistive load increases, less voltage is delivered from the SCs to the load, hence more potential difference remains in the SCs and since the leakage current has an exponential relationship with the potential difference over the SC, the leakage current remains higher due to the larger potential difference between the two ends of the SC.

4. Summary and conclusion

In this paper, we present a simple equivalent circuit model for supercapacitors (SCs) energy module based on exploiting the experimental parameters of printed SCs. The model includes both the equivalent series resistance (ESR) and an exponential equation to account for the non-linearity of leakage current and self-discharge. These experimental parameters, which are unique for each SC, contribute to the effective simulation and design of future systems. In addition, this model can be used to predict important issues in the printing of devices, as well as the dependence of an energy module consisting of series connected SCs on different device to device electrical variables.

The proposed model was used to investigate the effect of leakage current while charging SCs in four energy modules. In addition, the results of the self-discharge of each module and the amount of energy delivered to the different loads by four energy modules were compared with the model reported in the literature [50]. Finally, the effect of changing the resistive load on the time-dependent leakage current of SCs in an energy module was investigated. Furthermore, an analysis of the effect of device-to-device variations on the performance of the modules showed that typical variations in printed devices are not sufficient to cause significant problems in operation.

As SCs have been widely discussed in the literature as a promising

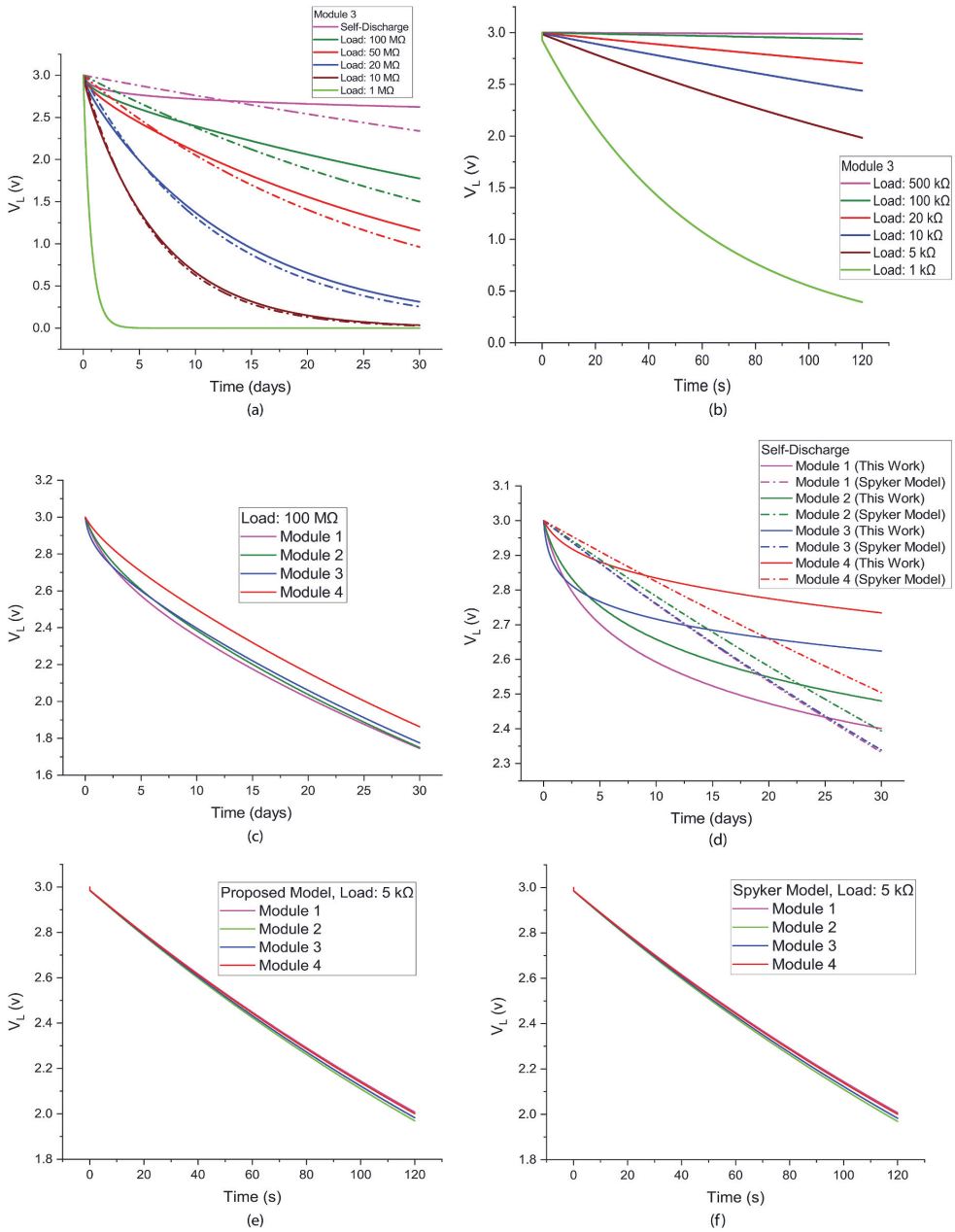

Fig. 7. a) Self-discharge behavior and the voltage delivered to the different large loads by the energy module 3 over time using the modified Spyker model and the model proposed in this work; The modified spyker and the proposed model are shown with dash-dotted and straight lines, respectively. (b) Voltage delivered to the different small loads by the energy module 3 over time using the model proposed in this work. (c) Comparing the voltage delivered to a 100 MΩ resistive load by four different energy modules. (d) Self-discharge behavior of four energy modules using the Spyker model and the proposed model; The modified spyker and the proposed model are shown with dash-dotted and straight lines, respectively. e) Comparison of the voltage delivered to a 5 kΩ resistive load by four different energy modules in short-term using the proposed model. f) Comparison of the voltage delivered to a 5 kΩ resistive load by four different energy modules in short-term using the Spyker model.

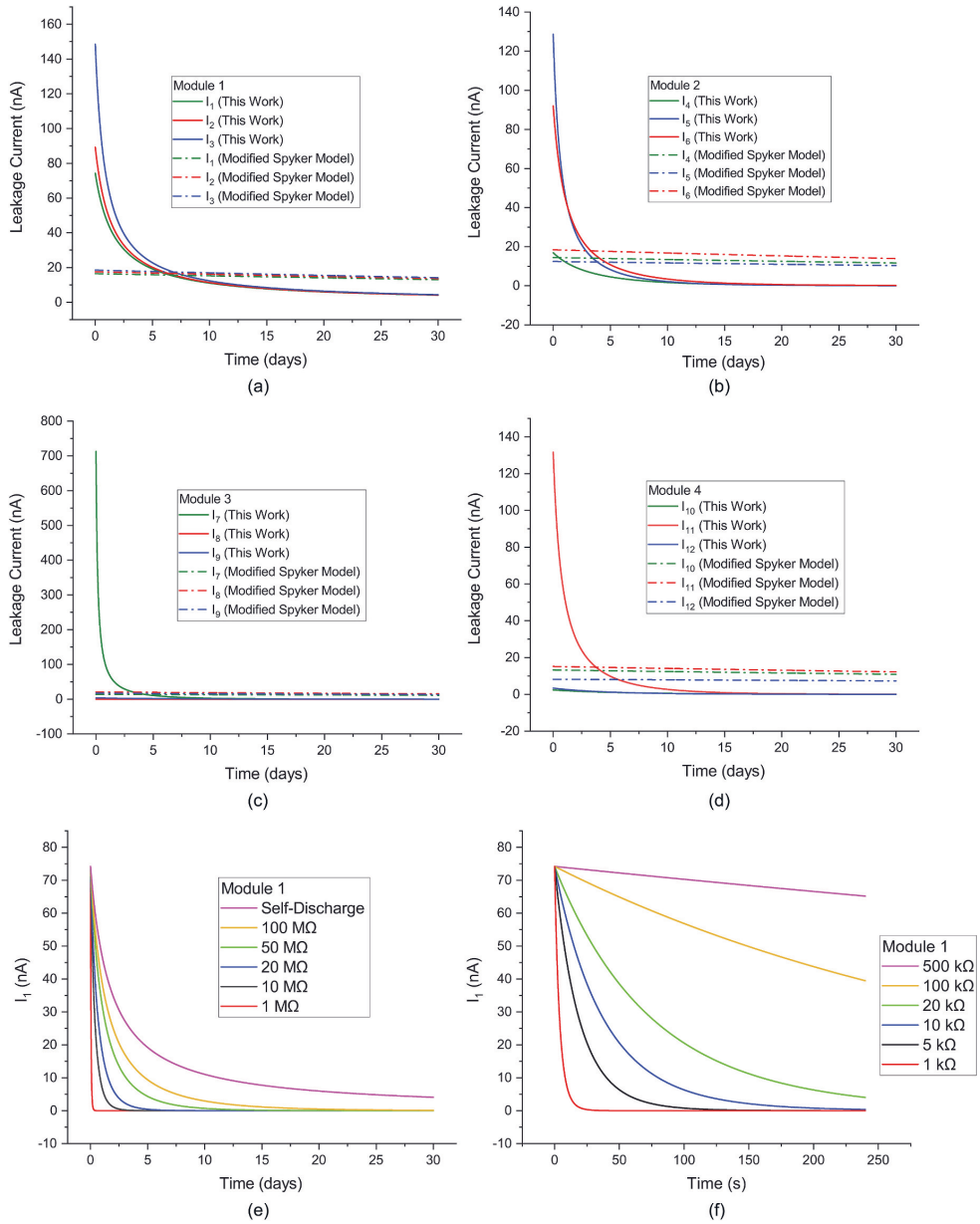

Fig. 8. a, b, c, d) Leakage behavior of SCs forming four energy modules using the proposed model and the modified Spyker model. e, f) The effect of the resistance load change on the leakage current of SCs.

energy storage technology, modelling the charging and discharging behavior of SCs in the form of energy modules also gives a good view into their performance in various applications as energy storage systems. The models reported in the literature have more RC network elements and branches and are complex for use in supercapacitor modules connected in series. These models are also not accurate to simulate the nonlinear self-discharge effect of the supercapacitors in long-term. In addition, exponential models using variable leakage resistance (VLR) have been published in the literature that have several separate exponential functions to model the self-discharge behavior of a single supercapacitor in the short-term (several hours). Accordingly, in order to simulate the self-discharge behavior of energy modules consisting of several supercapacitors connected in series for a long time (one month) using exponential models reported in the literature, a very large number of distinct exponential functions and parameters definition steps are required. Since simple versions are required to implement the models in practical applications, the models presented in the literature, despite having many RC network elements and parameter determination

difficulties, are not suitable for long-term simulation of supercapacitor modules. To conclude, the reported approach in this work can simply model the SC internal charge/discharge redistribution and explain experimental results in long-term (31 days). Therefore, the work reported here provides a useful and applicable approach for testing the behavior of SC modules in energy storage systems and power management strategies. Potential applications of this type of SCs in which high power density and longevity are valuable features include energy autonomous Internet of Things (IoT), Energy-Harvesting Wireless Sensor Nodes and wearable self-charging power systems.

CRediT authorship contribution statement

Hamed Pourkheirollah: Conceptualization, Methodology, Software, Validation, Formal analysis, Investigation, Data curation, Writing – original draft, Visualization. **Jari Keskinen:** Conceptualization, Methodology, Resources, Writing – review & editing. **Matti Mäntysalo:** Conceptualization, Methodology, Resources, Writing – review & editing, Supervision. **Donald Lupo:** Resources, Writing – review & editing, Supervision, Project administration, Funding acquisition.

Declaration of competing interest

The authors declare that they have no known competing financial interests or personal relationships that could have appeared to influence the work reported in this paper.

Acknowledgements

This work has mainly received funding from the European Union's Horizon 2020 research and innovation programme under the Marie Skłodowska-Curie grant agreement No 814299 - CHARISMA. Parts of the research used Academy of Finland Research Infrastructure "Printed Intelligence Infrastructure" (PII-FIRI, Grant Number 320019).

References

[1] Mathew Aneke, Meihong Wang, Energy storage technologies and real-life applications–A state of the art review, Appl. Energy 179 (2016) 350–377.
[2] Chang Gao, Jian Gao, Changxiang Shao, Yukun Xiao, Yang Zhao, Liangti Qu, Versatile origami micro-supercapacitors array as a wind energy harvester, J. Mater. Chem. 6 (40) (2018) 19750–19756.
[3] D. Lau, N. Song, C. Hall, Y. Jiang, S. Lim, I. Perez-Wurfl, Z. Ouyang, A. Lennon, Hybrid solar energy harvesting and storage devices: the promises and challenges, Mater. Today Energy 13 (2019) 22–44.
[4] Jian Lv, Itthipon Jeerapan, Farshad Tehrani, Yin Lu, Cristian Abraham Silva-Lopez, Ji-Hyun Jang, Davina Joshuia, et al., Sweat-based wearable energy harvesting-storage hybrid textile devices, Energy Environ. Sci. 11 (12) (2018) 3431–3442.
[5] Bilal Munir, Vladimir Dyo, On the Impact of mobility on battery-less RF energy harvesting system performance, Sensors 18 (11) (2018) 3597.
[6] Lin Li, Zhong Wu, Shuang Yuan, Xin-Bo Zhang, Advances and challenges for flexible energy storage and conversion devices and systems, Energy Environ. Sci. 7 (7) (2014) 2101–2122.
[7] El-Kady, F. Maher, Richard B. Kaner, Scalable fabrication of high-power graphene micro-supercapacitors for flexible and on-chip energy storage, Nat. Commun. 4 (1) (2013) 1–9.
[8] Xue Chen, , Nicolo Simone Villa, Yanfeng Zhuang, Linzhe Chen, Tianfu Wang, Zida Li, Tiantian Kong, Stretchable supercapacitors as emergent energy storage units for health monitoring bioelectronics, Adv. Energy Mater. 10 (4) (2020) 1902769.
[9] Michal Prauzek, Jaromir Konecny, Monika Borova, Karolina Janosova, Jakub Hlavica, Petr Musilek, Energy harvesting sources, storage devices and system topologies for environmental wireless sensor networks: a review, Sensors 18 (8) (2018) 2446.
[10] David Newell, Maeve Duffy, Review of power conversion and energy management for low-power, low-voltage energy harvesting powered wireless sensors, IEEE Trans. Power Electron. 34 (10) (2019) 9794–9805.
[11] Yuzhen Ma, Qing Ji, Song Chen, Gangbing Song, An experimental study of ultra-low power wireless sensor-based autonomous energy harvesting system, J. Renew. Sustain. Energy 9 (5) (2017), 054702.
[12] Xicai Yue, Janice Kiely, Des Gibson, M. Emmanuel, Drakakis, Charge-based supercapacitor storage estimation for indoor sub-mW photovoltaic energy harvesting powered wireless sensor nodes, IEEE Trans. Ind. Electron. 67 (3) (2019) 2411–2421.
[13] Andrey Somov, Raffaele Giaffreda, Powering IoT Devices: Technologies and Opportunities, IEEE IoT Newsletter, 2015.
[14] Swati Sucharita Roy, Deepak Puthal, Suraj Sharma, Saraju P. Mohanty, Albert Y. Zomaya, Building a sustainable Internet of Things: energy-efficient routing using low-power sensors will meet the need, IEEE Consumer Electronics Magazine 7 (no. 2) (2018) 42–49.
[15] Tanveer Ahmad, Dongdong Zhang, Using the Internet of Things in Smart Energy Systems and Networks, Sustainable Cities and Society, 2021, p. 102783.
[16] Ibrar Yaqoob, Ejaz Ahmed, Ibrahim Abaker Targio Hashem, Abdelmuttlib Ibrahim Abdalla Ahmed, Abdullah Gani, Muhammad Imran, Mohsen Guizani, Internet of things architecture: recent advances, taxonomy, requirements, and open challenges, IEEE Wireless Commun. 24 (3) (2017) 10–16.
[17] Taiyang Wu, Fan Wu, Jean-Michel Redoute, Mehmet Rasit Yuce, An autonomous wireless body area network implementation towards IoT connected healthcare applications, IEEE Access 5 (2017) 11413–11422.
[18] Thirumalesu Kudithi, R. Sakthivel, High-performance ECC processor architecture design for IoT security applications, J. Supercomput. 75 (1) (2019) 447–474.
[19] Sandeep Pirbhulal, Heye Zhang, Md Eshrat E Alahi, Hemant Ghayvat, Subhas Chandra Mukhopadhyay, Yuan-Ting Zhang, Wanqing Wu, A novel secure IoT-based smart home automation system using a wireless sensor network, Sensors 17 (1) (2017) 69.
[20] Fernández-Caramés, M. Tiago, Paula Fraga-Lamas, Towards the Internet of smart clothing: a review on IoT wearables and garments for creating intelligent connected e-textiles, Electronics 7 (12) (2018) 405.
[21] Xiong Pu, Weiguo Hu, Zhong, Lin Wang, Toward wearable self-charging power systems: the integration of energy-harvesting and storage devices, Small 14 (1) (2018), 1702817.
[22] Hui Yu, Nan Li, Ni Zhao, How far are we from achieving self-powered flexible health monitoring systems: an energy perspective, Adv. Energy Mater. 11 (9) (2021), 2002646.
[23] Libu Manjakkal, Abhilash Pullanchiyodan, Nivasan Yogeswaran, Ensieh S. Hosseini, Ravinder Dahiya, A wearable supercapacitor based on conductive PEDOT: PSS-coated cloth and a sweat electrolyte, Adv. Mater. 32 (24) (2020), 1907254.
[24] Afriyanti Sumboja, Jiawei Liu, Wesley Guangyuan Zheng, Zong Yun, Hua Zhang, Zhaolin Liu, Electrochemical energy storage devices for wearable technology: a rationale for materials selection and cell design, Chem. Soc. Rev. 47 (15) (2018) 5919–5945.
[25] Jayoung Kim, Rajan Kumar, Amay J. Bandodkar, Wang Joseph, Advanced materials for printed wearable electrochemical devices: a review, Adv. Electronic Mater. 3 (1) (2017), 1600260.
[26] Qi Xue, Jinfeng Sun, Yan Huang, Minshen Zhu, Zengxia Pei, Hongfei Li, Yukun Wang, Na Li, Haiyan Zhang, Chunyi Zhi, Recent progress on flexible and wearable supercapacitors, Small 13 (45) (2017), 1701827.
[27] Pavlos Giannakou, Mehmet O. Tas, Brice Le Borgne, Maxim Shkunov, Water-transferred, inkjet-printed supercapacitors toward conformal and epidermal energy storage, ACS Appl. Mater. Interfaces 12 (7) (2020) 8456–8465.
[28] Tiance An, Wenlong Cheng, Recent progress in stretchable supercapacitors, J. Mater. Chem. 6 (32) (2018) 15478–15494.
[29] Michal Prauzek, Jaromir Konecny, Monika Borova, Karolina Janosova, Jakub Hlavica, Petr Musilek, Energy harvesting sources, storage devices and system topologies for environmental wireless sensor networks: a review, Sensors 18 (8) (2018) 2446.
[30] Kwadwo Mensah-Darkwa, Camila Zequine, Pawan K. Kahol, Ram K. Gupta, Supercapacitor energy storage device using biowastes: a sustainable approach to green energy, Sustainability 11 (2) (2019) 414.
[31] Jiandong Duan, Shaogui Fan, Fengjiang Wu, Li Sun, Guanglin Wang, Power balance control of micro gas turbine generation system based on supercapacitor energy storage, Energy 119 (2017) 442–452.
[32] Richa Dubey, Velmathi Guruviah, Review of carbon-based electrode materials for supercapacitor energy storage, Ionics 25 (4) (2019) 1419–1445.
[33] Brian E. Conway, Electrochemical Supercapacitors: Scientific Fundamentals and Technological Applications, Springer Science & Business Media, 2013.
[34] Max Lu, Supercapacitors: Materials, Systems, and Applications, John Wiley & Sons, 2013.
[35] Jiří Libich, Josef Máca, Jiří Vondrák, Ondřej cech, and Marie sedlaříková. "Supercapacitors: properties and applications, J. Energy Storage 17 (2018) 224–227.
[36] Kriti Sharma, Anmol Arora, Surya Kant Tripathi, Review of supercapacitors: materials and devices, J. Energy Storage 21 (2019) 801–825.
[37] Muhammad Zahir Iqbal, Mian Muhammad Faisal, Syeda Ramsha Ali, Integration of supercapacitors and batteries towards high-performance hybrid energy storage devices, Int. J. Energy Res. 45 (2) (2021) 1449–1479.
[38] Manu Kujala, Terho Kololuoma, Jari Keskinen, Donald Lupo, Matti Mäntysalo, M. Thomas, Kraft, Bending reliability of screen-printed vias for a flexible energy module, npj Flexible Electronics 4 (1) (2020) 1–8.
[39] Maedeh Arvani, Jari Keskinen, Railanmaa Anna, Sanna Siljander, Tomas Björkqvist, Sampo Tuukkanen, Donald Lupo, Additive manufacturing of monolithic supercapacitors with biopolymer separator, J. Appl. Electrochem. 50 (6) (2020) 689–697.
[40] Maedeh Arvani, Jari Keskinen, Donald Lupo, Mari Honkanen, Current collectors for low resistance aqueous flexible printed supercapacitors, J. Energy Storage 29 (2020), 101384.
[41] Patrice Simon, Yury Gogotsi, Bruce Dunn, Where do batteries end, and supercapacitors begin? Science 343 (6176) (2014) 1210–1211.

[42] Jari Keskinen, Railanmaa Anna, Donald Lupo, Monolithically prepared aqueous supercapacitors, J. Energy Storage 16 (2018) 243–249.
[43] Lei Zhang, Xiaosong Hu, Zhenpo Wang, Fengchun Sun, David G. Dorrell, A review of supercapacitor modeling, estimation, and applications: a control/management perspective, Renew. Sustain. Energy Rev. 81 (2018) 1868–1878.
[44] Jeongbin Lee, Jaeshin Yi, Daeyong Kim, Chee Burm Shin, Kyung-Seok Min, Jongrak Choi, Ha-Young Lee, Modeling of the electrical and thermal behaviors of an ultracapacitor, Energies 7 (12) (2014) 8264–8278.
[45] Alberto Berrueta, Idoia San Martin, Andoni Hernández, Alfredo Ursúa, Pablo Sanchis, Electro-thermal modelling of a supercapacitor and experimental validation, J. Power Sources 259 (2014) 154–165.
[46] Maximilian Kaus, Julia Kowal, Dirk Uwe Sauer, Modelling the effects of charge redistribution during self-discharge of supercapacitors, Electrochim. Acta 55 (25) (2010) 7516–7523.
[47] Thibaut Kovaltchouk, Bernard Multon, Hamid Ben Ahmed, Judicael Aubry, Venet Pascal, Enhanced aging model for supercapacitors taking into account power cycling: application to the sizing of an energy storage system in a direct wave energy converter, IEEE Trans. Ind. Appl. 51 (3) (2014) 2405–2414.
[48] Mustafa Ergin Şahİn, Frede Blaabjerg, Ariya Sangwongwanİch, Modelling of supercapacitors based on simplified equivalent circuit, CPSS Trans. Power Electr. Appl. 6 (1) (2021) 31–39.
[49] Lisheng Shi, M.L. Crow, Comparison of ultracapacitor electric circuit models, in: IEEE Power and Energy Society General Meeting-Conversion and Delivery of Electrical Energy in the 21st Century, IEEE, 2008, pp. 1–6, 2008.
[50] Russell L. Spyker, R. Mark Nelms, Classical equivalent circuit parameters for a double-layer capacitor, IEEE Trans. Aero. Electron. Syst. 36 (3) (2000) 829–836.
[51] R. Faranda, A new parameters identification procedure for simplified double layer capacitor two-branch model, Elec. Power Syst. Res. 80 (4) (2010) 363–371.
[52] Yasser Diab, Venet Pascal, Hamid Gualous, Gérard Rojat, Self-discharge characterization and modeling of electrochemical capacitor used for power electronics applications, IEEE Trans. Power Electron. 24 (2) (2008) 510–517.
[53] Ying Zhang, Hengzhao Yang, Modeling and characterization of supercapacitors for wireless sensor network applications, J. Power Sources 196 (8) (2011) 4128–4135.
[54] Hengzhao Yang, Ying Zhang, Self-discharge analysis and characterization of supercapacitors for environmentally powered wireless sensor network applications, J. Power Sources 196 (20) (2011) 8866–8873.
[55] Ghanbari, Teymoor, Ehsan Moshksar, Sara Hamedi, Fatemeh Rezaei, and Zahra Hosseini. "Self-discharge modeling of supercapacitors using an optimal time-domain based approach." J. Power Sources 495 (2021): 229787.
[56] Jari Keskinen, Suvi Lehtimäki, Arman Dastpak, Sampo Tuukkanen, Timo Flyktman, Thomas Kraft, Railanmaa Anna, Donald Lupo, Architectural modifications for flexible supercapacitor performance optimization, Electr. Materials Let. 12 (6) (2016) 795–803.
[57] Jari Keskinen, Saara Tuurala, Sjödin Martin, Kaisa Kiri, Leif Nyholm, Timo Flyktman, Maria Strømme, Maria Smolander, Asymmetric and symmetric supercapacitors based on polypyrrole and activated carbon electrodes, Synth. Met. 203 (2015) 192–199.
[58] Jari Keskinen, Supercapacitors on Flexible Substrates for Energy Autonomous Electronics, 2018.
[59] Jari Keskinen, Railanmaa Anna, Donald Lupo, Monolithically prepared aqueous supercapacitors, J. Energy Storage 16 (2018) 243–249.
[60] Anna Railanmaa, Suvi Lehtimäki, Jari Keskinen, Donald Lupo, Non-toxic printed supercapacitors operating in sub-zero conditions, Sci. Rep. 9 (1) (2019) 1–8.
[61] Anna Railanmaa, Ayat Soltani, Suvi Lehtimäki, Nazanin Pournoori, Jari Keskinen, Mikko Hokka, Donald Lupo, Skin-conformable printed supercapacitors and their performance in wear, Sci. Rep. 10 (1) (2020) 1–9.
[62] International Electrochemical Commission, International Standard: Fixed Electric Double-Layer Capacitors for Use in Electronic Equipment, First. IEC, 2006, 62391-1.

PUBLICATION II

A Modified Exponential Equivalent Parallel Resistance (EPR) Model for Predicting Self-Discharge Behavior of Printed Flexible Supercapacitors

Hamed Pourkheirollah; Jari Keskinen; Donald Lupo; Matti Mäntysalo

2022 IEEE 9th Electronics System-Integration Technology Conference (ESTC)

https://doi.org/10.1109/ESTC55720.2022

A Modified Exponential Equivalent Parallel Resistance (EPR) Model for Predicting Self-Discharge Behavior of Printed Flexible Supercapacitors

Hamed Pourkheirollah
Faculty of Information Technology and Communication Sciences/ Electrical Engineering
Tampere University
Tampere, Finland
hamed.pourkheirollah@tuni.fi

Jari Keskinen
Faculty of Information Technology and Communication Sciences/ Electrical Engineering
Tampere University
Tampere, Finland
jari.keskinen@tuni.fi

Donald Lupo
Faculty of Information Technology and Communication Sciences/ Electrical Engineering
Tampere University
Tampere, Finland
donald.lupo@tuni.fi

Matti Mäntysalo
Faculty of Information Technology and Communication Sciences/ Electrical Engineering
Tampere University
Tampere, Finland
matti.mantysalo@tuni.fi

***Abstract*— Typically, batteries are used to power interconnected Internet of Things (IoT) devices. Intermittent manual replacement of batteries or recharging them after complete depletion is one of their major disadvantages, which increases the cost of maintaining and restricts the large-scale use of devices. Considering the longevity of devices and battery limitations, and in order to achieve the integrated and efficient operation of IoT devices, the development of alternative power sources and power management strategies is inevitable. The supercapacitor is a suitable energy storage option for energy-harvesting powered autonomous wireless sensor nodes in IoT applications. The leakage current value provided for the supercapacitors by the manufacturers is tested after the supercapacitor has been floated at a constant voltage for a long time. This raises concerns about the uncertainty of dynamic leakage current behavior during repeated charging and discharging of the supercapacitor in IoT applications. At present, there is no effective method to estimate and predict leakage current and the discharging behavior of supercapacitors in IoT applications with the aim of achieving optimal performance. In this work, an improved simplified exponential model is presented in order to simulate the non-linear discharge behavior of our fabricated printed flexible supercapacitors in long-term (31 days). The printed supercapacitors are disposable and have been fabricated using low-cost and non-toxic processes and materials. The model proposed in this work is very well adapted to the experimentally measured self-discharge results of the supercapacitors. In addition, according to the experimental and data fitting results of 10 fabricated supercapacitors, all the parameters defined in this model show good statistical values and have a Gaussian (normal) distribution.**

Keywords—supercapacitors, printed supercapacitors, energy storage, self-discharge, leakage current, supercapacitor modeling, supercapacitor simulation, equivalent parallel resistance, EPR model, VLR model

I. INTRODUCTION

Over the past two decades, supercapacitors (SCs) also called electric double layer capacitors (EDLCs), have received intensive study as a potential form of energy storage [1]. A SC consists of two electrodes with porous microstructures , separated by an electrolyte and separator layer [2]. As compared to conventional capacitors, SCs are larger in capacitance value and have a greater energy density. In addition to their higher power density and higher charge/discharge efficiency, SCs have a shorter charging time and a longer cycle life compared to batteries, making them ideal for a large number of applications [3,4]. In a variety of applications, SCs can handle fast fluctuations in the energy level [5] and be employed both as auxiliary energy storage devices and as a primary power source [6]. It has been proposed that SCs can be used as energy storage systems in a wide variety of industrial applications including energy autonomous self-powered wireless sensor networks (WSNs), Internet of Things (IoT) and flexible and wearable electronic devices [7-9]. Moreover, an innovative energy storage textile was recently developed using graphene and manganese oxide as part of a flexible SC [10]. The fabric based SCs that are generated exhibit high specific capacitance, excellent electric conductivity, high flexibility, and a long cycle life [10].

Self-discharge and leakage current have been identified as a limiting factor for the practical application of SCs [11]. A self-discharge occurs when a SC is left in open circuit, in which the voltage of the SC spontaneously decreases with an effectively infinite external resistance. The effects of the self-discharge cannot be ignored, since they also have a considerable effect on SC's dynamic during rest periods, which can be disruptive to its function and may result in the loss of stored energy [12]. Three different main processes result in self-discharge, including Ohmic leakage, charge redistribution, and Faradaic reactions [13]. Almost certainly, Faradaic reactions are the dominant cause of the self-discharge phenomenon in SCs [14]. On the other hand, SC's leakage current refers to the tiny current that flows while the rated voltage continues to be applied to the capacitor [15]. The leakage current eventually becomes stable over time as it diminishes. Considering the detrimental effects of the self-

discharge and leakage current, it is necessary to consider these characteristics when designing an electronic circuit with a SC. However, self-discharge and leakage current appear to have received less attention in the literature.

Various approaches for modeling the self-discharge in SCs have been reported in previous studies. A good modeling of this phenomenon enables us to obtain a reasonable estimate of the amount of available energy in the SCs at any given time. Earlier studies demonstrated that the SC dynamics can be physically described by various equivalent circuit models, such as classical [16], two-branch [17], multi-branch [18], ladder circuit models [19], etc. Based on equivalent circuit models, series and parallel resistances and capacitances are typically used to represent the resistance of porous carbon electrodes and the capacitance of carbon electrodes and electrolyte, respectively [20]. Models with two and three branches are more widely discussed in the literature. In order to take leakage current into account, a resistance branch is generally considered to be parallel to the other branches [21]. In some earlier publications [16], self-discharge/leakage current is modeled using a constant series or in-parallel resistance that is connected to an ideal capacitor (classical model). However, simply considering a constant resistance in classical model is not sufficient to simulate the self-discharge process over the long-term. In some other works [21], an equivalent circuit model based on variable leakage resistances (VLRs) has been proposed as a means of effectively describing the self-discharge effects of SCs. In these models, self-discharge is represented by a VLR parallel to the equivalent capacitance. VLRs can illustrate the dynamic charge leakage mechanism within SCs during the rest period. Moreover, there have been some studies in the literature on polynomial equivalent circuit models that incorporate VLR as a function of the terminal voltage [22]. Various time constants are present in these models during different self-discharge time and voltage intervals. In consequence, these models also contain several exponential functions and leakage resistances. The parameters of such models for long-term simulations would, however, be subject to a great number of exponential functions for a wide range of voltages and time periods, which would result in a huge number of parameter determination steps. Furthermore, it would be even more difficult to identify the parameters if the equivalent circuit model included multiple VLRs in SC energy modules in which a number of SCs are connected in series or in parallel. Besides, identifying the parameters of the dynamic polynomial function under a variety of experimental conditions will be quite challenging. In summary, the two-branch model with EPR, the three-branch model and the VLR models described in the literature have multiple branches and many RC network elements, whereas in practical applications, simplified versions are necessary to facilitate model implementation.

II. Experimental, Methods and Statistical

A. Experimental

The printed SCs used to develop this model were fabricated by this group. The fabrication process steps and characterization of the printed SCs have been described in earlier works published by the authors [14,23]. For the purpose of determining the EPR exponential factors corresponding to the self-discharge, all SCs were charged to a voltage of around 1.0 V and were kept at this voltage for 24 hours. Having been fully charged, the SCs were disconnected from the power source and their potential difference was monitored and measured for 31 days. As the rate of the self-discharge is higher at the beginning and in the early days, more data were collected in this period.

B. Method

As discussed in the introduction, equivalent circuit models reported in the literature have proven ineffective for long-term applications due to inadequate consideration of leakage and self-discharge effects. In this study, a simple model is proposed to overcome this limitation, which models the nonlinearity of leakage and self-discharge in the long-term. For each SC in the proposed equivalent circuit model, a conventional capacitor is used to model capacitance value, a series resistor to model ESR and ohmic losses, and a variable exponential equivalent parallel resistor (EPR) to model self-discharge and leakage current. This model has the same elements as the model that we reported in our earlier paper [23], although the exponential equation used for EPR and the method of obtaining EPR parameters differ from the previous paper. The current work uses $I=V\times e^{-(a+b\times V)}$ as the exponential equation of EPR representing self-discharge and leakage current effects, which actually exhibits a better fit with self-discharge experimental data. In addition, this exponential equation shows better suitability for Monte-Carlo simulations, which will be the focus of the authors' next research work.

We use the capacitor's discharge potential difference formula in order to obtain the EPR equation.

$$V=V_0\times e^{(-t/R\times C)},\ R=-t/(C\times \ln(V/V0)) \quad (1)$$

The capacitance value 'C' has already been determined by the characterization of the printed SCs using the standard Maccor system [23,24]. On the other hand, based on the self-discharge experimental data of the SCs, we have already determined 'V0' as the initial potential difference, 't' as time and 'V' as the potential difference for each SC at a specific time. Therefore, the numerical value of the dynamic resistance can now be calculated for each data point and the resistance curve (R(V)) can then be plotted as a function of potential difference. On the subsequent step, we fit the exponential equation $e^{(a+b\times V)}$ to the R(V) data points. As a result, we can determine 'a' and 'b' parameters for each individual SC in this manner. For example, as illustrated in Fig. 1, for a SC, the R(V) experimental data points are fitted to the desired exponential function. According to the table in Fig. 1, the statistical fitting parameters for this fit, such as the R-square (COD) and Adj. R-square are very close to 1, indicating that the exponential fitting curve has a good fit with the experimental data points.

In order to be able to model the self-discharge and leakage of SCs, the leakage current for the SC must be defined as a function of the potential difference. As $R=V/I = e^{(a+b\times V)}$, hence $I=V\times e^{-(a+b\times V)}$ and this provides the SC's EPR for the proposed model. The equivalent circuit model of a SC presented in this work can be seen in Fig. 2.

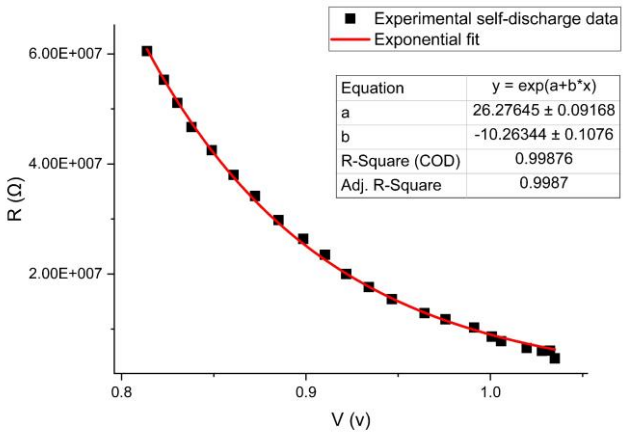

Figure 1. Exponential curve fitting of R(V) for a SC.

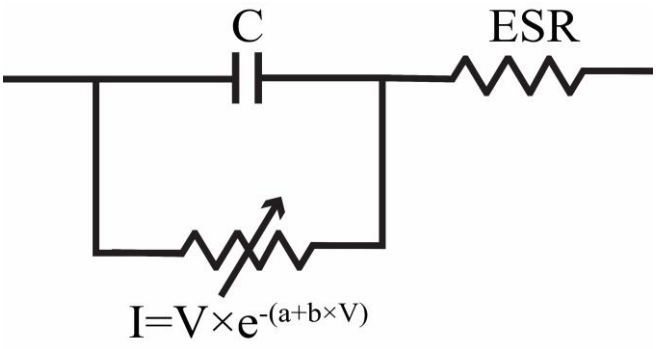

Figure 2. Proposed equivalent circuit model for a SC.

C. Statistical Tests of the Parameters

In order to develop the proposed model in this study, the characterization parameters ('C' and 'ESR'), self-discharge data, and EPR parameters ('a' and 'b') of 10 printed SCs were analyzed. The normal distribution (Gaussian distribution) was used to analyze the distribution of 10 SC parameters used in the development of the proposed model. Fig. 3 illustrates the histogram chart of all four parameters of the model; the distribution and the Bell curve (blue curve) for each parameter are included in the figure.

Furthermore, a normality test was conducted on every parameter to evaluate whether the data set for each parameter can be well described by a normal distribution. The following table summarizes the descriptive statistics for each parameter based on the normality test. According to table 1, the descriptive statistics indicate that all four parameters of the model are normally distributed. P-value and the approximate equality of mean and median values for each of the four parameters indicate a positive result for the normality test and prove that the normality test has been passed for each of the parameters. Moreover, these statistical values have demonstrated promising adaptability to Monte Carlo simulations.

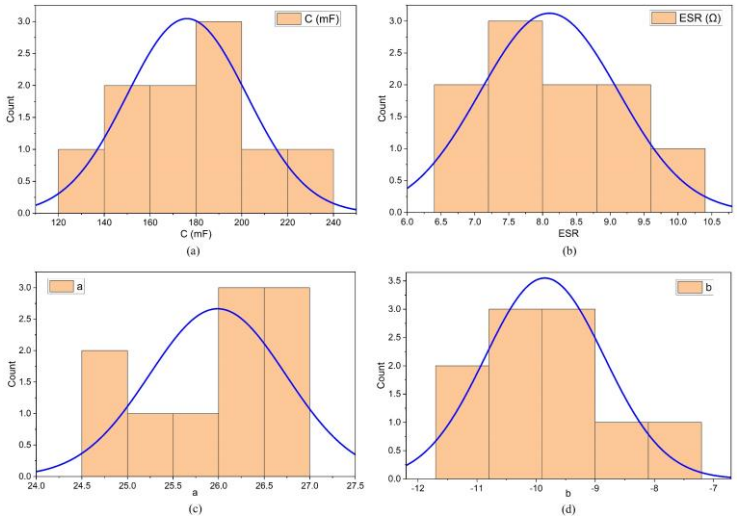

Figure 3. Histogram chart and Bell curve (normal distribution curve) for each parameter of the proposed model.

TABLE 1. DESCRIPTIVE STATISTICS FOR EACH OF THE FOUR SC'S PARAMETERS OF THE PROPOSED MODEL.

Parameters	C	ESR	a	b
N total	10	10	10	10
Mean	176.1	8.1	26	-9.9
Standard Deviation	26.2	1.0	0.75	1.0
Minimum	130	6.8	24.8	-11.6
Median	179.2	8.1	26.1	-9.9
Maximum	222.2	9.9	26.9	-8.0
p-value	0.98	0.62	0.36	1.0

III. RESULTS AND DISCUSSION

A. Accuracy of the proposed model in the self-discharge mode

For the purpose of evaluating the accuracy of the proposed model, the simulation results of the potential difference for four SCs in self-discharge mode were compared with experimental data collected for a period of 31 days. As can be seen in Fig. 4, there is no big difference between the experimental data and simulation results and a reasonable agreement can be observed between the simulation curve and the experimental data. After a period of 31 days, the difference between the measured experimental data and the simulation results is very small and the estimation error is less than two percent using the model presented in this paper.

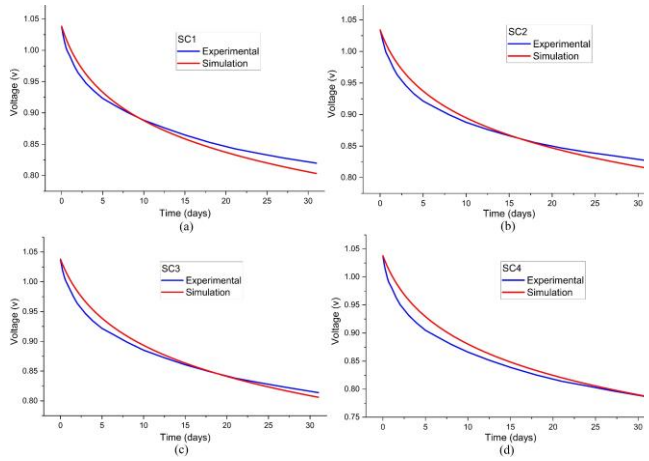

Figure 4. Experimental data and simulation results of the potential difference in self-discharge mode for four SCs over 31 days.

B. *Long-term Self-Discharge Behavior Simulation of SC Energy Modules.*

The printed SCs contain aqueous electrolytes, and because of the electrolytic window limitation, approximately 1.2 volts is the maximum voltage to which an individual SC can be charged [25]. Thus, for applications that require additional voltage, a SC energy storage module comprising a series connection of SCs will be needed. Our energy storage module is modeled by connecting three SCs in series. Charge and discharge circuits of an SC energy module consisting of three SCs connected in series are illustrated in [23]. We modeled three different energy storage modules using nine printed SCs. As can be seen in Fig. 5, the self-discharge behavior of different SC energy modules over the long term is simulated and compared. The simulation will enable us to estimate how much voltage each module will have at a specific time within 31 days. The final voltage of each module can also be predicted at the end of this period; based on that assessment, we can select the most appropriate module for our long-term application.

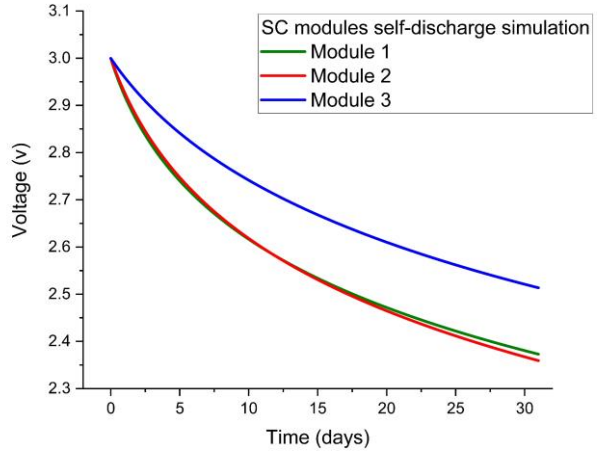

Figure 5. Simulation of the self-discharge behavior of three different SC energy storage modules over the long term. Each module consists of three SCs connected in series.

C. *Accuracy of the proposed model in the load-connected mode*

Furthermore, as a second experiment to verify the proposed model, the experimental and simulated results were compared in the context of a resistive load applied to SCs. This was accomplished by using discrete resistors as the resistance load connected to an SC energy module consisting of three SCs in series. In this experiment, the SC module was first charged up to 3 volts before a discrete resistor was connected to it. Using a digital multimeter, the voltage across the two ends of the discrete resistor was measured during discharge of the SC module. This experiment was repeated for three different discrete resistors and the experimental results were compared with the simulation results. As illustrated in Fig. 6, the differences between simulation and experimental results are negligible. In view of the results of this experiment and the previous experiment, it is evident that the proposed model can be considered well-validated in comparison with the experimental data.

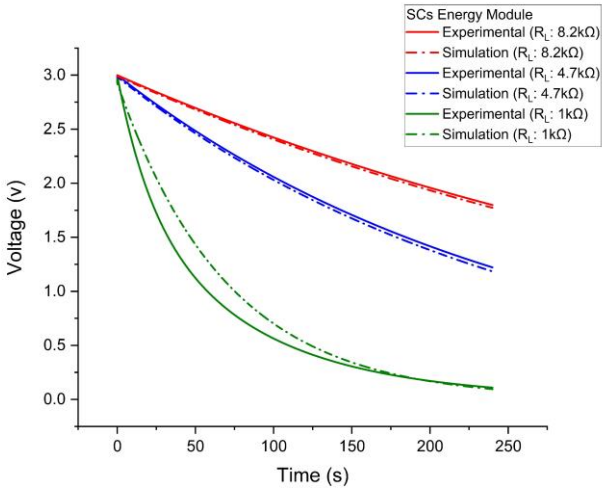

Figure 6. Verification of the proposed model accuracy against experiments using discrete resistors as resistive loads. Experimental and simulation behavior of an SC energy module.

IV. Conclusion

This paper presents a simple model in order to describe the dynamic self-discharge effects of printed supercapacitors. In order to model the non-linear behavior of self-discharge and leakage over the long term (31 days), a single exponential equation has been employed as the equivalent parallel resistance (EPR). On the basis of experimental results, it has been demonstrated that the proposed model is highly accurate for predicting the discharge behavior of printed supercapacitors in both self-discharge and load-connected modes. However, while the models reported in the literature have more RC network elements and branches, some of them have several separate exponential functions and also face difficulties determining the parameters, even in the short-term and are not accurate to simulate the long-term nonlinear self-discharge effect of the supercapacitors. Due to the need for simple versions for practical implementation, the model presented in this paper is more suitable for practical applications. Furthermore, the presented model can also be used to predict significant issues in the fabrication process of devices, as well as the behavior of a supercapacitor energy

storage module depending on varying electrical variables from device to device. In addition, according to the experimental and data fitting results of 10 fabricated supercapacitors, all the parameters defined in this model show good statistical values and have a Gaussian (normal) distribution. Therefore, this model exhibits good compatibility with Monte Carlo simulations, which is going to be part of our upcoming plans to simulate the supercapacitor's charge and discharge behavior.

ACKNOWLEDGMENT

This work has mainly received funding from the European Union's Horizon 2020 research and innovation programme under the Marie Skłodowska-Curie Grant Agreement Number 814299 - CHARISMA. Parts of the research used Academy of Finland Research Infrastructure "Printed Intelligence Infrastructure" (PII-FIRI, Grant Number 320019).

REFERENCES

[1] Olabi, Abdul Ghani, Qaisar Abbas, Ahmed Al Makky, and Mohammad Ali Abdelkareem. "Supercapacitors as next generation energy storage devices: Properties and applications." Energy 248 (2022): 123617.

[2] Zhang, Xinyu, Changzhong Jiang, Jing Liang, and Wei Wu. "Electrode materials and device architecture strategies for flexible supercapacitors in wearable energy storage." Journal of Materials Chemistry A 9, no. 13 (2021): 8099-8128.

[3] Riaz, Amna, Mahidur R. Sarker, Mohamad Hanif Md Saad, and Ramizi Mohamed. "Review on comparison of different energy storage technologies used in micro-energy harvesting, WSNs, low-cost microelectronic devices: Challenges and recommendations." Sensors 21, no. 15 (2021): 5041.

[4] Yaseen, Muhammad, Muhammad Arif Khan Khattak, Muhammad Humayun, Muhammad Usman, Syed Shaheen Shah, Shaista Bibi, Bakhtiar Syed Ul Hasnain et al. "A review of supercapacitors: materials design, modification, and applications." Energies 14, no. 22 (2021): 7779.

[5] Ma, Hailing, Yunyu Zhang, and Minghai Shen. "Application and prospect of supercapacitors in Internet of Energy (IOE)." Journal of Energy Storage 44 (2021): 103299.

[6] Şahin, Mustafa Ergin, Frede Blaabjerg, and Ariya Sangwongwanich. "A comprehensive review on supercapacitor applications and developments." Energies 15, no. 3 (2022): 674.

[7] Mohsen, Saeed, Abdelhalim Zekry, Khaled Youssef, and Mohamed Abouelatta. "A self-powered wearable wireless sensor system powered by a hybrid energy harvester for healthcare applications." Wireless Personal Communications 116, no. 4 (2021): 3143-3164.

[8] Aman, Azana Hafizah Mohd, Norazuwana Shaari, and Roszita Ibrahim. "Internet of things energy system: Smart applications, technology advancement, and open issues." International Journal of Energy Research 45, no. 6 (2021): 8389-8419.

[9] Wen, Jianfeng, Bingang Xu, Yuanyuan Gao, Meiqi Li, and Hong Fu. "Wearable technologies enable high-performance textile supercapacitors with flexible, breathable and wearable characteristics for future energy storage." Energy Storage Materials 37 (2021): 94-122.

[10] Li, Zengqing, Mingwei Tian, Xuantong Sun, Hongtao Zhao, Shifeng Zhu, and Xiansheng Zhang. "Flexible all-solid planar fibrous cellulose nonwoven fabric-based supercapacitor via capillarity-assisted graphene/MnO2 assembly." Journal of Alloys and Compounds 782 (2019): 986-994.

[11] Haque, Mazharul, Qi Li, Anderson D. Smith, Volodymyr Kuzmenko, Per Rudquist, Per Lundgren, and Peter Enoksson. "Self-discharge and leakage current mitigation of neutral aqueous-based supercapacitor by means of liquid crystal additive." Journal of Power Sources 453 (2020): 227897.

[12] Hamedi, Sara, Teymoor Ghanbari, Ehsan Moshksar, and Zahra Hosseini. "Time-varying model of self-discharge in a double layer supercapacitor with blocking layer." Journal of Energy Storage 40 (2021): 102730.

[13] Zhang, Wei, Wei Yang, Huanhuan Zhou, Zailei Zhang, Man Zhao, Qing Liu, Jing Yang, and Xianmao Lu. "Self-discharge of supercapacitors based on carbon nanotubes with different diameters." Electrochimica Acta 357 (2020): 136855.

[14] Keskinen, Jari, Suvi Lehtimäki, Arman Dastpak, Sampo Tuukkanen, Timo Flyktman, Thomas Kraft, Anna Railanmaa, and Donald Lupo. "Architectural modifications for flexible supercapacitor performance optimization." Electronic Materials Letters 12, no. 6 (2016): 795-803.

[15] Yuan, Siting, Xianhong Huang, Hao Wang, Lijing Xie, Jiayao Cheng, Qingqiang Kong, Guohua Sun, and Cheng-Meng Chen. "Structure evolution of oxygen removal from porous carbon for optimizing supercapacitor performance." Journal of Energy Chemistry 51 (2020): 396-404.

[16] Zhang, Lei, Xiaosong Hu, Zhenpo Wang, Fengchun Sun, and David G. Dorrell. "A review of supercapacitor modeling, estimation, and applications: A control/management perspective." Renewable and Sustainable Energy Reviews 81 (2018): 1868-1878.

[17] Faranda, R. "A new parameters identification procedure for simplified double layer capacitor two-branch model." Electric Power Systems Research 80, no. 4 (2010): 363-371.

[18] Logerais, Pierre-Olivier, M. A. Camara, O. Riou, A. Djellad, A. Omeiri, F. Delaleux, and J. F. Durastanti. "Modeling of a supercapacitor with a multibranch circuit." international journal of hydrogen energy 40, no. 39 (2015): 13725-13736.

[19] Torregrossa, Dimitri, Maryam Bahramipanah, Emil Namor, Rachid Cherkaoui, and Mario Paolone. "Improvement of dynamic modeling of supercapacitor by residual charge effect estimation." IEEE Transactions on Industrial Electronics 61, no. 3 (2013): 1345-1354.

[20] Abouelamaiem, Dina Ibrahim, Guanjie He, Tobias P. Neville, Drasti Patel, Shan Ji, Rongfang Wang, Ivan P. Parkin et al. "Correlating electrochemical impedance with hierarchical structure for porous carbon-based supercapacitors using a truncated transmission line model." Electrochimica Acta 284 (2018): 597-608.

[21] Ghanbari, Teymoor, Ehsan Moshksar, Sara Hamedi, Fatemeh Rezaei, and Zahra Hosseini. "Self-discharge modeling of supercapacitors using an optimal time-domain based approach." Journal of Power Sources 495 (2021): 229787.

[22] Wang, Bin, Chaohui Wang, Qiao Hu, Le Zhang, and Zhiyu Wang. "Modeling the dynamic self-discharge effects of supercapacitors using a controlled current source based ladder equivalent circuit." Journal of Energy Storage 30 (2020): 101473.

[23] Pourkheirollah, Hamed, Jari Keskinen, Matti Mäntysalo, and Donald Lupo. "An improved exponential model for charge and discharge behavior of printed supercapacitor modules under varying load conditions." Journal of Power Sources 535 (2022): 231475.

[24] Lehtimäki, Suvi, Anna Railanmaa, Jari Keskinen, Manu Kujala, Sampo Tuukkanen, and Donald Lupo. "Performance, stability and operation voltage optimization of screen-printed aqueous supercapacitors." Scientific reports 7, no. 1 (2017): 1-9.

[25] Arvani, Maedeh, Jari Keskinen, Donald Lupo, and Mari Honkanen. "Current collectors for low resistance aqueous flexible printed supercapacitors." Journal of Energy Storage 29 (2020): 101384.

PUBLICATION III

Simplified exponential equivalent circuit models for prediction of printed supercapacitor's discharge behavior - Simulations and experiments

Hamed Pourkheirollah, Jari Keskinen, Matti Mäntysalo, Donald Lupo

Journal of Power Sources

https://doi.org/10.1016/j.jpowsour.2023.232932

Journal of Power Sources 567 (2023) 232932

Contents lists available at ScienceDirect

Journal of Power Sources

journal homepage: www.elsevier.com/locate/jpowsour

Simplified exponential equivalent circuit models for prediction of printed supercapacitor's discharge behavior - Simulations and experiments

Hamed Pourkheirollah *, Jari Keskinen, Matti Mäntysalo, Donald Lupo

Faculty of Information Technology and Communication Sciences, Tampere University, Tampere, Finland

HIGHLIGHTS

- A simple numerical exponential method to model supercapacitors' discharge behavior.
- Using experimental electrical parameters of supercapacitors to model self-discharge.
- Accurately modeling inherent non-linearity of self-discharge and leakage current.
- High accuracy prediction of long-term discharge behavior of supercapacitor modules.
- A practical approach to simulate supercapacitors' behavior based on only C and ESR.

ARTICLE INFO

Keywords:
Supercapacitors
Printed electronics
Energy storage
Self-discharge
Leakage current
Supercapacitor modelling and simulation

ABSTRACT

Although supercapacitors (SCs) are promising devices for energy storage systems due to their high-power density and long lifecycle, they suffer from high leakage current and self-discharge. In this work, a simple and practical exponential equivalent circuit model (ECM) and three sub-ECMs based on electrical parameters and self-discharge profile of 12 printed flexible SCs are proposed to account for non-linear leakage and self-discharge phenomena in SCs. The capacitance and equivalent series resistance (ESR) of SCs are determined from the experiments. Besides, rather than modelling different self-discharge mechanisms within a SC cell, an exponential current/voltage function is employed for each SC in this study as a variable leakage resistance (VLR). The proposed ECMs are based on empirical parameters, without considering the physical mechanisms. Using the ECMs and only knowing two to four parameters for each SC cell, the discharge behaviors of SCs, electrochemical double-layer capacitors (EDLCs) type may be predicted with a high degree of accuracy over the long term (maximum simulation error in 31 days: less than 4%). Accordingly, the proposed ECMs, in contrast to those published in the literature, have the potential to be used in practical applications in the long-term as a result of their simplicity and high accuracy.

1. Introduction

Due to the depletion of fossil fuels such as oil and natural gas, and the results of their CO_2 emissions, research into renewable sources of energy has increased significantly [1]. It is necessary to employ energy storage devices for optimum utilization of renewable energies since the captured form of resources may not always be available [2]. Energy storage systems are used as energy buffers to store the power harvested from energy sources like solar [3], radio frequency [4], mechanical vibration [5], human-body [6], and wind [7] and deliver the power to the system when needed. These systems play a key role in a wide variety of industrial applications such as energy autonomous Internet of Things (IoT) [8], energy-harvesting wireless sensor networks (WSNs) [9] and self-powered flexible and wearable electronic devices [10]. In choosing an energy storage system, power and energy density, safety, reliability, and longevity are the criteria that must be considered [11,12]. Rechargeable batteries such as NiMH [13] and Li-ion [14] have been widely used as primary energy storage devices due to their high energy density and low self-discharge. However, gradual increase in internal resistance and decrease in capacity over time because of the aging process of batteries during charge-discharge cycles, limits the lifetime of many applications [15]. Besides, due to their low power density, there is

* Corresponding author.
E-mail address: hamed.pourkheirollah@tuni.fi (H. Pourkheirollah).

https://doi.org/10.1016/j.jpowsour.2023.232932
Received 11 October 2022; Received in revised form 14 February 2023; Accepted 6 March 2023
Available online 16 March 2023

a possibility of disruption in their ability to deliver power under high current loads [16]. In addition, high current rates and transient load conditions severely affect the cycle life of rechargeable batteries [16]. Therefore, due to the limitation of the cycle life, it may be necessary to replace the batteries in applications after 1–2 years [16].

On the other hand, supercapacitors (SCs) also known as electric double-layer capacitors (EDLCs), have an energy density several orders of magnitude higher compared to conventional capacitors and despite having relatively low energy density compared to batteries, are a promising alternative to use in energy storage systems technology [17]. Essentially, a SC is composed of two electrodes with a large surface area and an electrolyte layer between them [18]. Charges are stored in SCs through these double layers at the interface between the active electrode and the electrolyte and thus, SCs are able to store a greater amount of energy than conventional capacitors [19]. In contrast to batteries, SCs have higher power density and charge-discharge efficiency, and lower internal resistance [18,19]. Furthermore, SCs benefit from fast charge-discharge characteristics [20], operation in a wide temperature range [21], longer cycle life, and recyclability [22]. In view of these advantages, they are suitable for use in a wide variety of applications, including uninterrupted power supplies [23], quick start, peak pulse power, fast charge, and memory backup applications, etc. [24–26]. In order to achieve "perpetual lifetime" in applications such as energy autonomous self-powered WSNs, IoT and wearable electronics, in some works reported in the literature, SCs have been used individually for storing the harvested energy [27] and in some other works, in combination with rechargeable batteries [28].

In spite of all this, SCs suffer from high leakage current, which limits some of their practical applications [29]. The self-discharge or leakage of a SC is the result of the inability of the SC to retain stored charge for a prolonged period of time. It is crucial to take self-discharge into account when determining the long-term performance of a SC and estimating the amount of energy available at any given time, such as in the case of power supply to WSNs, IoT, and wearable electronic devices. Despite the high importance of the self-discharge phenomenon and leakage current, SCs still remain largely unexplored in terms of these characteristics and thus far, a small number of studies have addressed the self-discharge mechanisms in SCs [30,31]. Mechanism of self-discharge in SCs is complicated due to the involvement of ions as well as a variety of electrode structures and contrary to conventional capacitors, cannot be explained solely by leakage resistance [32]. In addition, a number of material properties, including the structure and porosity of the electrode, presence of the impurities, ionic size of the electrolyte, accessible surface area etc., can also influence the self-discharge process [33]. However, the process of self-discharge is primarily attributed to three different mechanisms: charge redistribution, internal ohmic leakage, and diffusion-controlled Faradaic redox reactions [34]. Charge redistribution arises from differences in the accessibility of electrolyte ions to the electrode surfaces [34]. For the normal operation of the SCs, Faradaic redox reactions and internal ohmic leakage must be considered since charge redistribution can only occur if the cells are overcharged. The Faradaic redox reactions dominate the self-discharge during the first few hours while the internal ohmic leakage usually dominates the self-discharge during the rest of the open-circuit period [35]. Besides, leakage current in SCs is primarily caused by Faradaic redox reactions at the electrode-electrolyte interface [34,35].

In order to maximize the potential benefits of SCs in energy storage systems, understanding their electrical behavior is important. Moreover, since SCs are being used in a wide variety of applications, it is essential to have a simple model that represents their behavior in practical applications. Besides, as fast self-discharge causes charge/energy loss and voltage drop in SCs, it is necessary to understand the dynamic behavior of self-discharge in long-term and develop an accurate terminal voltage prediction model in order to optimally design power management systems and find the best system architectures. This can be achieved through the equivalent circuit model (ECM) of a SC, which is an easy, simple, and accurate method in contrast to the other models such as electrochemical models, which require high computational complexity [36]. Additionally, the ECM can also be used as an important tool to reveal the nonlinear behavior of charging and discharging in SCs, as well as the redistribution of charges and self-discharge processes before deploying SCs in practical applications. In the literature, various ECMs for SCs have been developed recently. The reported ECMs differ in representing the implementation of SCs in different applications, and for specific applications, specific ECMs are proposed. In some reports of modeling SCs through ECM and analyses in the time [37] or frequency domain [38], diverse resistive-capacitive (RC) networks are used. In the last work published by this group [39], several ECMs for SCs reported in the literature were reviewed. In this paper, we now refer to the ECMs that have been published in recent years.

SCs have been modeled using a two-branch approach (Fig. 1a) in some publications [40,41]. In these ECMs, in order to account for leakage current and self-discharge, a couple of parallel branches of constant RC networks were added. In accordance with the self-discharge behavior, circuit elements were determined experimentally. Nevertheless, based on the constant parallel resistance used in this ECM, only the internal ohmic leakage of the SC is considered. As a result, modeling the leakage and self-discharge with constant RC elements may not be accurate, due to their non-linear inherent nature. This leads to a large difference between simulation and experimental results over long times. Additionally, some other studies have reported an ECM with two RC branches and a variable leakage resistance (VLR) [37,42], as can be seen in Fig. 1b. In these ECMs, the two RC branches have different time constants, which characterize the charging-redistribution process, and the VLR characterizes the self-discharge process. There are several different exponential functions in the VLR used in this ECM to model the self-discharge characteristic, each of which has a different time constant at various voltages and times, resulting in varying leakage resistances. Nevertheless, a huge number of distinct exponential functions must be determined for many periods in order to analyze and study the SC's self-discharge behavior over the long-term using these VLR ECMs. Another publication [43] modeled a SC by adding a controlled current source to the two-branched ECM (Fig. 1c). In this improved two branch ECM, based on the terminal voltage of the SC and its change rate, the controlled current source was designed. This ECM with the controlled current source is suitable for middle-term simulation of SC behavior (less than 30 min). Nonetheless, firstly this ECM is still complex, requiring numerous parameter determination steps, and secondly, it is not suitable for long-term simulations. In other publications [35,44], researchers reported an ECM in which three RC branches and an additional equivalent parallel resistor (EPR) to consider the self-discharge phenomenon are connected in parallel (Fig. 1d). In these ECMs, the largest capacitor does not have a constant value and instead has a linear relationship with the voltage [35,44]. However, in spite of the complexity of the ECM and the increased number of RC network elements, a three-branch ECM is also not capable of accurately estimating the nonlinear self-discharge effect in SCs over the long-term. Furthermore, other researchers have also reported ECMs based on polynomial functions. In Ref. [45], Saha et al. presented a polynomial ECM for the self-discharge process dominated by charge redistribution in SCs. These polynomial ECMs also require numerous parameter determination steps, which makes them unsuitable for use in practice. A further challenge will also be the identification of the dynamic polynomial function parameters under a variety of experimental conditions in these ECMs. Moreover, a model of a SC with a blocking layer of a few nanometers in order to reduce the leakage effect was presented by Tevi et al. [46]. The blocking layer was modeled as a capacitor, connected in series with the main double-layer capacitor. Although their proposed ECM accurately predicts experimental data in the short term, no long-term simulation results have been reported. Besides, de Levie's transmission line model (TLM) has also been extensively used for modeling ions' short-term movement inside electric double-layer capacitors with porous

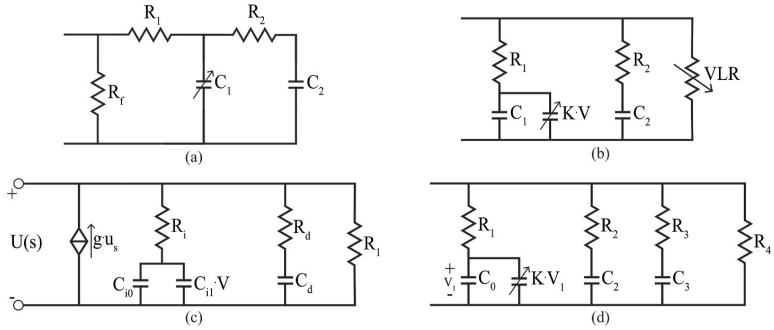

Fig. 1. ECMs for a single SC reported in the literature; a) Two-branch ECM [40,41]. b) Two-branch ECM with VLR [37,42]. c) Two-branch ECM with a controled current source [43]. d) Three-branch ECM with EPR [35,44].

electrodes [47].

A brief summary of the literature indicates that the reported different ECMs have multiple branches and more RC network elements, whereas in practical applications, simplified versions are required to facilitate the implementation of the ECMs. Besides, in order to form SC energy modules for the purposes of realizing energy storage systems and addressing the power requirements, several SCs need to be connected in series and/or parallel [48] into modules. Therefore, the reported ECMs are not suitable for long-term simulation in SC energy modules, as they would further increase the difficulty of parameter identification. Consequently, despite the complexity and the inclusion of more characterization steps, none of the ECMs reported in the literature adequately reflect the characteristics of the SCs in long-term, leading to inconsistent long-term results between simulations and experiments.

This work presents a simple numerical exponential method using experimental electrical parameters of printed SCs to model the non-linear behavior of self-discharge and leakage current in SCs, type of electrochemical double-layer capacitors (EDLCs). This proposed ECM is based on the previous model published by the authors [39,49], but the exponential function used in the EPR has now been modified and the method of obtaining EPR is also different than the previous works. This modified exponential function exhibits improved statistical parameters and is also compatible with Monte-Carlo simulations. This study simplifies the proposed ECM even further and proposes a super-simple ECM based on the numerical value of the capacitance solely to estimate the discharge and self-discharge behavior of SCs (EDLC type) over a prolonged period of time (31 days). This ECM contains only one branch and two RC elements, and since practical applications require simplified versions to facilitate model implementation, it is well suited for practical use. Accordingly, the presented ECM is simpler in comparison to the previous ECMs found in the literature and is therefore more suitable for use in energy storage modules containing several SCs integrated either in series or in parallel. The proposed ECM can also be used to predict how series-connected SC energy modules operate depending on the variation of electrical properties from device-to- device, which is a critical consideration in printed electronic devices. Thus, the reported super-simple ECM is not only capable of modeling the full charging and discharging behavior of SCs but can also be applied to analyzing how device-to-device variations in electrical parameters, such as the non-linear inherent of self-discharge and leakage current, affect the performance of series-connected SCs in energy modules.

Nonetheless, it should be noted that the proposed ECMs are based on empirical parameters without taking physical mechanisms into account and can only be used to predict the behavior of EDLC-type SCs. The ECMs reported in this work may not be necessarily applicable to the other types of SCs such as pseudo-capacitors or hybrids (combination of EDLCs and pseudo-capacitors). Furthermore, in order to gain an understanding of the mechanisms underlying the performance and aging of SCs, additional characterizations will be required.

2. Experimental and methods

2.1. Experimental

Printed SCs of the type of electrochemical double layer capacitors (EDLCs) are used in building the model presented in this paper and verifying the simulation results. Previous publications by the group have described in detail the process of fabricating these types of printed SCs [39,50–52]. However, the fabrication process is described in a very brief manner here. As a current collector, graphite ink was applied to the PET side of a double-sided flexible Al-PET substrate, while the Al layer serves only as a barrier. On the current collector layer, activated carbon ink was applied using an in-house formulation with chitosan as a binder to form an electrode layer. These two layers were deposited using a laboratory-scale doctor blade coater. On top of the electrode layer, NaCl: H_2O aqueous electrolyte was added, followed by a paper separator. In the final step of the process, an annealed adhesive material was used to heat-seal two electrodes face-to-face to form a SC.

We have also previously reported the characterization process for printed SCs using a Maccor workstation (Maccor Inc., USA) by which the key electrical parameters are obtained [39,50–52]. This process is, however, also summarized here. Three times of charging and discharging of SCs were conducted between 0 and 1.2 V with a constant current of 1, 3, and 10 mA. Following this, the SCs were maintained at 1.2 V for 30 min at constant voltage. Using a constant current discharge step between 0.96 V and 0.48 V, the capacitance was measured. A constant voltage of 1.2 V was then applied to the SCs for 1 h in order to determine the leakage current. The procedure was repeated for all three currents of 1, 3, and 10 mA. In the end, the ESR was calculated based on the IR drop in the measurement with a discharge current of 10 mA. In the supplementary material file, the characterization results for all SCs used to develop the model are provided. Among the electrical parameters of the SCs, capacitance (C) and equivalent series resistance (ESR) will be utilized in the model. The model is based on the characterization results of 12 printed SCs. After fabrication and characterization, each of the 12 SCs was charged up to approximately 1 V and then maintained at this constant voltage for 12 h (charging time: 12 h). The SCs were disconnected from the power source after charging and the potential difference data for each SC were monitored and recorded for 31 days during self-discharge.

2.2. Model

In order to model the internal parameters of a single SC in this study, a conventional capacitor (C), an equivalent series resistor (ESR), and a parallel variable exponential element as EPR (equivalent parallel

resistor) are used as illustrated in Fig. 2a. As mentioned above, the 'C' and 'ESR' values are determined using standard characterization. ESR represents the internal Ohmic losses of a SC caused by the combined effect of the current collector resistance, electrode contact resistance, electrolyte resistance, and the electrode/electrolyte interface resistance [53]. The variable exponential EPR models the nonlinearity of SC self-discharge and leakage current. In some respects, the proposed model is similar to the work published by the authors earlier; however, the exponential EPR function used in this model and the method for obtaining this element are different. This work uses $I = e^{(a+ b\times V)}$ as the exponential equation of EPR describing self-discharge and leakage current effects, which provides a better fit to the empirical data for self-discharge. This exponential equation has also the advantage of being suitable for Monte-Carlo simulations due to the normal distribution of the parameters in this equation.

2.3. Method

In this paper, a simple model is proposed to model the nonlinearity of leakage and self-discharge in the long-term (Fig. 2a). As discussed in the experimental section, the experimental self-discharge potential difference (voltage) data of each SC over time have been recorded to determine the exponential function of EPR. Using capacitance and current basic formulas (1), we can now calculate numerical values of the current (2) at any given voltage for each SC based on capacitance (C) and self-discharge. As can been seen in formula (2) and Fig. 2b, in order to determine the current at each data point, the difference between the values of that data and the previous data is used.

$$Q = C \times V,\ I = dQ/dt \tag{1}$$

$$I_m = C \times dV_m/dt_m = C \times (V_{m-1}-V_m)/(t_m-t_{m-1}) \tag{2}$$

With the current data-points calculated, we are now able to plot the diagram of the I (V) data-points for each SC as shown in Fig. 2c and . d. In the following step, we fit the exponential equation $e^{(a+ b\times V)}$ to the I (V) data points of each SC and as can be seen in Fig. 2c and d, SC's parameters 'a' and 'b' for two SCs are uniquely determined by fitting this exponential function. As a result of this exponential function, excellent statistical data fitting parameters, such as the R-square and Adj. R-square values, are evident. R-square, also referred to as coefficient of determination (COD), is a measure of how much variation in the response variable is explained by the fitted regression line. As a general rule, the closer the R-square is to 1, the better the fitted line would track the data. Accordingly, the fit line will explain all the variability around its mean if R-square is one. All 12 SCs in this study exhibit R-square values exceeding 0.99 using this exponential function, which shows excellent fit to the I (V) datapoints for all SCs. Based on this exponential function fit, we are now able to determine the numerical values of 'a' and 'b', parameters of the model, which are unique to each SC. With these two parameters, as well as the characterization parameters 'C' and 'ESR', all four parameters of this model are now revealed. This model (Fig. 2a) will be referred to as ECM 1 throughout this article.

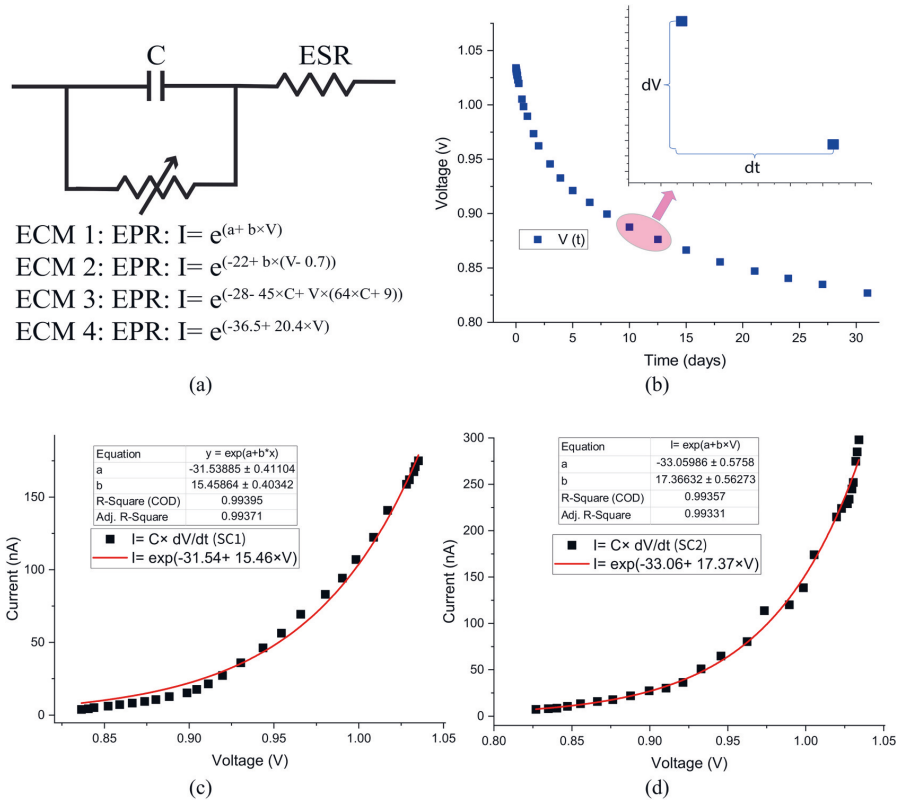

Fig. 2. a) Proposed ECMs for a single SC. b) Experimental self-discharge data of a SC. c) Fitting the exponential function to the I(V) datapoints of SC1. d) Fitting the exponential function to the I(V) datapoints of SC2.

2.3.1. Statistical study of parameters

In order to examine and analyze the distribution of each parameter in ECM 1 and assess whether the data set for each parameter can be adequately described by a normal distribution (Gaussian distribution), every parameter of this model is subjected to a normality test. Fig. 3 illustrates a histogram chart and normal probability plot for each of the four parameters in this model. In histogram charts (Fig. 3a, c, e, g), the distribution as well as the bell curve (blue line) for each parameter are included. Besides, it is also possible to evaluate substantive deviations from normality on the normal probability plots (Fig. 3b, d, f, h) by comparing data deviations from the reference line (red line); the closer the percentiles are to the reference line, the more normal the

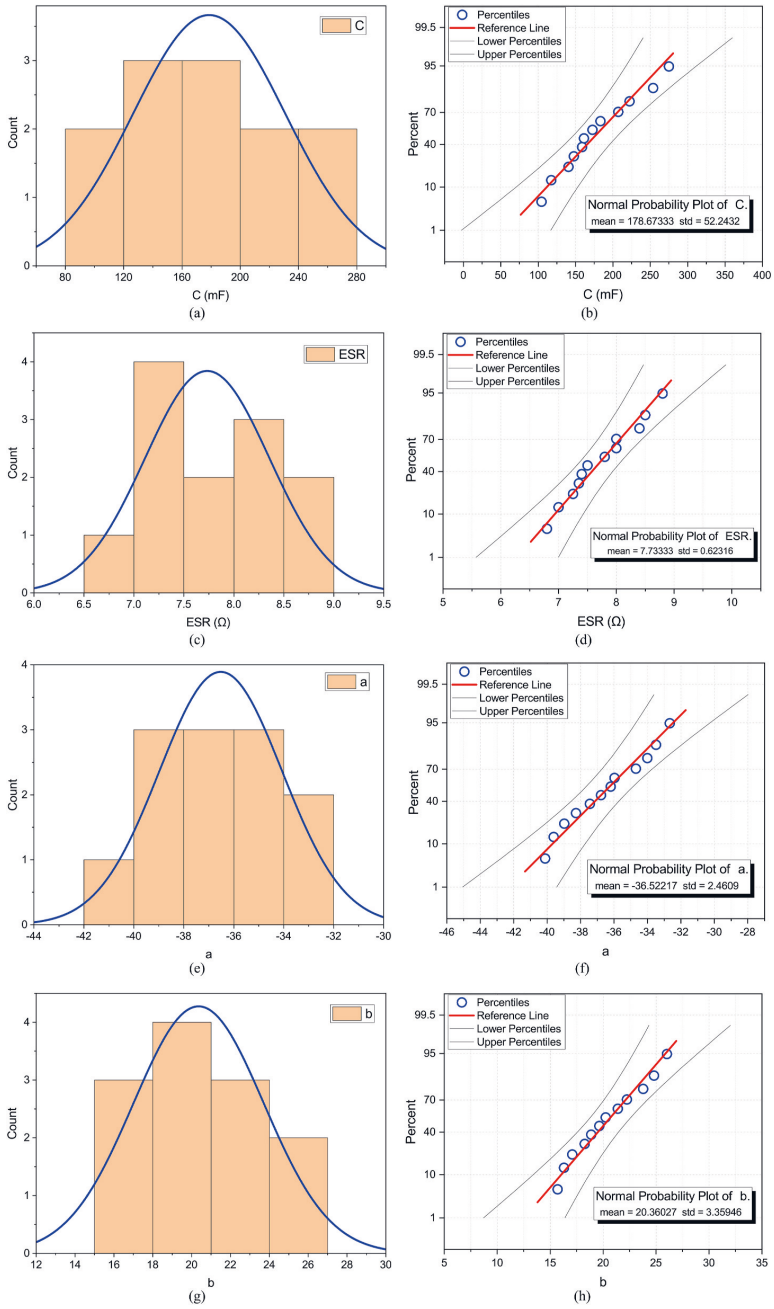

Fig. 3. a,c,e,g) Histogram chart of the ECM 1 parameters. b,d,f,h) Normal probabilty plot of the ECM 1 parameters.

distribution of the parameter appears. According to the normality test, Table 1 summarizes the descriptive statistics for each parameter. All four parameters of ECM 1 exhibit a normal distribution based on the numerical value of the descriptive statistics in Table 1. P-values for each of the four parameters are higher than 0.8, which strongly supports the normal distribution hypothesis. Besides, generally, a skewness value between −0.5 and 0.5 indicates that the probability distribution of a random variable is approximately symmetrical about its mean, as each parameter in ECM 1 is. Furthermore, since the mean and median values for each parameter in Table 1 are approximately equal, this indicates a positive result for the normality test and confirms that each parameter has passed the normality test. Additionally, the statistical values presented here have been found to be highly adaptable to Monte-Carlo simulations.

2.3.2. Simplifying ECM 1

As has already been discussed, ECM 1 presented in this work has four parameters (Fig. 2a). Compared to other models in the literature, this model is very simple and is well suited for long-term simulations, as discussed in the following section (section 3). As a result of its simplicity and accuracy, ECM 1 is already useful for practical applications. However, the objective is now to simplify the model even further since simpler models are easier to implement and more feasible to use in practical applications. Further simplifying this model requires reducing its parameters and for this, it is necessary to determine a relationship among the parameters in order to formulate the EPR exponential I(V) function based solely on one parameter. In Fig. 4a and b, it can be observed that 'C', 'a', and 'b', the parameters of ECM 1 for 12 printed SCs used in this model, exhibit a relatively good linear relationship. In order to obtain a good approximate representation of this relative linear relationship among the parameters, linear fits are used (Fig. 4a and b). It is worth mentioning that these two linear fits have R-square and Adj. R-square values (statistical data fitting parameters), above 0.97. Having defined the linear relationship among the parameters, the next step is to formulate the exponential equation for EPR based on only one parameter:

$$\text{EPR: } I = e^{(a + b\times V)},\ a = -0.7 \times b - 22 \rightarrow I = e^{(-22 + b\times(V - 0.7))}\text{:ECM 2} \quad (3)$$

$$b = 64 \times C + 9 \rightarrow I = e^{(-28 - 45\times C + V\times(64\times C + 9))}\text{:ECM 3} \quad (4)$$

The EPR exponential I(V) function has now been obtained once based on only parameter 'b' and once based on only parameter 'C'. During the following discussion in this paper, the ECM based on only parameter 'b' is referred to as ECM 2, and the ECM based on only parameter 'C' is referred to as ECM 3 (Fig. 2a). ECM 2 and ECM 3 are simpler than ECM 1, since they use three parameters rather than four.

An alternative approach to simplifying model 1 is also to replace the mean values of parameters 'a' and 'b' in the EPR exponential function. In this case, the EPR function would be $I = e^{(-36.5 + 20.4\times V)}$. This ECM is referred to as ECM 4 throughout this article (Fig. 2a). Compared with the previous ECMs in this paper, ECM 4 is extremely simple and straightforward, due to the advantage of having only two parameters ('C' and 'ESR') and not containing any parameters for the exponential EPR function.

Table 1
Descriptive statistics of ECM 1 parameters.

Parameters	C (mF)	ESR (Ω)	a	b
N total	12	12	12	12
Mean	178.7	7.7	−36.5	20.4
Minimum	104.4	6.8	−40.1	15.7
Median	167.0	7.6	−36.5	19.9
Maximum	274.9	8.8	−32.7	26.0
Std	52.2	0.6	2.5	3.4
P-value	0.83	0.86	0.9	0.91
Skewness	0.49	0.26	0.07	0.29

3. Results and discussion

3.1. Accuracy of the proposed ECMs

The accuracy of the proposed ECMs is evaluated in four different ways in this study. The first approach is to compare the simulation results with the experimental results of the SCs which were used to develop the ECMs. In the second approach, simulation, and experimental results of new SCs that were not used in the development of the ECMs are compared. The third accuracy test of the presented ECMs involves the comparison of experimental results with simulations of two commercially available SCs. Finally, in the fourth and last approach, two separate SC energy modules, each consisting of three SCs connected in series, are formed and each module is connected to a discrete resistor with different resistance values. Then, the amount of voltage delivered to the discrete resistor during the discharge of the SC module is compared with the simulation results.

3.1.1. SCs used to develop the ECMs: simulation results vs. experiments

Approach one for evaluating the accuracy of the proposed ECMs is as follows: A random selection of four SCs is made out of the 12 used to build the ECMs, and the simulation results based on different proposed ECMs in the self-discharge phase are compared to the experimental results. Fig. 5 illustrates both the potential difference graph of the SCs over time during self-discharge in the long-term (31 days) as well as the residual voltage graph over time (residual voltage = experiments – simulations). As shown in Fig. 5, the simulation results based on all ECMs are in good agreement with the experimental results over a period of 31 days. According to this figure, ECM 1, which includes four parameters ('C', 'ESR', 'a', and 'b') for a single SC, is extremely accurate; in fact, the maximum error in the self-discharge phase based on ECM 1 within 31-days is about 10 mV (Fig. 5d and f), which is roughly 1.2% of the SC's final voltage (the final voltage of SCs drops to about 0.8 V after 31 days of self-discharge). ECM 2 including three parameters for a single SC (EPR function in ECM 2 is based only on 'b') in the long term, has a maximum error of 21 mV (2.5%). However, ECM 3 and 4, which are the most simplified ECMs proposed in this work with only two parameters for each SC ('C' and 'ESR'), have a maximum error of around 33 mV (4%) (Figs. 5h) and 18 mV (2.2%) (Fig. 5d) respectively, in the long-term. Therefore, based on ECM 4 and by only knowing 'C' and 'ESR' values of a SC, its self-discharge behavior can be estimated with a very good approximation (2.2% error) over the long term (31 days). Table 2 summarizes the maximum simulation error based on each ECM, according to the self-discharge experimental and simulation results for these four random SCs.

3.1.2. SCs not used to develop the ECMs: simulation results vs. experiments

As a second way to verify the accuracy of the proposed ECMs, the ECMs are applied to new SCs that have not been used for the development of the ECMs. Towards this objective, the experimental results of the self-discharge behavior of four randomly selected SCs are compared with the simulation results based on the ECMs. In this study, to evaluate the comprehensiveness of the ECMs, both SCs similar to the previous ones used to build the ECMs and other SCs with different substrates have been used. All 12 SCs used in the development of the ECMs in this work are printed on Al/PET substrate, and SC1 and SC2 in this test are also printed on Al/PET substrate with the same fabrication process. SC3 and SC4 have different substrates (PET/PLA and Al/PLA, respectively), but the fabrication process is the same. As can be seen in Table 3, the capacitance values of SCs 1, 2, and 3 are within the range of the capacitances of SCs used in the development of the ECMs (104–275 mF), whereas the capacitance of SC 4 exceeds this range. In fact, these SCs are printed in different batches, which explains the difference in capacitance values. By using this fabrication process, eight SCs are printed in each batch, and since the doctor blade tool is adjusted to the same thickness in each batch, approximately the same amount of activated carbon ink will

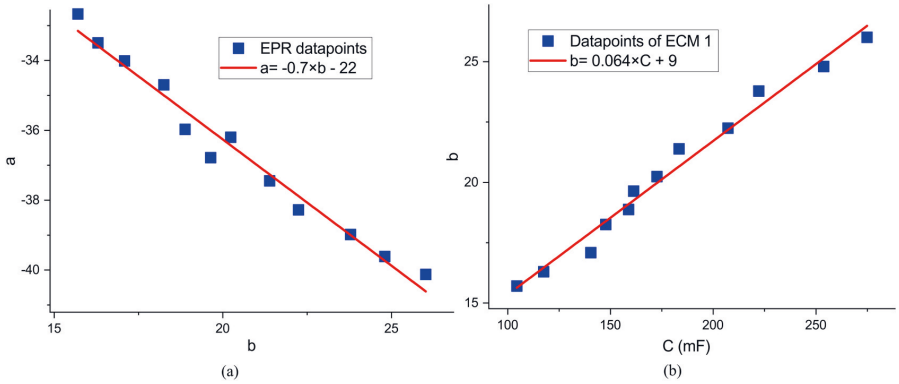

Fig. 4. a) A linear relationship with a good approximation between parameters 'a' and 'b' of ECM 1. b) A linear relationship with a good approximation between parameters 'b' and 'C' of ECM 1.

be printed on the graphite ink for all 16 SC cells, resulting in the almost same capacitance value for each SC (this process of fabricating SCs has been discussed in detail in Ref. [39]). Therefore, due to the thickness adjustment of the doctor blade tool, the different amount of activated carbon ink will be printed in different batches which will result in different capacitance values for the SCs. However, the ESR values of the selected SCs are all higher than those used in developing the ECMs (6.8–8.8 Ω). The selection of SCs with these values of capacitance and ESR has no particular purpose, and as mentioned all four SCs are selected at random.

Fig. 6 illustrates how well all the proposed ECMs work for the new SCs as well, and the self-discharge simulation and experimental results are in good agreement over the long-term (31 days). In addition, Table 3 provides a summary of the maximum simulation error for each ECM. According to this table, ECM 1 has a maximum error of 17.64 mV (2.21% of the SC's final voltage value) (Fig. 6e and 6f). The maximum error for ECM 2 is 26.49 mV (3.29%), for ECM 3 is 12.48 mV (1.56%), and for ECM 4 is 13.87 mV (1.74%). There is an interesting observation that ECMs 3 and 4, which are the simplest ECMs presented in this work, including only two parameters ('C' and 'ESR') for a single SC, are slightly more accurate than ECMs 1 and 2 with a maximum error of less than 2%, although the difference is within the experimental uncertainty. In other words, using proposed ECMs 3 and 4, one can predict the self-discharge behavior of a SC in the long term (31 days) with an error of less than 2% only by knowing the numerical value of capacitance and ESR. Considering the simplicity of the ECMs, it can be concluded that the maximum simulation error obtained for the new SCs based on all ECMs is negligible over the long term, and all ECMs have excellent accuracy.

3.1.3. Verification using commercial SCs (EDLC type): simulation results vs. experiments

As for the third part of the verification process of the proposed ECMs, self-discharge experimental results of two commercially available SCs, type of electrochemical double layer capacitors (EDLCs), are compared with the simulation results based on ECM 4. This ECM is the most simplified ECM in this study and by knowing only the capacitance and ESR value, the charge and discharge behavior of SCs can be simulated. The self-discharge experimental results for the two commercial SCs used in this test were obtained from the literature [54,55]. Commercial SC1 is a carbon-based SC with acetonitrile electrolyte and a capacitance of 600 F [54]. Commercial SC2 is also a carbon-based SC with organic electrolyte and a capacitance of 2600 F [55]. SC1 was charged up to 1.3 V and kept at that voltage for 24 h (charging time: 24 h) [54]. SC2 was charged up to 1.5 V with a charging time of 1 h [55]. After the charging process, the open circuit potential difference (self-discharge behavior) of SC1 and SC2 was monitored and recorded for 15 and 7 days, respectively [54,55]. Fig. 7a illustrates how closely the simulation results follow the experimental results for both SCs over time. The residual voltage over time for both SCs is also shown in Fig. 7b. As can be seen, the maximum simulation error for SC1 and SC2 is approximately 34 mV and 17 mV, respectively. Accordingly, the maximum simulation error for SC1 in 15 days is approximately 2.6% of the initial voltage and for SC2 in 7 days is 1.1% of the initial voltage, demonstrating that the proposed ECM is highly accurate for these two commercial SCs (EDLC type) as well.

As the printed SCs used in this study are of the EDLC type, commercial EDLC SCs are also used for verification. Therefore, the ECMs proposed in this work may not be applicable to other types of SCs such as pseudo-capacitors, and hybrid types formed by a combination of EDLCs and pseudo-capacitors.

3.1.4. Verification using discrete load resistors: simulation results vs. experiments

For an additional comparison of experimental results to the predictions of the model, discrete resistors in two different values (R_L:1.0 and 4.7 kΩ) are used to verify the accuracy of the proposed ECMs. First, two SC energy modules are formed, each consisting of three SCs connected in series using the 12 SCs used to develop the ECMs. Compared to module 1, the SCs of module 2 have a larger capacitance value difference. SC modules are first fully charged to a voltage of 3 V each and as soon as the energy module is fully charged, the main power source is disconnected. The discrete resistor is then used as the resistive load connected to the SC module and the voltage value between two ends of the discrete resistor during discharge of the SC module is measured using a digital multimeter. The ECM of the SC module and the resistive load is shown in Fig. 7c. In the ECM, the main 3V power source is connected to the module at $t = 0$, and the energy module is fully charged to 3 V. Each SC in the module is fully charged and stores the potential difference corresponding to its capacitance and then the main power source is disconnected at $t > 0$.

Fig. 7d, e, f, and g depict the discharge of the SC energy module. Fig. 7d and f illustrate the simulation and experimental results of the potential difference of the resistive load during the discharge of the SC module 1 and 2, respectively in the short-term (2 min) (In Ref. [39], the experimental results in Fig. 7d and f have already been published). According to these figures, the simulation results are consistent with the experimental results with a good degree of accuracy, and the difference between the simulations and experiments is small. In both modules, this difference is very close to zero for the resistive load of 4.7 kΩ. Fig. 7e and g shows the residual voltage for SC modules 1 and 2, which can be used to obtain the simulation error for each module by calculating the

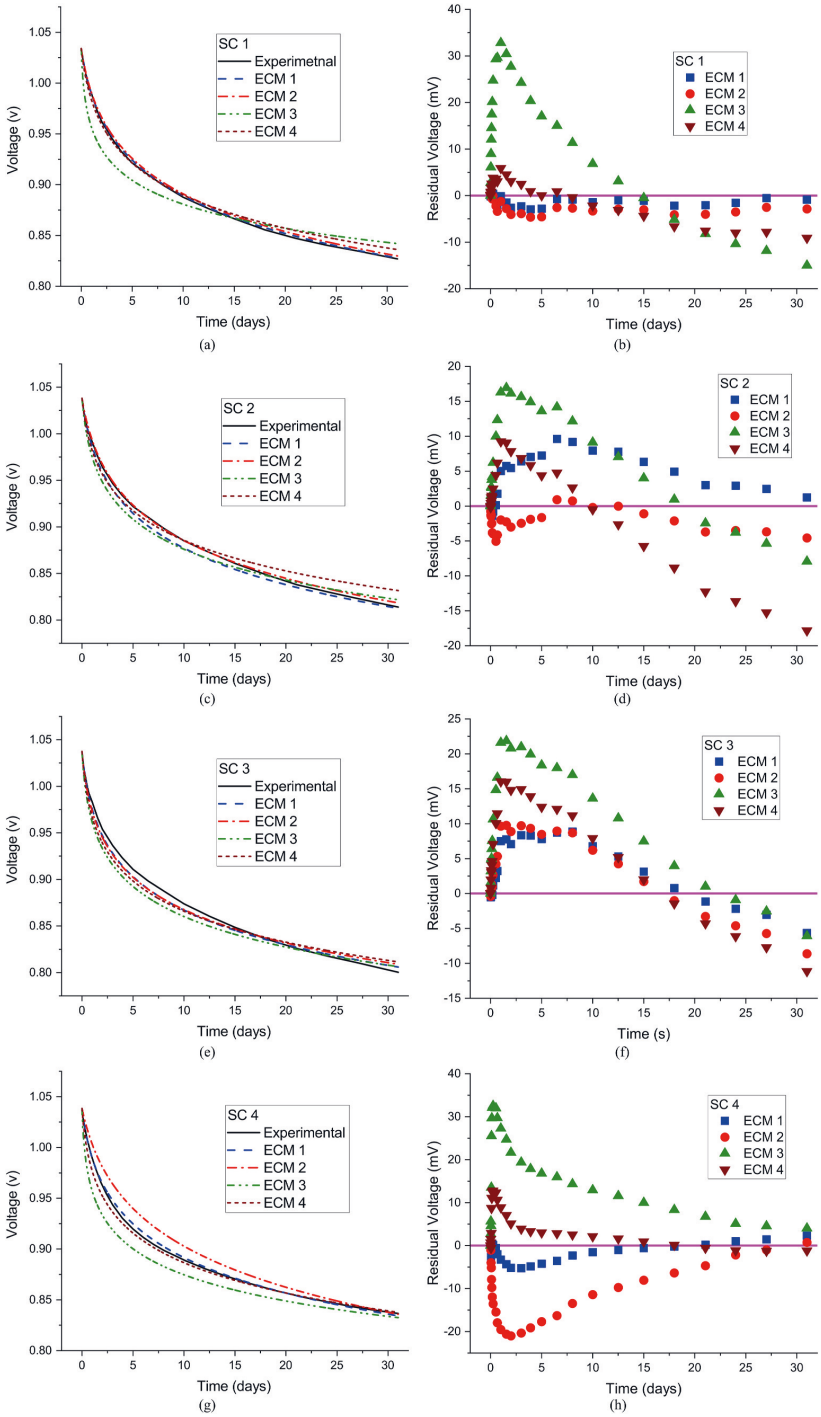

Fig. 5. a,c,e,g) Self-discharge experimental and simulation results in 31 days based on proposed ECMs for four randomly selected SCs used to develop the ECMs. b,d, f,h) Residual voltage (the difference between experiments and simulations).

Table 2
Maximum self-discharge simulation error in 31 days based on proposed ECMs for four randomly selected SCs used to develop the ECMs.

	SC 1	SC 2	SC 3	SC 4
ECM1	2.95 mV (0.36%)	9.6 mV (1.18%)	8.87 mV (1.11%)	5.26 mV (0.63%)
ECM2	4.61 mV (0.56%)	5.04 mV (0.62%)	9.76 mV (1.22%)	20.98 mV (2.51%)
ECM3	32.8 mV (3.97%)	16.93 mV (2.08%)	21.86 mV (2.73%)	32.54 mV (3.89%)
ECM4	9.1 mV (1.1%)	17.82 mV (2.19%)	16.04 mV (2%)	12.78 mV (1.53%)

Table 3
Maximum self-discharge simulation error in 31 days based on proposed ECMs for four randomly selected SCs not used to develop the ECMs.

	SC 1, (Al/PET)	SC 2 (Al/PET)	SC 3 (PET/PLAU)	SC 4 (Al/PLA)
C (mF)	126.4	211.2	157.7	326.5
ESR (Ω)	10.3	11	13	12.4
ECM 1	4.16 mV (0.5%)	13.8 mV (1.71%)	17.64 mV (2.21%)	2.53 mV (0.3%)
ECM 2	11.35 mV (1.37%)	26.49 mV (3.29%)	15.13 mV (1.89%)	14.53 mV (1.74%)
ECM 3	9.03 mV (1.09%)	10.46 mV (1.3%)	12.48 mV (1.56%)	1.81 mV (0.22%)
ECM 4	7.73 mV (0.94%)	11.38 mV (1.41%)	13.87 mV (1.74%)	12.59 mV (1.51%)

absolute value of this residual voltage over time. As a result, for the resistive load of 1 kΩ, the maximum simulation error for module 1 is 47 mV, for module 2 the error is 243 mV, corresponding to 1.57% and 8.1% of the module's initial voltage, respectively. In addition, an interesting aspect of these short-term simulations (2 min) is the full compliance among the simulation results based on ECMs 1 to 4, which implies that leakage and self-discharge do not play any significant role in the short term and have almost no influence in the initial minutes of SC discharge behavior. In contrast, the capacitance value of SCs is a more important factor in the discharge behavior of SCs over a short period of time. Consequently, it may therefore be argued that the higher simulation error of module 2 compared to module 1 can be caused by the larger difference in the capacitance value of its SCs.

All in all, based on the results of all methods of accuracy analysis, the estimation accuracy of all proposed ECMs can generally be assessed as acceptable in view of their simplicity.

3.2. Self-discharge behavior of SC modules: simulation results vs. experiments

The power that can be stored in a single SC may not be sufficient for some applications. Due to the limited potential window of SCs, it is not possible to store voltage beyond a certain limit, so the solution is to connect several SCs in series to form a SC energy module. Since the stored potential difference in a SC does not remain constant during its resting phase (open circuit) and decreases with time as a result of self-discharge, hence, in the long term, it is crucial to estimate the amount of power stored in the energy module that is available and ready to be delivered at any given time. Based on the ECMs presented in this work, it is now possible to predict the voltage over each SC energy module at any given time.

In this regard and as an illustration, four SC energy modules are formed, each consisting of three SCs connected in series based on the 12 SCs used to develop the ECMs. An ECM of this energy module in charge and discharge mode is already shown in Fig. 7. c, but in this case, there is no resistive load, and the module is at the rest phase (open circuit or self-discharge). Table 4 presents the parameters of the three SCs that form each module. As can be seen in this table, from module 1 to module 4, the difference in capacitance value among the SCs forming each module increases; accordingly, module 4 has the largest difference in the capacitance value of its SCs. Despite this, the total capacitance value of the modules is not significantly different. In addition to experimental results, Fig. 8 presents an estimation of the voltage still remaining in each of the four modules on the basis of the proposed ECMs over a period of 31 days.

According to experimental and simulation results, the voltage still remaining in module 4 on day 31 is lower than the voltage remaining in the other modules, as can be seen in Fig. 8 and Table 5. These results reveal that the larger the difference in capacitance value among the three SCs in a module, the lower the final voltage value still stored in the module will be in the long-term (self-discharge and leakage will have more effect). Specifically, as demonstrated in Table 5, module 1 with a smaller capacitance value difference among its SCs has a higher experimental and estimated final voltage value as compared to module 4 with a larger capacitance value difference. Therefore, in order to maximize power storage in an energy module, it is best to select SCs with the same capacitance or with a small difference so that, in the long term, more power can still be stored in the module. In this regard, one important motivation of the modelling work reported here is to gain understanding of the effects of the device-to-device variation in printed SCs on the performance of an energy module including several SCs connected in series.

Furthermore, the simulation results of the four ECMs can also be used as a method to predict the minimum and maximum voltage still remained in the energy module at any given time. In Table 5, the estimated final value of the voltage remained in each module (voltage at the end of day 31) based on different ECMs is given. According to this table, it is possible to determine the predicted minimum and maximum final voltage values for each module, and based on these values, one can approximate the possible final voltage range window over each module at the end of the 31st day. In support of this claim, as can be found in Table 5, the experimental result of voltage for each module at the end of day 31st is within the predicted final voltage range window.

4. Summary and conclusion

This study proposes a simplified equivalent circuit model (ECM) based on the experimentally identified parameters of supercapacitors (SCs) (EDLC type) in order to analyze their discharge and self-discharge characteristics. The proposed ECM utilizes experimental parameters of SCs such as capacitance value and ESR as well as an exponential function based on the experimental self-discharge profile of SCs to represent the nonlinear phenomena of self-discharge and leakage current. This article also proposes three very simple sub-ECMs by finding a linear relationship among the different parameters of the SCs used in developing the first ECM. Using these super-simple ECMs and merely knowing the capacitance and ESR value of the SCs, the discharge and self-discharge behavior of the EDLC-type SCs can be predicted over a long period of time with reasonable accuracy. In order to verify the accuracy of the proposed ECMs, simulation results for both the SCs used in the development of the ECMs and other SCs including two commercial EDLC-type SCs are compared with the experimental results and an excellent agreement is found. Moreover, a good match is observed between the simulation and experimental results of the discharge behavior of two SC energy modules, each consisting of three series connected SCs, connected to discrete resistive loads.

Literature-reported ECMs have more RC network elements and branches and are too complex to be used for multi-cell SC energy modules. Furthermore, those ECMs are not accurate in simulating the nonlinear self-discharge effect of SCs over a long period of time. In addition, some of the ECMs reported in the literature require a huge number of steps to define exponential functions and parameters to

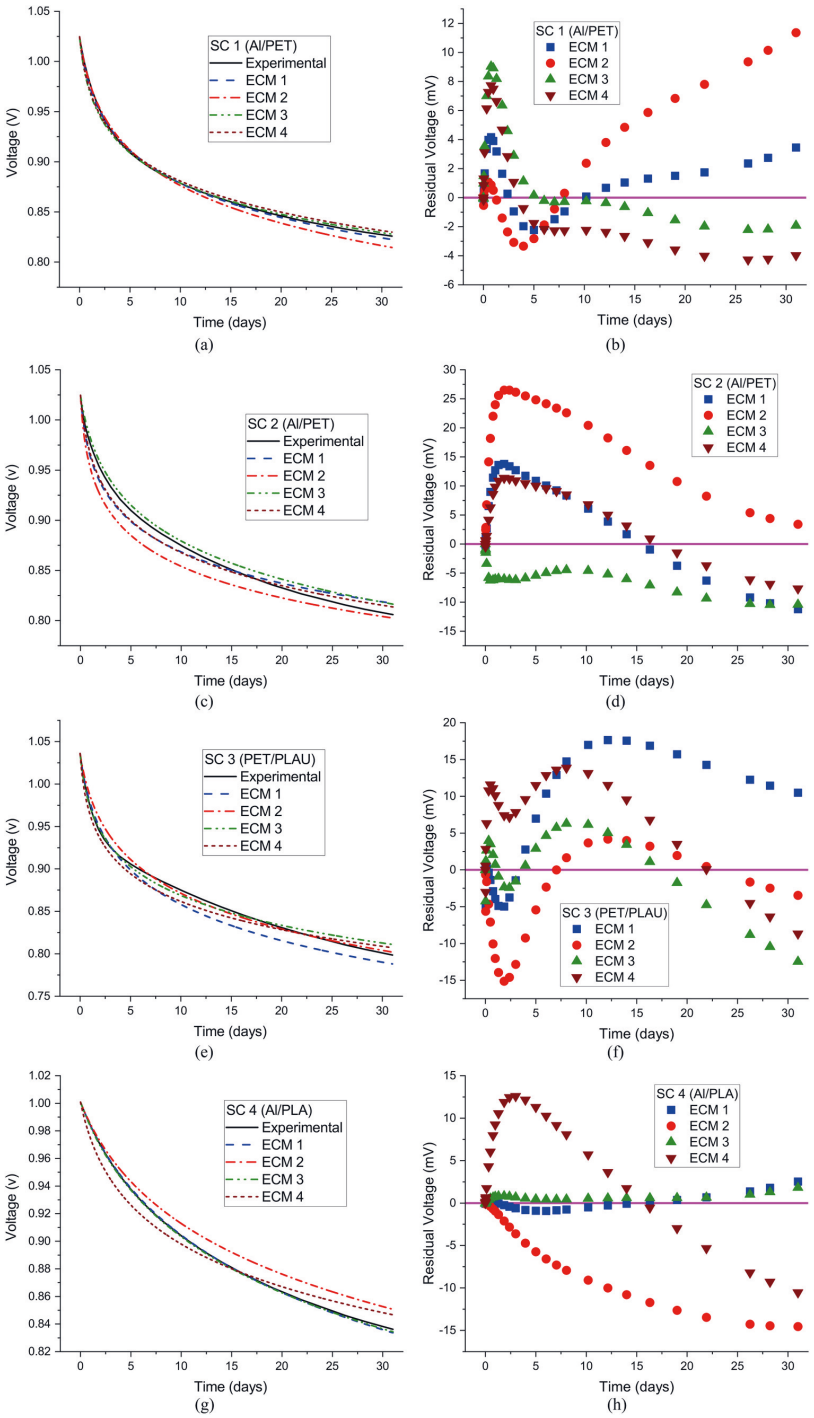

Fig. 6. a,c,e,g) Self-discharge experimental and simulation results in 31 days based on proposed ECMs for four randomly selected SCs not used to develop the ECMs. b,d,f,h) Residual voltage (the difference between experiments and simulations).

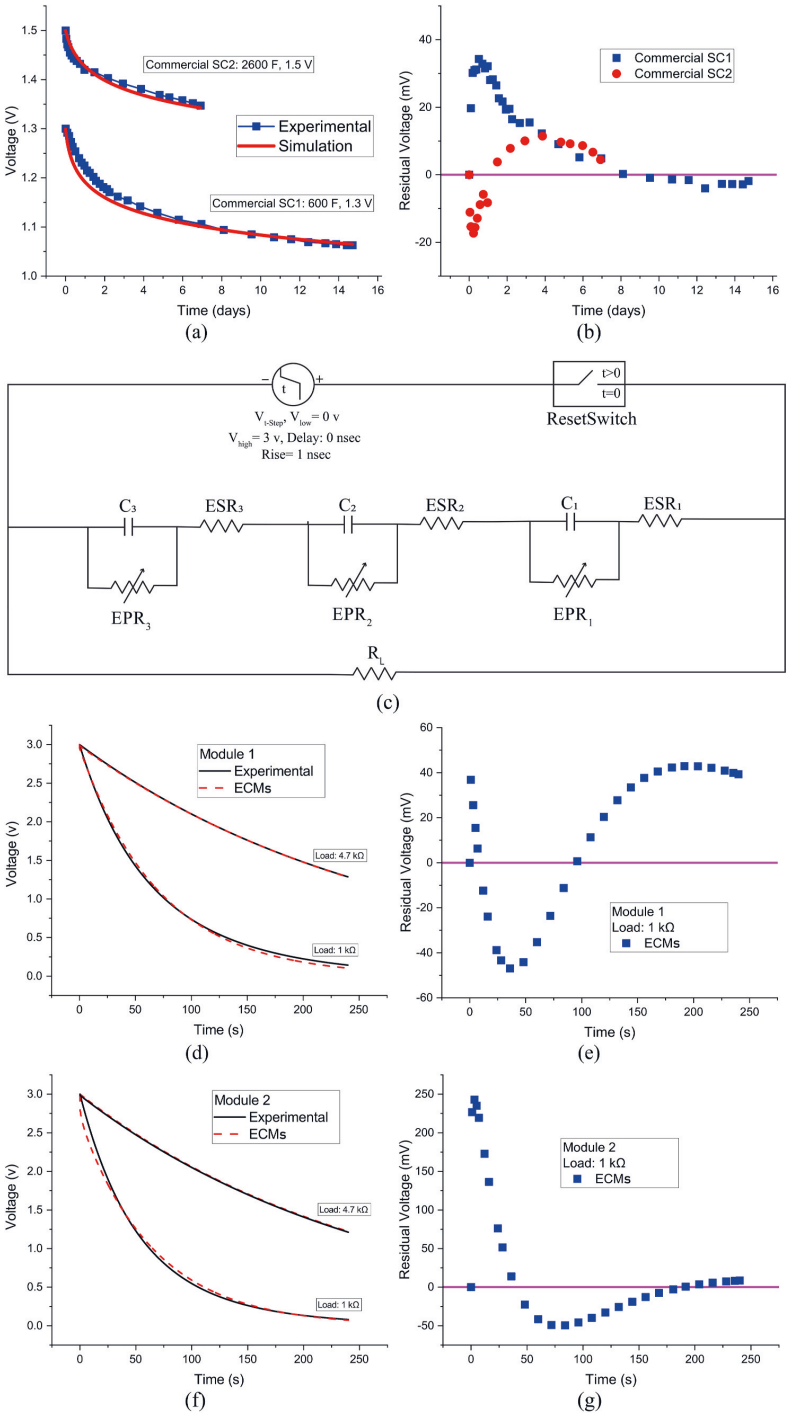

Fig. 7. a) Self-discharge experimental and simulation results based on ECM 4 of two commercially available SCs. b) Residual voltage (the difference between experiments and simulations) for the self-discharge of two commercial SCs. c) Charge and discharge ECM of a SC energy module (three series connected SCs) connected to a resistive load. d,f) Experimental and simulation results based on the proposed ECMs of the resistive load voltage during the discharge of the energy module. e,g) Residual voltage of the resistive load during the discharge of the module.

Table 4
ECM parameters of four SC energy modules, each consisting of three SCs connected in series.

Module 1	SC1	SC2	SC3	Module 2	SC1	SC2	SC3
C (mF)	147.7	158.8	161.3	**C (mF)**	140.5	183.4	222.2
ESR (Ω)	7.3	8	8	**ESR (Ω)**	7.2	7.8	8.8
a (EPR)	−34.7	−36.0	−36.8	**a (EPR)**	−34.0	−37.4	−39.0
b (EPR)	18.3	18.9	19.6	**b (EPR)**	17.1	21.4	23.8
C-total (mF)	51.9			**C-total (mF)**	58.6		
Module 3	**SC1**	**SC2**	**SC3**	**Module 4**	**SC1**	**SC2**	**SC3**
C (mF)	117.4	176.5	253.7	**C (mF)**	104.4	207.2	274.9
ESR (Ω)	7.5	7.4	8.4	**ESR (Ω)**	6.8	7	8.5
a (EPR)	−33.5	−36.2	−39.6	**a (EPR)**	−32.7	−38.3	−40.1
b (EPR)	16.3	20.2	24.8	**b (EPR)**	15.7	22.2	26.0
C-total (mF)	54.8			**C-total (mF)**	55.4		

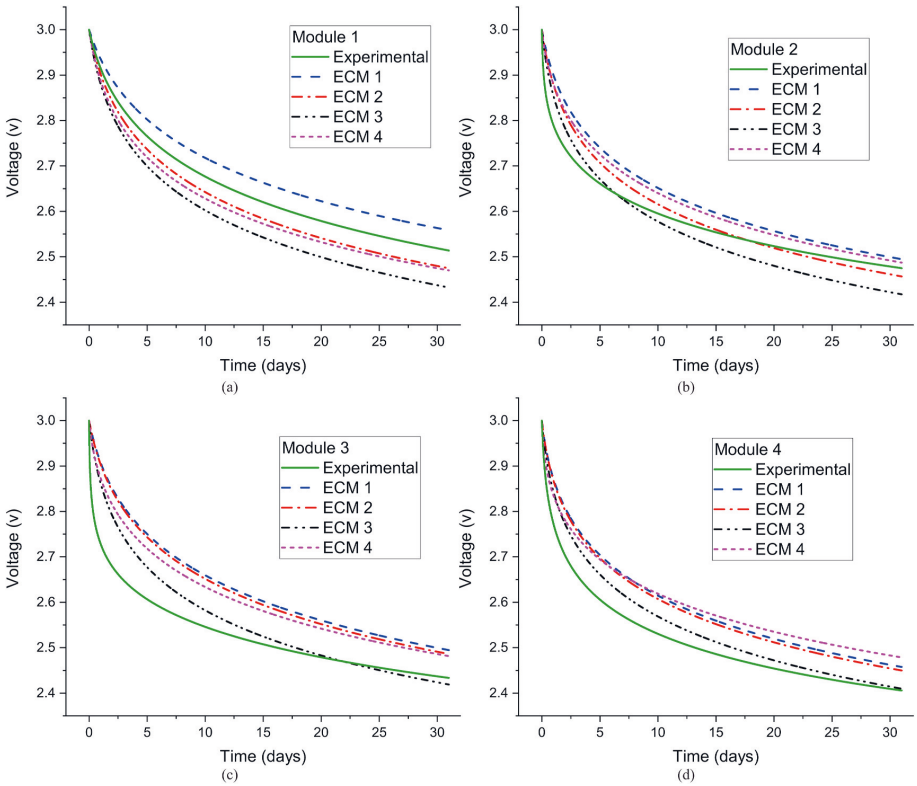

Fig. 8. Self-discharge behavior experimental and simulation results based on the proposed ECMs of four SC energy modules over time.

Table 5
Predicted final value of the voltage remained in each module (voltage at the end of day 31) based on proposed ECMs and experiments.

	Module 1	Module 2	Module 3	Module 4
ECM 1	2.56 V	2.49 V	2.49 V	2.46 V
ECM 2	2.47 V	2.46 V	2.49 V	2.45 V
ECM 3	2.43 V	2.42 V	2.42 V	2.41 V
ECM 4	2.47 V	2.49 V	2.48 V	2.48 V
Min.	2.43 V	2.42 V	2.42 V	2.41 V
Max.	2.56 V	2.49 V	2.49 V	2.48 V
Experiment	2.51 V	2.47 V	2.43 V	2.41 V

simulate the discharge behavior of SC modules over the long term. Due to the requirement for simple versions in order to implement the ECMs in practical applications, the ECMs presented in the literature are not suitable for long-term simulation of SC modules, despite their extensive RC network elements and difficulty in determining parameters. To conclude, the work presented in this paper, however, demonstrates a simple, practical, and accurate approach for studying the behavior of SC energy modules consisting of several SCs (EDLC type) connected in series/parallel, which can be used in the design of future energy storage systems and power management strategies. Furthermore, these ECMs may also be used to predict important aspects of printed electronics as well as the effect of different electrical variables that vary from device to device on the behavior of a SC energy module. Accordingly, depending

on the applications, the proposed ECMs may affect the choice of materials and layer thicknesses to reduce the leakage current in SCs. A deeper investigation of these cases utilizing the Monte Carlo simulation tool will be the subject of the authors' upcoming research work in the near future.

Declaration of competing interest

The authors declare that they have no known competing financial interests or personal relationships that could have appeared to influence the work reported in this paper.

Data availability

Data will be made available on request.

Acknowledgements

This project has received funding from the European Union's Horizon 2020 research and innovation programme under the Marie Skłodowska-Curie grant agreement No 814299 - CHARISMA. Parts of the research used Academy of Finland Research Infrastructure "Printed Intelligence Infrastructure" (PII-FIRI, Grant Number 320019).

Appendix A. Supplementary data

Supplementary data to this article can be found online at https://doi.org/10.1016/j.jpowsour.2023.232932.

References

[1] Anam Kalair, Naeem Abas, Muhammad Shoaib Saleem, Ali Raza Kalair, Nasrullah Khan, Role of energy storage systems in energy transition from fossil fuels to renewables, Energy Storage 3 (2021) e135–1.
[2] Shaqsi, A.L. Ahmed Zayed, Kamaruzzaman Sopian, Amer Al-Hinai, Review of energy storage services, applications, limitations, and benefits, Energy Rep. 6 (2020) 288–306.
[3] Guruprasad Alva, Yaxue Lin, Guiyin Fang, An overview of thermal energy storage systems, Energy 144 (2018) 341–378.
[4] Mustafa Cansiz, Dogay Altinel, Gunes Karabulut Kurt, Efficiency in RF energy harvesting systems: a comprehensive review, Energy 174 (2019) 292–309.
[5] Yunqi Cao, José Figueroa, Juan J. Pastrana, Wei Li, Zhiqiang Chen, Zhong Lin Wang, Sepúlveda Nelson, Flexible ferroelectret polymer for self-powering devices and energy storage systems, ACS Appl. Mater. Interfaces 11 (19) (2019) 17400–17409.
[6] Jian Lv, Jian Chen, Pooi See Lee, Sustainable wearable energy storage devices self-charged by human-body bioenergy, SusMat 1 (2) (2021) 285–302.
[7] Zhiwen Wang, Carriveau Rupp, David S-K. Ting, Wei Xiong, Zuwen Wang, A review of marine renewable energy storage, Int. J. Energy Res. 43 (12) (2019) 6108–6150.
[8] Azana Hafizah Mohd Aman, Norazuwana Shaari, Roszita Ibrahim, Internet of things energy system: smart applications, technology advancement, and open issues, Int. J. Energy Res. 45 (6) (2021) 8389–8419.
[9] Adu-Manu, Kofi Sarpong, Nadir Adam, Cristiano Tapparello, Hoda Ayatollahi, Wendi Heinzelman, Energy-harvesting wireless sensor networks (EH-WSNs) A review, ACM Trans. Sens. Netw. 14 (2) (2018) 1–50.
[10] Jiangqi Zhao, Jiajia Zha, Zhiyuan Zeng, Chaoliang Tan, Recent advances in wearable self-powered energy systems based on flexible energy storage devices integrated with flexible solar cells, J. Mater. Chem. A 9 (35) (2021) 18887–18905 (2021).
[11] Tarik Kousksou, Pascal Bruel, Abdelmajid Jamil, T. El Rhafiki, Youssef Zeraouli, Energy storage: applications and challenges, Sol. Energy Mater. Sol. Cell. 120 (2014) 59–80.
[12] Canan Acar, A comprehensive evaluation of energy storage options for better sustainability, Int. J. Energy Res. 42 (12) (2018) 3732–3746.
[13] A.R. Dehghani-Sanij, E. Tharumalingam, M.B. Dusseault, R. Fraser, Study of energy storage systems and environmental challenges of batteries, Renew. Sustain. Energy Rev. 104 (2019) 192–208.
[14] George Crabtree, Elizabeth Kócs, Trahey Lynn, The energy-storage frontier: lithium-ion batteries and beyond, MRS Bull. 40 (12) (2015) 1067–1078.
[15] Wenlu Zhou, Qiang Lu, Yanping Zheng, Review on the selection of health indicator for lithium ion batteries, Machines 10 (7) (2022) 512.
[16] Rajender Boddula, Ramyakrishna Pothu, Abdullah M. Asiri (Eds.), Rechargeable Batteries: History, Progress, and Applications, John Wiley & Sons, 2020.
[17] Muhammad Yaseen, Muhammad Arif Khan Khattak, Muhammad Humayun, Muhammad Usman, Syed Shaheen Shah, Shaista Bibi, Bakhtiar Syed Ul Hasnain, et al., A review of supercapacitors: materials design, modification, and applications, Energies 14 (22) (2021) 7779.
[18] Prerna Sinha, Kamal K. Kar, Introduction to supercapacitors, in: Handbook of Nanocomposite Supercapacitor Materials II, Springer, Cham, 2020, pp. 1–28.
[19] Priyanka Sharma, Vinod Kumar, Current technology of supercapacitors: a review, J. Electron. Mater. 49 (6) (2020) 3520–3532.
[20] Soma Banerjee, Kamal K. Kar, Conducting polymers as electrode materials for supercapacitors, in: Handbook of Nanocomposite Supercapacitor Materials II, Springer, Cham, 2020, pp. 333–352.
[21] Yonghong Xu, Hongguang Zhang, Fubin Yang, Liang Tong, Yan Dong, Yifan Yang, Jing Ren, Lili Ma, Yan Wang, State of charge estimation of supercapacitors based on multi-innovation unscented Kalman filter under a wide temperature range, Int. J. Energy Res. 46 (12) (2022) 16716–16735.
[22] Mehdi Shahedi Asl, Raha Hadi, Laleh Salehghadimi, Amin Goljanian Tabrizi, Sana Farhoudian, Babapoor Aziz, Majid Pahlevani, Flexible all-solid-state supercapacitors with high capacitance, long cycle life, and wide operational potential window: recent progress and future perspectives, J. Energy Storage 50 (2022), 104223.
[23] Dipanwita Majumdar, Manas Mandal, Swapan Kumar Bhattacharya, Journey from supercapacitors to supercapatteries: recent advancements in electrochemical energy storage systems, Emergent Materials 3 (3) (2020) 347–367.
[24] T.P. Sumangala, M.S. Sreekanth, Ariful Rahaman, Applications of supercapacitors, in: Handbook of Nanocomposite Supercapacitor Materials III, Springer, Cham, 2021, pp. 367–393.
[25] Alberto Cavallo, Antonio Russo, Giacomo Canciello, Control of supercapacitors for smooth EMA operations in aeronautical applications, in: 2019 American Control Conference (ACC), IEEE, 2019, pp. 4948–4954.
[26] Ravi Nigam, Kapil Dev Verma, Tanvi Pal, Kamal K. Kar, Applications of supercapacitors, in: Handbook of Nanocomposite Supercapacitor Materials II, Springer, Cham, 2020, pp. 463–481.
[27] Amna Riaz, Mahidur R. Sarker, Mohamad Hanif Md Saad, Ramizi Mohamed, Review on comparison of different energy storage technologies used in micro-energy harvesting, WSNs, low-cost microelectronic devices: challenges and recommendations, Sensors 21 (15) (2021) 5041.
[28] Kai Dong, Zhong Lin Wang, Self-charging power textiles integrating energy harvesting triboelectric nanogenerators with energy storage batteries/supercapacitors, J. Semiconduct. 42 (10) (2021), 101601.
[29] Brian Kihun Kim, Sy Serubbable, Aiping Yu, Jinjun Zhang, Electrochemical supercapacitors for energy storage and conversion, Handbook of clean energy systems (2015) 1–25.
[30] Francesca Soavi, Catia Arbizzani, Marina Mastragostino, Leakage currents and self-discharge of ionic liquid-based supercapacitors, J. Appl. Electrochem. 44 (4) (2014) 491–496.
[31] Mazharul Haque, Li Qi, D. Anderson, Smith, Volodymyr Kuzmenko, Per Rudquist, Per Lundgren, and Peter Enoksson. "Self-discharge and leakage current mitigation of neutral aqueous-based supercapacitor by means of liquid crystal additive, J. Power Sources 453 (2020), 227897.
[32] Jingwei Chen, Pooi See Lee, Electrochemical supercapacitors: from mechanism understanding to multifunctional applications, Adv. Energy Mater. 11 (6) (2021), 2003311.
[33] Binoy K. Saikia, Santhi Maria Benoy, Mousumi Bora, Joyshil Tamuly, Mayank Pandey, Dhurbajyoti Bhattacharya, A brief review on supercapacitor energy storage devices and utilization of natural carbon resources as their electrode materials, Fuel 282 (2020), 118796.
[34] Innocent S. Ike, Iakovos Sigalas, and Sunny Iyuke. "Understanding performance limitation and suppression of leakage current or self-discharge in electrochemical capacitors: a review, Phys. Chem. Chem. Phys. 18 (2) (2016) 661–680.
[35] Ji-Fu Shen, Yi-Jun He, Zi-Feng Ma, A systematical evaluation of polynomial based equivalent circuit model for charge redistribution dominated self-discharge process in supercapacitors, J. Power Sources 303 (2016) 294–304.
[36] Lei Zhang, Xiaosong Hu, Zhenpo Wang, Fengchun Sun, David G. Dorrell, A review of supercapacitor modeling, estimation, and applications: a control/management perspective, Renew. Sustain. Energy Rev. 81 (2018) 1868–1878.
[37] Teymoor Ghanbari, Ehsan Moshksar, Sara Hamedi, Fatemeh Rezaei, Zahra Hosseini, Self-discharge modeling of supercapacitors using an optimal time-domain based approach, J. Power Sources 495 (2021), 229787.
[38] Gustavo Navarro, Nájera Jorge, Jorge Torres, Marcos Blanco, Miguel Santos, Marcos Lafoz, Development and experimental validation of a supercapacitor frequency domain model for industrial energy applications considering dynamic behaviour at high frequencies, Energies 13 (5) (2020) 1156.
[39] Hamed Pourkheirollah, Jari Keskinen, Matti Mäntysalo, Donald Lupo, An improved exponential model for charge and discharge behavior of printed supercapacitor modules under varying load conditions, J. Power Sources 535 (2022), 231475.
[40] Mustafa Ergin Şahİn, Frede Blaabjerg, Ariya Sangwongwanİch, Modelling of supercapacitors based on simplified equivalent circuit, CPSS Transactions on Power Electronics and Applications 6 (1) (2021) 31–39.
[41] Ali Mohsen Alsabari, M.K. Hassan, C.S. Azura, Ribhan Zafira, Experimental design for an enhanced parametric modeling of supercapacitor equivalent circuit model, Indonesian Journal of Electrical Engineering and Computer Science 23 (1) (2021) 63–74.
[42] Hengzhao Yang, Ying Zhang, A study of supercapacitor charge redistribution for applications in environmentally powered wireless sensor nodes, J. Power Sources 273 (2015) 223–236.
[43] Dan Xu, Le Zhang, Bin Wang, Guangliang Ma, Modeling of supercapacitor behavior with an improved two-branch equivalent circuit, IEEE Access 7 (2019) 26379–26390.

[44] F. Naseri, S. Karimi, E. Farjah, E. Schaltz, Supercapacitor management system: a comprehensive review of modeling, estimation, balancing, and protection techniques, Renew. Sustain. Energy Rev. (2021), 111913.
[45] Pankaj Saha, Satadru Dey, Munmun Khanra, Modeling and state-of-charge estimation of supercapacitor considering leakage effect, IEEE Trans. Ind. Electron. 67 (1) (2019) 350–357.
[46] Tete Tevi, Arash Takshi, Modeling and simulation study of the self-discharge in supercapacitors in presence of a blocking layer, J. Power Sources 273 (2015) 857–862.
[47] Clarisse Péan, Benjamin Rotenberg, Patrice Simon, Mathieu Salanne, Multi-scale modelling of supercapacitors: from molecular simulations to a transmission line model, J. Power Sources 326 (2016) 680–685.
[48] Lei Zhang, Xiaosong Hu, Zhenpo Wang, Jiageng Ruan, Chengbin Ma, Ziyou Song, David G. Dorrell, Michael G. Pecht, Hybrid electrochemical energy storage systems: an overview for smart grid and electrified vehicle applications, Renew. Sustain. Energy Rev. 139 (2021), 110581.
[49] Hamed Pourkheirollah, Jari Keskinen, Donald Lupo, Matti Mäntysalo, A modified exponential equivalent parallel resistance (EPR) model for predicting self-discharge behavior of printed flexible supercapacitors, in: 2022 IEEE 9th Electronics System-Integration Technology Conference (ESTC), IEEE, 2022, pp. 264–268.
[50] Maedeh Arvani, Jari Keskinen, Donald Lupo, Mari Honkanen, Current collectors for low resistance aqueous flexible printed supercapacitors, J. Energy Storage 29 (2020), 101384.
[51] Anna Railanmaa, Ayat Soltani, Suvi Lehtimäki, Nazanin Pournoori, Jari Keskinen, Mikko Hokka, Donald Lupo, Skin-conformable printed supercapacitors and their performance in wear, Sci. Rep. 10 (1) (2020) 1–9.
[52] Jari Keskinen, Suvi Lehtimäki, Arman Dastpak, Sampo Tuukkanen, Timo Flyktman, Thomas Kraft, Railanmaa Anna, Donald Lupo, Architectural modifications for flexible supercapacitor performance optimization, Electron. Mater. Lett. 12 (6) (2016) 795–803.
[53] Ravi Muchakayala, Shenhua Song, Jingwei Wang, Youhua Fan, Manjunatha Bengeppagari, Jianjun Chen, Manlin Tan, Development and supercapacitor application of ionic liquid-incorporated gel polymer electrolyte films, J. Ind. Eng. Chem. 59 (2018) 79–89.
[54] Julia Kowal, Esin Avaroglu, Fahmi Chamekh, Armands Šenfelds, Tjark Thien, Dhanny Wijaya, Dirk Uwe Sauer, Detailed analysis of the self-discharge of supercapacitors, J. Power Sources 196 (1) (2011) 573–579.
[55] Yasser Diab, Venet Pascal, Hamid Gualous, Gérard Rojat, Self-discharge characterization and modeling of electrochemical capacitor used for power electronics applications, IEEE Trans. Power Electron. 24 (2) (2008) 510–517.

PUBLICATION IV

Statistical analysis and Monte-Carlo simulation of printed supercapacitors for energy storage systems

Hamed Pourkheirollah, Jari Keskinen, Matti Mäntysalo, Donald Lupo

Journal of Power Sources

https://doi.org/10.1016/j.jpowsour.2023.233626

Journal of Power Sources 585 (2023) 233626

Contents lists available at ScienceDirect

Journal of Power Sources

journal homepage: www.elsevier.com/locate/jpowsour

Statistical analysis and Monte-Carlo simulation of printed supercapacitors for energy storage systems

Hamed Pourkheirollah *, Jari Keskinen, Matti Mäntysalo, Donald Lupo

Faculty of Information Technology and Communication Sciences, Tampere University, Tampere, Finland

HIGHLIGHTS

- A novel method maintaining safe voltage storage via capacitance std regulation.
- Predictive energy range informs better system management and reliability.
- MC simulations ensure stable charging, predict post-self-discharge voltage range.
- ECM analysis confirms parameter normality; MC enhances module reliability.
- Proposed study empowers printed SC energy decisions, aids performance assessment.

ARTICLE INFO

Keywords:
Printed supercapacitors
Printed electronics
Energy storage systems
Statistical analysis
Monte-Carlo simulation
Self-discharge
Supercapacitor modelling and simulation

ABSTRACT

This study presents a comprehensive statistical analysis of experimental parameters for 12 printed supercapacitors (SCs) using previously proposed equivalent circuit models (ECMs). Statistical distributions and descriptive statistics, including mean, P-value, and standard deviation (std), are reported indicating a normal distribution for various SC parameters. A statistical method is introduced to determine the maximum potential std in capacitance of multiple SCs within an energy storage module, ensuring voltage limits are not exceeded. A linear relationship is discovered between the applied voltage on the module comprising three SCs in series and the maximum potential std of capacitance, ensuring safe operation. Additionally, a statistical method predicts the energy window range of the SC module after operating an IC chip, enabling better decision-making and system management. Monte-Carlo (MC) simulations predict the long-term charge and discharge performance of individual SCs and the series-connected modules. Results indicate that as long as the parameters' std remains below a defined threshold, charging behavior remains consistent. The MC simulations provide insight into voltage window ranges after 31 days of self-discharge, aiding in performance prediction and risk assessment. The statistical study approach empowers researchers in the field of printed SC energy storage, supporting performance evaluation, design validation, and evidence-based decision-making.

1. Introduction

It is becoming increasingly necessary to convert and store clean and renewable energy as a result of the depletion of fossil fuel sources, climate change, and global warming [1]. Concurrently, with the advent of renewable energy generation technology and the need for portable power, efficient storage of electrical energy has become increasingly important [2]. One example occurs in the context of the Internet of Things (IoTs), whereas a wide range of objects are interconnected via ubiquitous, inexpensive, thin, and flexible sensors [3]. There are several challenges associated with powering these devices using conventional methods, such as wiring them to the power outlets or using batteries that must be recharged or replaced on a regular basis [3]. In particular, currently available battery approaches, in spite of having high storage capacities, are limited in terms of aging effects, low charge/discharge rates, inflexibility, and safety and disposal issues because of the use of toxic or strategically problematic materials [4]. Consequently, some practical applications may be limited due to these issues. On the other hand, harvesting of energy from the ambient environment, wind, light, or temperature gradients presents a promising alternative. These sources, however, generate irregular and uneven power outputs [5].

The development of environmentally friendly energy storage

* Corresponding author.
E-mail address: hamed.pourkheirollah@tuni.fi (H. Pourkheirollah).

https://doi.org/10.1016/j.jpowsour.2023.233626
Received 6 June 2023; Received in revised form 18 August 2023; Accepted 10 September 2023
Available online 21 September 2023

technologies, such as electrochemical double-layer capacitors (EDLCs), has therefore received intensive research attention in recent years [6]. An EDLC, also called a supercapacitor (SC), is composed of two electrodes that contain a liquid electrolyte between which stores energy electrostatically by physically separating charge from electrolytic ion sorption on the electrode surface with a highly reversible mechanism [7]. As a result, they possess a higher power density in comparison with batteries [8]. Moreover, SCs are capable of being charged and discharged frequently at high current densities, with exceptional cycling stability [9]. As another advantage, it is also possible to manufacture SCs from non-toxic materials that are safer and more stable, which makes them ideal for a wide range of applications and easy to dispose of with minimal environmental impact [10,11]. When fabricated via printing techniques, SCs can also exhibit significant flexibility, which enables utilizing them in the development of energy-autonomous flexible and wearable electronic systems like electronic skin [12–14]. Therefore, SCs are extremely promising as next-generation energy storage devices for future electronic systems.

The field of printed electronics (PE) is considered to be an emerging field that is attracting growing research attention [15]. As opposed to conventional electronics, PE technology is highly efficient in the preparation of stacks of microscale/nanoscale devices [16]. In addition to being simple, time and material saving, cost-effective, versatile, eco-friendly, and high-volume production scalable, PE also offers a variety of manufacturing technologies for different SC architectures (micro, asymmetric, flexible, etc.) by utilizing a wide range of flexible substrates that can unleash the full potential of SCs [17].

Statistical analysis is a tool that can enable researchers to plan and conduct their experiments more precisely, analyze their data more effectively, and interpret their findings as well as identify trends in spending [18,19]. In addition, the purpose of this tool is to determine whether the differences, relationships, or congruencies observed are meaningful or merely coincidental [18,19]. In the field of PE, which involves high-volume sheet-to-sheet and roll-to-roll manufacturing processes, statistical analysis may also be considered to play a significant role. In particular, a number of statistical studies have been published in the literature concerning the behavior and properties of SCs. For example, in SCs with nanopore electrode structures, classical density functional theory (CDFT) has been reported to be used to investigate how capacitance and energy storage behavior are affected by pore size [20]. As part of another study, Ghamari et al. conducted a statistical survey based on AFM data in order to examine the effect of textural characteristics on the performance of SCs constructed with modified MOF electrodes [21]. In another article [22], researchers described how they developed a statistical model based on Monte-Carlo simulation to determine the capacity distributions for battery-supercapacitor hybrid energy storage systems in autonomous microgrids. In addition, the hybrid SC was also statistically modeled from manufacturing perspective with the input factors related to electrodes, while the specific capacitance was used as an output parameter [23]. Moreover, the researchers have also published a report concerning the investigation of a statistical and systematic approach for determining the optimum proportion of three component materials in graphene-based SC electrodes [24]. Furthermore, in Ref. [25], a support vector machine-based statistical analysis was employed to accurately predict the capacitance of carbon-based SCs depending on the structural characteristics such as specific surface area, calculated pore size, N-doping level, and applied voltage window.

Herein, we analyze the charge and discharge behavior of printed SCs using statistical techniques. It is possible to use the presented statistical study to predict how series-connected SC energy modules behave depending on the variation in electrical properties among the devices, a factor of serious importance when dealing with PE devices. As well as predicting critical aspects of PE, this statistical study can also be applied to determine the effect of various electrical variables that vary from device to device on the behavior of an energy module consisting of several SCs connected in series and/or in parallel. In other words, this work may also be used to the analysis of how variations in electrical parameters from device-to- device, such as self-discharge and leakage current in SCs, affect the performance of series-connected SCs in an energy module. In this study, Monte-Carlo (MC) simulation has been employed for the statistical analysis of the charge and self-discharge behavior of the printed SCs.

Nevertheless, it is important to highlight that the statistical analysis undertaken in this study relies on the equivalent circuit models (ECMs) that have been previously documented. In these prior ECMs, the charging current of printed SCs within an energy storage module has been treated as infinite.

2. Method

In this work, 12 printed SCs of the EDLC type are used to conduct the statistical analysis. These 12 printed SCs were manufactured utilizing an identical fabrication process throughout the production. A detailed description of the fabrication and characterization process of these kind of printed SCs has already been published by the authors [26–33] and this study utilizes the parameters of the 12 fabricated SCs for the statistical analysis purposes.

This study utilizes the MC simulation method in order to perform statistical analysis. The MC method is capable of performing an extensive number of simulations and producing an approximate range or distribution of the possible outcomes [34]. MC simulation involves building models that predict possible results by substituting a range of values -a probability distribution-for any factor that has inherent uncertainty [35]. Probability distributions are used in order to represent the various possible values of uncertain inputs, as well as their probability of occurring. As a result, the system calculates the possible outcomes repeatedly using a different set of random values generated by the probability functions. In addition to calculating the probabilities of different outcomes in their forecasts, researchers are also able to perform a wide range of additional analyses using this data on possible results. Therefore, MC simulation is significantly superior to "best/-worst/most likely" guess analyses in light of the fact that probability distributions describe uncertainty in variables much more realistically. Accordingly, in PE, MC method can greatly accelerate the research process and result in significant saving of time, energy, and costly materials by eliminating the need to fabricate large quantities of devices.

In order to model the printed SCs and apply MC, the same equivalent circuit models (ECMs) as previously proposed by the authors are utilized in here [36,37] (Fig. 1). The reported ECMs are extremely simple, as they require the specification of only two to four parameters for each SC.

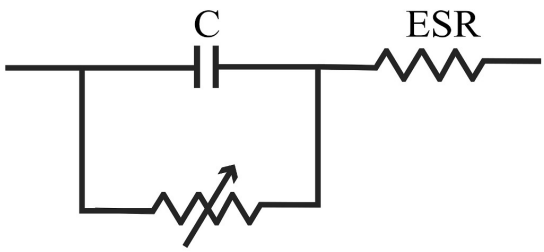

$$\text{ECM 1: EPR: } I = e^{(a + b \times V)}$$

$$\text{ECM 2: EPR: } I = e^{(-22 + b \times (V - 0.7))}$$

$$\text{ECM 3: EPR: } I = e^{(-28 - 45 \times C + V \times (64 \times C + 9))}$$

$$\text{ECM 4: EPR: } I = e^{(-36.5 + 20.4 \times V)}$$

Fig. 1. Proposed ECMs for a single printed SC [36].

Based on their simplicity, the presented ECMs are very suitable for use in energy storage modules containing multiple SCs connected either in series or parallel. These ECMs were found to be highly accurate in long-term, as a very significant correlation between the simulation and experimental results over a prolonged period of time (31 days) was reported. In these ECMs, capacitance (C), equivalent series resistance (ESR), and equivalent parallel resistance (EPR) parameters (a & b) are considered as four parameters that are subject to inherent uncertainty in the fabrication process of a single printed SC. In order to obtain capacitance and ESR value, a Maccor workstation (Maccor Inc., USA) was used to electrically characterize the SCs individually according to an international industrial standard (IEC 62391-1) (see Refs. [26,36] for more detailed information). Besides, the EPR (a & b) parameters were also determined from the self-discharge profile of the SCs (as discussed in detail in Refs. [36,37]).

As discussed above, in order to employ the MC tool, it is necessary to specify the probability distribution of each of the four parameters with inherent uncertainty for 12 printed SCs used in this study. Hence, every parameter in this ECM has been subjected to a normality test in order to determine whether the data can be described adequately by a normal distribution (Gaussian distribution). In probability theory, a normal distribution is a distribution that is symmetric around the mean, representing that data near the mean are more likely to occur than data further away from the mean [38]. Accordingly, each parameter's distribution as well as the bell curve are represented in the histogram charts (Fig. 2). The normal quantile-quantile (Q-Q) probability plot for each parameter of the ECM are also shown in the supplementary material (Fig. 2). As can be seen in the histogram charts and the Q-Q plots, all the four parameters follow a normal distribution.

Furthermore, a summary of the descriptive statistics and normality test results such as mean value, standard deviation (Std), P-value, and skewness for each parameter can be found in Table 1. It is also evident from the numerical results of the descriptive statistics that all four parameters exhibit a normal distribution. For instance, there is a strong support for the hypothesis of normal distribution based on the P-value of the four parameters, which range between 0.74 and 0.98. Moreover, the mean and median values for each of the four parameters are almost identical, representing another proof of passing the normal distribution test by all four variables. Besides, the skewness, an indicator of the degree of distribution asymmetry, ranges between 0.30 and 0.52 for the four parameters, indicating that the probability distributions of all variables are approximately symmetrical.

Table 1
Descriptive statistics and normality test results of the ECM parameters.

Parameters	C (mF)	ESR (Ω)	a	b
N total	12	12	12	12
Mean	179.0	7.7	−35.6	20.0
Minimum	169.1	6.3	−38.6	16.9
Median	178.2	7.6	−35.8	20.0
Maximum	192.0	9.3	−31.3	23.8
Std	7.18	0.92	2.21	2.07
P-Value	0.83	0.82	0.74	0.98
Skewness	0.35	0.41	0.52	0.30

3. Results and discussion

3.1. Quantifying capacitance variation in series-connected SC energy modules using statistical analysis

The voltage stored in a single SC cannot exceed a certain amount, as it is limited by the electrochemical potential window of the electrolyte [39]. This maximum potential value for the printed SCs used in this work is 1.2 V. However, there may be circumstances where this limited voltage is not sufficient for a particular application, so the solution is to connect multiple SCs in series in order to form a SC energy module. Nevertheless, the standard deviation (std) among the capacitance value of the SCs must be considered when connecting several SCs in series, as the larger the difference among the capacitance of series connected SCs is in a module, the larger the difference among the voltage stored over each SC will be, once the charging phase has completed (there will be more voltage over the SC with the lowest capacitance). On the basis of the capacitive division of the total charging voltage, the potential difference across each SC can be calculated using Eq. (1). Consequently, if the std of capacitance of SCs within a module is above a certain

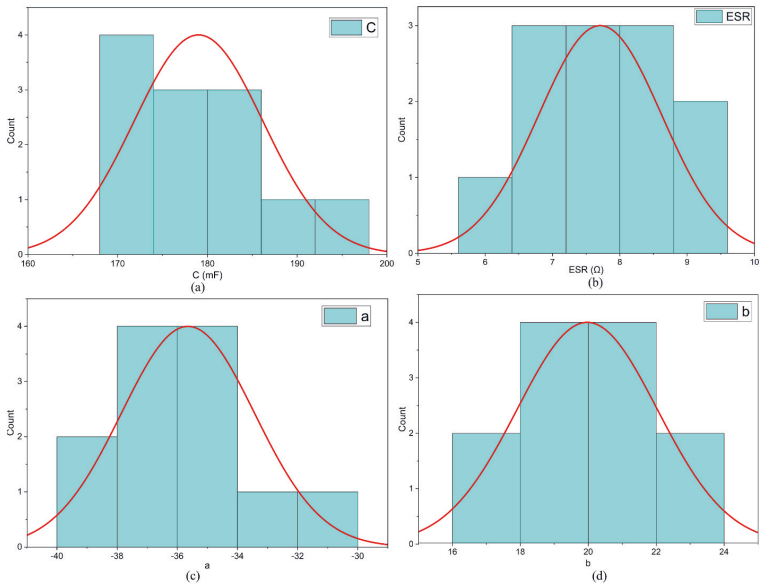

Fig. 2. Histogram chart of the ECM parameters.

threshold, some SCs will have voltage that exceeds the electrochemical potential window of the electrolyte, resulting in the entire module malfunctioning. Statistical analysis is therefore essential for determining the maximum capacitance std of series-connected SCs within a module.

$$V_{SCi} = V_0 / \ (C_i \times (1/C_1 + 1/C_2 + 1/C_3 + \ldots + 1/C_N)), \quad (1)$$

As V_{SCi} represents the voltage stored across SC_i, V_0 represents the charging voltage, C represents the capacitance, and N represents the number of SCs connected in series.

In the previous section, the normality test and descriptive statistics indicated that the capacitance of the printed SCs follows a normal distribution. Now, using the statistical analysis tools, our objective is to determine: if we fabricate 300 printed SCs with some standard deviation (std) on their capacitance (10, 15, and 20%), and if we would form 100 SC energy modules using three SCs connected in series per module, and if we would charge each module up to 3 V, how many of the modules will contain at least one SC with stored voltage higher than 1.2 V? The statistical study results for this investigation are presented in Table 2. In light of the results, if we have a 10% standard deviation on the capacitance value of the 300 printed SCs, we will have only one module with at least one SC with a voltage higher than 1.2 V. Accordingly, with a standard deviation of 15% and 20% on the capacitance of 300 SCs, there will be 12 and 31 modules with at least one SC with a voltage of more than 1.2 V, respectively. Thus, the maximum std allowed on the capacitance of three series-connected printed SCs is less than 10%, in order to prevent the module from malfunctioning when charged up to 3 V.

For this statistical investigation, Fig. 3 also shows the distribution plots of the SC's stored voltage within a module. It is evident from the distribution plots that the number of SCs with a voltage more than 1.2 V increases as the capacitance std increases and it may even reach about 1.6 V in the case of 20% std. Likewise, the violin-shaped plots of the SC's stored voltage across a module can be found in the supplementary material (Fig. 3).

3.2. Statistical analysis of capacitance std in series-connected printed SCs for charging voltage optimization

Before applying a specific voltage to the energy storage module, statistical analysis can be employed to determine the maximum std of capacitance of printed SCs connected in series within the module. As a result, the determination of the potential maximum std for the capacitance of series-connected printed SCs will protect the energy storage systems from malfunctioning.

Our objective is now to determine how much maximum std should be allowed for the capacitance of 300 printed SCs, if a specific voltage in the range of 2.5–3.5 V is applied to the three series-connected SCs module, in order to ensure that there are no SCs with voltage exceeding 1.2 V. A summary of the results of this statistical analysis is presented in a table in the supplementary material. The maximum allowed std of capacitance is inversely proportional to the voltage applied to the module, as shown in the table. For example, in order to safely store 3.5 V power to the energy storage module, the maximum capacitance std of the printed SCs must be 1.4%, while for 2.5 V, it can be increased up to 16.1%.

Furthermore, as shown in Fig. 4, the relationship between the maximum std of the capacitance and the total voltage stored in the module is linear with a high degree of accuracy (based on the R-square values of the linear fit). As a result of this linear relationship, the following equation can be derived:

Table 2
Number of SC energy modules with at least one SC exceeding 1.2 V stored voltage, based on different capacitance std (10%, 15%, and 20%).

	Std (10%)	Std (15%)	Std (20%)
Number of modules	1	12	31

$$C - Std_{max} = 54.61 - (15.2 \times V_T) \quad (2)$$

Where C-Std_{max} represents the maximum std allowed for the capacitance of 300 printed SCs, and V_T represents the maximum voltage that can be safely stored over a three series-connected SC energy module.

3.3. Energy window range of the printed SC modules

In order to ensure reliable operation during power outages or interruptions, it is crucial to accurately determine the amount of energy that an energy storage module is capable of continuously providing in various applications. With the std in the capacitance of the printed SCs during mass production, statistical analysis can therefore provide insight into the energy window range of the SC modules well in advance of the energy storage systems deployment in the applications. Additionally, awareness of the energy range that can be supplied by a printed SC module to a specific application facilitates the optimization of energy management, enhances system performance, extends the module's lifespan, minimizes the environmental impact, and guarantees safe operation [40].

As a result of Eq. (2), it is now possible to calculate the maximum potential std of the capacitance of printed SCs within a module in order to safely store a particular potential difference. Our aim is now to determine how much the energy window range of each module would be if we form 100 SC modules using 300 printed SCs and store a particular voltage (2.5–3.5 V) within each module. The energy window range of the three series-connected SC modules can be seen in Fig. 5a when a specific potential difference of 2.5–3.5 V is stored across the module. As an illustration, assuming a safe storage capacity of 3.5 V, the SC module has the capability to supply energy within the range of 358–370 mJ. While, if the safe storage capacity is reduced to 2.5 V, the SC module is expected to provide an energy output in the range of 125–225 mJ. Clearly, this indicates that lowering the stored voltage in the module results in increased std in the capacitance of the SCs, thus widening the energy window of the module (as shown in Fig. 5a, the energy window ranges from right to left becomes wider as the voltage decreases).

The utilization of printed SC modules in conjunction with integrated circuit (IC) chips is regarded as a significant and promising improvement, as the use of printed SCs can enable the development of more compact and energy-efficient IC chip systems [41]. Nonetheless, the integration of printed SC modules with IC chips presents several technical challenges that must be overcome. One significant challenge is the matching of the SCs module voltage with the operating voltage of the IC chip. The second challenge involves guaranteeing that sufficient energy is supplied to operate the IC chips. Hence, the voltage output of the SC module must be carefully controlled to avoid damaging the IC chip while still providing enough power to meet the chip's energy requirements. So far, the statistical analysis conducted in this study has partly demonstrated the approach to addressing these two concerns.

Subsequently, the remaining energy window of a printed SC module after operating an IC chip must also be considered, as it is important for several reasons. First, it can help to determine the operational efficiency of the SC module and the IC chip. If the remaining energy window is too low, it could indicate that the capacity of the SC module is insufficient to meet the energy requirements of the IC chip or that the energy transfer efficiency is low, leading to energy losses and decreased operational efficiency. Second, understanding the remaining energy window can help determine when the SC module needs to be recharged. If the remaining energy is low, it is essential to recharge the SC module before the energy is fully depleted in order to prevent potential shutdown of the IC chip. Third, knowledge of the remaining energy can help optimize the design of the system that incorporates the SC module and the IC chip. By understanding the energy requirements of the IC chip and the capacity of the SC module, the system can be designed to ensure that the SC module can provide sufficient energy to the IC chip for the desired

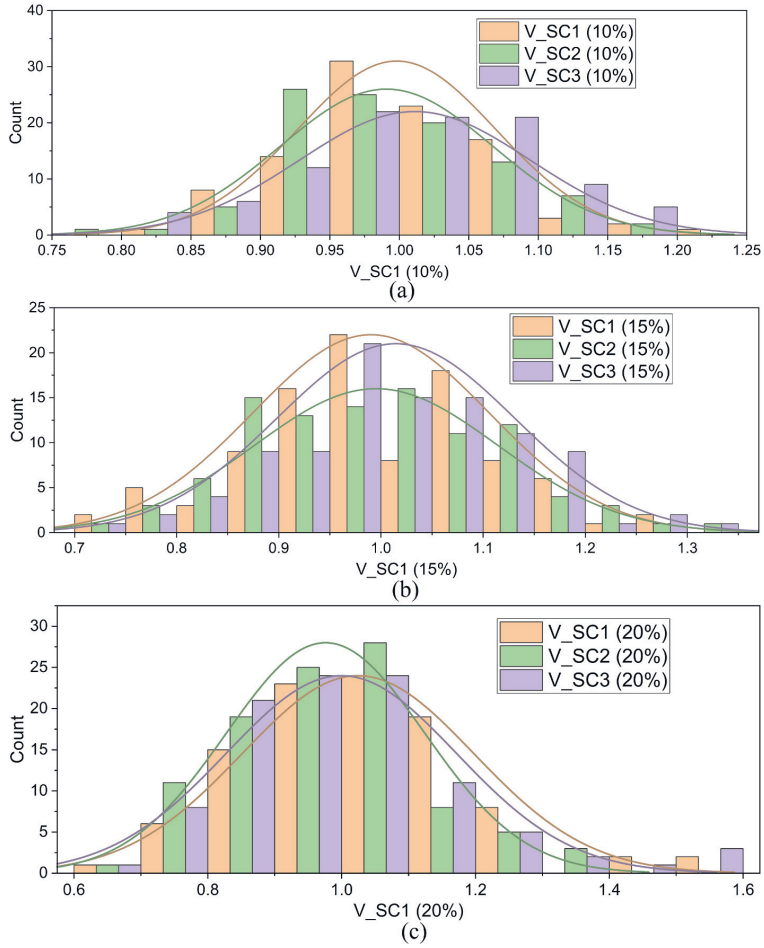

Fig. 3. (a–c) Distribution plots of the SC's stored voltage within a module based on 10, 15, and 20% std on the SCs' capacitance value, respectively.

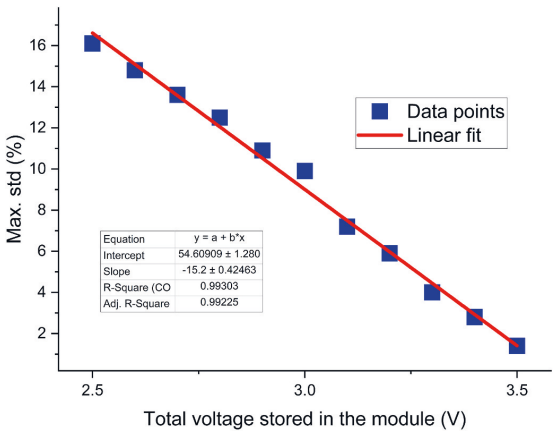

Fig. 4. Linear relationship between capacitance std and total stored voltage in series-connected SC Module.

duration of operation. In summary, knowing the remaining energy of a SC module after operating an IC chip is essential for determining operational efficiency, optimizing the design of the system, and preventing potential damage to the IC chip. The remaining energy available within the SC module can be computed using the following equation:

$$E = ½ \times C_{tot} \times \left(V^2_{module} - V^2_{app}\right)$$

where E is the remaining energy, C_{tot} is the total capacitance of the SC module, V_{module} is the stored voltage in the SC module, and V_{app} is the operational voltage of the IC chip.

The operation voltage of the IC chips varies depending on the specific chip and its design [42]. Modern IC chips typically operate at low voltages, usually around 2 V. This study assumes the use of printed SC modules to power IC chips with three distinct operation voltages (1.8, 2, and 2.2 V). The remaining energy window range of three series-connected printed SC modules after the operation of IC chips at voltages of 1.8, 2, and 2.2 V is illustrated in Fig. 5b–d, respectively, with no recharge applied. Based on the analysis depicted in Fig. 5b–d, it can be concluded that in case a printed SC module is charged up to 3.5 V and then utilized to power IC chips with voltages of 1.8, 2, and 2.2 V, a remaining energy range of 263–273, 241–250, and 217–224 mJ may be

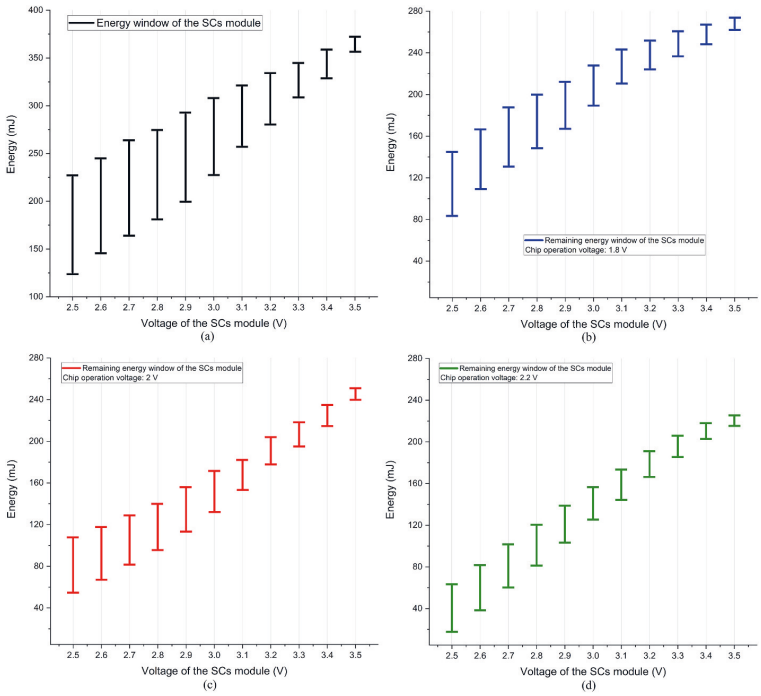

Fig. 5. (a) Energy window range of series-connected SC module with potential difference of 2.5–3.5 V (b–d) Remaining energy window range of series-connected printed SC modules after IC chip operation at voltages of 1.8 V, 2 V, and 2.2 V without recharge.

expected to be still available within the module, respectively. On the other hand, in the case of storing 2.5 V across the SC module, there will be a remaining energy range of 75–109, 56–107, and 19–62 mJ within the module after operating IC chips with voltages of 1.8, 2, and 2.2 V, respectively. Briefly, the determined energy window range values, obtained through statistical analysis, provide system designers with valuable information to select suitable energy modules and set realistic practical expectations for the duration of backup power supply.

3.4. Statistical analysis on charging and discharging behavior of SC module

In this section, we aim to employ MC simulation as a method for analyzing and predicting the charging and discharging behavior of individual printed SCs within a three series-connected SC energy module as well as the behavior of the entire module. The outcomes of MC simulation can provide detailed insights into the behavior of individual components, as well as the overall energy storage module, under varying conditions. These insights can be leveraged to evaluate the risk of failure or performance degradation of individual SCs and the module during charging and discharging cycles. Additionally, the utilization of MC simulation exhibits promising potential for mitigating the financial burdens associated with physical testing and prototyping, while concurrently reducing time expenditures. Through simulating the behavior of SC modules in a virtual setting, it is possible to detect potential issues early on in the design process, thereby minimizing the need for costly and time-consuming physical testing and prototyping. Furthermore, the results of MC simulation can be utilized to optimize the module's design and ensure that it satisfies the requisite specifications. In brief, by using MC simulation tool, designers and engineers can develop more efficient, reliable, and cost-effective SC modules.

Fig. 6. a illustrates the charging ECM of a SC module consisting of three printed SCs connected in series and charging up to 3 V. Fig. 6b also presents the discharge ECM of the SC module. In order to model the initial potential difference of the SCs when discharging, a switch and a DC voltage source have been employed for each SC. The value of the DC voltage source is calculated using capacitive voltage division of the three SCs. Besides, ESR (equivalent series resistance), refers to the internal resistance of the SC electrodes and electrolyte, as well as the resistance of the connections. On the other hand, EPR (equivalent parallel resistance), describes the nonlinearity associated with the SC's self-discharge and leakage current. The exponential function of EPRs for all four ECMs are already displayed in Fig. 1. The authors have previously provided a comprehensive description of these ECMs in their prior publication [36].

As discussed earlier in this work, in order to utilize MC simulation, it is necessary to define the various variables in an ECM, as well as their distribution, mean value and standard deviation (std). The four ECMs utilized in this work have different number of variables for each single SC (see Fig. 1). For a single SC, ECM1 has four variables (C, ESR, a, and b), ECM2 has three variables (C, ESR, and b), and ECMs 3 and 4 have two variables each (only C and ESR). Besides, as outlined in the 'Method' section, this work utilizes 12 printed SCs' parameters to conduct MC simulations, with all four parameters of the SCs following a normal distribution. Table 3 provides a summary of the EPR function for each ECM, along with the variables included in each ECM and their respective mean value (M) and std (the abbreviation 'N/A' denotes that the particular variable is not applicable to the corresponding ECM). In this research, the charging and discharging behavior of the printed SCs module is analyzed through 100 trials conducted using the MC simulation tool.

3.4.1. Monte-Carlo charging results using the proposed ECMs

Fig. 6c and d presents the charging behavior of one of the individual SCs (SC 1) and the entire module. The charging behavior of the three

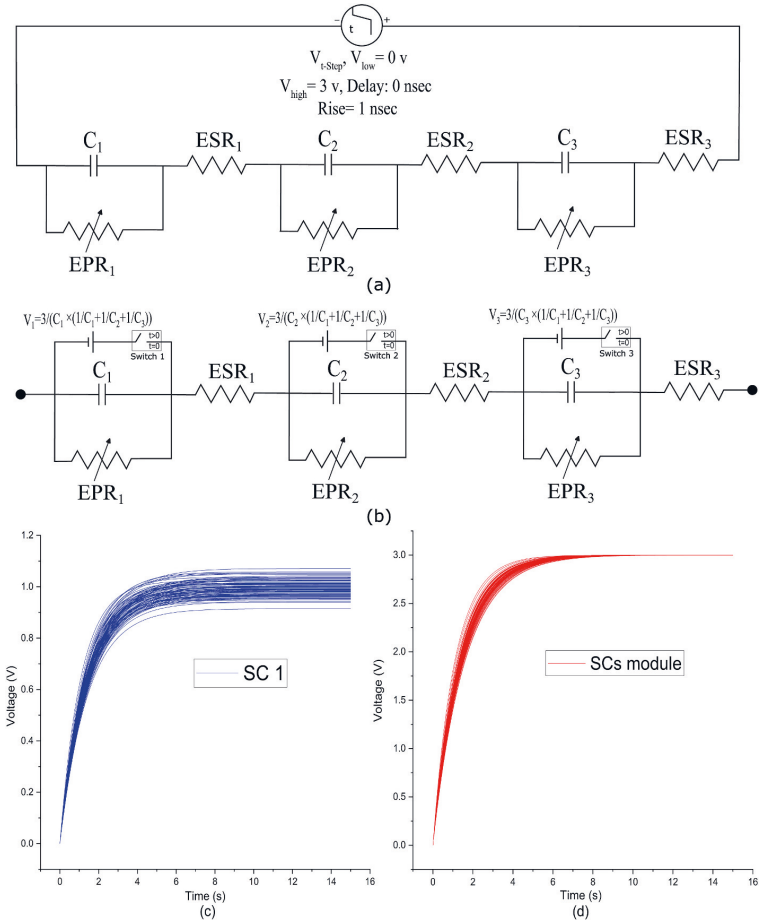

Fig. 6. (a) Charging ECM of a three series-connected SC module. (b) Discharging ECM of a three series-connected SC module. (c) Charging behavior of individual SCs within a SC module. (d) Charging behavior of the whole SC module.

Table 3
Summary of ECMs' variables, EPR function elements, mean value (M), and std.

Variables	C (mF)	ESR (Ω)	a	b
ECMs				
ECM 1	M: 179.0	M: 7.7	M: −35.6	M: 20.0
EPR: $I = e^{(a+b\times V)}$	Std: 7.18	Std: 0.92	Std: 2.21	Std: 2.07
ECM 2			N/A	
EPR: $I = e^{(-22+b\times(V-0.7))}$				
ECM 3				N/A
EPR: $I = e^{(-28\ -45\times C+V\times(64\times C+9))}$				
ECM 4				
EPR: $I = e^{(-36.5+20.4\times V)}$				

printed SCs exhibit a high degree of similarity, as evidenced in the supplementary material (Fig. 6). On the other hand, none of the SCs reaches a charging voltage of 1.2 V. The observed similarity in the charging behavior and the maintenance of the charging voltage below 1.2 V for each individual SC can be attributed to two factors. Firstly, the printed SCs exhibit low std in capacitance and ESR values (7.18% and 0.92% respectively). As previously discussed in this article, this ensures the safe storage of each individual printed SC within the three series-connected SC module when connected to a 3 V power source, as long as the std of the capacitance remains below 9.9% (see table in the supplementary material). Secondly, the authors' previous work demonstrated that the charging behavior of SCs is minimally affected by the EPR when the charging current is excessively high [26]. Additionally, Fig. 6d depicts the charging behavior of the entire module, which stores 3 V in approximately 10 s.

3.4.2. *Monte-Carlo self-discharge results using the proposed ECMs*

The utilization of the MC simulation tool facilitates an extensive comprehension of the self-discharge characteristics exhibited by printed SCs and SC energy storage modules, particularly when considering extended time duration scenarios. First, by studying the long-term self-discharge behavior, researchers can assess the energy storage capabilities of printed SCs and SC modules over extended periods. This evaluation helps in determining their suitability for practical applications that require prolonged energy storage. Second, knowledge of long-term self-discharge behavior aids in evaluating the reliability and durability of the printed SCs and modules. It allows researchers to identify potential

degradation mechanisms, estimate the loss of stored energy, and assess the impact of self-discharge on the overall system performance. Third, the long-term self-discharge behavior data can be used to develop predictive models that estimate the energy losses over time. These models can aid in system-level optimization, performance prediction, and decision-making processes regarding the use of printed SCs and modules in various applications. Fourth, comparing the self-discharge behavior of different printed SCs and modules over the long-term allows for performance comparison and benchmarking. This analysis helps to identify superior designs, materials, or fabrication techniques that exhibit lower self-discharge rates, higher energy retention, and improved long-term stability.

Figs. 7 and 8 depict the long-term (31 days) simulated self-discharge characteristics of one of the individual SCs within the module (SC 1) as well as the entire three series-connected SC energy module, employing four ECMs, through the utilization of the MC. The results for all three individual SCs are presented in the supplementary material (Figs. 7 and 8). The figures clearly demonstrate that ECM 1 predicts the broadest window range of results on day 31, whereas ECM 3 and 4 predict the narrowest window range. This difference in the width of the predicted window range can be attributed to the application of the MC tool on four variables in ECM 1, while only two variables are considered in ECM 3 and 4. Nonetheless, ECM 3 and ECM 4 are likely to yield the most probable final outcomes, given that the range of final outcomes produced by these two ECMs falls within the range of highest data concentration observed for ECM 1. Table 4 presents the MC simulated voltage outcomes of both individual SCs and the entire module after 31 days, utilizing four ECMs. Based on the table, when employing ECM 1, the SC energy storage module is projected to retain a minimum of 1.87 V power after 31 days of self-discharge in the worst-case scenario. Conversely, in the best-case scenario, the module is anticipated to possess a maximum of 2.89 V power on the 31st day. When ECM 2 is employed, the energy window range of the module on the 31st day is estimated to be between 2.41 and 2.56 V. However, when utilizing ECM 3 and 4, this range becomes more narrower, spanning approximately 2.40–2.43 V. Accordingly, these numerical values indicate that the final results produced by ECM 3 and ECM 4 are roughly equivalent to the average value of the final results generated by ECM1.

It should be noted that excellent concordance was observed between the experimental results and simulations conducted with four ECMs, as previously published by the authors [36,37].

4. Summary and conclusion

In this study, a thorough statistical analysis is conducted on experimental parameters of 12 printed supercapacitors (SCs) utilizing the equivalent circuit models (ECMs) previously proposed by the authors. Statistical distribution and descriptive statistics of different parameters of printed SCs such as mean, P-value, and standard deviation (std), etc. are reported in this work. In conclusion, it is observed that all four parameters of printed SCs exhibit a normal (Gaussian) distribution. Besides, a beneficial statistical method is proposed to establish the maximum potential std in the capacitance value of multiple SCs within an energy storage module. To summarize, this method ensures that none of the SCs store a voltage exceeding the electrochemical potential window of the electrolyte, which could potentially lead to system malfunction. In addition, a strong linear relationship with high accuracy is discovered between the applied voltage on the energy storage module comprising three printed SCs connected in series and the maximum potential std of capacitance of SCs, ensuring the safe operation of the energy module. Furthermore, a statistical method is proposed to predict the energy window range of the SC energy storage module after operating an IC chip. This method offers valuable insights that can contribute to performance optimization, resource planning, system reliability, energy harvesting strategies, and safety considerations. By providing information on the expected energy range, it enables better decision-making and management strategies to ensure the efficient and reliable operation of the overall system.

Subsequently, leveraging the obtained statistical characteristics of the experimental parameters and employing the Monte-Carlo (MC) simulation tool with 100 trials on the ECMs, the long-term (31 days) charge and discharge performance of individual single printed SCs and the three series-connected SC energy storage modules are predicted. The MC simulation results demonstrate that as long as the std of the parameters remains below the defined threshold, the charging behavior of SCs exhibits similarity. This is also attributed to the negligible impact of the equivalent parallel resistance (EPR) parameters during the charging phase. Moreover, The MC results provide a predicted window range of

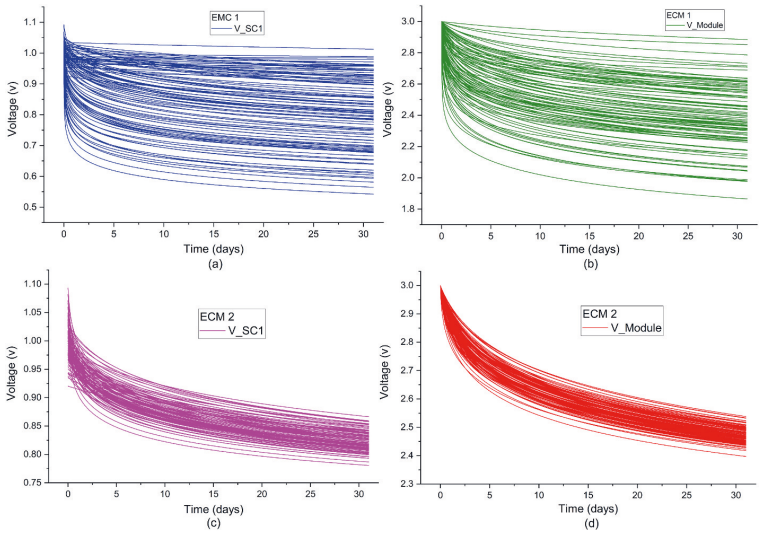

Fig. 7. MC simulated long-term (31 days) self-discharge characteristics of individual SCs and entire series-connected SC energy module using ECM 1 (a, b) and ECM 2 (c, d).

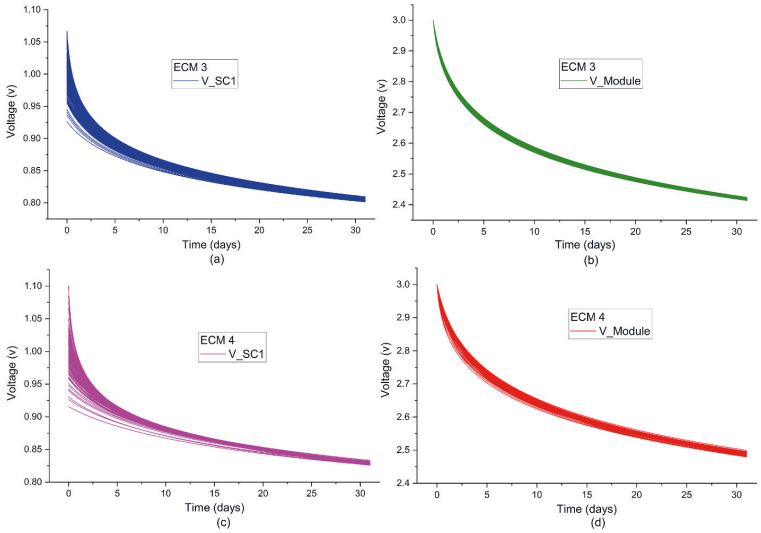

Fig. 8. MC simulated long-term (31 days) self-discharge characteristics of individual SCs and entire series-connected SC energy module using ECM 3 (a, b) and ECM 4 (c, d).

Table 4
MC simulated voltage outcomes of individual SCs and module after 31 days using four ECMs.

	Voltage of module on day 31 (V)	Voltage of single SC on day 31 (V)
ECM 1	Min: 1.87	Min: 0.44
	Max: 2.89	Max: 1.03
ECM 2	Min: 2.41	Min: 0.78
	Max: 2.56	Max: 0.90
ECM 3	Min: 2.415	Min: 0.80
	Max: 2.427	Max: 0.81
ECM 4	Min: 2.405	Min: 0.82
	Max: 2.428	Max: 0.83

voltage for the energy module after 31 days of self-discharge. The estimated range of results may provide valuable insights into the potential power variations and uncertainties that can occur over time. This information allows for better understanding and prediction of the energy module's performance under real-world conditions. By accounting for various factors and conducting multiple trials, the MC simulation helps in assessing the robustness and reliability of the energy storage system, aiding in effective planning, optimization, and risk mitigation strategies. Besides, the MC simulation results obtained from ECM 3 and 4, which have a smaller number of parameters, are considered the most likely outcomes. This is due to the fact that these results align with the range of data that exhibits the highest concentration in ECM 1, which has a larger number of parameters.

Overall, the statistical study approach proposed in this article may empower researchers in the field of printed SC energy storage modules by providing data-driven insights, performance evaluation, risk assessment, design validation, decision support, and predictive capabilities. These tools enhance understanding, support optimization, and facilitate evidence-based decision-making in this specialized research field.

Credit author statement

Hamed: Conceptualization, Methodology, Software, Validation, Formal analysis, Investigation, Data curation, Writing – original draft, Visualization. Jari: Conceptualization, Methodology, Resources, Writing – review & editing. Matti: Conceptualization, Methodology, Resources, Writing – review & editing, Supervision. Donald: Resources, Writing – review & editing, Supervision, Project administration, Funding acquisition.

Declaration of competing interest

The authors declare that they have no known competing financial interests or personal relationships that could have appeared to influence the work reported in this paper.

Data availability

Data will be made available on request.

Acknowledgements

This project has received funding from the European Union's Horizon 2020 research and innovation programme under the Marie Skłodowska-Curie grant agreement No 814299 – CHARISMA. Parts of the research used Academy of Finland Research Infrastructure "Printed Intelligence Infrastructure" (PII-FIRI, Grant Number 320019).

Appendix A. Supplementary data

Supplementary data to this article can be found online at https://doi.org/10.1016/j.jpowsour.2023.233626.

References

[1] Jerry L. Holechek, Hatim ME. Geli, MohammedN. Sawalhah, Raul Valdez, A global assessment: can renewable energy replace fossil fuels by 2050? Sustainability 14 (8) (2022) 4792.
[2] Anam Kalair, Naeem Abas, MuhammadShoaib Saleem, AliRaza Kalair, Nasrullah Khan, Role of energy storage systems in energy transition from fossil fuels to renewables, Energy Storage 3 (2021) e135–1.
[3] Abhishek Khanna, Sanmeet Kaur, Internet of things (IoT), applications and challenges: a comprehensive review, Wireless Pers. Commun. 114 (2020) 1687–1762.
[4] Arindam Dutta, Shirsendu Mitra, Mitali Basak, Tamal Banerjee, A comprehensive review on batteries and supercapacitors: development and challenges since their inception, Energy Storage 5 (1) (2023) e339.

[5] Hasan Eroğlu, Erdem Cuce, Pinar Mert Cuce, Fatih Gul, Abdulkerim Iskenderoğlu, Harmonic problems in renewable and sustainable energy systems: a comprehensive review, Sustain. Energy Technol. Assessments 48 (2021), 101566.
[6] Hui Shao, Yih-Chyng Wu, Zifeng Lin, Pierre-Louis Taberna, Patrice Simon, Nanoporous carbon for electrochemical capacitive energy storage, Chem. Soc. Rev. 49 (10) (2020) 3005–3039.
[7] KabirO. Oyedotun, JoshuaO. Ighalo, JamesF. Amaku, Chijioke Olisah, Adedapo O. Adeola, Kingsley O. Iwuozor, Kovo G. Akpomie, Jeanet Conradie, Kayode A. Adegoke, Advances in supercapacitor development: materials, processes, and applications, J. Electron. Mater. 52 (1) (2023) 96–129.
[8] Abdul Ghani Olabi, Qaisar Abbas, Ahmed Al Makky, Mohammad Ali Abdelkareem, Supercapacitors as next generation energy storage devices: properties and applications, Energy 248 (2022), 123617.
[9] Asl Mehdi Shahedi, Raha Hadi, Laleh Salehghadimi, Amin Goljanian Tabrizi, Sana Farhoudian, Babapoor Aziz, Majid Pahlevani, Flexible all-solid-state supercapacitors with high capacitance, long cycle life, and wide operational potential window: recent progress and future perspectives, J. Energy Storage 50 (2022), 104223.
[10] Anna Railanmaa, Manu Kujala, Jari Keskinen, Terho Kololuoma, Donald Lupo, Highly flexible and non-toxic natural polymer gel electrolyte for printed supercapacitors for IoT, Appl. Phys. A 125 (2019) 1–7.
[11] Guillaume Ah-Lung, Benjamin Flamme, Manuel Maréchal, Fouad Ghamouss, Johan Jacquemin, A comprehensive formulation of aqueous electrolytes for low-temperature supercapacitors, ChemSusChem 16 (10) (2023), e202202323.
[12] Libu Manjakkal, Carlos García Núñez, Wenting Dang, Ravinder Dahiya, Flexible self-charging supercapacitor based on graphene-Ag-3D graphene foam electrodes, Nano Energy 51 (2018) 604–612.
[13] García Núñez, Libu Manjakkal Carlos, Ravinder Dahiya, Energy autonomous electronic skin, npj Flexible Electron. 3 (2019), 1, 1.
[14] Li Liu, Feng Yu, Wei Wu, Recent progress in printed flexible solid-state supercapacitors for portable and wearable energy storage, J. Power Sources 410 (2019) 69–77.
[15] Abhishek Singh Dahiya, Dhayalan Shakthivel, Yogeenth Kumaresan, Zumeit Ayoub, Adamos Christou, Ravinder Dahiya, High-performance printed electronics based on inorganic semiconducting nano to chip scale structures, Nano Convergence 7 (2020) 1–25.
[16] Lixin Liu, Zhigang Shen, Xiaojing Zhang, Ma Han, Highly conductive graphene/carbon black screen printing inks for flexible electronics, J. Colloid Interface Sci. 582 (2021) 12–21.
[17] Yi-Zhou Zhang, Yang Wang, Tao Cheng, Lan-Qian Yao, Xiangchun Li, Wen-Yong Lai, Wei Huang, Printed supercapacitors: materials, printing and applications, Chem. Soc. Rev. 48 (12) (2019) 3229–3264.
[18] Chin Long Chiang, Statistical Methods of Analysis, World Scientific, 2003.
[19] Kathleen F. Weaver, Vanessa C. Morales, Sarah L. Dunn, Kanya Godde, Pablo F. Weaver, An Introduction to Statistical Analysis in Research: with Applications in the Biological and Life Sciences, John Wiley & Sons, 2017.
[20] S. Zhou, A statistical mechanics study on relationship between nanopore size and energy storage in supercapacitors, J. Phys. Chem. Solid. 148 (2021), 109705.
[21] Fatemeh Ghamari, Davood Raoufi, Saber Alizadeh, Jalal Arjomandi, Davood Nematollahi, Construction of highly efficient new binder-free bimetallic metal–organic framework symmetric supercapacitors: considering surface statistical and morphological analyses, J. Mater. Chem. A 9 (27) (2021) 15381–15393.
[22] Hongjie Jia, Yunfei Mu, Yan Qi, A statistical model to determine the capacity of battery–supercapacitor hybrid energy storage system in autonomous microgrid, Int. J. Electr. Power Energy Syst. 54 (2014) 516–524.
[23] Deepu Jha, Vispi Nevile Karkaria, P.B. Karandikar, R.S. Desai, Statistical modeling of hybrid supercapacitor, J. Energy Storage 46 (2022), 103869.
[24] Sung Deuk Lee, Han Sung Lee, Jin Young Kim, Jaesik Jeong, Yung Ho Kahng, A systematic optimization for graphene-based supercapacitors, Mater. Res. Express 4 (8) (2017), 085604.
[25] Majedeh Gheytanzadeh, Alireza Baghban, Sajjad Habibzadeh, Mohaddespour Ahmad, Otman Abida, Insights into the estimation of capacitance for carbon-based supercapacitors, RSC Adv. 11 (10) (2021) 5479–5486.
[26] Hamed Pourkheirollah, Jari Keskinen, Matti Mäntysalo, Donald Lupo, An improved exponential model for charge and discharge behavior of printed supercapacitor modules under varying load conditions, J. Power Sources 535 (2022), 231475.
[27] Maedeh Arvani, Jari Keskinen, Railanmaa Anna, Sanna Siljander, Tomas Björkqvist, Sampo Tuukkanen, Donald Lupo, Additive manufacturing of monolithic supercapacitors with biopolymer separator, J. Appl. Electrochem. 50 (2020) 689–697.
[28] Maedeh Arvani, Jari Keskinen, Donald Lupo, Mari Honkanen, Current collectors for low resistance aqueous flexible printed supercapacitors, J. Energy Storage 29 (2020), 101384.
[29] Jari Keskinen, Suvi Lehtimäki, Arman Dastpak, Sampo Tuukkanen, Timo Flyktman, Thomas Kraft, Railanmaa Anna, Donald Lupo, Architectural modifications for flexible supercapacitor performance optimization, Electron. Mater. Lett. 12 (2016) 795–803.
[30] Jari Keskinen, Saara Tuurala, Sjödin Martin, Kaisa Kiri, Leif Nyholm, Timo Flyktman, Maria Strømme, Maria Smolander, Asymmetric and symmetric supercapacitors based on polypyrrole and activated carbon electrodes, Synth. Met. 203 (2015) 192–199.
[31] Jari Keskinen, Railanmaa Anna, Donald Lupo, Monolithically prepared aqueous supercapacitors, J. Energy Storage 16 (2018) 243–249.
[32] Anna Railanmaa, Suvi Lehtimäki, Jari Keskinen, Donald Lupo, Non-toxic printed supercapacitors operating in sub-zero conditions, Sci. Rep. 9 (1) (2019) 1–8.
[33] Anna Railanmaa, Ayat Soltani, Suvi Lehtimäki, Nazanin Pournoori, Jari Keskinen, Mikko Hokka, Donald Lupo, Skin-conformable printed supercapacitors and their performance in wear, Sci. Rep. 10 (1) (2020) 1–9.
[34] Christopher Rausch, Mohammad Nahangi, Carl Haas, Wanhua Liang, Monte Carlo simulation for tolerance analysis in prefabrication and offsite construction, Autom. ConStruct. 103 (2019) 300–314.
[35] https://www.palisade.com/monte-carlo-simulation/.
[36] Hamed Pourkheirollah, Jari Keskinen, Matti Mäntysalo, Donald Lupo, Simplified exponential equivalent circuit models for prediction of printed supercapacitor's discharge behavior-Simulations and experiments, J. Power Sources 567 (2023), 232932.
[37] Hamed Pourkheirollah, Jari Keskinen, Donald Lupo, Matti Mäntysalo, A modified exponential equivalent parallel resistance (EPR) model for predicting self-discharge behavior of printed flexible supercapacitors, in: 2022 IEEE 9th Electronics System-Integration Technology Conference (ESTC), IEEE, 2022, pp. 264–268.
[38] https://statisticsbyjim.com/basics/normal-distribution/.
[39] Fang Wan, Jiacai Zhu, Shuo Huang, Zhiqiang Niu, High-voltage electrolytes for aqueous energy storage devices, Batteries Supercaps 3 (4) (2020) 323–330.
[40] Sambit Satpathy, Sanchali Das, Bidyut Kumar Bhattacharyya, How and where to use super-capacitors effectively, an integration of review of past and new characterization works on super-capacitors, J. Energy Storage 27 (2020), 101044.
[41] Yang Zhou, Hualei Qi, Jinyuan Yang, Bo Zheng, Feng Huang, Mohammad Saiful Islam, Xunyu Lu, et al., Two-birds-one-stone: multifunctional supercapacitors beyond traditional energy storage, Energy Environ. Sci. 14 (4) (2021) 1854–1896.
[42] Ahmed, Farid Uddin, Zarin Tasnim Sandhie, Liaquat Ali, H. Masud, Chowdhury. "A brief overview of on-chip voltage regulation in high-performance and high-density integrated circuits", IEEE Access 9 (2020) 813–826.

PUBLICATION V

Integration of Supercapacitors to Trigger In-Situ Electropolymerization for Irreversible Visual Indicators

E. L. Howard*, H. Pourkheirollah*, C. Pinheiro, C. A. T. Laia, A. J. Parola, M. Mäntysalo, D. Lupo

*Authors contributed equally to this work

2023 IEEE International Conference on Flexible, Printable Sensors and Systems (IEEE FLEPS)

https://doi.org/10.1109/FLEPS57599.2023.10220370

Integration of Supercapacitors to Trigger In-Situ Electropolymerization for Irreversible Visual Indicators

E. L. Howard[1,3*], H. Pourkheirollah[2*], C. Pinheiro[3], C. A. T. Laia[1], A. J. Parola[1], M. Mäntysalo[2], D. Lupo[2]
[1]LAQV-REQUIMTE, Departamento de Química, Faculdade de Ciências e Tecnologia, Universidade NOVA de Lisboa, Caparica, Portugal
[2]Faculty of Information Technology and Communication Sciences, Tampere University, Tampere, Finland
[3] Ynvisible GmbH, Engesserstrasse 4a, 79108, Freiburg im Breisgau, Germany
*Authors contributed equally to this work

***Abstract*— Printed supercapacitors (SCs) are demonstrated to activate 1x1 cm² Irreversible Visual Indicators (IVIs) based on four different monomer systems: 3,4-Ethylenedioxythiophene (EDOT), bis-3,4-Ethylenedioxythiophene (BiEDOT), 2,2'-Bithiophene (Bithiophene), and 2,2':5',2''-Terthiophene (Terthiophene). The key parameters which determine whether the IVIs can be fully activated (Δ Optical Density > 0.9) are the activation potential, the coloration efficiency (CE) of the IVI's, and the initial voltage and charge density of the SCs. All four monomer systems can be fully activated by three of the printed SCs connected in series (3.55 V), but only BiEDOT and TerThiophene can be fully activated by two series connected printed SCs (2.35 V).**

Keywords—Electrochromic Displays; Supercapacitors; Printed Electronics; Circuit Integration; Smart Labels; Irreversible Systems; Electropolymerization

I. Introduction

Electrochromic indicators and displays have commercial interest in the logistics, retail, and healthcare sectors as a dynamic form to convey information [1]. While a traditional approach to produce electrochromic displays consists of depositing or coating the chromogenic material during the manufacturing process, researchers such as Sotzing have put forward the concept of 'in-situ' electropolymerization as a simpler route for electrochromic display fabrication [2]–[5]. Using this technique, an electrochromic polymer is formed inside of the display electrochemically after the device has been fully manufactured.

While in-situ electropolymerization has been demonstrated as a method to generate electrochromic displays for conventional reversible cycling [6], the color transformation produced in the electropolymerization process can be utilized to create an Irreversible Electrochromic Indicator (IVI). This is envisioned for use in applications such as spoilage labels, or tamper labels, where a stark color change is necessary that cannot be removed, see Fig. 1. Commercial application of IVIs requires integration with a switching circuit and a power source that can trigger the electropolymerization reaction during use. Over the past decade, researchers around the world have become increasingly interested in supercapacitors (SCs), since SCs are regarded as an alternative to batteries for electrical energy storage [7]. The benefits of SCs as a promising energy storage system over conventional rechargeable batteries include high power density, light weight, exceptionally longer cycle life, lower internal resistance, short charge/discharge times, wide temperature range of operation, recyclability, and a low environmental impact [7]–[14]. While previous studies [15] have demonstrated reversible switching of electrochromic displays using SCs, electropolymerization requires a significantly greater voltage and charge than reversible redox switching of the corresponding homopolymer.

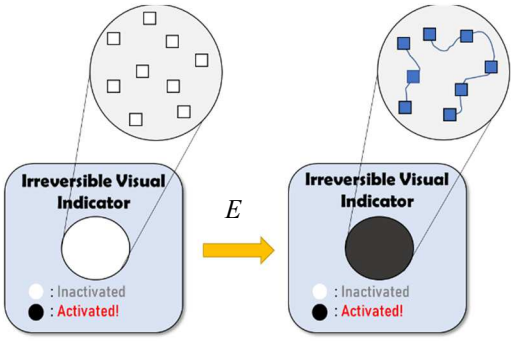

Fig. 1. Schematic of an irreversible visual indicator via electropolymerization

In this study, printed SCs are used to trigger in-situ electropolymerization of devices with four different monomer systems: 3,4-Ethylenedioxythiophene (EDOT), bis-3,4-Ethylenedioxythiophene (BiEDOT), 2,2'-Bithiophene (bithiophene), and 2,2':5',2"-Terthiophene (terthiophene). These monomer systems were selected as they present a broad range of activation potentials (E_a) and coloration efficiencies (CEs). The results of the activation with the printed SCs are evaluated and compared to a 3 V coin-cell battery. Overall, the study finds that for high coloration efficiency monomer systems, SCs can deliver sufficient voltage and charge to fully activate 1 x 1 cm² indicators, making them a promising candidate for activation of in-situ electropolymerization indicators.

II. Materials and Methods

A. Fabrication of Indicators

The electrolyte is composed of ethylene carbonate, propylene carbonate and lithium perchlorate in a 1:0.47:0.098

ratio. Gel electrolytes were formulated by incorporation of 9.95 wt% Zeospan 8030 triblock copolymer from ZEON Chemicals, and 0.5 wt% Phenylbis(2,4,6-trimethylbenzoyl)phosphine oxide photo initiator using a stainless-steel blade mixer. 10 mg/ml of monomer was mixed into the gel electrolyte.

Flexible devices were fabricated using a vertical device architecture composed of two 80 Ω□-1 PET-ITO electrodes (Eastman, FLEXVUE) and a 220 µm adhesive spacer material. The working area is a 1 cm^2. The electrolyte is cured using a LOCTITE 500 W mercury vapor bulb for 120 s. Copper tape was added to improve the electrical contact to the power source.

B. Fabrication of Supercapacitors

The authors have already published a detailed description of the process for fabricating and characterization of the printed SCs used in this study [16]–[19]. This paper provides only a brief overview of the fabrication process. A double-sided flexible Al/PET substrate was coated with graphite ink (Acheson Electrodag PF-407C) as a current collector on the PET side, while the Al layer served only as a barrier. In order to form an electrode layer, activated carbon ink (Kuraray YP-80F) was applied on the current collector layer using an in-house formulation containing chitosan as a binder. The two layers were achieved using laboratory-scale doctor blade coaters. Afterwards, NaCl:H_2O aqueous electrolyte and a paper separator were added, and the two electrodes were then heat-sealed upside down with an annealed adhesive material to form an SC of the electrochemical double-layer capacitor (EDLC) type.

C. Measurements

Optical spectroscopy was performed on an Agilent Cary 300 UV-Vis Spectrophotometer. The activation of the indicators was measured by following the transmittance at 555 nm, the peak of human photopic vision. Potentiostatsic and cyclic voltametric measurements were performed with an AUTOLAB PGSTAT100N potentiostat. The voltage of the SCs was measured using a FLUKE® 115 handheld multimeter digital CAT III 600 V display (counts): 6000.

III. Results and Discussion

A. Electrical and Optical Characterization of IVI systems

Two key electrical properties for IVIs are Ea and CE. The Ea of an IVI is primarily determined by the oxidation potential of the monomer system, and the CE is primarily determined by the number of electrons transferred in each cross-linking step (typically in the range of 2.07-2.60 F·mol−1 per monomer reacting [20]), as well as the length and absorptivity of the polymer formed. However, other parameters including the solvent, salt, monomer concentration, and electrical activation protocol can influence these values.

The first scan of cyclic voltammetry measurements of IVIs with all four monomers are shown in Fig. 2a. The onset of polymer film formation is identified by the rapid increase in the current density from monomer oxidation and subsequent cross-linking steps. The change in optical density as a function of charge during potentiostatic activation is shown in Fig. 2b. A summary of the Ea and CE for all four monomers is shown in Table I. As the conjugation length of a monomer species increases, the oxidation potential decreases, fewer cross-linking steps are required to form the same length of polymer. Thus, the CE of BiEDOT compared to EDOT and TerThiophene compared to BiThiophene are more than double, and the Ea decrease by 0.5 and 0.3 V respectively.

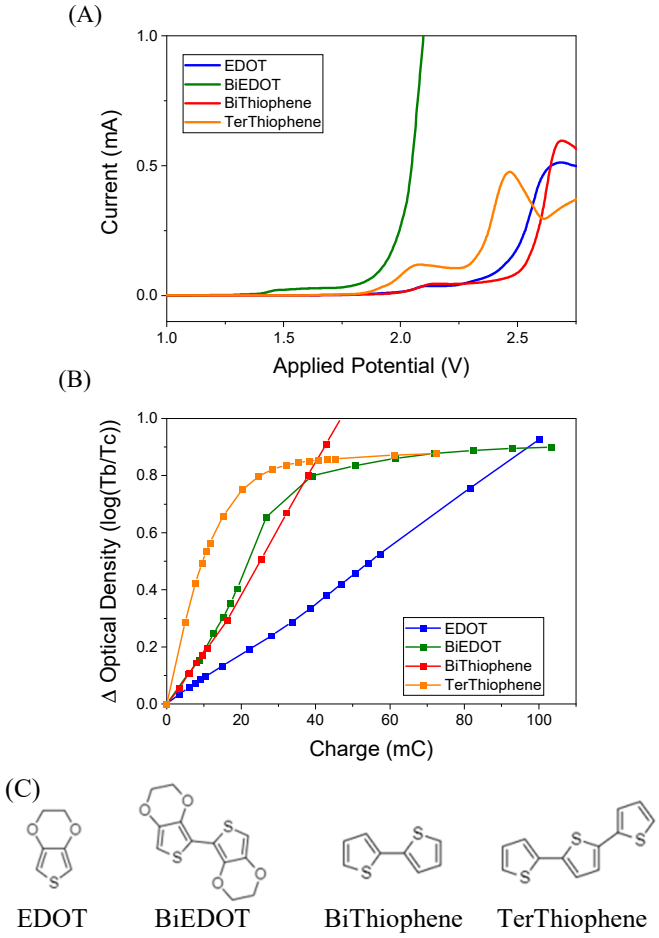

Fig. 2. (A) First forward scan of cyclic voltammetry of indicators at 10 mV/s (B) change in optical density at 555 nm as a function of current when activated potentiostatically at 3 V (C) chemical structure of EDOT, BiEDOT, BiThiophene and TerThiophene monomers.

TABLE I. KEY ELECTRICAL PROPERTIES OF IRREVERSIBLE INDICATORS BASED ON DIFFERENT MONOMER SYSTEMS

Monomer System	Activation Potential (V)	Coloration Efficiency (Cm^2/C)
EDOT	2.5	9
BiEDOT	2.0	24
BiThiophene	2.6	21
TerThiophene	2.3	49

[a] Measured at 555 nm during 3V potentiostatic activation

B. Activation of IVIs with SCs and Coin-Cell Battery

The key electrical properties of SCs are the initial voltage (E0), capacitance (C), and equivalent series resistance (ESR). The values for these properties are shown in Table II.

TABLE II. KEY ELECTRICAL PROPERTIES OF SUPERCAPACITORS CONNECTED IN SERIES

Number of SCs	Initial Voltage (V)	Overall Capacitance (mF)	Equivalent Series Resistance (Ω)
1	1.2	170	7.5
2	2.4	85	15
3	3.55	60	22

All four IVI systems were activated using two and three SCs connected in series. The transmittance across the IVIs and the voltage across the SCs were recorded simultaneously. The results are shown in Fig. 3. When the SCs are connected in series with the IVIs, if the E_0 of the SC is greater than the E_a of the IVI then the in-situ-polymerization will begin. The film forming process will proceed as the SC module discharges until the voltage of the module drops below the E_a of the IVI. At this point, the potential is too low to oxidize further monomers within the IVI and feed the electropolymerization reaction.

While both two and three SCs in series have a high enough E_0 to begin the activation with the EDOT, since the CE of EDOT is so low, 9 cm^2/C, three SCs in series are required to fully activate the IVI with $\Delta T > 80$ %. When only two SCs are used, a ΔT of only 55 % is achieved. BiThiophene likewise shows full activation with three SCs, but only a ΔT of 33 % when two SCs are used. Both BiEDOT and TerThiophene can be fully activated with both two and three SCs in series.

For all the monomer systems tested, faster activation is observed with three SCs than with two SCs, as the speed is dependent on the voltage. The transmittance data for activation with a 3 V coin-cell battery is also shown in Fig. 3, as this would be an alternative to SCs and light harvesting modules in a label.

IV. CONCLUSION

Overall, this study finds that IVIs based on in-situ polymerization can be effectively activated by printed SCs – showing potential for use in the emerging smart label market. This study shows that the contrast, as measured by Δ %T, and the activation speed can be modified by the selection of monomer system used in the IVI, as well as the number of SCs connected in series. BiEDOT and TerThiophene IVI systems are particularly promising systems due to their low E_a, and high CE during electropolymerization, however additional studies should be conducted to determine whether this has a detrimental impact on the long-term stability of the indicator. This system can be further optimized by modification of the IVI working area size and monomer concentration, and future work will include integration of these elements with a thermal sensor and an energy storage system on a flexible substrate as a prototype for use in the cold-chain market.

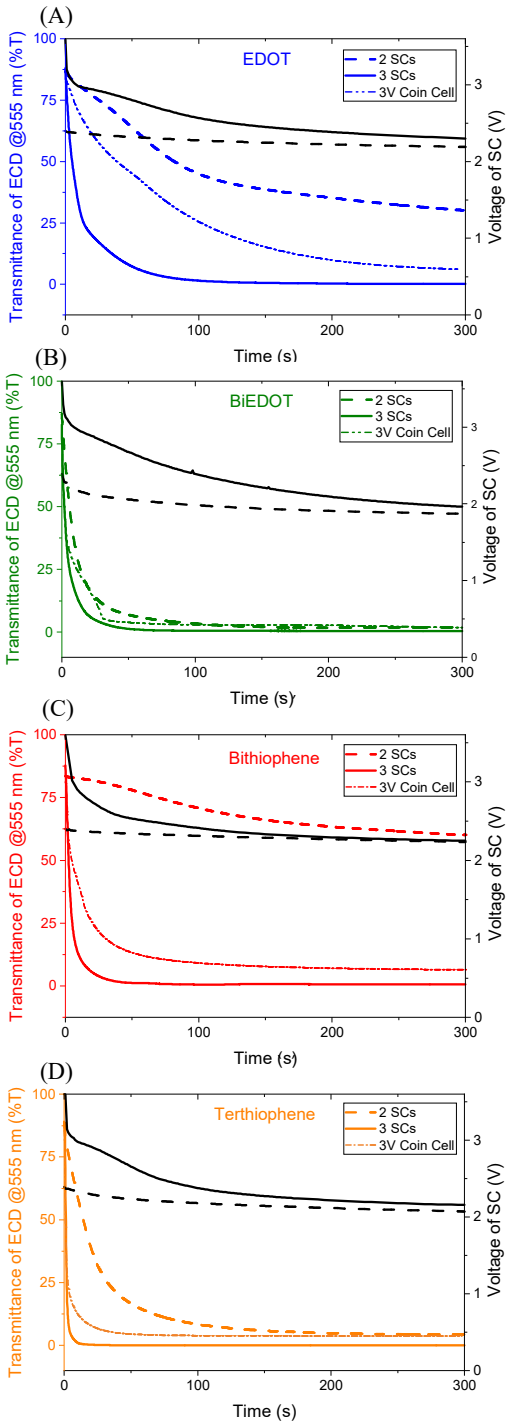

Fig. 3. Transmittance of IVIs during activation with two SCs, three SCs and a 3 V coin-cell battery for (A) EDOT, (B) BiEDOT, (C) BiThiophene, and (D) TerThiophne. Right y-axis shows the voltage of the SCs during activation. The black straight lines and the black dashed lines show the voltage of three and two series-connected SCs during activation, respectively.

ACKNOWLEDGMENT

This project has received funding from the European Union's Horizon 2020 research and innovation program under the Marie Skłodowska-Curie grant agreement No 81429.

REFERENCES.

[1] E. L. Howard, A. M. Österholm, D. E. Shen, L. P. Panchumarti, C. Pinheiro, and J. R. Reynolds, "Cost-Effective, Flexible, and Colorful Dynamic Displays: Removing Underlying Conducting Layers from Polymer-Based Electrochromic Devices," *ACS Appl. Mater. Interfaces*, p. acsami.1c00463, Mar. 2021, doi: 10.1021/acsami.1c00463.

[2] Y. Ding, M. A. Invernale, D. M. D. Mamangun, A. Kumar, and G. A. Sotzing, "A simple, low waste and versatile procedure to make polymer electrochromic devices," *J. Mater. Chem.*, vol. 21, no. 32, pp. 11873–11878, Aug. 2011, doi: 10.1039/C1JM11141H.

[3] A. Kumar, M. T. Otley, F. A. Alamar, Y. Zhu, B. G. Arden, and G. A. Sotzing, "Solid-state electrochromic devices: relationship of contrast as a function of device preparation parameters," *J. Mater. Chem. C*, vol. 2, no. 14, pp. 2510–2516, Mar. 2014, doi: 10.1039/C3TC32319F.

[4] Y. Tao, K. Zhang, C. Zhang, H. Cheng, C. Jiao, and Y. Zhao, "Electrochemical synthesis of copolymers based on 2-(anthracen-9-yl)thiophene: A facile and efficient route to a series of multicolor electrochromic polymers," *Mater. Sci. Semicond. Process.*, vol. 56, pp. 66–75, Dec. 2016, doi: 10.1016/j.mssp.2016.07.019.

[5] Y. Tao, H. Cheng, Z. Zhang, X. Xu, and Y. Zhou, "Multielectrochromic copolymers of 3,4-ethylenedioxythiophene and naphthalene prepared via electropolymerization in boron trifluoride diethyl etherate," *J. Electroanal. Chem.*, vol. 689, pp. 142–148, Jan. 2013, doi: 10.1016/j.jelechem.2012.10.033.

[6] A. M. Österholm, D. E. Shen, A. L. Dyer, and J. R. Reynolds, "Optimization of PEDOT Films in Ionic Liquid Supercapacitors: Demonstration As a Power Source for Polymer Electrochromic Devices," *ACS Appl. Mater. Interfaces*, vol. 5, no. 24, pp. 13432–13440, Dec. 2013, doi: 10.1021/AM4043454.

[7] A. G. Olabi, Q. Abbas, A. Al Makky, and M. A. Abdelkareem, "Supercapacitors as next generation energy storage devices: Properties and applications," *Energy*, vol. 248, p. 123617, Jun. 2022, doi: 10.1016/J.ENERGY.2022.123617.

[8] B. Du *et al.*, "Fabricating lignin-based carbon nanofibers as versatile supercapacitors from food wastes," *Int. J. Biol. Macromol.*, vol. 194, pp. 632–643, Jan. 2022, doi: 10.1016/J.IJBIOMAC.2021.11.107.

[9] X. Chang *et al.*, "3D Graphene Network with Covalently Grafted Aniline Tetramer for Ultralong-Life Supercapacitors," *Adv. Funct. Mater.*, vol. 31, no. 32, Aug. 2021, doi: 10.1002/ADFM.202102397.

[10] S. Satpathy, S. Das, and B. K. Bhattacharyya, "How and where to use super-capacitors effectively, an integration of review of past and new characterization works on super-capacitors," *J. Energy Storage*, vol. 27, p. 101044, Feb. 2020, doi: 10.1016/J.EST.2019.101044.

[11] M. Cakici, K. R. Reddy, and F. Alonso-Marroquin, "Advanced electrochemical energy storage supercapacitors based on the flexible carbon fiber fabric-coated with uniform coral-like MnO2 structured electrodes," *Chem. Eng. J.*, vol. 309, pp. 151–158, Feb. 2017, doi: 10.1016/J.CEJ.2016.10.012.

[12] H. Dai *et al.*, "Polymer gel electrolytes for flexible supercapacitors: Recent progress, challenges, and perspectives," *Energy Storage Mater.*, vol. 34, pp. 320–355, Jan. 2021, doi: 10.1016/J.ENSM.2020.09.018.

[13] S. Ghosh, S. Yadav, A. Devi, and T. Thomas, "Techno-economic understanding of Indian energy-storage market: A perspective on green materials-based supercapacitor technologies," *Renew. Sustain. Energy Rev.*, vol. 161, p. 112412, Jun. 2022, doi: 10.1016/J.RSER.2022.112412.

[14] A. Riaz, M. R. Sarker, M. H. M. Saad, and R. Mohamed, "Review on Comparison of Different Energy Storage Technologies Used in Micro-Energy Harvesting, WSNs, Low-Cost Microelectronic Devices: Challenges and Recommendations," *Sensors (Basel).*, vol. 21, no. 15, Aug. 2021, doi: 10.3390/S21155041.

[15] S. Tuukkanen, M. Välimäki, S. Lehtimäki, T. Vuorinen, and D. Lupo, "Behaviour of one-step spray-coated carbon nanotube supercapacitor in ambient light harvester circuit with printed organic solar cell and electrochromic display," *Sci. Reports 2016 61*, vol. 6, no. 1, pp. 1–9, Mar. 2016, doi: 10.1038/srep22967.

[16] M. Arvani, J. Keskinen, D. Lupo, and M. Honkanen, "Current collectors for low resistance aqueous flexible printed supercapacitors," *J. Energy Storage*, vol. 29, p. 101384, Jun. 2020, doi: 10.1016/J.EST.2020.101384.

[17] A. Railanmaa *et al.*, "Skin-conformable printed supercapacitors and their performance in wear," 123AD, doi: 10.1038/s41598-020-72244-8.

[18] J. Keskinen *et al.*, "Architectural Modifications for Flexible Supercapacitor Performance Optimization," *Electron. Mater. Lett.*, vol. 12, no. 6, pp. 795–803, Nov. 2016, doi: 10.1007/S13391-016-6141-Y.

[19] H. Pourkheirollah, J. Keskinen, M. Mäntysalo, and D. Lupo, "An Improved Exponential Model for Charge and Discharge Behavior of Printed Supercapacitor Modules under Varying Load Conditions," *J. Power Sources*, vol. 535, Jul. 2022, doi: 10.1016/j.jpowsour.2022.231475.

[20] J. Heinze, B. A. Frontana-Uribe, and S. Ludwigs, "Electrochemistry of conducting polymers-persistent models and new concepts," *Chem. Rev.*, vol. 110, no. 8, pp. 4724–4771, Aug. 2010, doi: 10.1021/cr900226k.